

INTEGRATED PHOTO-CATALYTIC AND ANAEROBIC TREATMENT OF INDUSTRIAL WASTEWATER FOR BIOGAS PRODUCTION

Report to the
WATER RESEARCH COMMISSION

by

OCHIENG AOYI, SETH O. APOLLO, JOHN AKACH, KWENA Y. PETE
Centre for Renewable Energy and Water,
Vaal University of Technology

WRC Report No 2105/1/14
ISBN 978-1-4312-0648-3

March 2015

Obtainable from

Water Research Commission
Private Bag X03
GEZINA, 0031

orders@wrc.org.za or download from www.wrc.org.za

DISCLAIMER

This report has been reviewed by the Water Research Commission (WRC) and approved for publication. Approval does not signify that the contents necessarily reflect the views and policies of the WRC, nor does mention of trade names or commercial products constitute endorsement or recommendation for use.

EXECUTIVE SUMMARY

Introduction: Anaerobic treatment of high strength wastewater is a widely accepted practice in the industry due to the fact that it converts the organic pollutants into biogas, which is a mixture of methane and carbon dioxide. As a result, this process leads to the reduction in chemical oxygen demand (COD) of industrial wastewater. Moreover, the biogas produced is a source of energy which can be used in industry or for domestic purposes to offset the ever increasing energy demand. Waste removal and methane yield are the key parameters used in the evaluation of an anaerobic digester (AD) performance in the anaerobic digestion process. The performance of ADs is inadequate in removing some biorecalcitrant wastes effectively. For this reason, advanced oxidation processes (AOPs) such as photocatalytic degradation as well as integrated techniques have attracted a lot of interest in the recent years. Several photocatalysts have been investigated, of which TiO_2 is most commonly applied. The catalyst and liquid mixture can be in form of slurry. The material in the slurry could be of nano- or macro-size TiO_2 particle. Used in this way, the photocatalysts pose an additional challenge with regard to the separation of the mixture. To address this problem, the catalysts can be deposited onto a support material such as zeolite. In such an application, zeolite has a dual function of adsorption and that of providing support for the catalyst. However, this creates yet another set of problems. One of such problems is that, in some cases, the degradation of the toxic wastes through photocatalysis results in compounds that are more toxic than the original one. The structures of the intermediate and final products are influenced by the operating conditions. It is important to identify the intermediate products in order to determine the photodegradation pathway which depends both on the properties of the parent compound, the characteristics of the support material and those of the reaction mixture. The presence of ions in the solution influences the properties of both TiO_2 and the toxic waste. Also, given that adsorption processes depend on the adsorbent surface area available and the presence of the active sites, the interaction between the support material and the catalyst influences both the adsorption and photo-degradation processes. The other problem is the light penetration in a system that has non-transparent liquid and opaque support materials. These problems are compounded by the fact that mass transfer limitations increase with an increase in biomass support loading.

Aim: The aim of the project was to analyse the performance of the anaerobic digester (AD) and advanced oxidation process (AOP) systems separately in degrading high strength wastes and to develop an integrated AD-AOP system to improve biogas production rate and methane yield. The treatment of high strength wastes such as molasses, textile, heavy metals and pharmaceutical was investigated under different experimental conditions.

Methodology: The approach was such that the work started with the preparation of catalysts and testing them on desk top experimental set ups at the Vaal University of Technology (VUT) and Tshwane University of Technology (TUT). Preliminary anaerobic digestion studies focused on molasses wastewater (MWW), pharmaceutical wastes and methyl blue (MB) dye. The photocatalyst (TiO_2) was attached onto zeolite and silica adsorbents. The adsorbents served two purposes of supporting both the catalyst (in the photodegradation process) and the microorganisms (in anaerobic digestion). In the photodegradation process ultraviolet lamps and sunlight were the sources of irradiation. For the solar photodegradation experiments, fluidised bed reactors (FBR) were employed to adsorb and photodegrade pharmaceuticals.

The TiO_2 was attached to powdered activated carbon (PAC) using silica xerogel. The PAC was used instead of clinoptilolite due to its favourable adsorption of pharmaceuticals and also due to the fact that it could be easily fluidised in the fluidised bed reactor.

Results and discussion: The investigation has been steadily increasing in depth and complexity in the aspects of the microbiology, photochemistry, design and modelling. This has resulted in an exponential growth in the number of researchers progressing from master to doctoral degree studies. The report is a summary of the results obtained by these young scholars. The biodegradation of MWW was observed to increase with an increase in the initial substrate concentration. However, the degradation of MB, a model textile wastewater, was inhibited at high concentrations (concentrations above 2000 mg/L). In both wastewater types, it was found that the use of zeolite as biomass support material improved biodegradation efficiency. Specifically, biogas production improved by five folds when treating MB and ten folds when treating MWW when zeolite was used in the FBR compared to reactors without zeolite. Similarly, chemical oxygen demand (COD) removal also showed the same trend with zeolite improving COD removal by about 20% in both cases. However, biodegradation was found to be suitable for colour removal only for the MB but not MWW. Colour removal of about 80% was achieved with the MB while an increment in colour was observed for MWW after the biodegradation process. Due to the fact that AD treatment could not remove the colour of the MWW and also due to the toxic nature exhibited by the MB dye, photodegradation of these kinds of wastewater was studied.

For the photodegradation studies, composite photocatalysts comprising TiO_2 and an adsorbent (zeolite, silica or activated carbon) was prepared and the proportion of TiO_2 in the composite ranged between 10-20%, depending on both the adsorbent and the pollutant to be removed. Given the energy cost associated with the application of UV, the use of solar irradiation was investigated. Solar photodegradation experiments were performed in fluidized bed battery of reactors, in which 90% removal of the pharmaceutical substrates was realized. This system was employed to study the hydrodynamics of and adsorption in the solar fluidized bed reactor. The optimum hydrodynamic condition was obtained when the reactor inclination angle and superficial air velocity were 75° and 0.014 m/s, respectively. However, a reactor inclination angle of 75° and a superficial velocity of 0.007 m/s gave the best adsorption and photodegradation of the substrates. These results show that the use of the synthesised composite catalyst in the fluidised bed reactor provided a stable and efficient system capable of long term use. The results from this work also show that this system can be used for the removal of pharmaceutical substrates at low concentrations. However, with zeolite TiO_2 was detaching with repeated use whilst silica was found to be a better binder than zeolite. Further, effects of ions on photodegradation were investigated using the UV reactor and silica as a binder for TiO_2 for the treatment of mixed dye and Cr(VI) wastewater. It was found that there was a good dispersion of TiO_2 on the surface of silica. The degradation of dye/ TiO_2 -silica binary system proceeded faster than that of the respective ternary dye/Cr(VI)/ TiO_2 -silica system at neutral pH. Results showed that the photo reduction of Cr(VI) was much faster in the mixed system than in the single one. The studies using separate photodegradation and biodegradation revealed limitations and advantages of each process, which were further employed by integrating the two processes.

Conclusion and recommendations: An Integrated AD and AOP using South African zeolite was applied in the treatment of methylene blue dye in up-flow fixed bed bioreactor and UV photoreactor. The optimal operating conditions obtained in the separate AOP and AD were applied in the treatment of methylene blue dye in an integrated up-flow fixed bed bioreactor and photoreactor. Results showed that, compared to the separate systems, the integrated AOP-AD system achieved better degradation with colour and COD reductions of 81% and 80%, respectively. Moreover, it was found that UV photodegradation pre-treatment improved the biodegradability of the MB dye by 3- folds after irradiation time of 60 minutes. Thus integration of the two processes in such a way that UV photodegradation precedes the AD process led to higher biogas production than that of the stand-alone AD process.

ACKNOWLEDGEMENT

We acknowledge the support, advice and stimulating discussions, initiated by Dr Valerie Naidoo, that helped shape the direction of the project. We are very grateful to Dr Francois Talbot for donating to us a mobile wastewater treatment plant (fondly referred to as mobile wastewater clinic) and Prof Maurice Onyango for his role in the adsorption aspect of the work and Thabo Brooms for his contribution in material characterization. The contributions by the members of the reference group are gratefully acknowledged.

Reference Group

Dr V Naidoo	Water Research Commission (Chairperson)
Prof MS Onyango	Tshwane University of Technology
Dr P Stegmann	Vaal University of Technology
Ms P Welz	Cape Peninsula University of Technology
Prof A Botha	Stellenbosch University
Dr P Osifo	Vaal University of Technology
Dr EB Naidoo	Vaal University of Technology
Dr J-F Talbot	Talbot & Talbot Ltd
Prof L Chimuka	University of the Witwatersrand
Prof T Majazi	University of the Witwatersrand
Mr CM Esterhuysen	City of Tshwane Metropolitan Municipality
Dr K Foxon	University of KwaZulu-Natal
Mr M Lindeque	Council for Scientific and Industrial Research
Ms G Munganga	University of Cape Town
Mr V Mabeer/Ms L Moodley	eThekweni municipality

TECHNOLOGY TRANSFER

Capacity development: The funds obtained from the WRC supported both BTech final year projects and postgraduate projects. The support for the BTech students was in form of equipment and materials only while for the MTech students, the support included either partial or full bursary. In case of partial bursary, the other portion came from, either the National Research Foundation (NRF), VUT or TUT.

MTech degrees, graduated

	Name	Year completed	Nationality
1	Ojijo V	2011	Kenyan
2	Mohlala MM	2012	South African
3	Apollo S	2013	Kenyan
4	Atiba AO	2013	Nigerian
5	Pete KY	2014	South African

In progress, MTech and DTech

	Name	Degree	Nationality	Institution
1	Munyai MH	MTech	South African	TUT
2	Mlungisi AM	MTech	South African	TUT
3	Nyembe N	MTech	South African	VUT
4	Akach J	DTech	Kenyan	VUT
5	Apollo S	DTech	Kenyan	VUT
6	Brooms T	DTech	South African	TUT

Publications

Journal article publications are from the postgraduate students projects while the conferences are from the work of both postgraduate and undergraduate projects.

Journal articles

1. Seth Apollo, Maurice S. Onyango, Aoyi Ochieng (2014), Integrated UV photodegradation and anaerobic digestion of textile dye for efficient biogas production using natural zeolite, *Journal of Chemical Engineering*, 245(1), 241-247.
2. Seth Apollo, Mannana Ntoampe, Maurice S. Onyango, Aoyi Ochieng, (2013) UV/H₂O₂/TiO₂/Zeolite Hybrid System for Treatment of molasses wastewater, submitted to the *Iranian Journal of Chemical Engineering*.
3. Seth Apollo, Aoyi Ochieng, Onyango, S. Maurice (2013). An integrated anaerobic digestion and UV photocatalytic treatment of distillery wastewater. *Journal of Hazardous Materials* 261, 435-442. (IF 4.7).
4. Apollo, S., Onyango, M. S., and Ochieng, A., (2013). UV photodegradation and anaerobic digestion of methylene blue dye. *Advanced Material Research*, (781-784).
5. Aoyi Ochieng, Rita. L.L. Pambi, P. Netshitangani, John Akach, Maurice S. Onyango, (2012). Solar/uv photocatalytic degradation of two commercial textile dyes *Journal of sustainable development and environmental protection*, 2(1) 36-48.

Conference presentations

1. Kwena Y Pete and Aoyi Ochieng (2014), Analysis of Kinetic Models in Heterogeneous Catalysis of Methyl Orange Using TiO₂/Silica Composite Photocatalyst, International Conference on Chemical and Metallurgical Engineering'2014, Plenary Scientific Research Centre (PSRC), Johannesburg, South Africa, 15-16 April 2014, ISBN 9789382242710, pp 172-176, www.pscentre.org.

2. John Akach, Maurice S. Onyango, Aoyi Ochieng (2014), Adsorption and photodegradation of sulfamethoxazole in a three phase fluidised bed reactor; *International Conference on "Environmental Technology and Sustainable Development*, Lucknow, India, 21-23 February 2014.
3. John Akach, Maurice S. Onyango, and Aoyi Ochieng (2014), Adsorption and Solar Photocatalytic Degradation of Diclofenac in Wastewater, *International Conference on Chemical and Metallurgical Engineering'2014*, Plenary Scientific Research Centre (PSRC), Johannesburg, South Africa, 15-16 April 2014, ISBN 9789382242710, pp 195-198, www.psrcentre.org
4. Malaka Mpho Sandra, Aoyi Ochieng, Akach John, Stanley Moyo (2014), Solar Photodegradation of Phenol and Dichlorophenol on Zeolite Supported TiO₂ Catalyst, *Annual Conference on Engineering & Information Technology (ACEAIT 2014)*, Tokyo, Japan, 28-30 March 2014, ISBN 978-986-89298-6-9, pp326-338.
5. Jeffrey Baloyi, Tumelo Seadira, Mpfunzeni Raphulu, Aoyi Ochieng (2014), Synthesis of dandelion-like TiO₂ structure as photocatalyst for industrial wastewater treatment containing Cr(VI) and Hg(II), *International Conference on Chemical and Metallurgical Engineering'2014*, Plenary Scientific Research Centre (PSRC), Johannesburg, South Africa, 15-16 April 2014, ISBN 9789382242710, pp 141-148, www.psrcentre.org.
6. Aoyi Ochieng, Kwena Y. Pete, (2014) Impact of Cr (VI) on the photodegradation of dye Using TiO₂/silica composite as photocatalyst, *International Conference on Composite Materials and Renewable Energy Applications (ICCMREA-2014)*, Sousse, Tunisia, 22-24 January 2014.
7. Mlungisi A. Mavuso, Maurice S. Onyango and Aoyi Ochieng (2014), Photodegradation of reactive Black-5 (Rb-5) dye Annular photoreactor, *International Conference on Chemical and Metallurgical Engineering'2014*, Plenary Scientific Research Centre (PSRC), Johannesburg, South Africa, 15-16 April 2014, ISBN 9789382242710, pp189-194, www.psrcentre.org.
8. Jeffrey Baloyi, Tumelo Seadira, Mpfunzeni Raphulu, Aoyi Ochieng (2014), Simultaneous photocatalytic reduction of Cr(VI) and oxidation of citric acid, *International Conference on Chemical and Metallurgical Engineering'2014*, Plenary Scientific Research Centre (PSRC), Johannesburg, South Africa, 15-16 April 2014, ISBN 9789382242710, pp149-155, www.psrcentre.org.
9. Tumelo Seadira, Jeffrey Baloyi, Mpfunzeni Raphulu, Richard Moutloali, Aoyi Ochieng (2014), Acid Mine Drainage Treatment Using Constructed Wetland, *International Conference on Chemical and Metallurgical Engineering'2014*, Plenary Scientific Research Centre (PSRC), Johannesburg, South Africa, 15-16 April 2014, ISBN 9789382242710, pp 134-140, www.psrcentre.org.
10. Thabo J Brooms, Maurice Onyango, Aoyi Ochieng (2014), Photocatalytic activity of polyaniline/TiO₂/ZnO composites for degradation of aromatic compounds on abattoir wastewater, *International Conference on Chemical and Metallurgical Engineering'2014*, Plenary Scientific Research Centre (PSRC), Johannesburg, South Africa, 15-16 April 2014, ISBN 9789382242710, pp 127-133, www.psrcentre.org.
11. Seth Apollo, Maurice S. Onyango, Aoyi Ochieng, (2013), Integrated UV photodegradation and anaerobic digestion of textile dye for efficient biogas production, *3rd International Conference on Chemical Engineering and Advanced Materials*, Guangzhou, China, 4-6 July 2013.
12. Apollo, S., Onyango, M. S., and Ochieng, A., Photocatalytic degradation of industrial wastewater using South African natural zeolite as TiO₂ support material. Paper presented at *WISA 2012 Biennial Conference and Exhibition*, Cape Town, South Africa, 6-10, May 2012.
13. Akach, J., Onyango, M. S., and Aoyi Ochieng, Solar Photocatalytic degradation of biorecalcitrant wastes. Paper presented at *WISA 2012 Biennial Conference and Exhibition*, Cape Town, South Africa, 6-10 May 2012.
14. Apollo, S., Onyango, M. S., and Ochieng, A., UV photodegradation of molasses wastewater using South African natural zeolite as catalyst support. *Paper presented at SAChE conference 2012*, Champagne Sports Resort, South Africa, 16-19 September 2012.
15. Akach, J., Onyango, M. S., and Aoyi Ochieng, Solar photocatalytic decolourization of molasses and Mauritian blue dye. *Paper presented at SAChE conference 2012*, Champagne Sports Resort, South Africa, 16-19 Sep. 2012.

16. Pambi, R. L. L., Akach, J., Aoyi, Ochieng, and Osifo, P., Solar photocatalytic degradation of textile water using chitosan-TiO₂ beads catalyst. *Paper presented at SAChE conference 2012*, Champagne Sports Resort, South Africa, 16-19 Sep. 2012.
17. Apollo, S., Onyango, M. S., and Aoyi Ochieng, Application of South African natural zeolite to enhance biogas production in anaerobic treatment of industrial wastewater. Paper presented at Academy of Science of South Africa, Pretoria, South Africa, 16-18 Oct. 2012.
18. Aoyi Ochieng, Rita. L.L. Pambi, P. Netshitangani, John P Akach, Maurice S. Onyango, Solar/UV photocatalytic degradation of two commercial textile dyes, pp 36-48, Sustainable Development and Environmental Protection Conference, 20-22 March 2012, Ota, Nigeria.
19. Vincent O. Ojijo, Maurice S. Onyango, Aoyi Ochieng and Fred A.O. Otieno, (2011). Combined Adsorption and Biodegradation of Synthetic Melanoidin, *The 21st Annual International Conference on Soil, Water, Energy, and Air and AEHS Foundation Annual Meeting March 14-17, 2011*, San Diego, USA.

BTech degrees, graduated

The students listed here are only those that worked on BTech final year projects funded by this WRC project.

2011			2012			2013		
#	Name	Nationality	#	Name	Nationality	#	Name	Nationality
1	Serepa TM	SA	1	Msimango N	SA	1	Mabitsela T	SA
2	Nedambale TM		2	Malaka M	SA	2	Xorile P	SA
3	Moloko KP	SA	3	Matsimela M	SA	3	Komane DM	SA
4	Mokgobu NC	SA	4	Tsheshla T	SA	4	Malindi MJ	SA
5	Valashiya ZB	SA	5	Balepe G	DRC	5	Maga R	SA
6	Pambi RLL	DRC	6	Kwena YP	SA	6	Bataatweng	Botswana
7	Baloyi SJ	SA	7	Godlo N	SA	7	Modipa	SA
8	Hlahane RTPC	SA	8	Matjebe T	SA	8	Malaka A	SA
9	Seribe MS	SA	9	Mashego V	SA	9	Manayati MK	Botswana
10	Netsgitangani P		10	Makhubele G	SA	10	Mfeya	SA
11	Shabangu PD	SA	11	Ramoshaba I	SA	11	Mokone	SA
12	Khoro TE	SA	12	Thobejane I	SA	12	Tshehlakgolo DIM	SA
13	Motale I	SA	13	Mthembi F	SA	13	Mangwale SE	Botswana
14	Maloka MM	SA	14	Moyahabo J	SA	14	Masina A	SA
15	Seadira TWP	SA	15	Siaga T	SA	15	Ndlovu T	SA
16	Masemola MJ	SA	16	Magaraba V	SA	16	Makwala W	SA
17	Mokua E	SA	17	Ndashi G	SA	17	Moshoea GA	SA
18	Mkhize ZE	SA	18	Msimango N	SA	18	MabuoA A	SA
19	Kubheka ZN	SA	19	Malaka M	SA	19	Thobejane L	SA
20	Nxumalo LH	SA	20	Matsimela M	SA	20	Chitray G	SA
21	Mutalama L		21	Tsheshla T	SA	21	Phala W	SA
22	Kgopotso		22	Balepe G	DRC	22	Tsie ME	SA
23	Shabangu N	SA	23	Kwena YP	SA	23	Mohatla GN	SA
24	Lukhele JT	SA	24	Godlo N	SA	24	Molongoane R	SA
25	Pretorius J	SA	25	Matjebe T	SA	25	Tjale A	SA
26	Bali M					26	Smith J	SA
27	Nkosana					27	Nelushi T	
28	Bongani					28	Ithenga	SA
29	Govendor	SA				29	Mashego VM	SA
						30	Ngobeni MK	SA
						31	Ongunsula TM	Nigeria
						32	Meyer D	SA
						33	Phungula Dz	
						34	Matsimela RP	SA
						35	Machaba GM	SA
						36	Sibiya MO	SA
						37	Mazibuko SG	SA
						38	Mlambo JE	SA
						39	Makubo S	SA

Contents

Acknowledgement	vi
List of Tables	xv
List of Figures	xv
List of abbreviations	xix
List of Symbols	xx
CHAPTER 1	1
1 Introduction	1
1.1 MOTIVATION AND RESEARCH PROBLEM	1
1.2 AIMS AND OBJECTIVES	1
1.2.1 Specific objectives	1
1.2.2 Layout of the report.....	2
CHAPTER 2	3
2 Review of wastewaters and treatment methods	3
2.1 CHARACTERISTICS OF INDUSTRIAL WASTEWATER	3
2.2 MOLASSES INDUSTRY WASTEWATER AND DISTILLERY SPENT WASH	3
2.3 TEXTILE INDUSTRY WASTEWATER	4
2.4 EMERGING PHARMACEUTICAL CONTAMINANTS	5
2.5 ANAEROBIC DIGESTION (AD)	7
2.5.1 Energy potential of industrial wastewater	7
2.5.2 Digester performance	7
2.5.3 Methane yield.....	8
2.5.4 Application of zeolite in anaerobic wastewater treatment process.....	8
2.5.5 Challenges of the AD in the treatment of textile and molasses wastewater.....	8
2.6 ADVANCED OXIDATION PROCESSES.....	9
2.6.1 Mechanism of photodegradation.....	9
2.6.2 Support materials for photocatalyst	10
2.6.3 Natural zeolite as photocatalyst support material	11
2.6.4 Preparation of TiO ₂ supported on zeolite.....	11
2.6.5 Light source.....	11
2.6.6 Heterogeneous solar photocatalysis.....	11
2.6.7 Challenges in photocatalytic wastewater treatment.....	12
2.7 INTEGRATED ADSORPTION AND PHOTODEGRADATION.....	12
2.8 INTEGRATED PHOTODEGRADATION AND BIODEGRADATION (IPB).....	13
2.9 CONCLUSION AND INADEQUACY OF BOTH AOP AND AD	16
REFERENCES	16
CHAPTER 3	21
3 Anaerobic digestion	21
3.1 INTRODUCTION	21
3.2 METHODOLOGY.....	21

3.2.1	Equipment.....	21
3.2.2	Experimental procedure.....	22
3.3	RESULTS AND DISCUSSION	22
3.3.1	Effect of substrate concentration and zeolite addition	22
3.3.2	Effect of nutrient addition on MB degradation.....	24
3.3.3	Methane yield.....	24
3.3.4	Effect of zeolite dosage.....	25
3.3.5	Biogas production	27
3.3.6	COD and colour reductions.....	28
3.4	CONCLUSION	29
	REFERENCES	30
CHAPTER 4		32
4	UV photodegradation of molasses wastewater and methylene blue dye	32
4.1	INTRODUCTION	32
4.2	METHODOLOGY.....	32
4.2.1	Preliminary photocatalytic degradation experiments	32
4.2.2	Catalyst preparation.....	33
4.2.3	Experimental analysis	33
4.3	RESULTS AND DISCUSSION	33
4.3.1	Catalyst characterization.....	33
4.3.2	Preliminary photodegradation for molasses wastewater (MWW).....	35
4.3.3	Preliminary photodegradation of methylene blue dye	42
4.4	CONCLUSION	45
	REFERENCES	45
CHAPTER 5		47
5	Solar photodegradation AND adsorption of emerging pharmaceuticals	47
5.1	INTRODUCTION	47
5.2	METHODOLOGY.....	47
5.2.1	Equipment.....	47
5.2.2	Materials.....	49
5.2.3	Experimental methods	50
5.2.4	Chemical analyses.....	51
5.2.5	Experimental design	52
5.2.6	Data analyses	52
5.3	RESULTS AND DISCUSSION	53
5.3.1	Solar radiation at VUT.....	53
5.3.2	Catalyst characterization.....	56
5.3.3	Catalyst composition and performance	61
5.3.4	Hydrodynamics	69
5.3.5	Effect of hydrodynamics on adsorption and photodegradation	73
5.3.6	Solution characteristics	77
5.4	CONCLUSION	80
	REFERENCES	80

CHAPTER 6	83
6 Photocatalytic degradation of dyes in the presence of ions	83
6.1 INTRODUCTION	83
6.2 METHODOLOGY	83
6.2.1 Synthesis of TiO ₂ /silica composite photocatalysts	83
6.2.2 Characterization of composite photocatalysts	84
6.2.3 Photocatalysis experiments	84
6.3 RESULTS AND DISCUSSION	84
6.3.1 SEM- EDS analysis	84
6.3.2 Raman spectra analysis	85
6.3.3 Isoelectric point measurements (IEP)	86
6.3.4 Photocatalytic degradation of methyl orange dye by TiO ₂ /silica photocatalyst	86
6.3.5 Effect of photocatalyst composite loading	87
6.3.6 Effect of dye initial concentration	88
6.3.7 Effect of solution pH	89
6.3.8 Photodegradation isotherms and kinetics of methyl orange	89
6.3.9 Photocatalytic reduction with a single substrate: Cr(VI)	93
6.3.10 Photocatalytic degradation of the dye and reduction of Cr(VI), ternary system	94
6.4 CONCLUSION	96
REFERENCES	96
CHAPTER 7	98
7 Integrated biodegradation and photodegradation	98
7.1 INTRODUCTION	98
7.2 METHODOLOGY	99
7.2.1 Materials	99
7.2.2 Inoculum and wastewater preparation	99
7.2.3 Experimental set-up	99
7.2.4 Photodegradation and biodegradation experiments	100
7.2.5 Experimental analysis	101
7.2.6 Statistical Analysis	101
7.3 RESULTS AND DISCUSSION	101
7.3.1 Distillery wastewater	101
7.3.2 Textile wastewater	109
7.4 CONCLUSION	116
REFERENCES	116
CHAPTER 8	120
8 Continuous photodegradation of distillery effluent	120
8.1 INTRODUCTION	120
8.2 METHODOLOGY	120
8.2.1 Materials	120
8.2.2 Experimental set up	120
8.2.3 Experimental procedure	120
8.3 RESULTS AND DISCUSSION	121
8.3.1 Effect of UV type and reactor construction material	121
8.3.2 Effect of concentration	122

8.3.3	Air flow rate and effluent flow rate	122
8.3.4	Catalyst loading.....	123
8.4	CONCLUSION	124
	REFERENCES	124
CHAPTER 9	125
9	Conclusions and Recommendations	125
9.1	CONCLUSIONS.....	125
9.1.1	Anaerobic digestion of molasses wastewater and methylene blue dye	125
9.1.2	UV photodegradation of molasses wastewater and methylene blue dye.....	125
9.1.3	Adsorption and solar photodegradation of pharmaceutical wastewater	125
9.1.4	Photodegradation of methyl orange in the presence of ions	125
9.1.5	Integrated anaerobic biodegradation and photodegradation of molasses wastewater and methylene blue.....	126
9.1.6	Continuous photodegradation of distillery effluent.....	126
9.2	RECOMMENDATIONS.....	126
Appendices	127
A1	REACTOR DESIGN AND PICTURES.....	127
A2	SUPPLEMENTARY DATA	131
A3	WORKSHOP/CONFERENCES.....	132
A4	OTHER OUTPUTS	132

LIST OF TABLES

Table 2.1: Characteristics of distillery spentwash generated from cane molasses.....	4
Table 2.2: Data on consumption, excretion and environmental concentration of diclofenac, sulfamethoxazole and carbamazepine	6
Table 2.3: Methane production potential of some industrial wastewater effluents.....	7
Table 4.1: EDX results for elemental composition of South African natural zeolite	35
Table 4.2: Rate constant and R ² values	41
Table 5.1: Properties of diclofenac, sulfamethoxazole and carbamazepine	49
Table 5.2: The parameters investigated during the experiments using OFAT experimental design	52
Table 5.3: Percentage of rutile and anatase in the P-25 TiO ₂ and CTS composite	60
Table 5.4: Carbon free basis XRF results vs theoretical compositions for various silica loadings	61
Table 5.5: Adsorption, adsorption equilibrium time and photodegradation of SMX, DCF and CBZ	63
Table 5.6: Performance characteristics of CTS composites with different PAC/TiO ₂ ratios	67
Table 5.7: Langmuir and Freundlich isotherms of the adsorption of SMX onto the CTS composite	80
Table 6.1: Isotherms constants and correlation coefficients for the degradation of Methyl orange onto TiO ₂ /silica composite photocatalyst.....	91
Table 6.2: Kinetic parameters for degradation of methyl orange	93
Table 7.1: Wastewater characteristics.....	102
Table 7.2: Colour and COD reduction by adsorption in the photoreactor and bioreactor	104
Table 7.3: pH variation during the anaerobic degradation process.....	106
Table 7.4: Wastewater characteristics.....	110
Table 7.5: Comparison between UV pre-treatment and AD pre-treatment in colour reduction	112
Table 7.6: Adsorption on TiO ₂ /zeolite and zeolite surface in the reactors	112

LIST OF FIGURES

Fig. 2.1: Publications treating photocatalysis and the share treating solar-driven photocatalysis.	9
Fig. 2.2: Process of photocatalysis.....	10
Fig. 2.3: UV radiation wavelengths.....	12
Fig. 2.4: Overview of methods of AC regeneration	13
Fig. 2.5: Integrated biological and photodegradation	15
Fig. 3.1: Laboratory scale fixed bed anaerobic reactor	22
Fig. 3.2: Effect of substrate concentration on anaerobic degradation.....	23
Fig. 3.3: Effect of addition of nutrients in the degradation of MB dye.....	24
Fig. 3.4: Effect of zeolite on methane yield.....	25
Fig. 3.5: Effect of zeolite dosage on COD removal during anaerobic treatment of MWW, MB dye and distillery wastewater.....	26
Fig. 3.6: Variation in colour removal with zeolite mass in the degradation of MWW, MB and distillery	26

Fig. 3.7: Cumulative biogas production in the FBR	27
Fig. 3.8: Biogas production coefficient in the FBR	28
Fig. 3.9: COD removal in the FBR after 27 days of degradation.....	29
Fig. 3.10: Colour removal in the FBR	29
Fig. 4.1: XRD result for TiO ₂ powder	34
Fig. 4.2: Results of EDX analysis of zeolite.....	34
Fig. 4.3: SEM analysis for zeolite, TiO ₂ and TiO ₂ -zeolite catalyst before degradation and after degradation	35
Fig. 4.4: Effect of initial concentration of MWW on the degradationd	36
Fig. 4.5: Effect of hydrogen peroxide dosage on photocatalytic degradation of molasses wastewater in acidic medium.....	37
Fig. 4.6: Effect of TiO ₂ loading on zeolite at initial concentration of 20 g/L and pH of 4	38
Fig. 4.7: Adsorption and effect of H ₂ O ₂ on the photodegradation process at pH 4 and concentration of 20 g/L.....	39
Fig. 4.8: UV-Vis spectral changes.	39
Fig. 4.9: Effect of photodegradation on COD and colour removal	40
Fig. 4.10: Effect of pH on H ₂ O ₂ /TiO ₂ /UV/zeolite hybrid system pH 4, pH 7 and pH 10.....	41
Fig. 4.11: The effect of TiO ₂ loading on Zeolite.....	42
Fig. 4.12: The effect of catalyst (TiO ₂ -zeolite) dosage	43
Fig. 4.13: The effect of pH on photodegradation of MB using zeolite as catalyst support.....	44
Fig. 4.14: Colour removal by photodegradation and adsorption	44
Fig. 5.1: Experimental set up.....	48
Fig. 5.2: Monthly solar radiation for May to November 2012 at VUT	54
Fig. 5.3: Daily solar radiation for October 2012 at VUT.....	54
Fig. 5.4: Solar radiation data for 24 th October 2012 and 31 st October 2012 at VUT	55
Fig. 5.5: SEM images of pure silica xerogel, CTS composite, PAC and TiO ₂	56
Fig. 5.6: High magnification SEM images of silica xerogel, small sized PAC and large sized PAC, TS composite and CTS composite.....	57
Fig. 5.7: SEM images of various CTS composites with varying PAC/TiO ₂ ratios	58
Fig. 5.8: SEM images of various CTS composites with varying silica xerogel loading	59
Fig. 5.9: XRD spectra of CTS, TiO ₂ , PAC and pure silica xerogel	60
Fig. 5.10: Effect of proportion of silica xerogel in the CTS composite on the rate of adsorption and photodegradation of SMX, DCF and CBZ.....	62
Fig. 5.11: Effect of proportion of silica xerogel in the composite on the turbidity of SMX, DCF and CBZ	65
Fig. 5.12: Effect of PAC/TiO ₂ ratio on the rate of adsorption and photodegradation of SMX, DCF and CBZ.	66
Fig. 5.13: Effect of mass of the CTS composite on the adsorption and photodegradation of SMX, DCF and CBZ.....	68
Fig. 5.14: The effect of aspect ratio and superficial air velocity on gas holdup.....	70
Fig. 5.15: The effect of inclination angle on gas holdup.....	70

Fig. 5.16: Variation of solid concentration with distance from the distributor at different superficial air velocities and inclination angles	71
Fig. 5.17: Mean catalyst loading and standard deviation of samples at different distances from the distributor at different inclination angles and superficial air velocities.....	72
Fig. 5.18: Effect of reactor inclination angle on the rate of adsorption and photodegradation of DCF, SMX and CBZ.....	74
Fig. 5.19: Effect of superficial air velocity on the rate of adsorption and photocatalysis of SMX, DCF and CBZ.....	76
Fig. 5.20: Effect of substrate initial concentration on the adsorption and photodegradation of SMX, DCF and CBZ.....	78
Fig. 5.21: Effect of initial pH of solution on the adsorption and photodegradation of SMX.....	79
Fig. 6.1: Experimental setup.....	84
Fig. 6.2: SEM images and EDS spectra of silica alone and 15% TiO ₂ /silica	85
Fig. 6.3: Raman spectra of TiO ₂ /silica before and after the photocatalysis treatment	85
Fig. 6.4: Zeta potential of TiO ₂ /silica as a function of pH	86
Fig. 6.5: Adsorption of methyl orange over TiO ₂ /silica; photocatalytic degradation of methyl orange	87
Fig. 6.6: Effect of TiO ₂ /silica composite photocatalyst concentration on dye degradation.....	88
Fig. 6.7: Effect of initial concentration on TiO ₂ /silica photocatalyst.....	88
Fig. 6.8: Effect of solution pH on TiO ₂ /silica photocatalyst.....	89
Fig. 6.9: Linear transform of Langmuir and Freundlich isotherm	90
Fig. 6.10: Photodegradation isotherms of methyl orange on TiO ₂ /silica	91
Fig. 6.11: Pseudo-first-order plot for the photocatalytic degradation of methyl orange dye onto TiO ₂ /silica ..	92
Fig. 6.12: Pseudo-second-order plot for the photocatalytic degradation of methyl orange dye onto TiO ₂ /silica	92
Fig. 6.13: Photoreduction of Cr(VI) on TiO ₂ /silica.....	93
Fig. 6.14: Effect of TiO ₂ /silica photocatalyst concentration on dye degradation in the presence of Cr(VI).....	94
Fig. 6.15: Effect of TiO ₂ /silica concentration on Cr(VI) reduction in the presence of dye.	95
Fig. 6.16: Effect of Cr(VI) initial concentration on dye degradation.....	95
Fig. 7.1: The integrated photocatalytic degradation and anaerobic digestion set up.....	100
Fig. 7.2: SEM analysis for TiO ₂ -zeolite catalyst before and after photodegradation.....	101
Fig. 7.3: Photodegradation of MWW and distillery wastewater in the annular photocatalytic reactor.....	103
Fig. 7.4: Anaerobic degradation of MWW and distillery wastewater streams	103
Fig. 7.5: Cumulative biogas production during the anaerobic process	104
Fig. 7.6: VFA removal during the anaerobic process	105
Fig. 7.7: Nitrates removal during the anaerobic process.....	106
Fig. 7.8: Phosphates removal during the anaerobic process	107
Fig. 7.9: Overall colour removal for the integrated system.....	108
Fig. 7.10: Overall COD reduction for the integrated system.....	109

Fig. 7.11: Photodegradation in the annular photocatalytic reactor.....	110
Fig. 7.12: Anaerobic degradation of UV pre-treated wastewater sample.....	111
Fig. 7.13: Biogas production and methane composition during the anaerobic process.....	113
Fig. 7.14: VFA removal during AD process and Degradation kinetics of the VFAs	113
Fig. 7.15: Nitrate and phosphate removal during the anaerobic process.....	114
Fig. 7.16: Overall COD reduction for the integrated system.....	115
Fig. 8.1: Reactor set up	121
Fig. 8.2: Effect of construction material and UV type on photodegradation	122
Fig. 8.3: Effect of the initial wastewater concentration on the colour removal efficiency	122
Fig. 8.4: Effect of air flow rate in the degradation of distillery effluent.....	123
Fig. 8.5: Effect of liquid flow rate in the degradation of distillery effluent	123
Fig. 8.6: Effect of catalyst loading on degradation of distillery effluent	124

LIST OF ABBREVIATIONS

AC	Activated carbon
AD	Anaerobic digestion
ADs	Anaerobic digesters
AOPs	Advanced Oxidation Processes
BOD	Biochemical Oxygen Demand
CBZ	Carbamazepine
COD	Chemical Oxygen Demand
CSTR	Continuously stirred tank reactor
CTS	Activated carbon – TiO ₂ – silica xerogel composite
CVD	Chemical vapor decomposition
DCF	Diclofenac
DON	Dissolved organic nitrogen
EDCs	Endocrine disrupting compounds
EDX	Energy Dispersive X-ray
FAU	Formazin attenuation units
FBB	Fluidized bed bioreactor
FBR	Fixed bed reactor
GC	Gas Chromatography
HPLC	High Performance Liquid Chromatography
HRT	Hydraulic retention time
IPB	Integrated Photodegradation and Biodegradation
LCFAs	Low carbon fatty acids
LPM	Litres per minute
MB	Methylene blue
MWW	Molasses Wastewater
NSAIDs	Non-steroidal anti-inflammatory drugs
PAC	Powdered activated carbon
PPCPs	Pharmaceutical and personal care products
SAWS	South African Weather Services
SEM	Scanning Electron Microscopy
SGB	Silica gel beads
SMX	Sulfamethoxazole
SSD	Solid Solid Dispersion
TCD	Thermal Conductivity Detector
TiO ₂	Titanium (IV) oxide
TOC	Total Organic Carbon
TS	TiO ₂ and silica xerogel composite
TZ	Titanium dioxide/zeolite
UASB	Up-flow anaerobic sludge blanket
UKZN	University of KwaZulu-Natal
US	University of Stellenbosch
UV	Ultraviolet
UV-vis	Ultraviolet-visible
VFAs	Volatile fatty acids
VUT	Vaal University of Technology
WWTPs	Wastewater treatment plants
XRD	X-ray diffraction
XRF	X-ray fluorescence
ZPC	Zero point charge

LIST OF SYMBOLS

$1/n$	Freundlich intensity parameter
C_0	Initial substrate concentration (mg/L)
C_e	Equilibrium substrate concentration (mg/L)
I_A	Intensity of anatase (101) phase of TiO_2
I_R	Intensity of the rutile (110) phase of TiO_2
K_F	Freundlich capacity factor ($mg/g(1/mg)^{1/n}$)
Q_{EA}	Equilibrium adsorption capacity of the fresh PAC (mg/g)
Q_{EAP}	Equilibrium adsorption capacity of the spent PAC due to photocatalytic regeneration (mg/g)
m_{AP}	Mass of the substrates adsorbed during the second adsorption due to photocatalytic regeneration (g)
m_{AT}	Mass of substrates adsorbed by the spent PAC during the second adsorption (g)
m_{AU}	Mass of the substrates adsorbed by unsaturated sites during the second adsorption (g)
q_m	Maximum Langmuir adsorption capacity (mg/g)
A_0	Initial absorbance
A_t	Absorbance at time t
I_A	Intensity of anatase
I_R	Intensity of rutile
K	Langmuir equilibrium adsorption constant (L/mg)
K	Reaction rate constant (Min^{-1})
m	Mass of the adsorbent (g)
\emptyset	% colour removal
R^2	Correlation coefficient
V	Volume of the substrate solution (L)
X_R	Mass fraction of rutile
E	Methane production coefficient (CH_4 L/g COD removed)
χ	Weight fraction of rutile phase of TiO_2
RE	Regeneration efficiency (%)

CHAPTER 1

1 INTRODUCTION

1.1 Motivation and research problem

Biological wastewater treatment systems are typically employed to treat industrial wastewater, however, the performance of these systems is inadequate in removing biorecalcitrant wastes. For this reason, advanced methods such as photocatalytic degradation as well as integrated photocatalysis and adsorption techniques have attracted a lot of interest in the recent years. Several photocatalysts have been investigated, of which TiO_2 is the one that is most commonly applied. This is due to the fact that it is less costly compared to the other types, non-toxic and chemically resistant to photo-corrosion. The catalyst and liquid mixture can be in the form of slurry. The material in the slurry could be of nano or macro-size TiO_2 particle. Used in this way, the photocatalyst poses an additional challenge with regard to the separation of the mixture. To address this problem, the catalysts can be deposited on the support material such as adsorbent. In such an application, the adsorbent has a dual function of adsorption and that of providing support for the catalyst. However, this poses yet another set of problems. One of such problems is that in some cases the degradation of the toxic wastes through photocatalysis results in compounds that are more toxic than the original one. The structures of the intermediate and final products are influenced by the operating conditions. It is important to identify the intermediate products in order to determine the photodegradation pathway, which depends both on the properties of the parent compound, the characteristics of the support material and those of the reaction mixture. Most wastewater streams contain a variety of pollutants including ions. The presence of ions in the solution influences the properties of both TiO_2 and the toxic waste. Also, given that adsorption processes depend on the adsorbent surface area available and the presence of the active sites, the interaction between the support material and the catalyst influences both the adsorption and photodegradation processes. The other problem is the penetration of the light through a system that has non-transparent liquid and opaque support materials. These problems are compounded by the fact that mass transfer limitations increase with an increase in biomass support loading. The key problems in this study include toxicity of the intermediate products as well as the influence of the clinoptilolite on the adsorption and reaction kinetics.

1.2 Aims and objectives

The aim of the project was to develop a photo-catalysed anaerobic digester and to improve biogas production rate and methane yield.

1.2.1 Specific objectives

- a. To review the trend of wastewater treatment techniques globally and in South Africa.
- b. To determine the optimum operating conditions for the anaerobic digestion of textile and molasses wastewater.
- c. To prepare and apply photocatalysis in the UV photocatalytic degradation of molasses wastewater and methylene blue.
- d. To design and apply a solar photoreactor to treat pharmaceutical wastes.
- e. To determine the reactor configuration for optimum COD and colour reduction as well as biogas production.
- f. To determine the effect of ions in the photodegradation of dyes.
- g. To apply continuous UV photodegradation and anaerobic digestion to treat distillery wastewater.

1.2.2 *Layout of the report*

This report consist of eight chapters. In Chapter 1, a brief background is given to the material in the report together with the motivation, significance and the objectives of the study. Chapter 2 discusses the anaerobic digestion of molasses and methylene blue in a shaker. Chapter 3 deals with the UV photodegradation of molasses and methylene blue dye in a shaker. In Chapter 4, the adsorption and solar photodegradation of pharmaceuticals in a fluidised bed reactor is discussed. Chapter 5 describes the UV photodegradation of methyl orange in the presence of Cr(VI) ions. In Chapter 6, the optimum order of anaerobic digestion and UV photodegradation treatment of molasses, distillery and methylene blue wastewater is determined. Chapter 7 describes the continuous photodegradation of distillery wastewater in a fluidised bed reactor. Chapter 8 gives a general conclusion and recommendations from the entire report.

CHAPTER 2

2 REVIEW OF WASTEWATERS AND TREATMENT METHODS

2.1 Characteristics of industrial wastewater

Treatment of wastewater from industries, municipalities and the agricultural sector has been of great concern due to the negative effects of such wastes on the environment. These wastewaters, if not appropriately handled, can percolate into ground water or contaminate surface water thereby causing an adverse impact on life. It has been realized that the increase in global industrialization has led to the increase in the amount of industrial wastewaters discharged into the environment. South Africa, in particular, is not an exception when considering the detrimental effect of industrial effluent on the existing natural water resources. The Department of Water Affairs (1986) reported that water pollution is rapidly increasing in South Africa. The major industries which are responsible for the discharge of large amounts of effluent in South Africa are: dairy industry, brewery industry, food industry, textile industry, mining industry and petrochemical industry. Many food industries produce wastewater that is readily biodegradable. However, distilleries and molasses wastewater streams are largely biorecalcitrant and need more advanced treatment techniques. Equally demanding are textile and pharmaceutical wastes.

2.2 Molasses industry wastewater and distillery spent wash

The increasing demand for sugar and molasses fermentation products such as ethanol and baker's yeast has led to rapid growth in the sugar cane processing industries. These industries are able to produce millions of tonnes of sugar for domestic and industrial uses while at the same time molasses is produced as a by-product. Most of the molasses produced is used by distillery industries to manufacture ethanol while some leave the sugar industry as waste in the effluent. Still at the distillery industry, a large amount of the molasses remains in the fermentation residues after product recovery. Berg (2004) reported that about 61% of the world's ethanol production is from molasses while Jain et al. (2002) estimated that about 88% of the molasses used in distillery industries is discharged as effluent.

The main stages in production of ethanol from cane molasses are feed preparation, fermentation and packaging. In the distillery process, molasses is suitably diluted to have the desired sucrose level, it is then supplemented with various nutrients like ammonium sulphate before fermenting using an active yeast culture. The fermented culture is then distilled, fractionated and rectified after the removal of the yeast sludge (Pathede, 2003). It is the residue of the fermented mash which comes out as distillery spent wash (Pathede, 2003; Sigh et al., 2004; Nandy et al., 2002). Some characteristics of distillery wastewater are listed in Table 2.1. Factors such as quality of molasses used, unit operation procedures employed during the alcohol production process and process recovery of alcohol determine the pollution load of the distillery effluent (Pandey et al., 2003). Saha et al. (2005) reported that in the distillery process, an average of 8-15 litres of effluent is generated for every litre of alcohol produced. Moreover, the amount of wastes generated during ethanol production is on the rise since there is an increase in alcohol distillery industries due to a wide spread industrial application of alcohol such as in food, pharmaceuticals, perfumery or even in transport industry as fuel supplement (Mohana et al., 2009). The wastewater from molasses processing plants presents a large amount of coloured substances that give a recalcitrant dark brown colour and high organic load to the effluents (Martins and van Boekel, 2004). Poorly treated distillery wastewater poses a serious threat to water quality in several regions around the world (Mohana et al., 2009).

Discharge of molasses wastewater into the receiving water causes environmental stress, largely to the aquatic organisms. This is because the molasses wastewater has high COD (80,000-100,000 mg/L), BOD (40,000-50,000 mg/L), strong odour and is acidic in nature (Satyawali and Balakrishnan, 2008). Worse still, the molasses wastewater contains a dark brown recalcitrant colour which impedes the penetration of sunlight to the aquatic photosynthetic plants and therefore reduces dissolved oxygen in river courses. The dark

brown pigment is generally called melanoidin formed due to Maillard amino-carbonyl reaction. It is a product of non-enzymatic reaction between sugars and amino compounds (Martins and van Boekel, 2004). It has been reported that melanoidin has an antioxidant property which renders it toxic to many micro-organisms such as those typically present in biological wastewater treatment plants (Kumar et al., 1997). The recalcitrance of melanoidins to degradation is evidenced by the fact that these compounds escape various stages of wastewater treatment plants and finally enter the environment. Pandey et al. (2003) reported that other recalcitrant compounds present in effluent of industries processing molasses are caramel, a variety of sugar decomposition products, anthocyanins, tanins and different xenobiotic compounds (Mohana, 2009). The effluent from industries consuming molasses or producing molasses also has a characteristic strong odour. This odour is caused by the presence of sulphur containing organic compounds such as skatoles and indoles in the wastewater stream (Sharma et al., 2007). Also, Kumar et al. (1997) explained that the high organic load, nitrogen and total phosphates content in this effluent may result in eutrophication of the natural water bodies.

Table 2.1: Characteristics of distillery spentwash generated from cane molasses (Satyawili and Balakrishnan, 2008)

Characteristic	Value
COD (mg/l)	65,000-130,000
BOD (mg/l)	40,000-70,000
Total solids (mg/l)	30,000-100,000
Total dissolved solids (mg/l)	80,000-87,000
Total nitrogen (mg/l)	1000-2000
Total Phosphorus (mg/l)	800-1,200
Potassium (mg/l)	8,000-12,000
Sulphates	2,000-6,000
pH	3-5.4

Studies have been conducted to evaluate the effect of distillery effluent on the growth of various organisms inhabiting different environments. Haematological alterations in fresh water catfish (*Channapunctatus*) exposed to distillery effluent have been reported (Kumar and Gopal, 2001). Oxygen consumption in fresh water fish (*Lebeorohita*) exposed to distillery effluent was also investigated by Saxena and Chauhan (2003). It was observed that the presence of inorganic and organic salts in the effluent interfered with the respiration in the fish. These pollutants led to coagulation of gill mucus of the fish, resulting in a decrease in dissolved oxygen consumption which caused asphyxiation. In addition to that, the effect of uncontrolled disposal of distillery spent wash on land surface has also been studied and it was found that these wastes are equally harmful to vegetation. Kumar et al. (1997) reported that this waste inhibits seed germination since it alters soil alkalinity and reduces manganese availability to plants.

2.3 Textile industry wastewater

The textile industry is considered as one of the largest water consumers in the world (Wouter et al., 1998). Ramgi and Buckely (2006) reported that in the current environmental legislation, textile industries have been labelled as high priority industry with respect to pollution and with specific regard to toxicity caused by recalcitrant wastes, high salt and heavy metals in their effluent. Wastewater which contains various pollutants is generated during various stages of the textile manufacturing process. Specifically, the major sources of wastewater generated by the textile industry originate from the washing (scouring) and bleaching of natural fibres and from dyeing and finishing steps (Chen et al., 2008). Based on the fact that varieties of fibres, dyes, process additives and finishing products are employed, these processes generate wastewater of high chemical complexity (Vandevivere et al., 1998). The recalcitrant nature of the organic pollutants generated from dye stuff has posed a great challenge in treating the textile industry effluent. It has been reported that during processing, up to about 15% of the total dye remains unreacted and is lost in the effluent (O'Neill et al., 1999). This fact has also been supported by other studies, Hao et al. (2000); Robert and

Sanjeev (2005), reported that out of more than one million tons of dyes produced, about 280,000 tons are annually discharged as effluent worldwide. Apart from the high effluent COD contributed by the dyes, their presence in wastewater, even in low amounts is highly visible, and this seriously affects the aesthetic quality of the receiving water bodies. The presence of dyes also causes poor penetration of light rays into natural water bodies therefore impacting negatively on the life of aquatic photosynthetic plants. The direct consequence of this is the reduction in dissolved oxygen in the aquatic ecosystem which can lead to death of the aquatic organisms. Studies have reported that most of these dyes are refractory to biological degradation (Wijetunga et al., 2008). Moreover, some of the dyes, dye precursors and dye degradation products are reported to be carcinogenic and mutagenic in nature (Henderson et al., 1997).

2.4 Emerging pharmaceutical contaminants

Emerging environmental contaminants are mainly organic micropollutants produced by human activities such as pharmaceutical and personal care products (PPCPs), Endocrine Disrupting Compounds (EDCs), illicit drugs, sweeteners, nanoparticles, flame retardants, perfluorinated compounds, organic solvents, complexing agents, plasticizers, pesticides and surfactants detected in trace amounts of several ng/L up to low µg/L in wastewater treatment effluents and water sources (Houtman, 2010). From domestic, agricultural and industrial sources, these emerging contaminants enter wastewater treatment plants (WWTPs) where their removal is usually incomplete mainly due to their biorecalcitrant nature. Wastewater treatment facilities have therefore been identified as the main pathway through which emerging contaminants enter surface and ground water (Baeza and Knappe, 2011).

Emerging pollutants have only become an issue in recent years with the development of better analytical techniques that are capable of detecting chemicals at low concentrations of up to ng/L level. The environmental toxicity of emerging pollutants to humans and wildlife is still not well understood. For this reason, most countries currently have little or no relevant legislation regulating the release of these contaminants into surface water. However, widespread production, use and continuous input into the environment, their persistence in the environment, bioaccumulation and potential chronic toxicity to aquatic biota even at low concentrations, have raised concerns over emerging contaminants in recent years (Houtman, 2010). With increasing research on the effects of emerging contaminants on the environment, these wastes are expected to be under regulation soon (Malato et al., 2009). Therefore there is a need to develop appropriate methods for treating emerging contaminants to be used when regulation starts.

Pharmaceutical products form a class of emerging pollutants which include human and veterinary medicines and their metabolites. To achieve their function, pharmaceutical drugs are designed to persist in the body in the form in which they were ingested and are often only slightly altered before excretion in urine and faeces (Fent et al., 2006). These drugs and their metabolites, once excreted, maintain their persistence in the environment, resisting degradation in WWTPs and surface waters. As a result, residues of pharmaceutical drugs have been ubiquitously detected in treated waters and surface waters in North America, Europe and Asia (Monteiro and Boxall, 2010).

Pharmaceutical products can enter aquatic systems from several sources. Drugs and their metabolites once excreted in urine and faeces of humans enter municipal WWTPs and this is the principal route by which pharmaceuticals enter surface water bodies. Other sources are hospital wastewater effluents, pharmaceutical factory effluents and expired or unused drugs that are improperly disposed of. Runoffs of manure applied to farmland, use of manure for aquaculture and wastewater from agricultural farms are significant sources of veterinary pharmaceutical pollution originating from drug excretion in urine and dung of animals (Fent et al., 2006).

The efficiency of the removal of pharmaceuticals in conventional WWTPs has been observed to be generally low although this varies widely from one plant to the other due to differences in construction, treatment processes used, hydraulic retention time (HRT), performance, operation and environmental conditions

(Zorita et al., 2009). Pharmaceuticals are removed from conventional WWTPs mainly through sorption to sludge and biodegradation, both of which are not effective. Therefore, most pharmaceutical pollutants enter the aquatic environment with the treated water (Fent et al., 2006).

In the aquatic environment, pharmaceuticals pose a considerable toxicity threat to aquatic life. Pharmaceuticals are designed to have physiological effects in higher organisms at trace concentrations (Hapeshi et al., 2010), and as such can cause similar effects in lower organisms (Zorita et al., 2009). Individual pharmaceuticals at low ng/L concentrations may not cause significant harm to aquatic life. However, as is usually the case, when mixtures of these drugs each at low concentrations are present, toxicity increases due to additive effects (Pomati et al., 2006). Although the risk of acute toxicity is minimal, that of chronic toxicity to aquatic species is considerably high as these organisms live in water and are thus exposed to the pollutants all their life. Humans could be affected indirectly through food toxicity if edible aquatic species bioaccumulate these pharmaceuticals (Fent et al., 2006). The presence of pharmaceutical pollutants in wastewater streams has contributed to the resistance by the public to the use of WWTPs effluents for irrigation and this has greatly affected sustainable water reuse (Snyder and Benotti, 2010).

Hundreds of pharmaceuticals have been detected in wastewater, in treatment plants and surface water bodies. Of these drugs, those with significant environmental impact are mostly drugs of considerable toxicity, environmental persistence and often, but not always, high production volumes (Fent et al., 2006). Pharmaceuticals with such environmental impact include diclofenac, sulfamethoxazole and carbamazepine. These three pharmaceuticals are some of the most investigated in regard to their removal from wastewater using advanced oxidation methods (Klavarioti et al., 2009). Some representative data on consumption, excretion rates and concentrations of sulfamethoxazole, diclofenac and carbamazepine in WWTP influent and effluent, rivers, lakes, groundwater and drinking water are shown in Table 2.2.

Table 2.2: Data on consumption, excretion and environmental concentration of diclofenac, sulfamethoxazole and carbamazepine nd – not detected; References: [1] – Fent et al. (2006); [2] – Monteiro and Boxall (2010)

Compound	Consumption (tonnes/year)	Excretion rates (%unchanged)	WWTP influent (µg/L)	WWTP effluent (µg/L)	Rivers (µg/L)	Ground water (µg/L)
Diclofenac	4.50-85.80 ^[1,2]	6.0-39 ^[2]	0.33-3 ^[1]	nd-5.45 ^[1,2]	nd-1.20 ^[2]	nd-3.5 ^[2]
Sulfamethoxazole	3.1-16.7 ^[2]	6.0-39 ^[2]		nd-2.14 ^[2]	nd-9 ^[2]	0.002-0.47 ^[2]
Carbamazepine	4.40-87.71 ^[1,2]	1.0-5 ^[2]	0.7 ^[1]	0.033-6.3 ^[1,2]	0.001-7.1 ^[2]	nd-15.9 ^[2]

Diclofenac is one of the most used Non-steroidal Anti-inflammatory Drugs (NSAIDs) for the treatment of inflammation, pain, fever and rheumatic diseases. The drug is only slightly removed in WWTPs and is therefore often detected in wastewater treatment plants, river water, wells and ground water. Diclofenac has been found to be acutely toxic to vultures feeding on animals treated with the drug. The toxicity of diclofenac to river biofilm communities and the rainbow trout has also been documented (Fent et al., 2006).

Sulfamethoxazole is the most used sulphonamide antimicrobial in the treatment of urinary tract infections. Only a portion of the antibiotic is degraded in the human body, the rest being excreted in urine and faeces which find their way into sewerage systems. Sulfamethoxazole has been found in hospital sewage and sewage from residential areas which empties into WWTPs. In WWTPs, like other antibiotics, most of the sulfamethoxazole is not biodegraded as it attacks the bacteria that are supposed to biodegrade it (Abellán et al., 2007). Some of the sulfamethoxazole that is not degraded is sorbed onto sludge but the majority of the sulfamethoxazole remains dissolved in the WWTP effluent which goes into the receiving waters. As a result,

sulfamethoxazole has been detected in WWTP effluents, sludge, rivers, river sediments, lakes, seas, groundwater and even drinking water of several countries. Antibiotics like sulfamethoxazole in aqueous systems and soil sediments have been linked to antibiotic resistance in humans and animals. This bacterial resistance occurs due to the fact that the low concentration of sulfamethoxazole in wastewater and soil sediments is too low to destroy bacteria but high enough to enable them develop resistant genes (Akiyama and Savin, 2010).

Carbamazepine is the primary neuroactive compound used in the treatment of psychomotor epilepsy. In WWTPs, the neutral and polar carbamazepine is hardly removed as it resists biodegradation even under long residence times. In the aquatic environment, carbamazepine has been found to damage the liver of rainbow trout and the immune system of mussels (Zhang et al., 2010) as well as poison *C. dubia* and the rotifer *B. calyciflorus* (Fent et al., 2006).

2.5 Anaerobic digestion (AD)

2.5.1 Energy potential of industrial wastewater

Anaerobic digestion has been employed for generation of energy from a wide range of effluents from various industries. Table 2.2, illustrates the range of some substrates that have been tested at laboratory or pilot scale and their potential energy recovery as reported by Burton et al., (2009). The methane yields are typically expressed in terms of gas production per unit COD or volatile solids (VS). The energy yield from methane is calculated based on calorific value of 890.3 kJ per mole of methane (or 11.04 kWh/m³) (Duerr et al., 2007). In Table 2.3 the capacity of the system employed is indicated by the hydraulic retention time (HRT) and organic loading rate (OLR).

Table 2.3: Methane production potential of some industrial wastewater effluents (Burton et al., 2009)

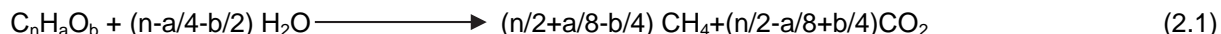
Feed	HRT (Days)	OLR	Potential Energy Recovery	Reference
Fruit and vegetable Wastes	20	2.8 g VS/L.d	0.45 l CH ₄ /g VS	Bouallagui et al., 2005
Brewery slurry	16	6.27 g COD/L.d	0.42 L CH ₄ /g COD	Zupancic et al., 2007
Molasses	7	7 g COD/L.d	0.23 L CH ₄ /g COD	Jimnez et al., 2004

2.5.2 Digester performance

The performance of an anaerobic process depends on the stability of the reactor. Reduction of COD of the wastewater and methane yield is the key parameters used in the evaluation of the digester performance in the anaerobic digestion process. One of the major problems encountered in operating a biogas digester in a continuous mode is the reactor instability. This occurs during both the start-up and operation of the anaerobic degradation process affecting the performance of the system due to the low specific growth rate of the methanogenic micro-organisms involved (Bjornsson et al., 1997). Under conditions of unstable operation, intermediates such as volatile fatty acids (VFAs) and alcohols accumulate at different rates depending on the cause of the instability. The most common causes of imbalance are hydraulic or organic overloading, presence of toxins/inhibitory substances, microbial washout and change in the substrate concentration. Several parameters are used as indicators of stress, such as variation in gas production rate, gas composition, pH and VFA concentration (Powell and Archer, 1989). The continuous accumulation of toxic by-products affects both the effectiveness of methanogens and the yield of methane.

2.5.3 Methane yield

The efficiency of a digester is evaluated on the basis of the rate of methane production and methane yield. For total substrate conversion, the theoretical product composition is given by (Maya-Altamira et al., 2008):



Wastewater from food processing industries typically contains carbohydrates (ϕ_{cb}), proteins (ϕ_{pt}), acetate (ϕ_{ac}), lipids (ϕ_{lp}) and propionate (ϕ_{pp}). Theoretical yield (Y) of methane based on the organic fraction of the substrate can be estimated as:

$$Y_\phi = 0.415 \phi_{cb} + 0.496 \phi_{pt} + 1.0140 \phi_{ac} + 0.373 \phi_{lp} + 0.530 \phi_{pp} \quad (2.2)$$

where Y_ϕ is the methane yield calculated on the basis of mole fraction. The value of ϕ is determined from the analytical measurement of the total volatile solids. The real methane yield can be determined by measuring the percentage of methane. Methane yield on the other hand depends on the system's operating parameters such as temperature, pH, hydraulic retention time and nutrient ratio (Maya-Altamira et al., 2008).

2.5.4 Application of zeolite in anaerobic wastewater treatment process

The structural composition of natural zeolites varies with geographical occurrence and therefore there are various types of natural zeolite. One of the best known zeolites for ion exchange is the clinoptilolite (Emadi et al., 2001), which is a low temperature zeolite. Jorgensen et al. (1976) were able to remove up to 14.4 g total ammonium nitrogen (TAN)/kg using clinoptilolite. They noted an increase in sorption with contact time, and also enhanced efficiency with smaller grain size. Mwale (2000) obtained cation exchange capacity close to 15 g/kg with South African zeolites. Rozic et al. (2002) used Croatian clinoptilolite to take up ammonium from aqueous solution and had a maximum loading in ammonia exchange of 13.2 g TAN/kg. Structural modification of zeolite can be carried out to improve its adsorption capacity for the various pollutants. The surface of zeolite has a net negative surface charge which may enhance the adsorption of positively charged ions. The adsorption of negative ions requires the modification of the surface of zeolite.

2.5.5 Challenges of the AD in the treatment of textile and molasses wastewater

Even with the use of zeolite to improve the anaerobic system, there are still some organic pollutants which cannot be effectively degraded due to their high toxicity or biorecalcitrant nature. Dye component of textile wastewater and melanoidin which is a constituent of wastewater containing molasses are typical examples. It has been reported that dyes are very difficult to degrade using standard biological methods (Adams et al., 1997). In fact, textile dyes are considered to be biorecalcitrant (Ganesh et al., 1994), a fact which makes them to be able to go through biological wastewater treatment without being eliminated (Chu and Tsui, 2002). The hazardous potential of textile dyes on bacterial strands has also been reported (Chun and Wang, 1999). On the other hand, Gonzalez et al. (1999) reported that biodegradability of melanoidin present in the wastewater containing molasses is very low. They reported that only biodegradation of about 6%-7% could be achieved. It was therefore observed that even after the anaerobic treatment, the wastewater still had the dark brown colour contributed by the melanoidin. This is an indication that this compound is also recalcitrant to biodegradation. These biorecalcitrant compounds can, however, be totally eliminated using photocatalysis.

Conventional WWTPs have been found to be inefficient in eliminating emerging pharmaceutical pollutants, which are biorecalcitrant in nature. As a result, new and efficient treatment systems such as chlorination, Advanced Oxidation Processes (AOPs), membrane processes (reverse osmosis, nanofiltration, ultrafiltration and ion exchange), adsorption and their combinations have been proposed for the removal of the pharmaceutical wastes from the environment (Homem and Santos, 2011). The disadvantage of these alternative treatment methods is that they are more costly than the conventional systems.

2.6 Advanced Oxidation Processes

Among the most promising technologies for the removal of recalcitrant pollutants are the AOPs such as photolysis, ozonation, electrochemical oxidation, ultrasound irradiation (sonolysis), sub-critical wet air oxidation, homogeneous photo-Fenton oxidation and heterogeneous semiconductor photocatalysis (Klavarioti et al., 2009). The use of AOPs is advantageous in that they destroy pollutants instead of simply transferring the pollutant to a different phase (Fernández-Ibáñez et al., 1999). This eliminates the need to regenerate or dispose of sludge produced in the process of treating wastewater (Zainudin et al., 2010). Of the many AOPs, heterogeneous semiconductor photocatalysis has attracted significant attention as a potential commercial system for the treatment of pharmaceutical wastes due to its low energy and chemical input requirements especially when powered by sunlight (Klavarioti et al., 2009).

Photocatalytic degradation is an advanced wastewater treatment technique that is employed to remove highly toxic compounds such as aromatic chlorophenols, dyes and pharmaceuticals. These compounds are biorecalcitrant and anaerobic degradation per se cannot efficiently be used to remove them from industrial effluents. Photocatalytic degradation involves the use of a semi-conductor (photocatalyst) in the presence of a light source to degrade such complex hydrocarbon compounds into simpler organic compounds. The semiconductors that can be used as photocatalyst are TiO_2 , WO, FeTiO and SrTiO. Compared to other semiconductors, TiO_2 has been used extensively due to its high photocatalytic activity, non-toxicity, low cost and chemical as well as thermal stability (Huang et al, 2008) while sunlight or UV irradiation has been used as source of light. The success of photocatalysis is dependent on the toxicity of the intermediate compounds. The identity of the intermediate compound can give an insight into the mechanism of the photodegradation process. There has been an increasing interest in photocatalysis evidenced by increasing number of scientific publications in this area (Fig. 2.1).

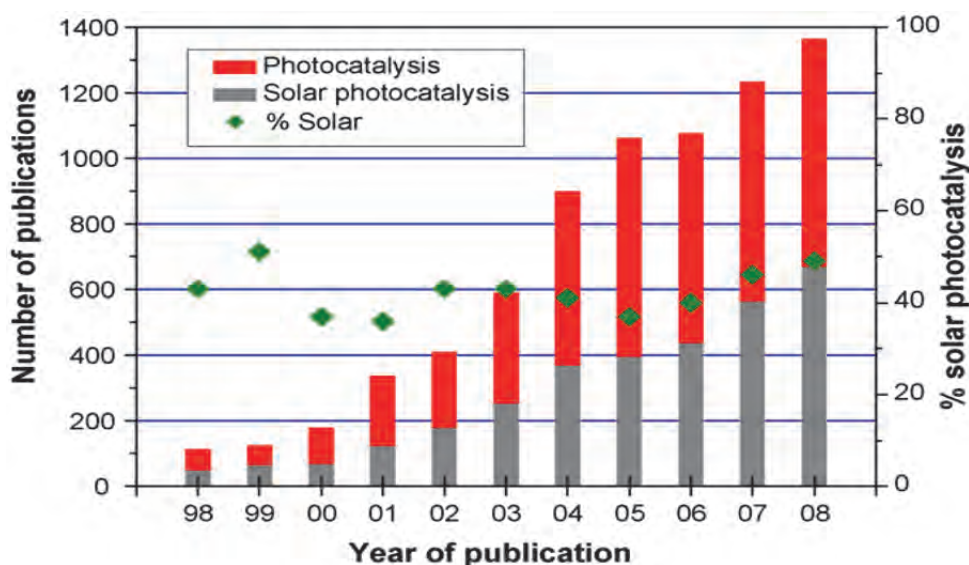


Fig. 2.1: Publications treating photocatalysis and the share treating solar-driven photocatalysis (source: <http://www.scopus.com>, 2009, search terms “photocatalysis” and “solar” within these results) (Cited from Malato et al., 2009).

2.6.1 Mechanism of photodegradation

To function as a catalyst, the semiconductor has to be first activated. The activation is carried out by irradiating the semiconductor with photons of light of energy greater than or equal to its band gap energy. When the semiconductor absorbs such a photon, an electron jumps from the valence band to the conduction band which creates a hole in the valence band (Herrmann, 1999). The electrons and holes thus created could combine within the semiconductor or migrate to the surface of the catalyst where they participate in redox reactions with electron acceptors and donors adsorbed on the surface. In aqueous media, water

molecules adsorbed onto the surface of the photocatalyst are oxidized by the holes into hydroxyl radicals (Eq. 2.3). The highly reactive hydroxyl radicals then attack organic pollutants (Eq. 2.4). Pollutants adsorbed onto the surface of the semiconductor catalyst are also oxidized directly by the holes on the semiconductor surface (Eq. 2.5). Dissolved oxygen and other dissolved electron acceptors scavenge electrons on the surface of the semiconductor (Eq. 2.6) (Gaya and Abdullah, 2008). In this way, dissolved oxygen may prevent the recombination of electron-hole pair by acting as an electron scavenger.

The combined attack of the hydroxyl radicals, semiconductor holes and other radical species on the organic pollutants successively breaks down the organics into simpler molecules. As the process continues, eventually all the intermediate degradation products will themselves be oxidized into CO₂, H₂O and mineral acids as generalized by Eq. 2.7 (Mills and Le Hunte, 1997). Semiconductor photocatalysis has been found to be effective for the oxidative degradation of over 800 molecules (Robert and Malato, 2002). The process is shown graphically in Fig. 2.2.

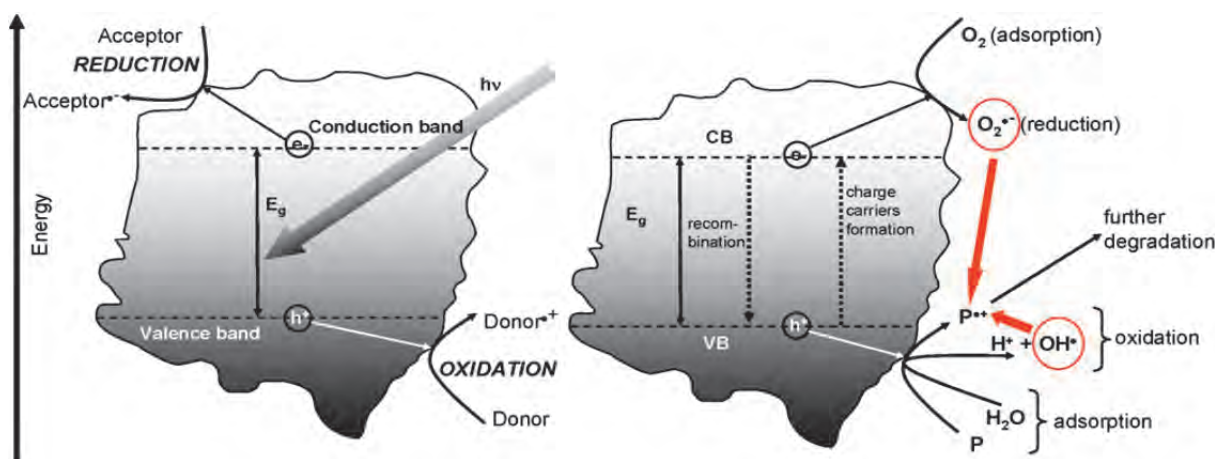
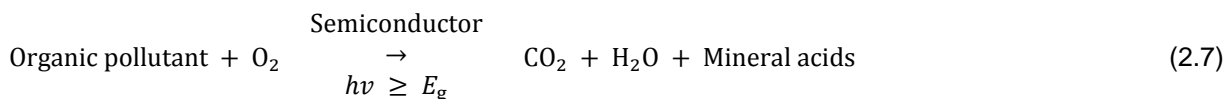


Fig. 2.2: Process of photocatalysis (Malato et al., 2009)



2.6.2 Support materials for photocatalyst

Over the last few decades, the scientific and engineering interest in the application of heterogeneous photocatalysis using TiO₂ powder for the decomposition of organic hazardous materials in liquid phases has grown exponentially (Brosillon et al., 2008; Shan et al., 2010; Nawi et al., 2012). However, in the aqueous phase, the inconvenience of using TiO₂ in the form of slurry is the need of recovering the TiO₂ powder. The recovery needs an additional treatment which may result in the process being more time consuming and more expensive (Shan et al., 2010). Attempts to immobilize TiO₂ on different support materials such as glass fibre, glass, quartz and stainless steel have been made with the aim to solve this problem. These methods were efficient in TiO₂ recovery, but there was a notable reduction in the catalyst activity due to mass transfer limitation of pollutants to the surface of the semiconductor. Consequently, porous support

materials such as activated carbon and zeolite have been proposed by various researchers since they have the ability to concentrate pollutants through adsorption around the loaded TiO₂ leading to a rapid degradation of the pollutants (Zhang and Lei, 2008). Of these two support materials, activated carbon is more costly while natural zeolite is affordable and readily available. Zeolite is therefore the most preferred support material.

2.6.3 Natural zeolite as photocatalyst support material

Zeolite is a promising support material for TiO₂ photocatalyst due to its regular pores and channel sizes, and good adsorption ability. Titanium dioxide supported on zeolite integrates the photocatalytic ability of TiO₂ with the adsorption properties of zeolite, which induces a synergistic effect, resulting in enhancement of photocatalytic efficiency (Huang et al., 2008). However, preparation of the catalyst coated support material (zeolite) should be carefully done to limit the interaction between the active sites of the material and the catalyst as this greatly affects performance of photodegradation (Durgakumari et al., 2002).

2.6.4 Preparation of TiO₂ supported on zeolite

A method of supporting TiO₂ on zeolite without losing the photosensitization of TiO₂ and the adsorption properties of zeolite is a very important aspect while preparing zeolite-based photocatalyst (Durgakumari et al., 2002). The ratio of TiO₂ to zeolite remains a very significant parameter under consideration when preparing the catalyst. At low TiO₂ loading on zeolite surface, adsorption is the predominant process while photodegradation is predominant at high TiO₂ loading. It is therefore important to determine the optimum ratio of TiO₂ to zeolite in order to optimally utilize the synergism of adsorption and photodegradation processes. Ochieng and Onyango, (2011) reported that at low TiO₂ loading (5 wt %), there was low photodegradation of acetic acid solution due to the low number of photocatalytically active sites. They recorded the highest degradation with 10% TiO₂ loading. However, decreased photodegradation was also observed with 15% TiO₂ loading due to the fact that at such a high catalyst loading, the TiO₂ tends to overcrowd and detach from zeolite surface therefore making the solution turbid thus hindering penetration of UV rays.

2.6.5 Light source

Photocatalytic degradation can be carried out using visible light, UV or sunlight which have different energy levels depending on the wavelength (Fig. 2.3). While sunlight is the most cost effective source of light, unfortunately, only 5% of the solar energy reaching the earth's surface can be absorbed by a typical photocatalyst such as TiO₂. Despite the fact that useful sunlight for photocatalysis is very low, its use is still of importance since it is free. A comparison of the three light sources on the decolourization of dye showed that the highest decolourization was achieved with UV followed by sunlight and lastly visible light (Mounir et al., 2007). Under light irradiation, photosensitization takes place, TiO₂ is excited and electron transferred from the valence band to the conduction band of the semi-conductor. These electrons and the hole participate in the redox reaction.

2.6.6 Heterogeneous solar photocatalysis

In heterogeneous solar photocatalytic detoxification, the near ultra-violet (UV) band of the solar spectrum (wavelength shorter than 400 nm which is more than the bandgap energy) is used to photoexcite a semiconductor catalyst TiO₂ in contact with water. The photogenerated holes interact with adsorbed water producing hydroxyl radicals, which attack organic contaminants progressively breaking them up yielding CO₂, H₂O and inorganic acids. The important issue governing the efficiency of the process is minimizing electron-hole recombination by maximizing the rate of interfacial electron transfer to capture the photogenerated electrons and/or holes (Malato et al., 2009). In comparing different semiconductors, TiO₂ has an additional advantage. The TiO₂ photocatalyst can use solar UV due to the fact that its bandgap energy can be surpassed by the energy content of a solar photon of wavelengths (390nm > λ > 300nm). The high operating cost of artificially generating photons can be reduced by using the sun. From a typical UV-

flux near the earth's surface of $20\text{-}30\text{ Wm}^{-2}$, $0.2\text{-}0.3\text{ mol photons m}^{-2}\text{ h}^{-1}$ in the $300\text{-}400\text{ nm}$ range can be used by the process. Of the many different sources of TiO_2 , Degussa P25 TiO_2 has become a standard (Serpone et al., 1996).

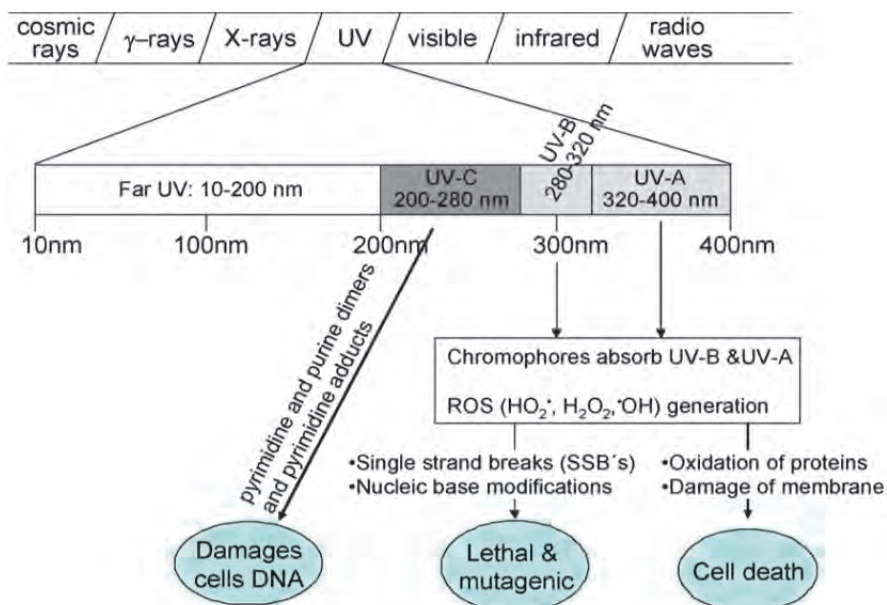


Fig. 2.3: UV radiation wavelengths (Malato et al., 2009)

2.6.7 Challenges in photocatalytic wastewater treatment

Although photodegradation performs well in mineralization of toxic and biorecalcitrant organic compounds, it is faced with some challenges. In the first place, the major challenge of this process is high energy requirement in cases where artificial irradiation such as UV light is used. In this case, the associated cost can often be prohibitive for wastewater treatment. Another problem is encountered in the treatment of wastewater with high colour intensity such as distillery and textile industry effluent. In this case, the high colour intensity hinders the penetration of light rays thus lowering the performance of the process. It therefore means that for photocatalytic degradation to perform better in the treatment of such wastewater high dilutions are required. This again is not economical as a larger reactor volume is required.

In this work, it is proposed that the solution to the challenges facing both the anaerobic degradation and photocatalytic degradation of organic pollutants lies in the integration of the two processes. This is based on the possibility that photocatalytic pre-treatment of toxic pollutants can increase their biodegradability before conducting the anaerobic process. This means that the photodegradation process will be carried out for a shorter period since complete mineralization is not required. Moreover, the cost of energy required by the photodegradation process can be offset by the energy generated by the anaerobic process.

2.7 Integrated adsorption and photodegradation

In adsorption, the pollutants in the wastewater accumulate on the surface of a solid (adsorbent) as a result of intermolecular attractions. Adsorbents are some of the best support materials for TiO_2 powder due to their capacity to adsorb and therefore concentrate reactants near the TiO_2 attached onto their surfaces. This concentration of reactants near the TiO_2 is especially advantageous when dealing with reactants at very low concentrations (Augugliaro et al., 2006). Since both the initial pollutant and degradation products are to be photodegraded, the adsorbent support would need to have a high affinity for a wide range of pollutants. As hydroxyl radicals produced by TiO_2 are very reactive, the adsorbent combined with TiO_2 must be inert to these radicals. If the adsorbent is not inert, its structure would be broken down and it will also compete with the pollutants for the hydroxyl radicals thus reducing the rate of the photocatalysis reaction.

Both synthetic (activated carbon, silica, alumina and zeolites) and natural adsorbents (natural zeolites, clays and chitosan) have been investigated for their effectiveness as a TiO₂ support (Durgakumari et al., 2002; Haque et al., 2005; Vega et al., 2011). Adsorbents such as clinoptilolite and silica are selective and only adsorb well certain organic chemicals. Clinoptilolite has been modified by organic surfactants to improve the number of organic chemicals it can adsorb. However, the surfactant portion of the surfactant modified clinoptilolite has been found to be susceptible to attack by hydroxyl radicals. Other organic adsorbents like chitosan have also been found to react with hydroxyl radicals and thus would not be good candidates for combination with TiO₂. Of all the adsorbents reviewed, AC has been found to be superior due to its resistance to hydroxyl radical attack and its ability to adsorb a wide range of organic chemicals.

The AC has been widely applied for the adsorption of a wide range of organic pollutants in wastewater and air. The major drawback of using AC for adsorption has been the fact that commercial AC is relatively costly as compared to other adsorbents. The high cost of the AC adsorbent lies in the fact that once the adsorbent is spent, it is usually disposed of. Regeneration of the AC adsorbent would significantly reduce the cost of operation. Several regeneration methods among them thermal regeneration, extractive regeneration and catalytic regeneration have been used to regenerate AC as reviewed by Sheintuch and Matatov-Meytal (1999). Most of these methods (Fig. 2.4) are costly in terms of chemical and energy input, produce toxic chemicals and only transfer pollutants from one phase to another without destroying the contaminants. In this regard, photocatalytic regeneration of the spent AC has been found to be better suited for the regeneration of AC due to the fact that it does not suffer these disadvantages.

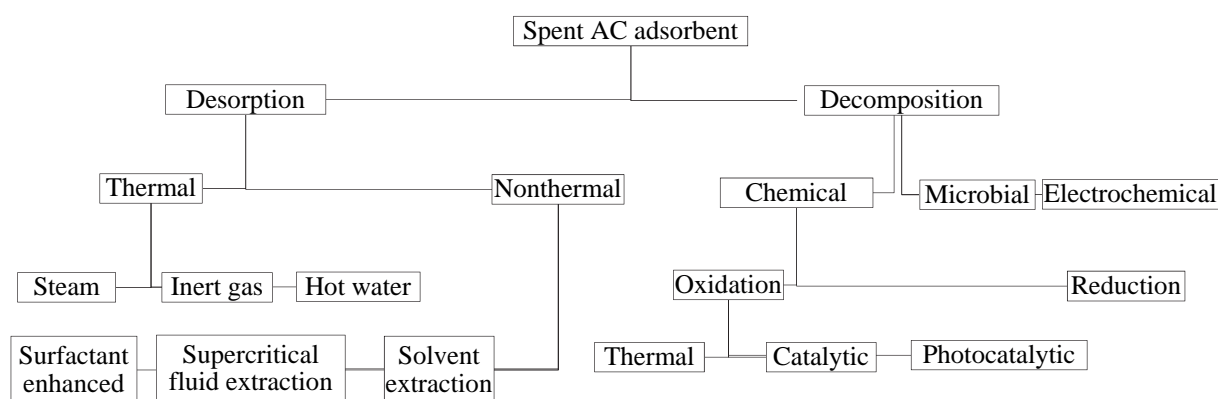


Fig. 2.4: Overview of methods of AC regeneration (Sheintuch and Matatov-Meytal, 1999)

Two modes of AC regeneration using photocatalysis have been investigated: desorption of the pollutants from the AC followed by pollutant photodegradation and combination of the AC and TiO₂ in which the TiO₂ photodegrades the pollutants adsorbed on the AC (Sheintuch and Matatov-Meytal, 1999). The former method suffers from long regeneration cycles due to the slow rate of desorption of the pollutants from the AC. The combined AC and TiO₂ system is advantageous due to the short diffusion paths of the pollutants from the AC to the TiO₂ which increases the rate of regeneration.

2.8 Integrated photodegradation and biodegradation (IPB)

Integration of the photodegradation and anaerobic digestion seems to have a high potential in the treatment of wastewater streams containing recalcitrant organic compounds. However, as much as the photocatalytic pre-treatment can lead to increased biodegradability of some recalcitrant organic contaminants, it can also produce some more toxic products which can be more difficult to biodegrade. It is therefore very important to determine whether the photodegradation should be conducted before the anaerobic degradation, or to be employed to finally polish the anaerobically treated wastewater, in order to get rid of the biorecalcitrant

component of the wastewater in question. This choice, however, depends on the type of wastewater to be treated. Improvement of the integrated photodegradation/biodegradation system can be achieved by using a porous adsorbent as a support material for microbes and the photocatalyst. The adsorbent concentrates the pollutants on its surface thereby bringing to close contact the organic pollutants and the catalyst or the microbes.

Figure 2.5 shows a scheme that can be used as a guide to determine the arrangements of the units for the integrated biological and photodegradation process. In this approach it is important to determine the sequence of the treatment method on the basis of the characteristics of the reactants and products such that the photodegradation unit can come after or before the biological process. It is a fact that photodegradation of organic pollutants is a competitive technique for wastewater treatment for the removal of those organic pollutants that are not easily treatable using biological methods due to their high chemical stability, high toxicity and/or low biodegradability. Although photodegradation for complete mineralisation can be expensive, its combination with biological treatment is reported to reduce operating cost (Oller et al., 2011). On the one hand, such a system can lead to an increase in methane yield if photodegradation is preceded by biodegradation. On the other hand, employing photodegradation as a post-treatment for an anaerobic degradation system may lead to thorough removal of traces of organic contaminants which might need long biodegradation time.

Scott and Ollis (1995) identified wastewater streams that are potentially treatable by integrated photodegradation and biodegradation as: wastewater containing biorecalcitrant compounds such as large macromolecules like soluble polymers that are not easily biodegradable due to their large size and lack of active centres, highly biodegradable industrial wastewater which still requires chemical post-treatment since it contains a large amount of biodegradable organic compounds in addition to small concentrations of recalcitrant compounds, and finally, wastewater containing inhibiting compounds which are toxic to certain microbial strains. Depending on the characteristics of the wastewater, the process shown in Fig. 2.5 can be followed to choose the treatment path for the organic pollutants.

Some of the significant targets when treating molasses wastewater from alcohol fermentation industry are COD and BOD reduction as well as colour removal. Various reports have indicated that this kind of wastewater has a high potential of energy generation in form of biogas when anaerobically treated. This results in appreciable COD and BOD reductions. Satyawili and Balakrishnan (2008) reported a BOD reduction of about 80% combined with energy recovery in terms of biogas. However, the colour is hardly removed by the conventional anaerobic treatment. In fact, some studies have reported an increase in colour during anaerobic degradation of molasses based distillery wastewater due to repolymerisation of compounds. Pefia et al. (1996); Pant and Adholeya (2007) reported an increment in colour during the anaerobic treatment of the molasses based distillery wastewater. Apart from the recalcitrant colour, another challenge facing the anaerobic treatment of the distillery wastewater is the long hydraulic retention time due to the presence of traces of toxic and recalcitrant organic compounds such as phenolics (Oller et al., 2011).

Similarly, AOPs have also been applied for the treatment of wastewater containing molasses. Beltran et al. (1999) reported that a combination of ozone and UV-C proved to enhance biodegradability of polyphenols, this method can therefore be employed in enhancing biodegradability of molasses wastewater since it totally mineralizes the toxic phenolic compounds in the wastewater. Pena et al. (2003), conducted UV/TiO₂ photodegradation of molasses wastewater, a high colour removal was achieved but notably low COD removal of about 25% was obtained. This was an indication that the photodegradation process was able to degrade the melanoidins which are responsible for colour thus leading to colour reduction. However, the resultant organic intermediates still demanded oxygen for their complete mineralization hence the low COD reduction recorded. Carboxylic acids have been identified as the products of melanoidin oxidation (Kim et al., 1985 and Hoigne and Bader, 1983). Since photodegradation is reported to achieve high colour removal for molasses wastewater but low COD removal, while anaerobic degradation is reported to be efficient in COD removal but poor in colour removal, an integration of the two processes in treatment of molasses

wastewater can be a very suitable approach in achieving both colour and COD removal. Besides, the effect of integration of the two processes in energy recovery is of interest.

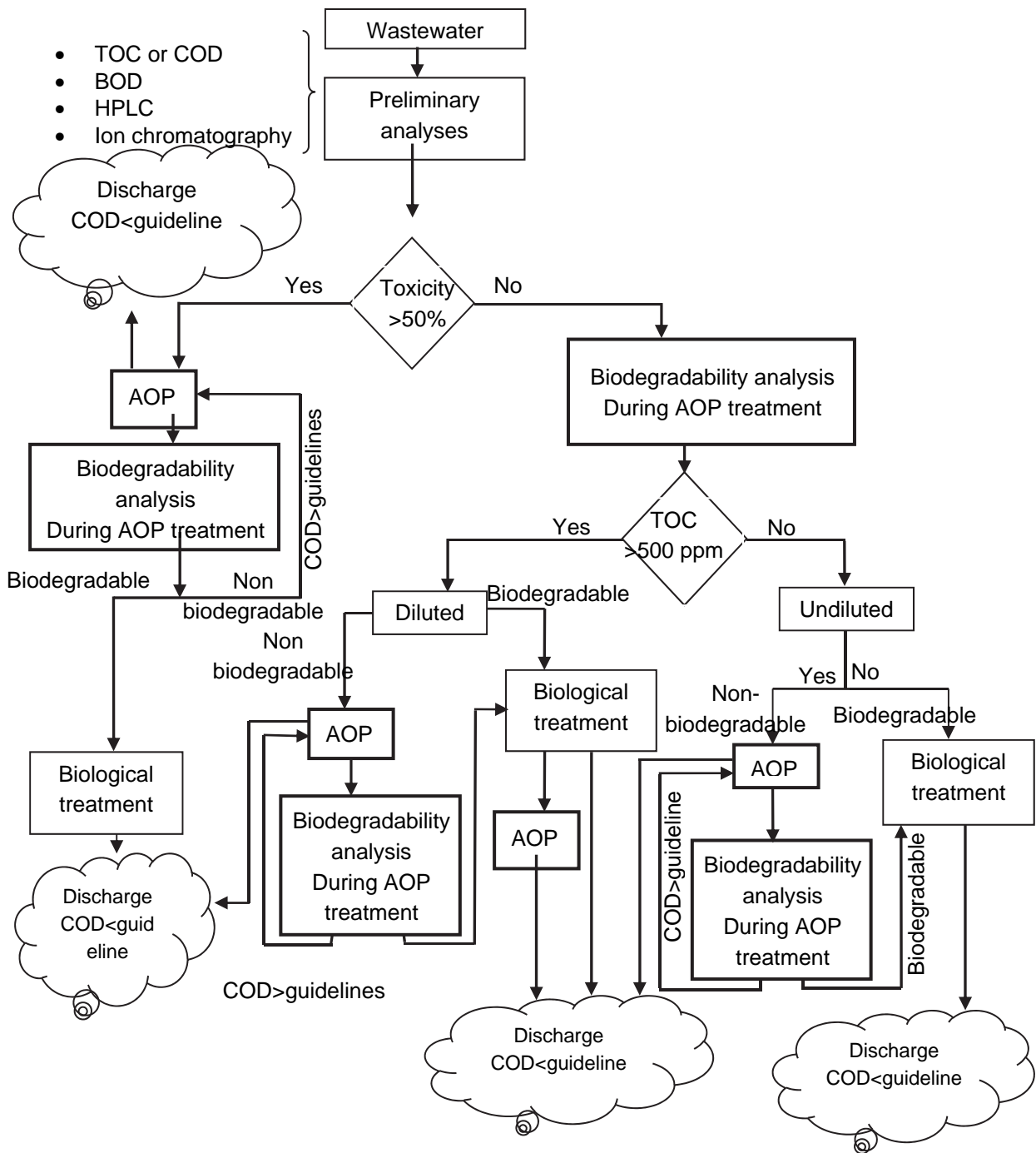


Fig. 2.5: Integrated biological and photodegradation, adopted from Oller et al. (2009)

Textile wastewater on the other hand, has high COD associated with biorecalcitrant compounds and an intense colour, contributed by the dyes, as the major pollutants. The organic content of the textile wastewater is reported to have low biodegradability (Savin and Butnaru, 2008). BOD_5/COD ratio has been used by various authors as a measure of biodegradability of various wastewater streams (Scott and Ollis, 1995; Chamarro et al., 2001). Wastewater can be considered substantially biodegradable if it has a BOD_5/COD ratio between 0.4 and 0.8 (Al-Momani et al., 2002). Conversely, the biodegradability (BOD_5/COD) of most dyes is reported to be below 0.3 (Al-Momani et al., 2002). Therefore, efficient biodegradation of dyes may require long acclimatization periods for special strains of microbes.

The AOPs have been widely reported to be promising in treating the textile industry wastewater. Nawi et al. (2012); Reddy and Kotahia, (2005) reported high removal efficiencies when using UV/TiO₂ photocatalysis in the treatment of wastewater containing reactive dyes. Also, Gomes de Moraes et al., (2000) reported a complete decolourization and total organic carbon (TOC) reduction of over 60% in the TiO₂-assisted photocatalysis of textile wastewater. Use of AOPs to enhance biodegradability of various dyes has also been studied. Al-Momani et al. (2002) used UV photolysis to improve the biodegradability of some selected recalcitrant dyes. It was observed that the biodegradability was enhanced with a reported BOD₅/COD ratio increment from about 0 to 0.42. Also, Chun and Wang (1999) reported an increase in the biodegradability index of up to 0.75 when using suspended TiO₂ in photodegradation of azo dyes. A study on the photodegradation of real textile wastewater reported an increment of biodegradability from 0 to 0.22 after irradiation time of 13 minutes (Al-Momani et al., 2002). The study also reported that the biodegradability of the real textile wastewater increased with irradiation time and attained a maximum BOD₅/COD value of about 0.45 after around 40 minutes.

Despite the availability of the valuable information on the role of photodegradation in the enhancement of the biodegradability of some recalcitrant organic compounds, up to now there is still inadequate information on how this can impact on energy generation from such wastewater. This is because most of the studies which have been conducted on the integrated photodegradation and biological treatment process have mainly concentrated on the aerobic digestion rather than the anaerobic one. This is amidst the huge interest in the generation of energy from wastewater. Prior to the integration of the two systems, critical analysis of separate AD and AOP is necessary.

2.9 Conclusion and inadequacy of both AOP and AD

Anaerobic digestion (AD) has been widely applied as a secondary treatment of several wastes. This is due to its low production of sludge, low cost and the production of high energy biogas. However, biorecalcitrant wastes such as distillery, textile and pharmaceutical wastewaters cannot be effectively removed by AD. Such wastes require advanced treatment methods such as photocatalysis to remove them. The disadvantage of photocatalysis is its high cost. Therefore, a combined AD-photocatalysis process for the treatment of wastes is desirable as a less costly and robust treatment method. This broad and multifaceted study looks into catalyst development, reactor optimisation and the treatment of a wide range of pollutants with the aim of investigating the feasibility of a combined AD-photocatalysis system.

References

- Abellán, M. N., Bayarri, B., Giménez, J., Costa, J. (2007). Photocatalytic degradation of sulfamethoxazole in aqueous suspension of TiO₂. *Applied Catalysis B: Environmental*, 74(3), 233-241.
- Adams, C. D., Cozzens, R. A., Kim, B. J. (1997). Effects of ozonation on the biodegradability of substituted phenols. *Water research*, 31(10), 2655-2663.
- Akiyama, T., Savin, M. C. (2010). Populations of antibiotic-resistant coliform bacteria change rapidly in a wastewater effluent dominated stream. *Science of the total environment*, 408(24), 6192-6201.
- Al-Momani, F., Touraud, E., Degorce-Dumas, J. R., Roussy, J., Thomas, O. (2002). Biodegradability enhancement of textile dyes and textile wastewater by VUV photolysis. *Journal of photochemistry and Photobiology A: Chemistry*, 153(1), 191-197.
- Augugliaro, V., Litter, M., Palmisano, L., Soria, J. (2006). The combination of heterogeneous photocatalysis with chemical and physical operations: a tool for improving the photoprocess performance. *Journal of Photochemistry and Photobiology C: Photochemistry Reviews*, 7(4), 127-144.
- Baeza, C., Knappe, D. R. (2011). Transformation kinetics of biochemically active compounds in low-pressure UV Photolysis and UV/H₂O₂ advanced oxidation processes. *Water research*, 45(15), 4531-4543.
- Beltrán, F. J., García-Araya, J. F., Álvarez, P. M. (1999). Wine distillery wastewater degradation. 1. Oxidative treatment using ozone and its effect on the wastewater biodegradability. *Journal of agricultural and food chemistry*, 47(9), 3911-3918.
- Berg, C. (2004). World fuel ethanol analysis and outlook. *The online distillery network for distilleries & fuel ethanol plants worldwide*, www.distill.com.

- Björnsson, L., Mattiasson, B., Henrysson, T. (1997). Effects of support material on the pattern of volatile fatty acid accumulation at overload in anaerobic digestion of semi-solid waste. *Applied Microbiology and Biotechnology*, 47(6), 640-644.
- Bouallagui, H., Touhami, Y., Ben Cheikh, R., Hamdi, M. (2005). Bioreactor performance in anaerobic digestion of fruit and vegetable wastes. *Process biochemistry*, 40(3), 989-995.
- Brosillon, S., Djelal, H., Merienne, N., Amrane, A. (2008). Innovative integrated process for the treatment of azo dyes: coupling of photocatalysis and biological treatment. *Desalination*, 222(1), 331-339.
- Burton, S., Cohen, B., Harrison, S., Pather-Elias, S., Stafford, W., van Hille, R., von Blottnitz, H. (2009). Energy from Wastewater-a Feasibility study. Technical report to Water research commission. *WRC Project k5/1732, Dept of Chem Eng, UCT*.
- Chamarro, E., Marco, A., Esplugas, S. (2001). Use of Fenton reagent to improve organic chemical biodegradability. *Water research*, 35(4), 1047-1051.
- Chen, Y., Cheng, J. J., Creamer, K. S. (2008). Inhibition of anaerobic digestion process: a review. *Bioresource technology*, 99(10), 4044-4064.
- Chu, W., Tsui, S. M. (2002). Modeling of photodecoloration of azo dye in a cocktail photolysis system. *Water research*, 36(13), 3350-3358.
- Chun, H., Yizhong, W. (1999). Decolorization and biodegradability of photocatalytic treated azo dyes and wool textile wastewater. *Chemosphere*, 39(12), 2107-2115.
- Crittenden, J. C., Trussell, R. R., Hand, D. W., Howe, K. J., Tchobanoglous, G. (2012). *MWH's Water Treatment: Principles and Design*. Wiley.
- Department of Water Affairs, (1986). Management of the water resources of the Republic of South Africa. Published by the Department of Water Affairs: Pretoria
- Duerr, M., Gair, S., Cruden, A., McDonald, J. (2007). Hydrogen and electrical energy from organic waste treatment. *International journal of hydrogen energy*, 32(6), 705-709.
- Durgakumari, V., Subrahmanyam, M., Subba Rao, K. V., Ratnamala, A., Noorjahan, M., Tanaka, K. (2002). An easy and efficient use of TiO₂ supported HZSM-5 and TiO₂+ HZSM-5 zeolite combine in the photodegradation of aqueous phenol and p-chlorophenol. *Applied Catalysis A: General*, 234(1), 155-165.
- Emadi, H., Nezhad, J. E., Pourbagher, H. (2001). In vitro Comparison of Zeolite(Clinoptilolite) and Activated Carbon as Ammonia Absorbants in Fish Culture. *Naga*, 24(1), 18-20.
- Fent, K., Weston, A. A., Caminada, D. (2006). Ecotoxicology of human pharmaceuticals. *Aquatic toxicology*, 76(2), 122-159.
- Fernández-Ibáñez, P., Malato, S., De Las Nieves, F. J. (1999). Relationship between TiO₂ particle size and reactor diameter in solar photoreactors efficiency. *Catalysis Today*, 54(2), 195-204.
- Ganesh, R., Boardman, G. D., Michelsen, D. (1994). Fate of azo dyes in sludges. *Water Research*, 28(6), 1367-1376.
- Gaya, U. I., Abdullah, A. H. (2008). Heterogeneous photocatalytic degradation of organic contaminants over titanium dioxide: a review of fundamentals, progress and problems. *Journal of Photochemistry and Photobiology C: Photochemistry Reviews*, 9(1), 1-12.
- Gomes de Moraes, S., Sanches Freire, R., Duran, N. (2000). Degradation and toxicity reduction of textile effluent by combined photocatalytic and ozonation processes. *Chemosphere*, 40(4), 369-373.
- Gonzalez Benito, G., Pena Miranda, M., Garcia Cubero, M. T., Uruena Alonso, M. A. (1999). Decolorization of molasses effluents by coagulation-flocculation process. *Zuckerindustrie (Germany)*.
- Hao, O. J., Kim, H., Chiang, P. C. (2000). Decolorization of wastewater. *Critical reviews in environmental science and technology*, 30(4), 449-505.
- Hapeshi, E., Achilleos, A., Vasquez, M. I., Michael, C., Xekoukoulotakis, N. P., Mantzavinos, D., Kassinou, D. (2010). Drugs degrading photocatalytically: kinetics and mechanisms of ofloxacin and atenolol removal on titania suspensions. *Water research*, 44(6), 1737-1746.
- Haque, F., Vaisman, E., Langford, C. H., Kantzas, A. (2005). Preparation and performance of integrated photocatalyst adsorbent (IPCA) employed to degrade model organic compounds in synthetic wastewater. *Journal of Photochemistry and Photobiology A: Chemistry*, 169(1), 21-27.

- Henderson, A. L., Schmitt, T. C., Heinze, T. M., Cerniglia, C. E. (1997). Reduction of malachite green to leucomalachite green by intestinal bacteria. *Applied and environmental microbiology*, 63(10), 4099-4101.
- Herrmann, J. M. (1999). Heterogeneous photocatalysis: fundamentals and applications to the removal of various types of aqueous pollutants. *Catalysis today*, 53(1), 115-129.
- Hoigné, J., Bader, H. (1983). Rate constants of reactions of ozone with organic and inorganic compounds in water –I: non-dissociating organic compounds. *Water Research*, 17(2), 173-183.
- Homem, V., Santos, L. (2011). Degradation and removal methods of antibiotics from aqueous matrices – a review. *Journal of environmental management*, 92(10), 2304-2347.
- Houtman, C. J. (2010). Emerging contaminants in surface waters and their relevance for the production of drinking water in Europe. *Journal of integrative environmental sciences*, 7(4), 271-295.
- Huang, M., Xu, C., Wu, Z., Huang, Y., Lin, J., Wu, J. (2008). Photocatalytic discolorization of methyl orange solution by Pt modified TiO₂ loaded on natural zeolite. *Dyes and Pigments*, 77(2), 327-334.
- Jain, N., Minocha, A. K., Verma, C. L. (2002). Degradation of predigested distillery effluent by isolated bacterial strains. *Indian journal of experimental biology*, 40(1), 101-105.
- Jiménez, A. M., Borja, R., Martín, A. (2004). A comparative kinetic evaluation of the anaerobic digestion of untreated molasses and molasses previously fermented with *Penicillium decumbens* in batch reactors. *Biochemical Engineering Journal*, 18(2), 121-132.
- Jorgensen, S. E., Libor, O., Lea Graber, K., Barkacs, K. (1976). Ammonia removal by use of clinoptilolite. *Water Research*, 10(3), 213-224.
- Kim, S. B., Hayase, F., Kato, H. (1985). Decolorization and degradation products of melanoidins on ozonolysis. *Agricultural and Biological Chemistry*, 49(3), 785-792.
- Klavarioti, M., Mantzavinos, D., Kassinos, D. (2009). Removal of residual pharmaceuticals from aqueous systems by advanced oxidation processes. *Environment international*, 35(2), 402-417.
- Kumar, S., Gopal, K. (2001). Impact of distillery effluent on physiological consequences in the freshwater teleost *Channa punctatus*. *Bulletin of environmental contamination and toxicology*, 66(5), 617-622.
- Kumar, V., Wati, L., FitzGibbon, F., Nigam, P., Banat, I. M., Singh, D., Marchant, R. (1997). Bioremediation and decolorization of anaerobically digested distillery spent wash. *Biotechnology Letters*, 19(4), 311-314.
- Malato, S., Fernández-Ibáñez, P., Maldonado, M. I., Blanco, J., Gernjak, W. (2009). Decontamination and disinfection of water by solar photocatalysis: recent overview and trends. *Catalysis Today*, 147(1), 1-59.
- Martins, S. I., Van Boekel, M. A. (2005). A kinetic model for the glucose/glycine Maillard reaction pathways. *Food Chemistry*, 90(1), 257-269.
- Maya-Altamira, L., Baun, A., Angelidaki, I., Schmidt, J. E. (2008). Influence of wastewater characteristics on methane potential in food-processing industry wastewaters. *Water research*, 42(8), 2195-2203.
- Mills, A., Le Hunte, S. (1997). An overview of semiconductor photocatalysis. *Journal of photochemistry and photobiology A: Chemistry*, 108(1), 1-35.
- Mohana, S., Acharya, B. K., Madamwar, D. (2009). Distillery spent wash: treatment technologies and potential applications. *Journal of hazardous materials*, 163(1), 12-25.
- Monteiro, S. C., Boxall, A. B. (2010). Occurrence and fate of human pharmaceuticals in the environment. In *Reviews of environmental contamination and toxicology* (pp. 53-154). Springer New York.
- Mounir, B., Pons, M. N., Zahraa, O., Yaacoubi, A., Benhammou, A. (2007). Discoloration of a red cationic dye by supported TiO₂ photocatalysis. *Journal of hazardous materials*, 148(3), 513-520.
- Mwale, M. (2000). *Ammonia removal from water by ion exchange using South African and Zambian zeolite samples* (Doctoral dissertation, Rhodes University).
- Nandy, T., Shastry, S., Kaul, S. N. (2002). Wastewater management in a cane molasses distillery involving bioresource recovery. *Journal of environmental management*, 65(1), 25-38.
- Nawi, M. A., Sabar, S. (2012). Photocatalytic decolourisation of Reactive Red 4 dye by an immobilised TiO₂/chitosan layer by layer system. *Journal of colloid and interface science*, 372(1), 80-87.
- O'Neill, C., Hawkes, F. R., Hawkes, D. L., Lourenco, N. D., Pinheiro, H. M., Delee, W. (1999). Colour in textile effluents – sources, measurement, discharge consents and simulation: a review. *Journal of Chemical Technology and Biotechnology*, 74(11), 1009-1018.

- Ochieng, A., Onyango, M. S., (2011) Biogas synthesis using photocatalysis Technical report part III submitted to the Water Research Commission
- Oller, I., Malato, S., Sánchez-Pérez, J. A. (2011). Combination of advanced oxidation processes and biological treatments for wastewater decontamination – a review. *Science of the total environment*, 409(20), 4141-4166.
- Pandey, R. A., Malhotra, S., Tankhiwale, A., Pande, S., Pathe, P. P., Kaul, S. N. (2003). Treatment of biologically treated distillery effluent-a case study. *International journal of environmental studies*, 60(3), 263-275.
- Pant, D., Adholeya, A. (2007). Biological approaches for treatment of distillery wastewater: a review. *Bioresource technology*, 98(12), 2321-2334.
- Pathade. G.R. (2003). A review of current technologies for distillery wastewater treatment, in: P.K. Goel (Ed.). *Advances in Industrial Wastewater Treatment*, ABD Publishers, Jaipur, India, 180-239.
- Miranda, M. P., Benito, G. G., Cristobal, N. S., Nieto, C. H. (1996). Color elimination from molasses wastewater by *Aspergillus niger*. *Bioresource Technology*, 57(3), 229-235.
- Pena, M., Coca, M., Gonzalez, G., Rioja, R., Garcia, M. T. (2003). Chemical oxidation of wastewater from molasses fermentation with ozone. *Chemosphere*, 51(9), 893-900.
- Pomati, F., Castiglioni, S., Zuccato, E., Fanelli, R., Vigetti, D., Rossetti, C., Calamari, D. (2006). Effects of a complex mixture of therapeutic drugs at environmental levels on human embryonic cells. *Environmental science & technology*, 40(7), 2442-2447.
- Powell, G. E., Archer, D. B. (1989). On-line titration method for monitoring buffer capacity and total volatile fatty acid levels in anaerobic digesters. *Biotechnology and bioengineering*, 33(5), 570-577.
- Reddy, S. S., Kotaiah, B. (2005). Decolorization of simulated spent reactive dye bath using solar/TiO₂/H₂O₂. *International Journal of Environmental Science & Technology*, 2(3), 245-251.
- Remigi, E. U., Buckley, C. A. (2006). *Co-digestion of High-strength/toxic Organic Effluents in Anaerobic Digesters and Wastewater Treatment Works*. Water Research Commission.
- Rezaee, A., Ghaneian, M. T., Hashemian, S. J., Moussavi, G., Khavanin, A., Ghanizadeh, G. (2008). Decolorization of Reactive Blue 19 Dye from Textile Wastewater by the UV/H₂O₂ Process. *Journal of Applied Sciences*, 8(6), 1108-1122.
- Robert, D., Malato, S. (2002). Solar photocatalysis: a clean process for water detoxification. *Science of the Total Environment*, 291(1), 85-97.
- Maas, R., Chaudhari, S. (2005). Adsorption and biological decolourization of azo dye Reactive Red 2 in semicontinuous anaerobic reactors. *Process Biochemistry*, 40(2), 699-705.
- Rozic, M., Cerjan-Stefanovic, S., Curkovic, L. (2002). Evaluation of Croatian clinoptilolite-and montmorillonite-rich tuffs for ammonium removal. *Croatica chemica acta*, 75(1), 255-269.
- Saha, N. K., Balakrishnan, M., Batra, V. S. (2005). Improving industrial water use: case study for an Indian distillery. *Resources, conservation and recycling*, 43(2), 163-174.
- Satyawali, Y., Balakrishnan, M. (2008). Wastewater treatment in molasses-based alcohol distilleries for COD and color removal: a review. *Journal of environmental management*, 86(3), 481-497.
- Savin, I. I., Butnaru, R. (2008). Wastewater characteristics in textile finishing mills. *Environmental Engineering Management Journal (EEMJ)*, 7(6), 859-864
- Saxena, K. K., Chauhan, R. R. S. (2003). Oxygen consumption in fish, *Labeo rohita* (HAM.) caused by distillery effluent. *Ecology Environment and Conservation*, 9, 357-360.
- Scott, J. P., Ollis, D. F. (1995). Integration of chemical and biological oxidation processes for water treatment: review and recommendations. *Environmental Progress*, 14(2), 88-103.
- Serpone, N., Sauve, G., Koch, R., Tahiri, H., Pichat, P., Piccinini, P., Hidaka, H. (1996). Standardization protocol of process efficiencies and activation parameters in heterogeneous photocatalysis: relative photonic efficiencies ζ . *Journal of photochemistry and photobiology A: Chemistry*, 94(2), 191-203.
- Shan, A. Y., Ghazi, T. I. M., Rashid, S. A. (2010). Immobilisation of titanium dioxide onto supporting materials in heterogeneous photocatalysis: a review. *Applied Catalysis A: General*, 389(1), 1-8.
- Sharma, S., Sharma, A., Singh, P. K., Soni, P., Sharma, S., Sharma, P., Sharma, K. P. (2007). Impact of distillery soil leachate on haematology of swiss albino mice (*Mus musculus*). *Bulletin of environmental contamination and toxicology*, 79(3), 273-277.

- Sheintuch, M., Matatov-Meytal, Y. I. (1999). Comparison of catalytic processes with other regeneration methods of activated carbon. *Catalysis Today*, 53(1), 73-80.
- Singh, P.N., Robinson, T. D., Singh. (2004). Treatment of industrial effluents-distillery effluent, in: A. Pandey (Ed.), *Concise Encyclopedia of Bioresource Technology*, Food Products Press, New York, USA, 135-141.
- Snyder, S. A., Westerhoff, P., Yoon, Y., Sedlak, D. L. (2003). Pharmaceuticals, personal care products, and endocrine disruptors in water: implications for the water industry. *Environmental Engineering Science*, 20(5), 449-469.
- Snyder, S., Benotti, M. (2010). Endocrine disruptors and pharmaceuticals: implications for water sustainability. *Water Science & Technology*, 61(1), 145-154
- Vandevivere, P. C., Bianchi, R., Verstraete, W. (1998). Review: Treatment and reuse of wastewater from the textile wet-processing industry: Review of emerging technologies. *Journal of Chemical Technology and Biotechnology*, 72(4), 289-302.
- Vega, A. A., Keshmiri, M., Mohseni, M. (2011). Composite template-free TiO₂ photocatalyst: Synthesis, characteristics and photocatalytic activity. *Applied Catalysis B: Environmental*, 104(1), 127-135.
- Somasiri, W., Li, X. F., Ruan, W. Q., Jian, C. (2008). Evaluation of the efficacy of upflow anaerobic sludge blanket reactor in removal of colour and reduction of COD in real textile wastewater. *Bioresource technology*, 99(9), 3692-3699.
- Delee, W., O'Neill, C., Hawkes, F. R., Pinheiro, H. M. (1998). Anaerobic treatment of textile effluents: a review. *Journal of chemical technology and biotechnology*, 73(4), 323-335.
- Zainudin, N. F., Abdullah, A. Z., Mohamed, A. R. (2010). Characteristics of supported nano-TiO₂ ZSM-5/silica gel (SNTZS): Photocatalytic degradation of phenol. *Journal of hazardous materials*, 174(1), 299-306.
- Zhang, W., Ding, Y., Boyd, Shygyg. A., Teppen, B. J., Li, H. (2010). Sorption and desorption of carbamazepine from water by smectite clays. *Chemosphere*, 81(7), 954-960.
- Zhang, X., Lei, L. (2008). Effect of preparation methods on the structure and catalytic performance of TiO₂/AC photocatalysts. *Journal of hazardous materials*, 153(1), 827-833.
- Zorita, S., Mårtensson, L., Mathiasson, L. (2009). Occurrence and removal of pharmaceuticals in a municipal sewage treatment system in the south of Sweden. *Science of the total environment*, 407(8), 2760-2770.
- Zupančič, G. D., Stražišar, M., Roš, M. (2007). Treatment of brewery slurry in thermophilic anaerobic sequencing batch reactor. *Bioresource technology*, 98(14), 2714-2722.

CHAPTER 3

3 ANAEROBIC DIGESTION

3.1 Introduction

The increase in world population which has subsequently led to an increase in demand for quality manufactured goods has brought about a high growth in the number of manufacturing industries. These industries discharge large volumes of contaminated effluent which, if not properly treated, will put the health of the world population at high risk. Moreover, the increase in the number of manufacturing industries has put a lot of pressure on the available energy resources and therefore alternative technologies of producing more and safer energy is needed. Biological processes have been widely used to treat different kinds of waste. However, there are some wastes such as textile and molasses wastewater which contain some biorecalcitrant compounds.

Discharge of molasses wastewater into the receiving water causes environmental stress, mainly to the aquatic organisms. This is because the molasses wastewater has high COD (80,000-100,000 mg/L), BOD (40,000-50,000 mg/L), strong odour and is acidic in nature (Satyawali and Balakrishnan, 2008). Worst still, the molasses wastewater contains a dark brown recalcitrant colour which impedes the penetration of sunlight to the aquatic photosynthetic plants and therefore reduces dissolved oxygen in river courses. On the other hand, textile industry is considered as one of the largest water consumers in the world (Wouter et al., 1998). Remigi and Buckely (2006) reported that in the current environmental legislation, textile industries have been labelled as high priority industry with regard to pollution and due to the problem of toxicity caused by the recalcitrant COD, high salt and heavy metals in their effluent. Apart from the high effluent COD contributed by the dyes, their presence in wastewater, even in low amounts is highly visible which seriously affects the aesthetic quality of receiving waters. Moreover, some of the dyes, dye precursors and dye degradation products are reported to be carcinogenic and mutagenic in nature (Henderson et al., 1997).

Anaerobic digestion is a viable technique for treating textile and molasses wastewater as it leads to the conversion of the organic contaminants into biogas. The efficiency of an anaerobic digestion can be improved by introducing a support material in the bioreactor in order to prevent microbial washout (Montalvo et al., 2012). Some of the solid support materials which have been used are glass beads, clay, zeolite, polypropylene, polyethylene and polyvinylchloride (Farhadian et al., 2007). Zeolites have been identified as good support material due to their good adsorption capacity, buffering capacity and ion exchange capacity (Montalvo et al., 2012). However, the performance of zeolite as a support material depends on its mineralogical composition which, in turn, varies with its geographical occurrence. The aim of this work is to study the effect of application of South African natural zeolite as biomass support in the anaerobic treatment of molasses wastewater and methylene blue dye, a model textile wastewater.

3.2 Methodology

3.2.1 Equipment

Anaerobic degradation experiments were conducted in 100 ml flasks and 500 ml fixed bed anaerobic reactors (Fig. 3.1). The synthetic wastewater contained methylene blue and molasses. A thermostatic shaker and water bath were used for incubation during the digestion period. Chemical oxygen demand (COD) measuring kit (Nanocolor) was used to measure COD during the degradation. UV-vis spectrophotometer DR 2800 (HACH 2000) was used for colour analysis while gas chromatography (GC) model SRI 8610C fitted with thermal conductivity detector (TCD) was used to quantify methane produced. The set up for the preliminary anaerobic digestion (AD) carried out in the laboratory scale fixed bed anaerobic digester is shown in Fig. 3.1.

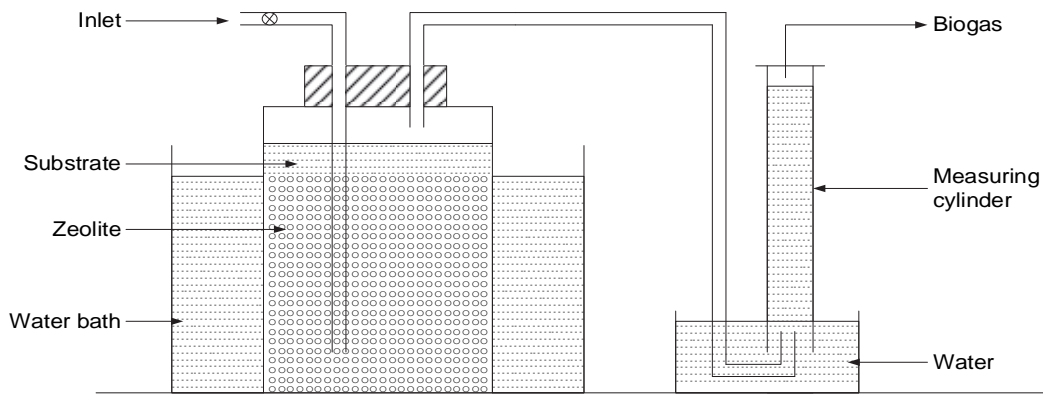


Fig. 3.1: Laboratory scale fixed bed anaerobic reactor

3.2.2 Experimental procedure

To evaluate the effect of operating parameters on anaerobic treatment of real distillery wastewater, commercial molasses wastewater (obtained from a commercial outlet) and methyl blue (MB) dye, batch experiments were performed. The experiments were carried out in 100 ml conical flasks in which inoculum and substrate were added. The inoculum was prepared from anaerobic sludge from a municipal wastewater treatment plant (50%), diluted cow dung (20%) and distillery wastewater (Heineken distilleries) 20%. Nutrients such as KHPO_4 , $\text{MgSO}_4 \cdot 7\text{H}_2\text{O}$, NiSO_4 , NH_4NO_3 , glucose and $\text{Ca}(\text{HCO}_3)_2$ were added. The substrate was added periodically for acclimatization purpose. The inoculum was kept for three months before use.

For the preparation of the digester solution, 60 ml of the substrate and 40 ml of inoculum were transferred into a 100 ml flask. The pH of the solution was then adjusted in the range of 6.8 to 7.2. Zeolite was added before purging with nitrogen for 5 minutes to eliminate any dissolved oxygen. The flasks were then covered with balloons to collect the produced biogas and incubated at 37°C in a thermostatic shaker. The parameters which were investigated were; substrate concentration, zeolite dosage and nutrients on the biodegradation process. COD, biogas produced and colour intensity were measured at the end of biodegradation.

3.3 Results and discussion

Preliminary experiments were performed to determine optimum operating conditions for the anaerobic digestion, in 100 ml conical flasks. These flasks were then incubated in a shaker at 37°C . The investigation focused on substrate concentration, effect of zeolite, zeolite dosage and nutrients addition on anaerobic degradation. All the experiments were conducted in duplicate and mean values recorded.

3.3.1 Effect of substrate concentration and zeolite addition on anaerobic degradation

To evaluate the effect of substrate concentration on the anaerobic digestion process, solutions of different concentrations of molasses, real distillery wastewater and methylene blue (MB) dye were prepared. The concentrations investigated were in the range of 1000 ppm to 4000 ppm, the corresponding COD values of these samples were then determined in $\text{mg O}_2/\text{L}$. The effect of zeolite as biomass support in the anaerobic process was also investigated. In this study 1.5 g of zeolite was added to 100 ml of solution to be digested, and digestion was carried out for 42 days. In one set of experiments, no zeolite was used, this acted as control. Also, the capacity of zeolite to adsorb the pollutants in the various wastewater samples was investigated in another set of experiments whereby no inoculum was added to the wastewater during the incubation period. The experiments were carried out in duplicate and the mean COD values are presented in Fig. 3.2.

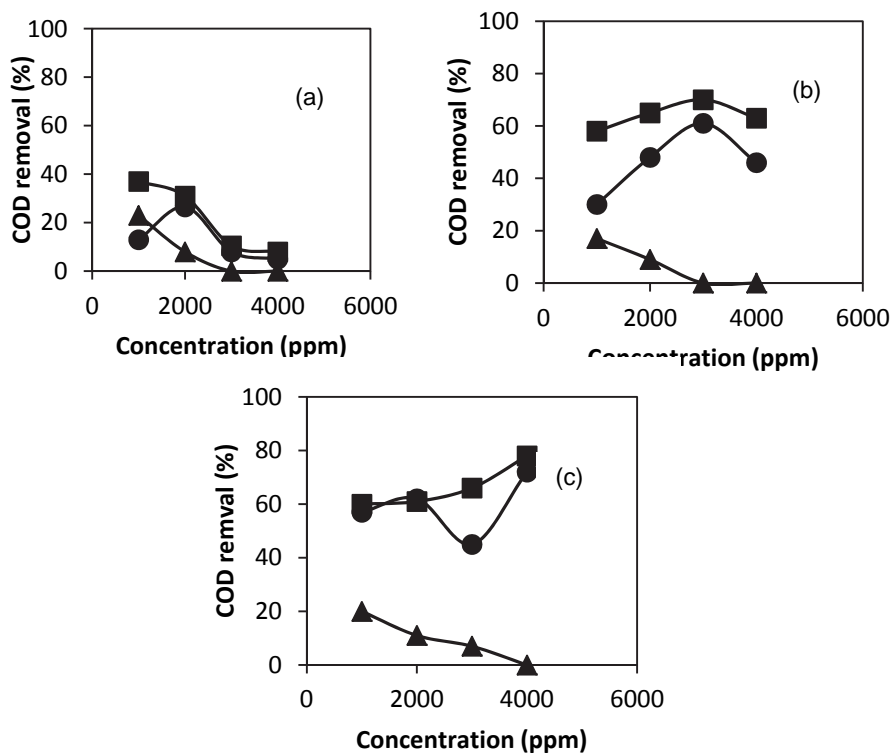


Fig. 3.2: Effect of substrate concentration on anaerobic degradation; (a) MB dye (b) distillery and (c) MWW; with zeolite (■) without zeolite (●) and adsorption (▲)

It can be seen (Fig. 3.2) that COD removal efficiencies increased with an increase in concentration for the molasses wastewater (MWW) and distillery wastewater (up to 3000 ppm for distillery) while it reduced with an increase in concentration for the dye solution in cases where zeolite was applied. It was also observed that in all concentrations investigated higher biodegradation was always achieved with MWW and distillery wastewater than with MB dye. This shows that the MWW and distillery wastewater were more easily biodegradable than MB. The low biodegradability of MB is due to its inhibition effects on the microorganisms activity. This effect is even elevated with an increase in concentration and therefore lower degradation is achieved at high concentrations. Chun and Wang (1999); Herrera et al. (1999) demonstrated the hazardous potential of textile dyes on bacterial strands.

It is worth noting that the adsorption onto zeolite surface attained equilibrium after 6 hours for the MB dye and after about 24 hours for the MWW and distillery wastewater. For the substrate removal by adsorption in Fig. 3.2, only adsorption values at equilibrium were used. In all cases, it can be seen that COD removal by adsorption decreased with an increase in substrate concentration. This may be due to the fact that since the mass of zeolite used was constant therefore there were a fixed number of adsorptive sites. This number of the active sites could only hold a specific amount of substrate. It therefore means that for higher concentration the total amount adsorbed was less (negligible) compared to the total amount of substrate available. It therefore follows that at high concentration of 4,000 ppm, no appreciable removal by adsorption could be obtained.

Further, it can also be seen in Fig. 3.2 that, generally, there was an increase in COD reduction in cases where zeolite was applied. Various studies aimed at determining the effect of different types of microbial support material on anaerobic degradation process have been documented. Jimenez et al. (2004) studied the use of Saponite and Esmectite as microbial support material in the treatment of molasses wastewater and reported a higher degradation than in control (where no support material was used). Milan et al. (2003)

and Montalivo et al. (2005) explained that the high performance of zeolite as support material is due to the high capacity for the immobilization of microorganisms.

3.3.2 Effect of nutrient addition on MB degradation

Since MB dye always recorded low biodegradation as shown in Fig. 3.2a, there was a need to investigate how addition of an external source of carbon (glucose) and other inorganic nutrients could impact on its degradation. There was no glucose addition for the results shown in Fig. 3.2a). Figure 3.3 shows the results for the effect of addition of nutrients on the degradation of MB dye. Lowest degradation was obtained when no nutrient was added. The addition of glucose only (0.5%) increased degradation by about 5%, while the addition of other inorganic nutrients (HPO_4^- (20 ppm), Ni^{+2} (10 ppm), K^{+1} (20 ppm), Ca^{+2} (20 ppm), NO_3^- 20 ppm), Fe^{+3} (5ppm) and Mg^{+2} (5 ppm)) alongside glucose increased the degradation by about 20%. This shows that the addition of micronutrients aided biodegradation, as nutrients are essential for microbial growth.

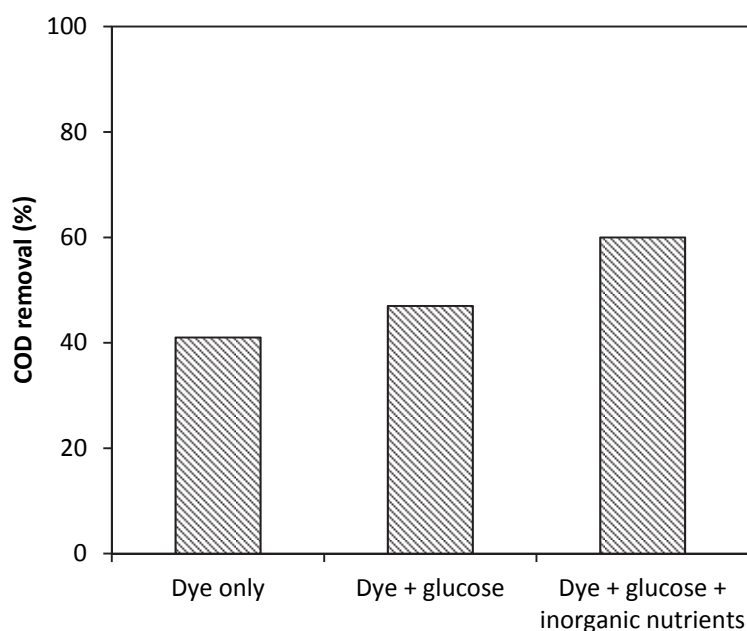


Fig. 3.3: Effect of addition of nutrients in the degradation of MB dye

3.3.3 Methane yield

The effect of application of zeolite on methane yield during the anaerobic digestion of the various wastewater streams was studied. In this study, the anaerobic digestion was carried out in 100 ml conical flasks covered with balloons for a period of 42 days and the methane produced was quantified using GC, and the results are shown in Fig. 3.4. Methane yield was calculated as a fraction of combined methane and carbon dioxide produced, while other trace gases produced were assumed to be negligible. The concentration of the wastewater streams were, MWW and distillery (4,000 ppm), while MB dye was (1,000 ppm). These concentrations were chosen because they were established to be the optimum during AD treatment of these wastewater streams as shown in Fig. 3.2.

In Fig. 3.4, it can be seen that the application of zeolite enhanced methane yield in all wastewater samples treated. This is because zeolite has a high capacity for immobilization of microorganisms; this makes the microorganisms to have a faster growth rate (Montalvo et al., 2012). The fast growth rate of the microorganisms subsequently leads to high degradation of the organic molecules and their subsequent conversion into methane by the methanogens. Kotsopoulos et al. (2008) and Duran-barrantes et al. (2008) conducted studies on the performance of zeolite in the anaerobic treatment of swine wastewater; they both observed an increase in methane production and reduction in volatile fatty acids (VFA) accumulation in

systems containing zeolite as compared to systems without zeolite. They explained that zeolite has the ability to prevent accumulation of VFA and thereby regulating the acidity of the system. It can further be argued that an increase in methanogens would lead to an increase in conversion of carboxylic acids into methane.

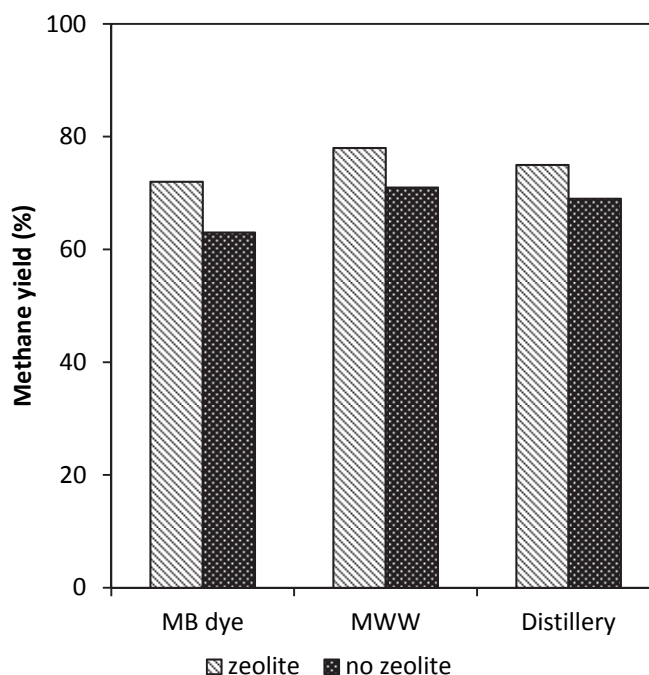


Fig. 3.4: Effect of zeolite on methane yield

3.3.4 Effect of zeolite dosage

The effect of zeolite dosage on the anaerobic degradation process was investigated using zeolite masses of 0, 10, 50, 100 and 200 g/L. The solutions were purged with nitrogen and covered with balloons then incubated in the shaker for a period of 42 days. For the MMW, distillery and MB dye, there was a general increment in the biodegradation with an increase in zeolite loading up to 100 g/L, after which the increment was negligible as shown in Fig. 3.5. The corresponding increment in degradation with the increment in zeolite dosage up to 100 g/L can be attributed to the increase in available surface area for micro-organisms attachment. In addition, zeolite is reportedly a good adsorbent, and therefore can concentrate the pollutants on its surface for easy degradation by the microorganisms attached on its surface. The addition of zeolite can only increase degradation up to a certain optimum dosage, above which it starts to hinder the degradation process. This is due to the fact that zeolite loading above the optimum increases the apparent viscosity of the medium resulting in a decrease in mass transfer between the substrate and the microorganisms responsible for the degradation process (Milan et al., 2001a). This observation is more prominent in systems where there is no circulation of influent. On the other hand, mass transfer in a packed bed reactor is enhanced by circulating the effluent across the bed.

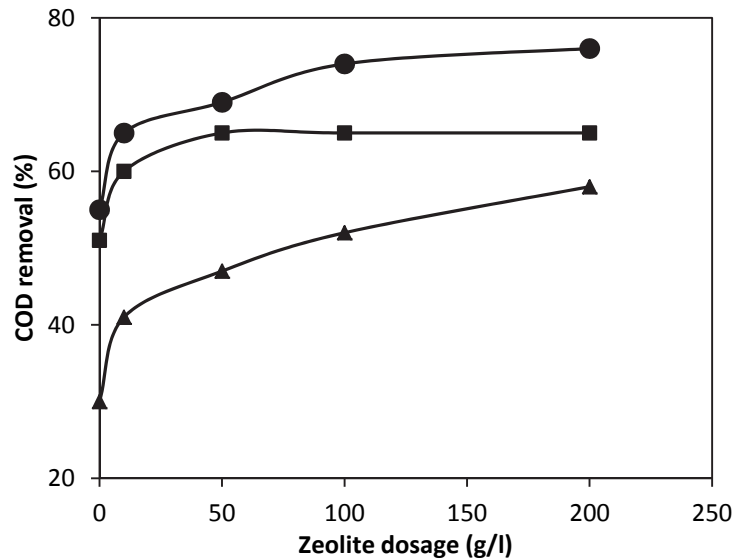


Fig. 3.5: Effect of zeolite dosage on COD removal during anaerobic treatment of; MWW (●) MB dye (■) and distillery wastewater (▲)

The effect of zeolite concentration on anaerobic digestion in a batch system has been studied by other researchers and their findings are in agreement with those of the present one, in that addition of zeolite is effective in increasing degradation only up to a certain optimum amount. Kotsopoulos et al. (2008) investigated the effect of addition of zeolite on batch thermophilic anaerobic digestion of piggery waste, doses of 0 to 12 g/L zeolite were evaluated, and high degradation was observed at dosage of 8 g/L. Milan et al. (2001a) also investigated the effect of zeolite dosage when treating piggery wastewater under mesophilic temperatures. Zeolite dosage in the range of 0.2-10 g/L was investigated where it was found that the maximum degradation was obtained with dosage between 2 to 4 g/L. Dosage above these values leads to a decrease in degradation due to mass transfer hindrance.

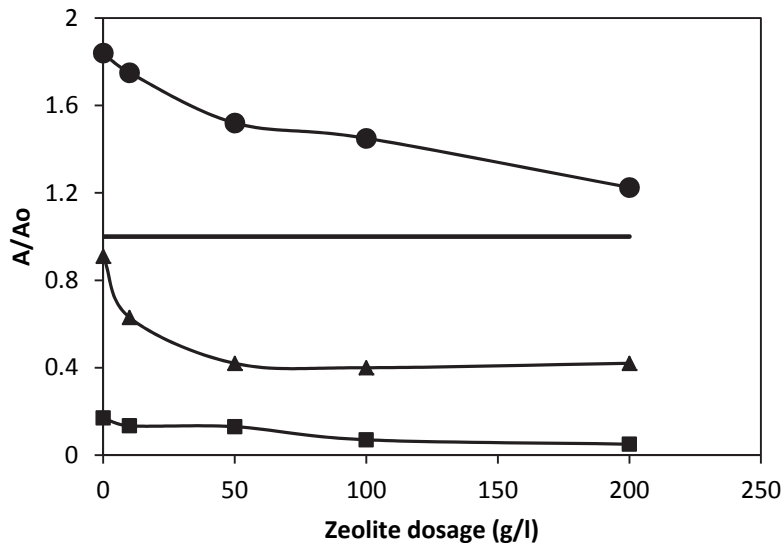


Fig. 3.6: Variation in colour removal with zeolite mass in the degradation of; MWW (●), MB (■), distillery (▲) and Ao/Ao (—)

The effect of zeolite dosage on colour removal was also investigated and the results in Fig. 3.6 show that colour removal with MB is very effective, achieving up to 95% removal. In contrast, it was found that the colour of MWW increased after degradation irrespective of the amount of zeolite added (Fig. 3.6). However,

the increase in colour recorded reduced with an increase in zeolite dosage as it can be seen that without zeolite addition the colour increased by about 60% while with addition of 200 g/L of zeolite the colour increased by about 20% only. Pefia et al. (1996) reported that colour increment during the biological treatment of MWW could be due to repolymerisation of compounds.

3.3.5 Biogas production

Based on the observations made in the preliminary experiments using conical flasks reported in the previous section, the anaerobic process was scaled up in a fixed bed anaerobic digester of capacity 500 ml, with a working volume of 400 ml. Attempts were made in this study to address some problems observed in the preliminary experiments when using the 100 ml conical flasks covered with the balloons. Some challenges were experienced in the first preliminary studies. Firstly, after some period of digestion the balloons would wear out and tear thus making the gas to escape, secondly, replacement of the balloons was then necessary, thus the amount of gas produced and COD removed on daily basis could not be determined. Finally, measuring and quantifying the biogas produced was cumbersome and inaccurate. In this method, therefore, the Mariotte water displacement method was used to collect the biogas produced, this made it easier to determine daily biogas production. The measuring cylinder used for gas collection was fixed with butyl rubber at its top to enable injection for gas analysis. Also the reactor had a sampling port which enabled periodical determination of COD reduction as well as colour removal. The performance of the packed bed reactor and un-packed bed reactor were evaluated in terms of COD and colour removal as well as biogas production.

Biogas produced when treating MWW, distillery wastewater and MB dye was recorded on daily basis for a period of 27 days. In all cases the wastewater treated had a COD of about 5000 mg/L, and the effect of zeolite on biogas production was investigated (Fig. 3.7). It was observed that a higher biogas production was achieved in packed bed reactor than in the un-packed reactor. This confirmed that zeolite performs well in the immobilization of micro-organisms thereby improving the process. It was observed that zeolite improved biogas production by 5 folds in the case of MWW, 1.2 times for distillery wastewater and 10 times in the case of MB dye. From Fig. 3.7, it can also be seen that the use of zeolite also decreased the lag phase for all the pollutants.

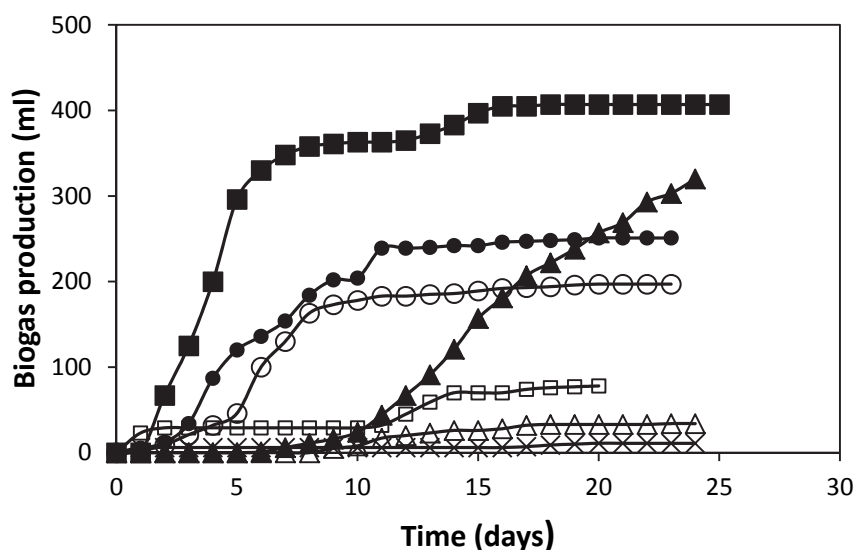


Fig. 3.7: Cumulative biogas production in the FBR; MWW with zeolite (■), MWW without zeolite (□), distillery with zeolite (●), distillery without zeolite (○), MB with zeolite (▲) MB without zeolite (△) and control (×)

Similar observations were reported by Umaña et al. (2008) when treating dairy manure using lab scale fixed bed anaerobic digester packed with zeolite. It was discovered that the reactors packed with zeolite produced 40% more biogas than the reactor without zeolite. Nikolaeva et al., 2009 also reported that kinetic constant for methane production was 29.4% higher in the reactor with zeolite than in the reactor without zeolite.

Figure 3.8 shows that MWW and distillery wastewater always had a higher biogas production coefficient than the MB dye. Further, in both cases the coefficient was higher in the packed digesters. For the MWW the coefficient increased with time up to the tenth day, after which it gradually started to decrease. An almost similar trend was recorded in the case of distillery wastewater, in which the coefficient was high by the tenth day then recorded a sharp decrease on the 15th day.

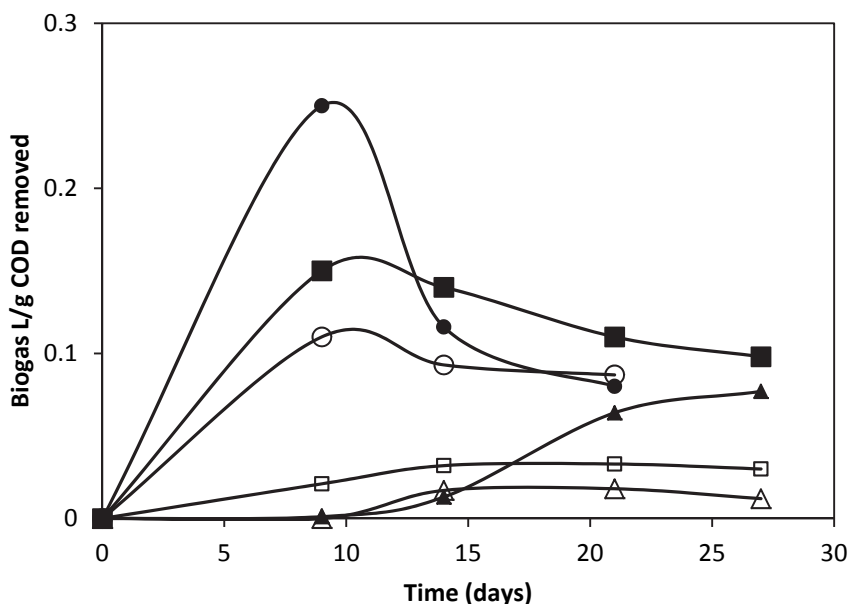


Fig. 3.8: Biogas production coefficient in the FBR, MWW with zeolite (■), MWW without zeolite (□), distillery without zeolite (●), distillery with zeolite (○), MB with zeolite (▲) MB without zeolite (△)

This observation can be attributed to the depletion of substrate after the 10th day. At the beginning of the digestion there was sufficient substrate which microorganisms could convert to biogas but after ten days of degradation, the substrate concentration started to reduce below the optimal amount. A longer lag phase was observed for MB, this could be due to the fact that MB is more toxic to microbes than MWW therefore, a longer acclimatization period was necessary. It was also observed that when treating the wastewater samples in the unpacked reactor, the biogas production coefficients picked up, then it leveled off after a few days. This may be due to steady state inhibition which might have been caused by accumulation of VFAs.

3.3.6 COD and colour reductions

The results for the final COD reduction in the FBR and the un-packed reactor in Fig. 3.9, shows that packed bed reactor performed better than the unpacked bed reactor. For MWW the packed bed achieved 84% COD reduction while the un-packed bed had 63%. For the distillery wastewater the packed and un-packed reactor achieved 65% and 56% COD reductions respectively, while in the case of MB, 70% and 46% degradation was achieved with packed and un-packed digesters, respectively. This confirms the trends obtained in the preliminary experiments.

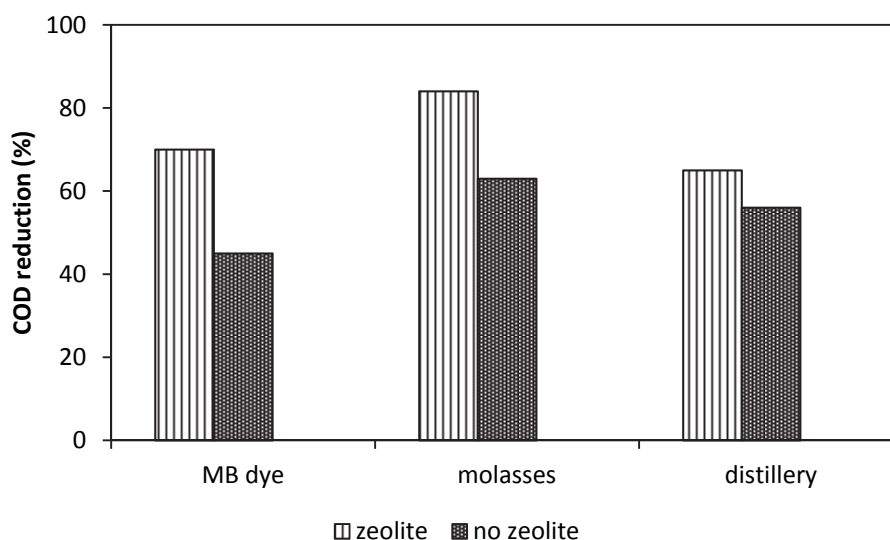


Fig. 3.9: COD removal in the FBR after 27 days of degradation

Colour removal achieved for M.B and distillery wastewater (Fig. 3.10) were 80% and 52%, respectively, whereas a general increment in colour for MWW was observed. Melanoidin which is responsible for colour in the MWW has been reported to resist biodegradation (Miranda et al., 1996, Benito et al., 1997; Miyata et al., 2000). Repolymerisation of melanoidin can lead to colour increment during anaerobic treatment of MWW as reported by Pefia et al. (1996). The colour removal by adsorption almost had a similar trend as that of the COD shown in Fig. 3.10, with MB achieving 54%, MWW 23% and distillery 18%.

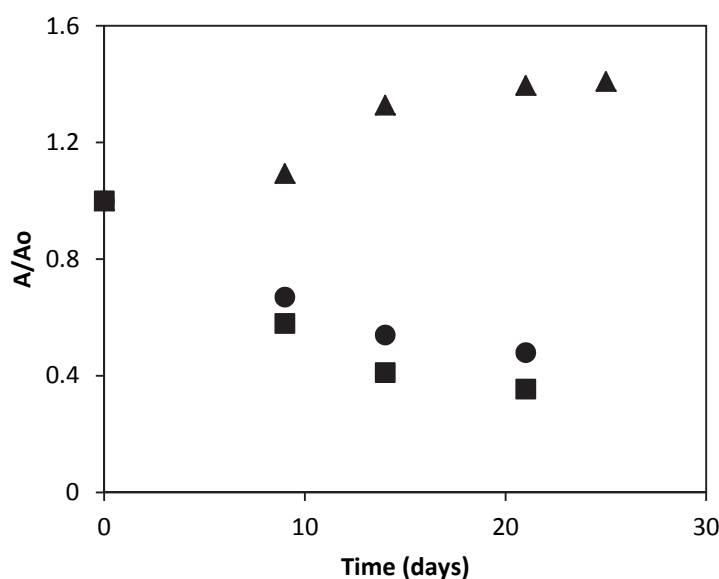


Fig. 3.10: Colour removal in the FBR; MWW (▲), distillery (●) and MB (■)

3.4 Conclusion

The study focused on anaerobic digestion of molasses wastewater (MWW) and methyl blue (MB) dye. The biodegradation of MWW was observed to increase with an increase in the initial substrate concentration. On the other hand, the degradation of MB, a model textile wastewater, was inhibited at high concentrations (concentrations above 2000 mg/L). In both wastewater types, it was found that the use of zeolite as biomass support material led to an improvement in biodegradation efficiency. Specifically, biogas production improved 5 folds when treating MB and 10 folds for MWW when zeolite was used in the FBR compared to

reactors without zeolite. Similarly, COD removal showed the same trend, with zeolite improving COD removal by above 20% in both cases. Biodegradation was found to be suitable for colour removal only for the MB but not MWW. Colour removal of about 80% was achieved with the MB while an increment in colour was observed for MWW after the biodegradation process. It was found that the addition of zeolite improved methane yield from 60% to 70% for MB dye and from 71% to about 75% for both MWW and distillery effluent. For COD reduction, the application of zeolite in packed bed reactor improved COD reduction from 63% in unpacked bed to 84% in packed bed for MWW. For MB dye COD reduction of 70% and 46% was achieved in packed bed and unpacked bed reactors.

Anaerobic digestion has been widely applied as a secondary treatment stage of most wastewater treatment plants. This is due to the fact that AD is low cost and produces biogas which can be used as a renewable energy. However, AD faces challenges in treating wastewater that is toxic or recalcitrant. In order to remove such wastes, advanced methods of treatment need to be employed. One such advanced method is UV photodegradation which will be looked at in the next section.

References

- Benito, G. G., Miranda, M. P., de los Santos, D. R. (1997). Decolorization of wastewater from an alcoholic fermentation process with *Trametes versicolor*. *Bioresource Technology*, 61(1), 33-37.
- Chun, H., Yizhong, W. (1999). Decolorization and biodegradability of photocatalytic treated azo dyes and wool textile wastewater. *Chemosphere*, 39(12), 2107-2115.
- Delee, W., O'Neill, C., Hawkes, F. R., Pinheiro, H. M. (1998). Anaerobic treatment of textile effluents: a review. *Journal of chemical technology and biotechnology*, 73(4), 323-335.
- Durán-Barrantes, M. M., Álvarez-Mateos, P., Carta-Escobar, F., Romero-Guzmán, F., Fiestas-Ros de Ursinos, J. A. (2008). Kinetics and effect of temperature in anaerobic fluidised bed reactors with clayey supports. *Chemical and Biochemical Engineering Quarterly*, 22(4), 393-399.
- Farhadian, M., Borghei, M., Umrana, V. V. (2007). Treatment of beet sugar wastewater by UAFB bioprocess. *Bioresource technology*, 98(16), 3080-3083.
- Henderson, A. L., Schmitt, T. C., Heinze, T. M., Cerniglia, C. E. (1997). Reduction of malachite green to leucomalachite green by intestinal bacteria. *Applied and environmental microbiology*, 63(10), 4099-4101.
- Herrera, F., Kiwi, J., Lopez, A., Nadtochenko, V. (1999). Photochemical decoloration of Remazol Brilliant Blue and Uniblue A in the presence of Fe³⁺ and H₂O₂. *Environmental science & technology*, 33(18), 3145-3151.
- Jiménez, A. M., Borja, R., Martín, A. (2004). A comparative kinetic evaluation of the anaerobic digestion of untreated molasses and molasses previously fermented with *Penicillium decumbens* in batch reactors. *Biochemical Engineering Journal*, 18(2), 121-132.
- Kotsopoulos, T. A., Karamanlis, X., Dotas, D., Martzopoulos, G. G. (2008). The impact of different natural zeolite concentrations on the methane production in thermophilic anaerobic digestion of pig waste. *Biosystems engineering*, 99(1), 105-111.
- Milán, Z., Montalvo, S., Ilangovan, K., Monroy, O., Chamy, R., Weiland, P., Borja, R. (2010a). The impact of ammonia nitrogen concentration and zeolite addition on the specific methanogenic activity of granular and flocculent anaerobic sludges. *Journal of Environmental Science and Health Part A*, 45(7), 883-889.
- Milán, Z., Villa, P., Sánchez, E., Montalvo, S., Borja, R., Ilangovan, K., Briones, R. (2003). Effect of natural and modified zeolite addition on anaerobic digestion of piggery waste. *Water Science & Technology*, 48(6), 263-269.
- Miranda, M. P., Benito, G. G., Cristobal, N. S., Nieto, C. H. (1996). Color elimination from molasses wastewater by *Aspergillus niger*. *Bioresource Technology*, 57(3), 229-235.
- Miyata, N., Mori, T., Iwahori, K., Fujita, M. (2000). Microbial decolorization of melanoidin-containing wastewaters: Combined use of activated sludge and the fungus *Coriolus hirsutus*. *Journal of Bioscience and bioengineering*, 89(2), 145-150.

- Montalvo, S., Díaz, F., Guerrero, L., Sánchez, E., Borja, R. (2005). Effect of particle size and doses of zeolite addition on anaerobic digestion processes of synthetic and piggery wastes. *Process biochemistry*, 40(3), 1475-1481.
- Montalvo, S., Guerrero, L., Borja, R., Sánchez, E., Milán, Z., Cortés, I., Angeles de la Rubia, M. (2012). Application of natural zeolites in anaerobic digestion processes: A review. *Applied Clay Science*, 58, 125-133.
- Nikolaeva, S., Sánchez, E., Borja, R., Raposo, F., Colmenarejo, M. F., Montalvo, S., Jiménez-Rodríguez, A. M. (2009). Kinetics of anaerobic degradation of screened dairy manure by upflow fixed bed digesters: effect of natural zeolite addition. *Journal of Environmental Science and Health Part A*, 44(2), 146-154.
- Remigi, E.U., Buckely, C.A. (2006). Co-digestion of high strength/toxic organic effluents in anaerobic digesters at wastewater treatment works, *Water Research Commission*
- Satyawali, Y., Balakrishnan, M. (2008). Wastewater treatment in molasses-based alcohol distilleries for COD and color removal: a review. *Journal of environmental management*, 86(3), 481-497.
- Umana, O., Nikolaeva, S., Sánchez, E., Borja, R., Raposo, F. (2008). Treatment of screened dairy manure by upflow anaerobic fixed bed reactors packed with waste tyre rubber and a combination of waste tyre rubber and zeolite: effect of the hydraulic retention time. *Bioresource technology*, 99(15), 7412-7417.

CHAPTER 4

4 UV PHOTODEGRADATION OF MOLASSES WASTEWATER AND METHYLENE BLUE DYE

4.1 Introduction

Photocatalytic oxidation involves the use of ultraviolet radiation, visible light or sunlight in the presence of a semiconductor catalyst to produce hydroxyl radicals which oxidizes the organic contaminants. Titanium dioxide is the most preferred semiconductor photocatalyst in the photocatalytic treatment of wastewater due to its high photocatalytic activity, high stability, non-environmental impact and affordable cost (Mounir et al., 2007). The TiO₂ is coated on zeolite surface to integrate its photocatalytic activity with the adsorption properties of the zeolite, which induces a synergistic effect, resulting in the enhancement of photodegradation efficiency. This also facilitates post-treatment separation of the catalyst from the treated water, an activity which becomes very tedious and expensive if suspended catalyst is used (Zhang and Lei, 2008). Advanced oxidation processes are typically employed to treat wastewater with biorecalcitrant compounds such as molasses and textile wastewater.

Discharge of molasses wastewater into the receiving water bodies causes environmental stress, largely to the aquatic organisms. Apart from high organic load of molasses wastewater, the molasses wastewater also contains a dark brown recalcitrant colour which impedes the penetration of sunlight to the aquatic photosynthetic plants and therefore reduces dissolved oxygen in river courses. The dark brown pigment is generally called melanoidin and is formed due to Maillard amino-carbonyl reaction. It is a product of non-enzymatic reaction between sugars and amino compounds (Martins and van Boekel, 2004). Another effluent which is also characterised by intense colour is wastewater from the textile industry. To solve the environmental problems associated with the molasses and textile wastewater, various treatment methods have been applied. Biological treatments with certain bacteria and fungi have been applied with achievement of high organic removal but notably low colour removal efficiencies for molasses wastewater (Miranda et al., 1996). In fact, Gumaraes et al. (1999) reported that the conventional anaerobic and aerobic treatment processes can accomplish the degradation of melanoidins only up to 6% or 7%, while Pefia et al. (1996) reported that colour can even increase during the biological treatment due to repolymerisation of compounds. For significant colour removal of molasses wastewater, studies have now focused on the use of photocatalysis. Similarly, biological treatment of textile effluent has been reported to be inefficient due to the recalcitrant dyes present in textile wastewater (Oller et al., 2011). Such wastewater can be treated using a single oxidation process or a hybrid of such processes.

Advanced oxidation processes can be combined in various ways to form hybrid systems that reduce degradation time and can treat a wide variety of recalcitrant organic pollutants in wastewater streams. Some of the hybrid systems which have been used for wastewater treatment include UV/H₂O₂, UV/ozone, UV/H₂O₂/ozone, UV/TiO₂ and UV/H₂O₂/TiO₂ (Rezaee et al., 2008; Crittenden et al., 2008; Huang et al., 2008). The aim of this work is to study the efficiency of the hybrid system constituting photocatalysis in which TiO₂ coated on South African natural zeolite (clinoptilolite) is used as catalyst, UV as radiation source and chemical oxidation where hydrogen peroxide is used as the oxidant in the COD removal and decolourization of methylene blue dye and molasses wastewater.

4.2 Methodology

4.2.1 Preliminary photocatalytic degradation experiments

Preliminary batch experiments were carried out in a temperature controlled shaker. The shaker was fitted with 30 W UV-C lamp and operated at 25°C to determine the best operating conditions such as catalyst loading, catalyst dosage, irradiation time, pH and amount of hydrogen peroxide as oxidant in the UV photodegradation processes. To synthesize molasses wastewater (MWW), commercial molasses syrup was dissolved in distilled water while stirring to form COD concentration of 20 g/L. Serial dilutions were then done to obtain lower concentrations of 5 g/L and 1 g/L solutions. A sample solution of 20 mg/L MB dye was

also prepared. In both cases, an appropriate mass of the TiO₂-zeolite catalyst was weighed then transferred into a 100 ml conical flask and 50 ml of the wastewater was then added. The composition of TiO₂ on the composite catalyst was varied between 5 wt% to 20 wt%. In the case of MWW, the effect of hydrogen peroxide addition in the range of 0.735 mM, 1.47 mM, 2.205 mM and 2.94 mM on the photodegradation was investigated. The flasks were then put in the thermostatic shaker for a specified period. At the same time, control for adsorption was also carried out whereby the samples were prepared in the same manner but wrapped with aluminium foil to block UV rays so as to prevent photodegradation. Also, photolysis was tested whereby the wastewater was put in the flask then irradiated without addition of the catalyst. Degraded wastewater was left to settle then filtered before measuring COD and absorbance to evaluate degradation efficiency. The absorbance of MB was measured at 664 nm while for MWW and distillery it was measured at 475 nm. The percentage colour removal (\emptyset) was calculated as;

$$\emptyset = \frac{(A_0 - A_t)}{A_0} \times 100 \quad (4.1)$$

where A_0 is the initial absorbance and A_t is the absorbance at time t . The optimum operating conditions obtained in the preliminary studies was then used in the photocatalytic reactor which was integrated with the bioreactor.

4.2.2 Catalyst preparation

For the UV photodegradation experiments, TiO₂ was supported on zeolite. The TiO₂ particles were supported on zeolite using the solid state dispersion (SSD) of TiO₂ procedure (Durgakumari *et al.*, 2002). In this method, an appropriate mass of TiO₂ was mixed with zeolite to give TiO₂ loading in the range of 2-20% (whole experimental analysis), and was thoroughly mixed with ethanol using a pestle. The mixing was done over a heating plate to remove the solvent by evaporation. Samples were later dried at 110°C and calcined in air at 450°C for 6 h. The product (TiO₂-zeolite) was obtained as TiO₂ supported on zeolite catalyst. An appropriate quantity of colloidal silica was mixed with TiO₂ in a plastic tube. The tube was then capped and shaken vigorously to disperse the TiO₂ uniformly in the colloidal silica.

4.2.3 Experimental analysis

Decolourization and COD reduction were used to evaluate the performance of the photodegradation process. Closed reflux method with potassium dichromate solution as oxidant was used to determine the COD. A UV-vis spectrophotometer was used to determine colour intensity. Scanning electron microscopy (SEM), model FEI NOVANO SEM 230, fitted with energy dispersive X-ray spectrophotometry (EDX) was used to study the surface morphology of the TiO₂-zeolite catalyst and the elemental composition of zeolite. X-ray diffractometer, model Bruker D8, was used to study the crystalline structure of the TiO₂ particles using nickel copper filtered Cu K (α) radiation (40 kv and 40 mA).

4.3 Results and discussion

4.3.1 Catalyst characterization

X-ray powder diffraction was used to analyse the crystalline structure of the catalyst (TiO₂ and zeolite) particles. In Fig. 4.1, the characteristic of XRD peaks of the anatase were observed at $2\theta = 25.4$, other peaks corresponding to anatase also appeared at $2\theta = 48.3$ and 54.9 as was earlier reported by Xiao *et al.* (2008).

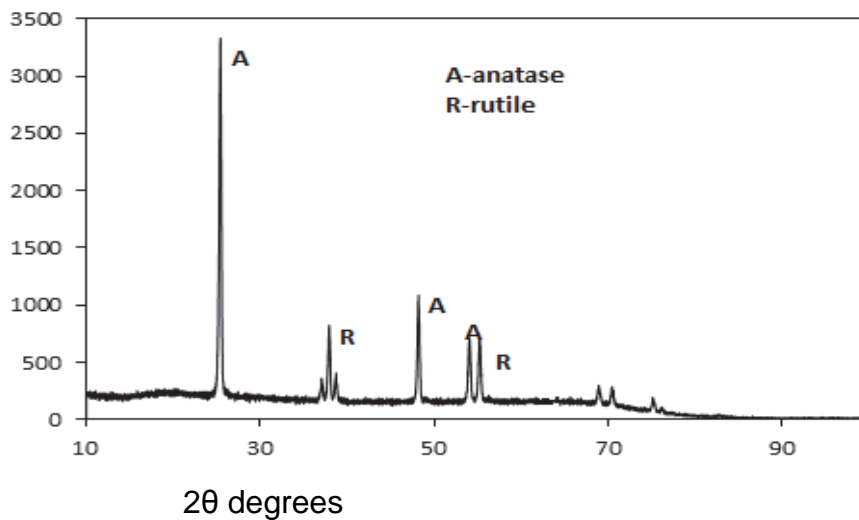


Fig. 4.1: XRD result for TiO₂ powder

The amount of rutile in the sample was calculated as (Xiao et al., 2008):

$$X_R = \frac{1}{\left(1 + \frac{0.8I_A}{I_R}\right)} \quad (4.2)$$

where X_R is the mass fraction of rutile, I_A and I_R are the intensities of anatase and rutile respectively. It was found that the TiO₂ powder had 95.6% anatase phase. For this reason, calcinations may be necessary only for the improvement of catalyst attachment on the zeolite but not for conversion of the amorphous phase to anatase in this case.

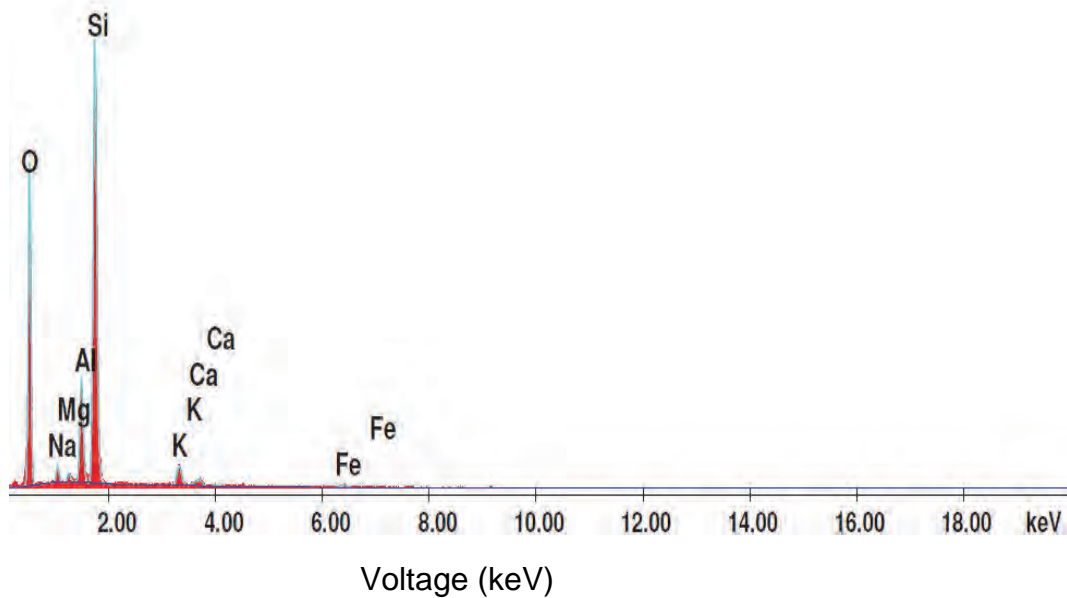


Fig. 4.2: Results of EDX analysis of zeolite.

To determine the elemental composition of the zeolite, EDX analysis was carried out. The results in Fig. 4.2 and Table 4.1 indicate that South African clinoptilolite has higher silicates than aluminates within its structure.

Table 4.1: EDX results for elemental composition of South African natural zeolite

Element	Wt%
OK	57.41
NaK	1.52
MgK	0.63
AlK	6.5
SiK	30.63
KK	1.99
CaK	0.73
FeK	0.57
Total	100%

From this observation, it can be confirmed that zeolite has an overall negative charge on its surface since the Si/Al ratio determines the overall surface charge of zeolites, zeolites with higher Si/Al ratio are negatively charged (Montalvo et al., 2012). Figure 4.3 shows the results for SEM analysis for zeolite, TiO₂ and the TiO₂/zeolite (TZ) composite catalyst before and after degradation. Comparing Fig. 4.3a (zeolite only) and Fig. 4.3c (TiO₂ attached on zeolite), it can be seen that the TiO₂ attached well on the surface of zeolite. It can also be seen that even after degradation (Fig. 4.3d) TiO₂ was still attached onto the zeolite. However, the density had reduced as some might have fallen off due to attrition of the particles caused by shaking/agitation during the reaction.

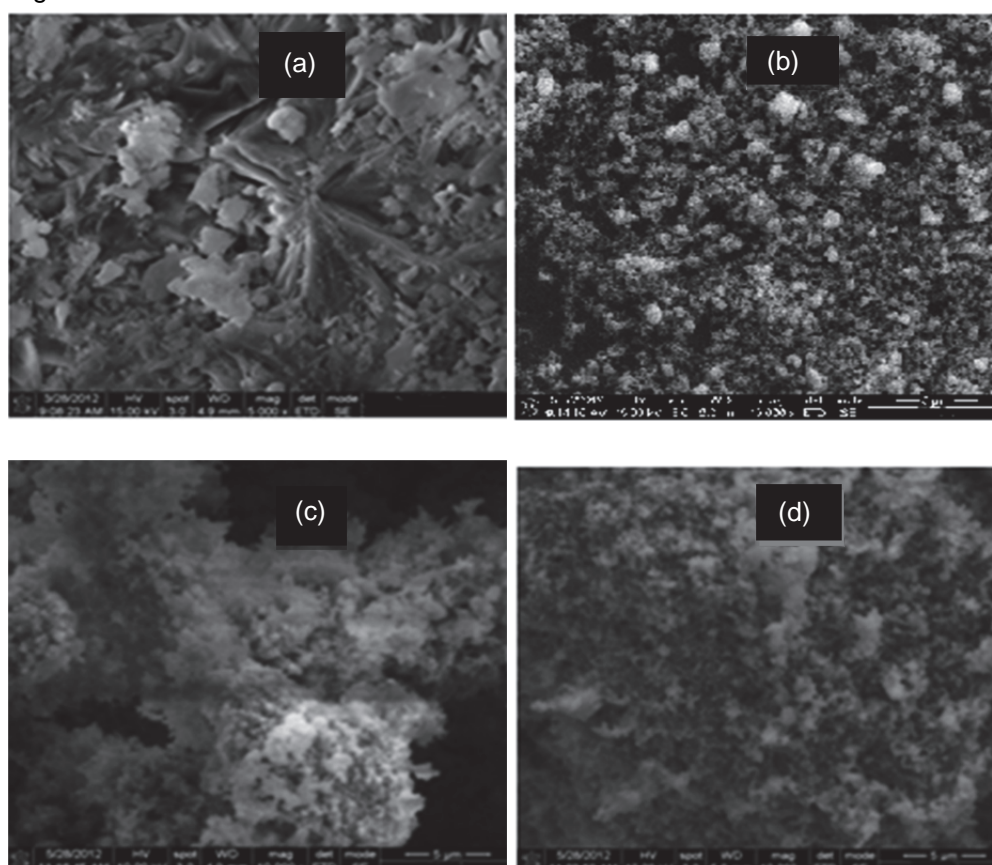


Fig. 4.3: SEM analysis for (a) zeolite (b) TiO₂ and TiO₂-zeolite catalyst (c) before degradation and (d) after degradation

4.3.2 Preliminary photodegradation for molasses wastewater (MWW)

Preliminary experiments to determine the optimum operating conditions for the photodegradation of MWW was carried out. Photodegradation operating parameters such as substrate concentration, pH of the

medium, effect of amount of TiO_2 loaded on zeolite in the $\text{TiO}_2/\text{zeolite}$ (TZ) catalyst (catalyst loading) and irradiation time were investigated.

4.3.2.1 Effect of the initial concentration

It has been reported that molasses wastewater and wastewater from distillery industries have a COD concentration of about 100 g/L (Satyawali and Balakrishnan, 2008). In this work, concentrations of 1 g/L to 20 g/L were studied since concentrations above 20 g/L did not show any appreciable degradation, probably because the colour was too intense for the UV rays to penetrate through.

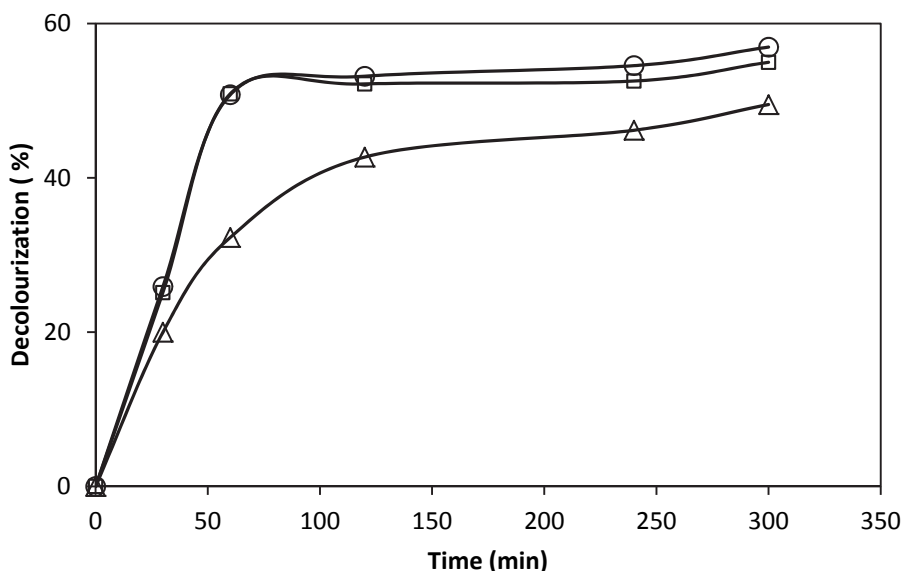


Fig. 4.4: Effect of initial concentration of MWW on the degradation; 20 g/L (Δ), 5 g/L (□) and 1 g/L (○)

Figure 4.4 shows the effect of the initial concentration on the UV photodegradation of the molasses wastewater (MWW) at its natural pH of 4 and when TiO_2 loading of 15 % was used. It was found that the degradation reduced with an increase in the initial concentration. This observation may be due to the fact that at high substrate concentrations the colour of the solution became more intense thus hindering the penetration of the UV light rays. The faster degradation observed during the first 100 minutes in each case may have been due to the fact that during this time, the molecules could be quickly adsorbed onto the catalyst surface as there were many adsorption sites available; this made the molecules to be in close contact with the catalyst therefore facilitating their photodegradation. However, the rate of degradation leveled off after about 125 minutes; this observation can be attributed to the fact that during this time the catalyst adsorptive sites had become choked and therefore the mechanism of concentrating the pollutants on the catalyst surface was hindered. It was also observed that the overall degradation achieved when a diluted solution of 1 g/L was used was not so much higher than that for 20 g/L (a 6% difference). It is therefore not economical to dilute the wastewater below 20 g/L before photodegradation in this study. It is also notable that UV/ TiO_2 photodegradation achieved low colour reduction. In order to improve the degradation efficiency of the 20 g/L, the effect of hydrogen peroxide dosage on the degradation was investigated.

4.3.2.2 Effect of H_2O_2 dosage on photodegradation

The effect of H_2O_2 dosage on the UV degradation of 20 g/L molasses wastewater was investigated at concentrations of 0.00 mM, 0.735 mM, 1.47 mM, 2.205 mM and 2.94 mM H_2O_2 (Fig. 4.5). These were the concentrations of H_2O_2 in the bulk liquid treated. It was observed that the decolourisation increased with an increase in H_2O_2 concentration from 0 to 1.47 mM, after which there was a decrease. In the photocatalytic

degradation process, addition of adequate H_2O_2 is beneficial to the formation of hydroxyl radicals as explained by the following chemical reaction (Konstantinou and Albanis, 2004).

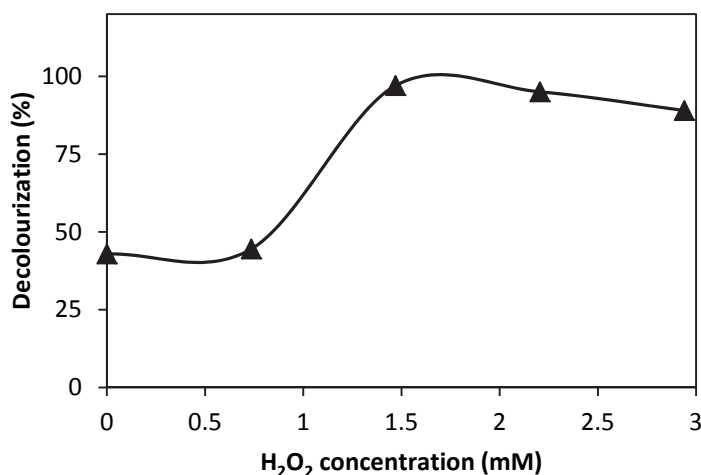
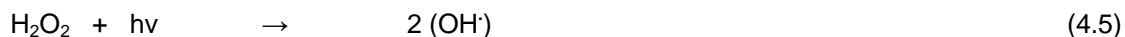
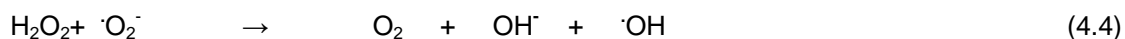
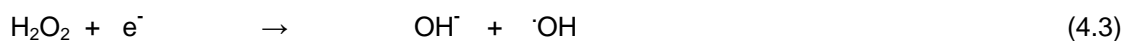
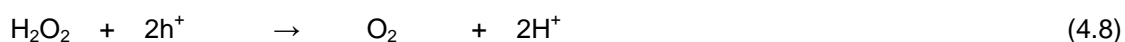


Fig. 4.5: Effect of hydrogen peroxide dosage on photocatalytic degradation of molasses wastewater in acidic medium

The hydroxyl radical ($\text{OH}\cdot$) is a super strong oxidant and a dominant species in the photocatalytic process that is able to oxidize a variety of organic substances completely on the surface of TiO_2 irradiated by UV light. Therefore, H_2O_2 will facilitate the generation of $\text{OH}\cdot$ and promote the photodegradation efficiency. However, under the condition of excess H_2O_2 concentration, it scavenges the hydroxyl radicals produced and the decolourisation reaction becomes retarded. Scavenging of the radicals takes place as in equations (4.6), (4.7) and (4.8). Similar observations were reported by Huang et al. (2008) in the hydrogen peroxide assisted photodegradation of methylene orange using TiO_2 coated on zeolite



4.3.2.3 Effect of catalyst loading (TiO_2 loading on zeolite)

The effect of catalyst loading on the degradation efficiency of MWW was investigated using TiO_2 loaded on zeolite to form compositions of 0, 5, 10, 15 and 20 wt%. Due to the high recalcitrant nature of molasses wastewater, H_2O_2 was added to the solution to form a concentration of 1.47 mM H_2O_2 . This is because the degradation without addition of the hydrogen peroxide was very low (Fig. 4.4) and a good trend could not be observed. For these experiments, 3 g catalyst and 50 ml molasses solution were used and irradiated for 6 hours. From the results shown in Fig. 4.6, it was observed that there was a general increase in the degradation with an increase in TiO_2 loading from 0% to 20%. Also, a rapid increase in the degradation when catalyst loading was increased from 0% to 15% was observed. Conversely, a negligible increase in the degradation when loading was increased from 15% to 20% was observed. These observations can be explained in terms of the availability of active sites on the catalyst surface and the penetration of the UV light into the solution (Goncalves et al., 1999). The total catalyst active sites increased with increasing catalyst

loading. At the same time, as the catalyst loading was increased above 15%, there was an increase in turbidity of the solution as the loading above 15% may be in excess and the catalyst particles started to fall off into the solution. The same observation was made by Daneshvar et al. (2004) during photocatalytic degradation of azo dye acid red 14.

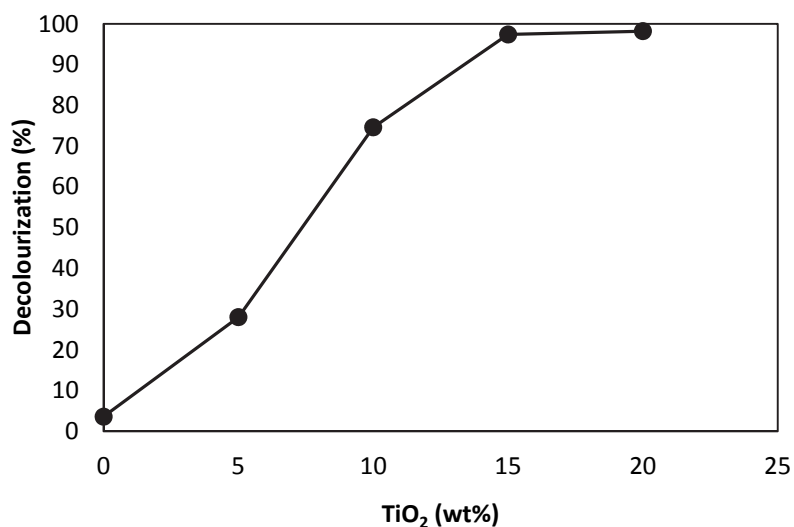


Fig. 4.6: Effect of TiO₂ loading on zeolite at initial concentration of 20 g/L and pH of 4

4.3.2.4 Colour removal by adsorption and effect of H₂O₂ on photodegradation

In Fig. 4.7, results for adsorption conducted in the absence of UV light are shown alongside the results for the effect of H₂O₂ on the photodegradation of molasses wastewater at pH 4. The adsorption on TiO₂/zeolite surface had the least colour removal of 4% compared to the systems comprising H₂O₂/UV/TiO₂/zeolite, H₂O₂ and UV. It can be deduced that there is a role played by adsorption on concentrating the organic pollutants on the surface of the catalyst, and this enhances photodegradation. The H₂O₂/UV/TiO₂/zeolite system gave the best performance since there was multiple sources of the reactive hydroxyl radicals viz. from the peroxide, UV, UV/TiO₂ and UV/H₂O₂. However, the adsorption process accounted for a negligible percentage reduction. This result could be related to those in Fig. 4.4. It can be concluded from the result in Fig. 4.6 that adsorption only enhanced photodegradation in Fig. 4.4.

Figure 4.7 shows that there was very little colour removal by UV photolysis alone as compared to H₂O₂ and UV/H₂O₂ systems. It means that UV photolysis produced less hydroxyl radicals compared to those of H₂O₂ and UV/H₂O₂ systems during the photodegradation process. However, these methods were not sufficient to bring about effective photodegradation. Also, UV/TiO₂/zeolite achieved slightly higher degradation as compared to those other methods. From this observation it can be deduced that holes generated by UV/TiO₂ could be more effective in the generation of hydroxyl radicals than in cases where only hydrogen peroxide was the major source of the hydroxyl radicals. The H₂O₂/UV/TiO₂/zeolite combination doubled the colour removal possibly due to the synergy in the hydroxyl generation process. In this system, a very high reaction rate was recorded in the first 100 minutes. This can be attributed to the high amount of hydroxyl radicals generated during this time period. Also, substrate was available therefore time could have been the limiting factor in the reaction. The reaction profile then leveled off after about 180 minutes suggesting that either the hydroxyl radicals or the substrate had been depleted. In fact, from the high colour removal of 97% attained, it can be deduced that it was the substrate that got depleted. However, in the other systems, lower reaction rates were observed. This may be due to low generation of hydroxyl radicals, and this implies that generation of the radicals was the limiting factor in these cases. The high degradation achieved with H₂O₂/UV/TiO₂ for the 20 g/L concentration of molasses is an indication that this concentration could be used for a higher concentration of molasses.

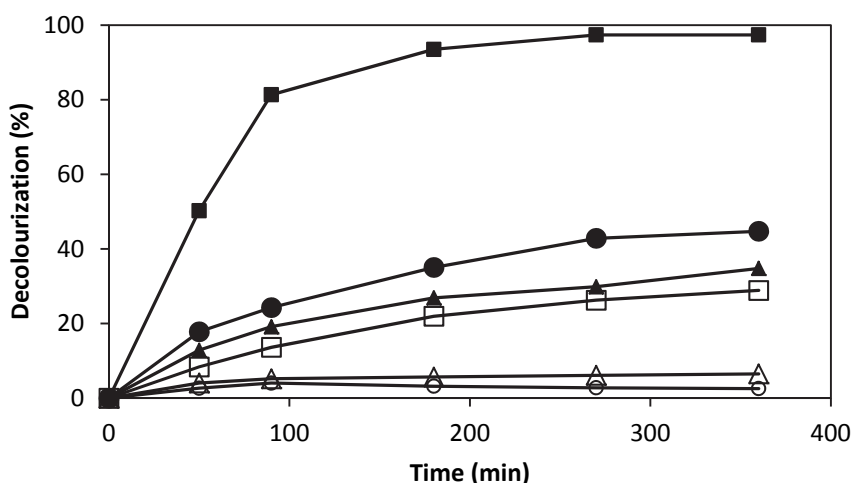


Fig. 4.7: Adsorption and effect of H₂O₂ (1.47 mM) on the photodegradation process at pH 4 and concentration of 20 g/L; H₂O₂/TiO₂/UV/zeolite (■), TiO₂/UV/zeolite (●), H₂O₂/UV (▲), H₂O₂ (□), UV photolysis (△) and adsorption (○)

4.3.2.5 UV-Vis spectral changes during photodegradation

UV-Vis scanning was conducted to give some insight into the degradation profile of the molasses wastewater under various conditions. This study was conducted with 2 g of catalyst for 180 minutes with

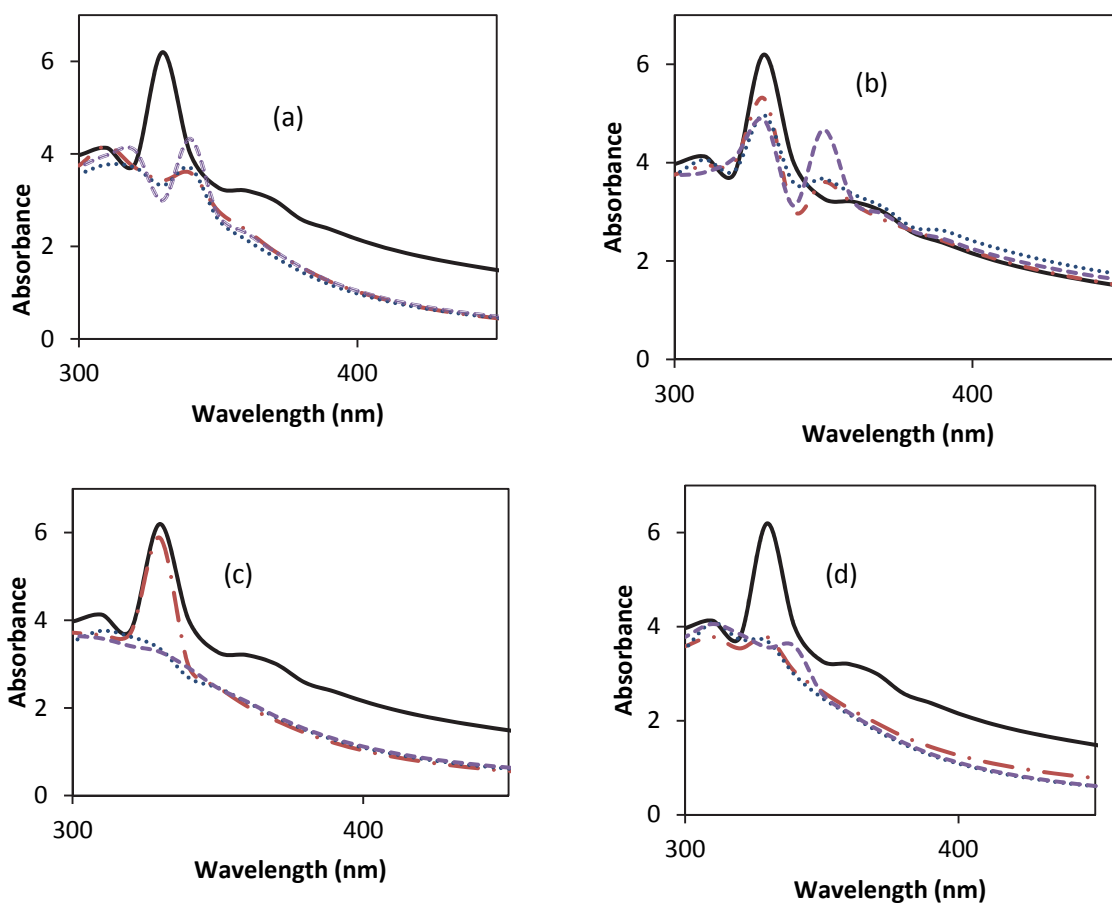


Fig. 4.8: UV-Vis spectral changes, (a) H₂O₂/UV/TiO₂/zeolite, (b) UV/TiO₂/zeolite, (c) UV/H₂O₂ and (d) H₂O₂, 0 hr (—), 1 hr (- - -), 2 hrs (·····) and 3 hrs (- - - -).

samples analysed after every hour. The untreated wastewater was found to have maximum absorbance at 330 nm as indicated by the graphs ($t=0$) in Fig. 4.8. Figure 4.8a represents the profile for $H_2O_2/UV/TiO_2/zeolite$ system where it is observed that after every hour there was a reduction in the absorbance at 330 nm but there is a peak which started to develop at around 340 nm. As degradation progressed with time, the second peak became progressively eminent while the peak at 330 nm continued to diminish. This is also observed in Fig. 4.8b (UV photolysis) where the second peak started to appear at 350nm as degradation progressed. This is an indication that under these two conditions there are some intermediates which were formed as the reaction proceeded. These intermediates had λ_{max} at 340 nm and 350 nm respectively as compared to that of the untreated wastewater which is at 330nm. A similar profile as that of Fig. 4.8a and Fig. 4.8b was also observed for a $UV/TiO_2/zeolite$ system. However, for UV/H_2O_2 (Fig. 4.8c) and H_2O_2 only (Fig. 4.8d) there were no intermediates observed since the peak at 330 nm progressively reduced with degradation time without emergence of other peaks elsewhere. In the cases where intermediates were formed (Fig. 4.8a and Fig. 4.8b) it is recommended that GC-MS analysis be conducted to identify these intermediates.

4.3.2.6 Effect of photodegradation on COD reduction

A study on the effect of photodegradation on COD removal in molasses wastewater was carried out and it was found that UV photolysis performed poorest with only 2% COD removal after 3 hours of radiation and 2 g (15 wt% TiO_2) catalyst (Fig. 4.9). The $H_2O_2/TiO_2/UV/zeolite$ hybrid system attained the highest COD reduction of about 15%. It was also observed that in all cases colour reduction was always higher than COD reduction and the order of colour removal and COD removal across all the systems was the same. Similar results were obtained by Penna et al. (2003), where COD removal of between 15% and 25% were obtained in a chemical treatment of wastewater from molasses fermentation with ozone. The low COD removal may be attributed to the fact that the brown compounds (melanoidin) present in the wastewater reacted with the generated hydroxyl radical, leading to organic compounds which still demand oxygen until their final degradation. It can therefore be concluded that there is some correlation between the colour of the wastewater and its COD. Carboxylic acids have been identified as products of melanoidin oxidation (Kim et al., 1985; Hoigne and Bader, 1983). In this study, photodegradation appears not to be an appropriate technology for COD removal in molasses wastewater because it attains very low COD removal. However, it is an efficient technology for colour removal since high efficiencies of colour removal can be obtained. The high colour removal associated with low COD reduction is an indication that photodegradation did not result in complete mineralization but rather in degradation of complex compounds to simpler ones.

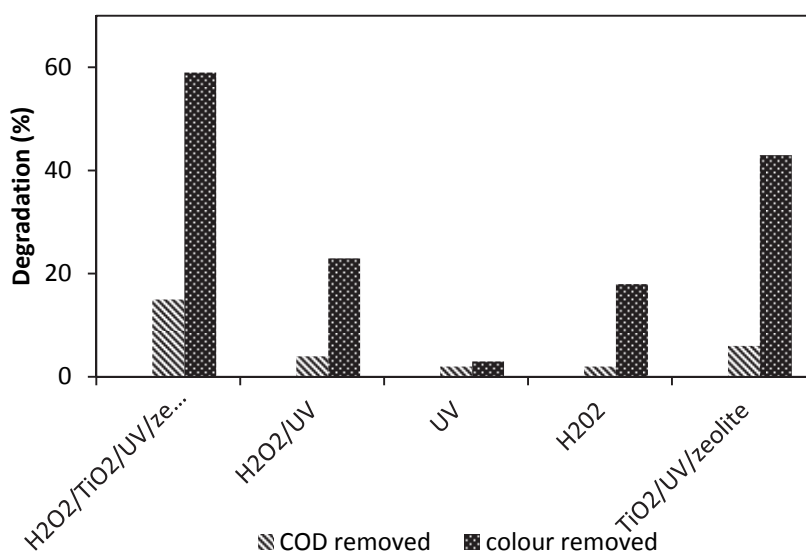


Fig. 4.9: Effect of photodegradation on COD and colour removal

As the photodegradation continues, the formation of intermediate compounds may have an influence on the solution pH. Therefore the study of the effect of pH on photodegradation becomes important.

4.3.2.7 Effect of pH on the H₂O₂/TiO₂/UV/zeolite hybrid process.

Performance of UV/H₂O₂/TiO₂/zeolite system was investigated under different pH conditions and with 10% hydrogen peroxide. Colour removal was investigated as a function of irradiation time and data were fitted to a pseudo first-order reaction model (equation (4.9)) as reported by various authors who have worked on photodegradation of various organic contaminants (Wong and Chu 2003; Muruganandham and Swaminathan (2004).

$$\ln\left(\frac{A_0}{A}\right) = kt \quad (4.9)$$

where A₀ and A_t are the respective absorbances of solution at irradiation times 0 and t, k the rate constant (min⁻¹) and t is the irradiation time (min).

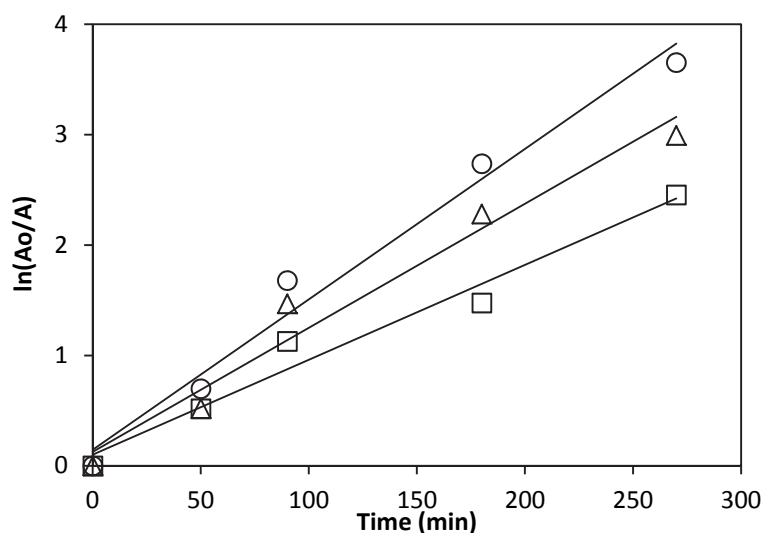


Fig. 4.10: Effect of pH on H₂O₂/TiO₂/UV/zeolite hybrid system pH 4 (○), pH 7 (Δ) and pH 10 (□)

Figure 4.10 and Table 4.2 show that the decolourisation reaction was fastest at pH 4 and slowest at pH 10. This can be attributed to the fact that under alkaline conditions some of the H₂O₂ undergoes photodecomposition to water and oxygen rather than to hydroxyl radical as shown by eqn (4.10) (Galindo and Kalt, 1998).

Table 4.2: Rate constant and R² values

pH	R ²	K (min ⁻¹)
4	0.9794	0.0136
7	0.9671	0.0112
10	0.9701	0.0086



Moreover, under alkaline medium the oxidising species hydroperoxy anion (HO_2^-) is formed (HO_2^- anion is the conjugated base of H_2O_2). This HO_2^- anion reacts with $\cdot\text{OH}$ radical and residual H_2O_2 according to equations (4.11) and (4.12) consequently lowering the removal rate. The same observation was made by Muruganandham and Swaminathan (2004) in a study of photodegradation of reactive azo dye with UV/ H_2O_2 process.



The difference in degradation rate under different pH medium may also be explained by the change in surface property of the composite catalyst under different pH conditions. Melanoidin, the main constituent of molasses wastewater, is negatively charged, similarly zeolite and TiO_2 also have negatively charged surfaces. It has been reported that TiO_2 has zero point charge of 6.25 (Kaur and Vasundhara, 2007). At low pH values the surface of TiO_2 -zeolite acquires positive charges and thus has the ability to attract the negatively charged melanoidin molecules onto its surface thereby increasing degradation rate. However, in a basic medium the surface of the catalyst acquires negative charges and therefore does not attract the negatively charged melanoidin molecules therefore lower degradation is obtained.

4.3.3 Preliminary photodegradation of methylene blue dye

4.3.3.1 Effect of TiO_2 loading on zeolite

The effect of catalyst loading on zeolite was investigated and it was found that 10 wt% TiO_2 had lower degradation as compared to 15 wt% and 20 wt% (Fig. 4.11). This may be due to the fact that the 10 wt% TiO_2 had fewer numbers of catalyst and therefore there were less catalyst reactive sites. From Fig. 4.11, it can be seen that there was no appreciable difference in degradation between catalyst loading of 15 wt% and 20 wt%. It means that for these loadings, the catalyst was sufficient and the catalyst reactive sites were not the limiting factor in the reaction. Also, the failure of 20 wt% to produce higher degradation than 15 wt% as may have been expected, might have been due to the fact that at this catalyst loading, the TiO_2 became excess and started falling off from the zeolite surface thereby making the solution turbid and consequently blocking the penetration of UV rays into the solution.

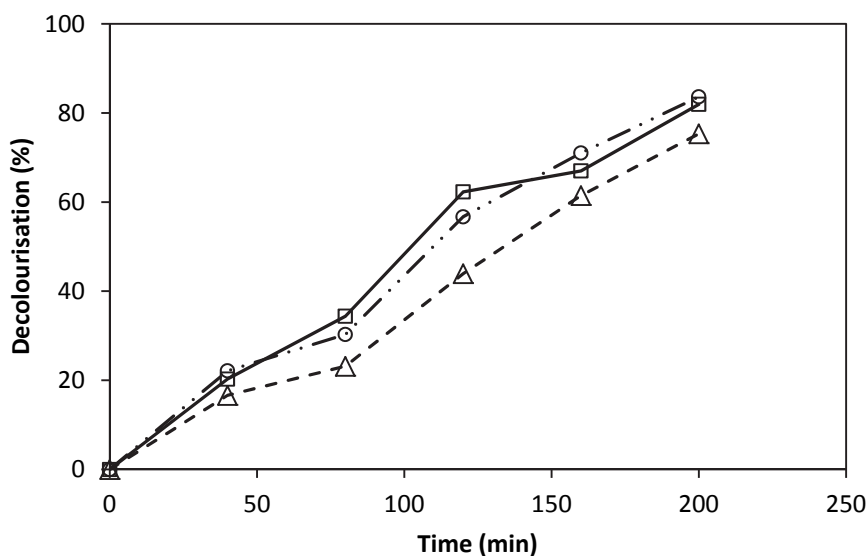


Fig. 4.11: The effect of TiO_2 loading on Zeolite, 10% (Δ), 15% (\square) and 20% (\circ)

4.3.3.2 Effect of composite catalyst dosage

The effect of the amount of the composite catalyst ($\text{TiO}_2/\text{zeolite}$) was studied using various amounts of catalyst (25 g/L, 50 g/L and 75 g/L) at constant MB concentration of 20 mg/L while catalyst loading was maintained at 15 wt% TiO_2 . It was found (Fig. 4.12) that low catalyst loading of 25 g/L had a low performance whereas 50 g/L seemed to have a better performance than the catalyst loading of 75 g/L after degradation time of 160 minutes. The increase in degradation when catalyst loading was increased from 25 g/L to 50 g/L can be attributed to the fact that as the amount of catalyst was increased, the number of photons absorbed and the number of dye molecules adsorbed also increased owing to an increase in the number of TiO_2 particles. The density of the particles in the area of illumination also increased and so the rate of reaction is enhanced.

It can also be seen that though 75 g/L catalyst dosage did not produce the highest degradation within 160 minutes, it had the highest initial rate of degradation. This can be attributed to the fact that initially the 75 g/L catalyst dose offers a high number of catalyst reactive sites and since the dye concentration was high enough, the reaction proceeded in such a way that neither the dye concentration nor the amount of catalyst limited the reaction. However, the rate reduced after some time most likely due to the decreased dye concentration. Subsequently, its diffusion onto the catalyst surface probably became slow as the high catalyst loading hindered the mass transfer process (Nawi et al., 2002). This effect is more prominent at low substrate concentrations and high catalyst loading. In addition, the high catalyst loading blocked the penetration of UV radiation. This meant that the performance of the 50 g/L catalyst loading therefore surpassed the 75 g/L after some time as shown in Fig. 4.12.

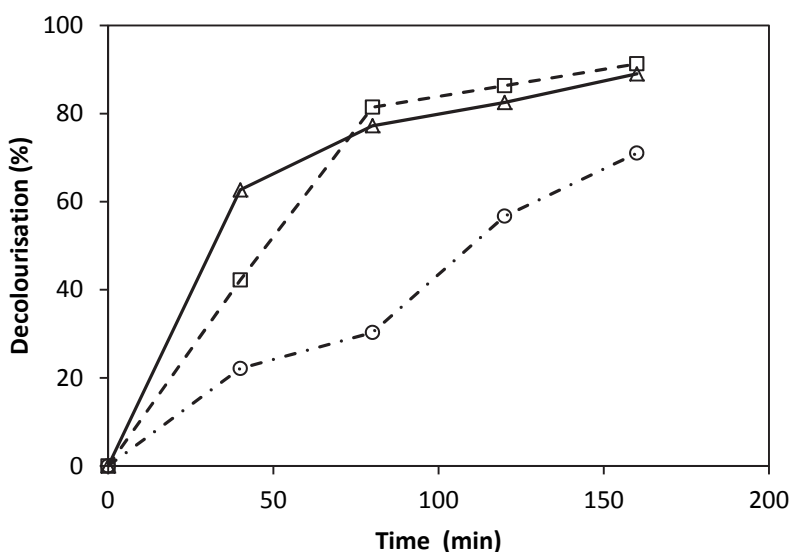


Fig. 4.12: The effect of catalyst (TiO_2 -zeolite) dosage using 15 % TiO_2 on zeolite, 25 g/L (○), 50 g/L (□), and 75 g/L (△)

4.3.3.3 Effect of solution pH

The solution pH is a very important operating parameter for the photocatalytic reaction. It was observed that the rate of MB degradation increased with an increase in pH (Fig. 4.13). This is indicative of the significant role of the surface property of the photocatalyst TiO_2 ; the acid-base property of the metal oxide surface has a considerable influence on the photocatalytic activity with varying pH. The pH effect can be explained on the basis of the zero point of charge of TiO_2 . The photodegradation efficiency as a function of pH value decreased in the order of $9 > 4 > 2$ as shown in Fig. 4.13. Similar observations were reported by Lakshmi et

al. (1995); Xiao et al. (2008) for the photodegradation of MB using TiO_2 as photocatalyst. It is generally accepted that the pH-dependent photodecomposition was mainly attributed to the variations of surface charge properties of a photocatalyst. Consequently, this changed the adsorption behaviour of a dye on the catalyst surface. Since methylene blue (MB) had a cationic configuration, its adsorption is favoured in alkaline solution and this increased photodegradation on the catalyst surface. On the other hand the adsorption of MB on the catalyst surface in acidic medium is poor because the surface of the catalyst was positively charged and therefore could not easily absorb the cationic dye.

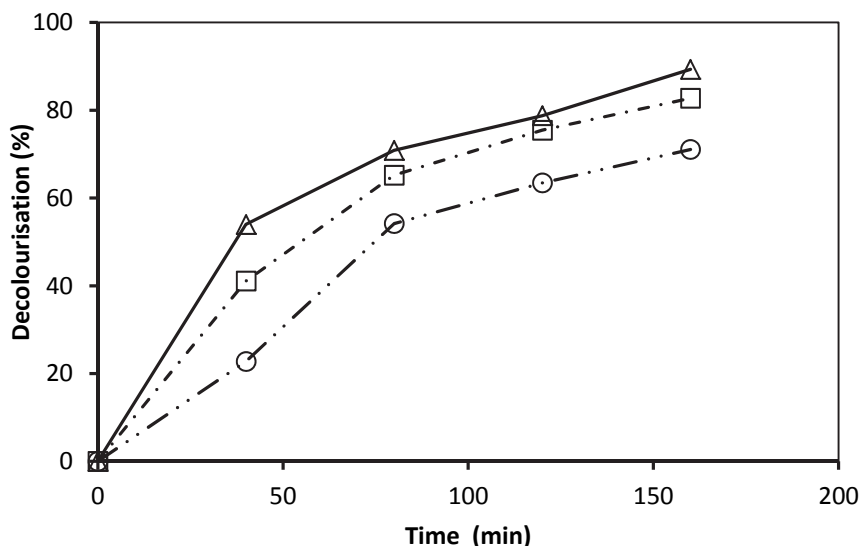


Fig. 4.13: The effect of pH on photodegradation of MB using zeolite as catalyst support, pH 2 (○), pH 4 (□) and pH 9 (△)

4.3.3.4 Adsorption and photodegradation

Figure 4.14 shows the comparison between the removal of methylene blue by the adsorption on TiO_2 /zeolite surface and that of the photodegradation. The study of methylene blue adsorption was performed at 298 K in the dark. It is observed that photodegradation achieved higher colour removal than adsorption. This is

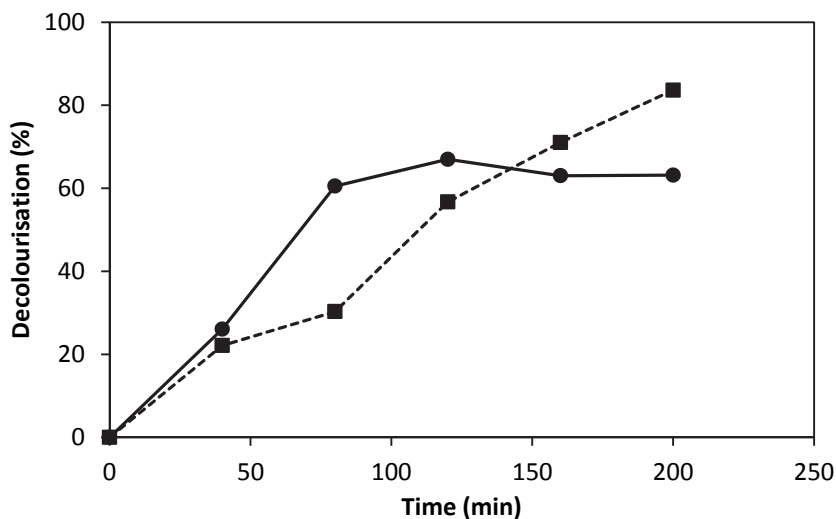


Fig. 4.14: Colour removal by; photodegradation (■) and adsorption (●)

due to the fact that the adsorption of the dye takes place up to a maximum level where equilibrium is achieved and thereafter no more adsorption can take place, while for photodegradation there is no equilibrium to be attained as the MB molecules are photodecomposed as soon as they are adsorbed onto the TiO₂/zeolite surface. However, adsorption is observed to take place faster than photodegradation within the first 100 minutes. This may be an indication that in the adsorptive photodegradation process for the treatment of wastewater containing MB, adsorption of the molecules onto the surface of the adsorbent takes place first followed by photodegradation. It can also be pointed out in Fig. 4.14 that colour removal by adsorption was 67% while photodegradation achieved 84% colour removal within a period of 200 minutes. Though adsorption onto TiO₂/zeolite performed relatively well in colour removal, it is better to integrate it with photodegradation in the treatment of textile industry effluent. This is due to the fact that adsorption alone only transfers pollutants from the solution to the adsorbent surface whereas photodegradation degrades the pollutants.

4.4 Conclusion

The effects of pH, catalyst loading, oxidant dosage and irradiation time on the COD reduction and decolourization of the molasses wastewater (MWW) during photodegradation was studied in a thermostatic shaker. The highest colour removal of more than 90% was achieved at pH 4 and oxidant dosage of 1.47 mM, while low COD removal (< 20%) was observed during photodegradation. The H₂O₂/UV/TiO₂ system achieved higher colour removal of 97% compared to the UV/TiO₂ system which achieved 44% while H₂O₂/UV system achieved 34% colour removal. The rate of decolourization was found to fit pseudo- first order reaction kinetics with the highest rate constant value of $1.36 \times 10^{-2} \text{ min}^{-1}$. Also, photodegradation of methylene blue dye was studied where it was found that TiO₂ loading on zeolite of 15% wt/wt had optimal performance and photodegradation was more efficient at pH 9.

Photodegradation using UV light generated from artificial lamps has been widely investigated. UV from artificial lamps has been found to be reliable and lamps generating high intensity of UV light can be used to increase the rate and reduce the duration of photodegradation. However, UV lamps are costly to acquire and operate due to their high consumption of electricity. UV lamps are also made of toxic materials such as mercury making them undesirable for large scale use. Therefore, there has been a search for an appropriate alternative UV light source for photocatalysis. Zeolite was also investigated as a support for TiO₂ using the solid state dispersion method. The SSD method of attachment faced the challenge of detachment of the TiO₂ from the zeolite substrate.

References

- Daneshvar, N., Salari, D., Khataee, A. R. (2004). Photocatalytic degradation of azo dye acid red 14 in water on ZnO as an alternative catalyst to TiO₂. *Journal of Photochemistry and Photobiology A: Chemistry*, 162(2), 317-322.
- Durgakumari, V., Subrahmanyam, M., Subba Rao, K. V., Ratnamala, A., Noorjahan, M., Tanaka, K. (2002). An easy and efficient use of TiO₂ supported HZSM-5 and TiO₂+ HZSM-5 zeolite combineate in the photodegradation of aqueous phenol and p-chlorophenol. *Applied Catalysis A: General*, 234(1), 155-165.
- Galindo, C., and Kalt, A. (1999). UV-H₂O₂ oxidation of monoazo dyes in aqueous media: a kinetic study. *Dyes and pigments*, 40(1), 27-35.
- Goncalves, M. S., Oliveira-Campos, A. M., Pinto, E. M., Plasência, P., Queiroz, M. J. R. (1999). Photochemical treatment of solutions of azo dyes containing TiO₂. *Chemosphere*, 39(5), 781-786.
- Guimaraes, C., Bento, L. S. M., Mota, M. (1999). Biodegradation of colorants in refinery effluents: potential use of the fungus *Phanerochaete chrysosporium*. *International Sugar Journal* 101 1205, 246-251.
- Hoigné, J., and Bader, H. (1983). Rate constants of reactions of ozone with organic and inorganic compounds in water – I: non-dissociating organic compounds. *Water Research*, 17(2), 173-183.
- Huang, M., Xu, C., Wu, Z., Huang, Y., Lin, J., Wu, J. (2008). Photocatalytic discolorization of methyl orange solution by Pt modified TiO₂ loaded on natural zeolite. *Dyes and Pigments*, 77(2), 327-334.

- Kaur, S., and Singh, V. (2007). TiO₂ mediated photocatalytic degradation studies of Reactive Red 198 by UV irradiation. *Journal of hazardous materials*, 141(1), 230-236.
- Kim, S. B., Hayase, F., Kato, H. (1985). Decolorization and degradation products of melanoidins on ozonolysis. *Agricultural and Biological Chemistry*, 49(3), 785-792.
- Konstantyinou, I. K., and Albanis, T. A. (2004). TiO₂-assisted photocatalytic degradation of azo dyes in aqueous solution: kinetic and mechanistic investigations. *A review, Applied Catalyst B: Environmental*, 49, 1-14.
- Lakshmi, S., Renganathan, R., Fujita, S. (1995). Study on TiO₂-mediated photocatalytic degradation of methyleneblue. *Journal of Photochemistry and Photobiology A: Chemistry* 88, 163-167.
- Martins, S. I., and Van Boekel, M. A. (2005). A kinetic model for the glucose/glycine Maillard reaction pathways. *Food Chemistry*, 90(1), 257-269.
- Miranda, M. P., Benito, G. G., Cristobal, N. S., Nieto, C. H. (1996). Color elimination from molasses wastewater by *Aspergillus niger*. *Bioresource Technology*, 57(3), 229-235.
- Montalvo, S., Guerrero, L., Borja, R., Sánchez, E., Milán, Z., Cortés, I., Angeles de la Rubia, M. (2012). Application of natural zeolites in anaerobic digestion processes: A review. *Applied Clay Science*, 58, 125-133.
- Mounir, B., Pons, M. N., Zahraa, O., Yaacoubi, A., Benhammou, A. (2007). Discoloration of a red cationic dye by supported TiO₂ photocatalysis. *Journal of hazardous materials*, 148(3), 513-520.
- Muruganandham, M., and Swaminathan, M. (2004). Photochemical oxidation of reactive azo dye with UV-H₂O₂ process. *Dyes and pigments*, 62(3), 269-275.
- Nawi, M. A., and Sabar, S. (2012). Photocatalytic decolourisation of Reactive Red 4 dye by an immobilised TiO₂/chitosan layer by layer system. *Journal of colloid and interface science*, 372(1), 80-87.
- Oller, I., Malato, S., Sánchez-Pérez, J. A. (2011). Combination of advanced oxidation processes and biological treatments for wastewater decontamination – a review. *Science of the total environment*, 409(20), 4141-4166.
- Pefia, M., Gonzfilez, B. G., San Cristoba N. L., Heras, N. C. (1996). Color elimination from molasses wastewater by aspergillusniger. *Bioresource Technology* 57, 229-235.
- Pena, M., Coca, M., Gonzalez, G., Rioja, R., Garcia, M. T. (2003). Chemical oxidation of wastewater from molasses fermentation with ozone. *Chemosphere*, 51(9), 893-900.
- Satyawali, Y., and Balakrishnan, M. (2008). Wastewater treatment in molasses-based alcohol distilleries for COD and color removal: a review. *Journal of environmental management*, 86(3), 481-497.
- Wong, C. C., and Chu, W. (2003). The direct photolysis and photocatalytic degradation of alachlor at different TiO₂ and UV sources. *Chemosphere*, 50(8), 981-987.
- Xiao, Q., Zhang, J., Xiao, C., Si, Z., Tan, X. (2008). Solar photocatalytic degradation of methylene blue in carbon-doped TiO₂ nanoparticles suspension. *Solar Energy*, 82(8), 706-713.
- Zhang, X., and Lei, L. (2008). Effect of preparation methods on the structure and catalytic performance of TiO₂/AC photocatalysts. *Journal of hazardous materials*, 153(1), 827-833.

CHAPTER 5

5 SOLAR PHOTODEGRADATION AND ADSORPTION OF EMERGING PHARMACEUTICALS

5.1 Introduction

The use of artificial UV light for photocatalysis has been found to be costly in terms of acquisition, environmental safety, operation and disposal. This cost can be reduced through the use of sunlight as the source of energy. In order to investigate the feasibility of utilising sunlight, the hourly, daily and monthly solar radiation data needs to be determined in order to examine the effect of time of day, cloud cover and seasons on solar intensity. Although supported TiO₂ has been found to be easier to separate from the reaction solution (Shan et al., 2010), the supported catalyst still suffers from low reaction rates and detachment of TiO₂ from its supports. The low reaction rates of supported TiO₂ has been increased by supporting the TiO₂ onto a strong adsorbent such as activated carbon (Sheintuch and Matatov-Meytal, 1999). The adsorbent brings the substrates into intimate contact with the TiO₂ thus increasing the rate of photocatalysis. The use of the SSD method for the attachment of TiO₂ onto zeolite has been affected negatively by the detachment of the TiO₂. The detachment of TiO₂ can be prevented by using a binder such as silica xerogel to attach TiO₂ onto its support.

Several reactor designs such as water bell, thin film, concentrating and compound parabolic concentrator have been used for photocatalysis (Braham and Harris, 2009). The complexity, low reactivity or high cost of such reactors has motivated the search for a better reactor system. One attractive alternative has been the air fluidised reactor due to the low cost of moving the fluidising air medium and the double use of the fluidising air as the electron scavenger (Kimura et al., 2004). In this study, a composite catalyst of TiO₂, activated carbon and silica xerogel was used to adsorb and photodegrade several pharmaceuticals in a fluidised bed reactor using sunlight as the source of activation energy. The aim of the study was to determine the optimum composition of the composite catalyst and the optimum hydrodynamic conditions of the fluidised bed reactor.

5.2 Methodology

5.2.1 Equipment

In order to carry out the experiments several equipment were procured and/or assembled on site. The different equipment were used to prepare the catalyst, carry out experiments, prepare samples for analysis and quantify solar radiation.

5.2.1.1 Experimental setup

The experimental set up (Fig. 5.1) consisted of ten fluidized bed photocatalytic reactors (1) mounted on a single frame. The frame could be tilted both East-West and North-South to obtain the required azimuth and inclination angles to the sun. Ten reactors were used simultaneously so that ten experiments could be run concurrently. It was necessary to carry out several experiments simultaneously in order to eliminate the effect of the variations of solar radiation intensity on the experiments. Air was supplied to the reactors from a compressor (2) through a common header (3) from where gas lines channelled the air into the respective reactors. Needle valves (4), rotameters (5) and non-return valves (6) were fitted to the gas lines from the header to control air flow, meter the volumetric flow of air and keep liquid from entering the gas lines, respectively.

The reactor consisted of an upper glass section screwed onto a bottom plastic section. The plastic section was connected to the non-return valves and it also held the gas distributor which was made of sintered glass of pore size 10-16 µm. A porous glass distributor was selected due to the fact that it could produce bubbles of very small sizes, which led to good fluidization and also high gas-liquid mass transfer rates. The pore size

of the glass distributor was chosen to be smaller than the catalyst size, in the range 38-75 μm , in order to prevent the catalyst from passing through the distributor. The upper glass section of the reactor consisted of the reactor body and a gas disengaging section made of clear borosilicate glass. Schott-Duran borosilicate glass was used for the glass section due to its high transmittance in the solar UV range. It has been suggested that solar photoreactors should have a diameter of 25-50 mm (Malato Rodríguez et al., 2004). Therefore, 32 mm was chosen as the internal diameter of the reactor body after considering the available commercial sizes of glass tubes. Detailed design features are shown in Fig. A1.

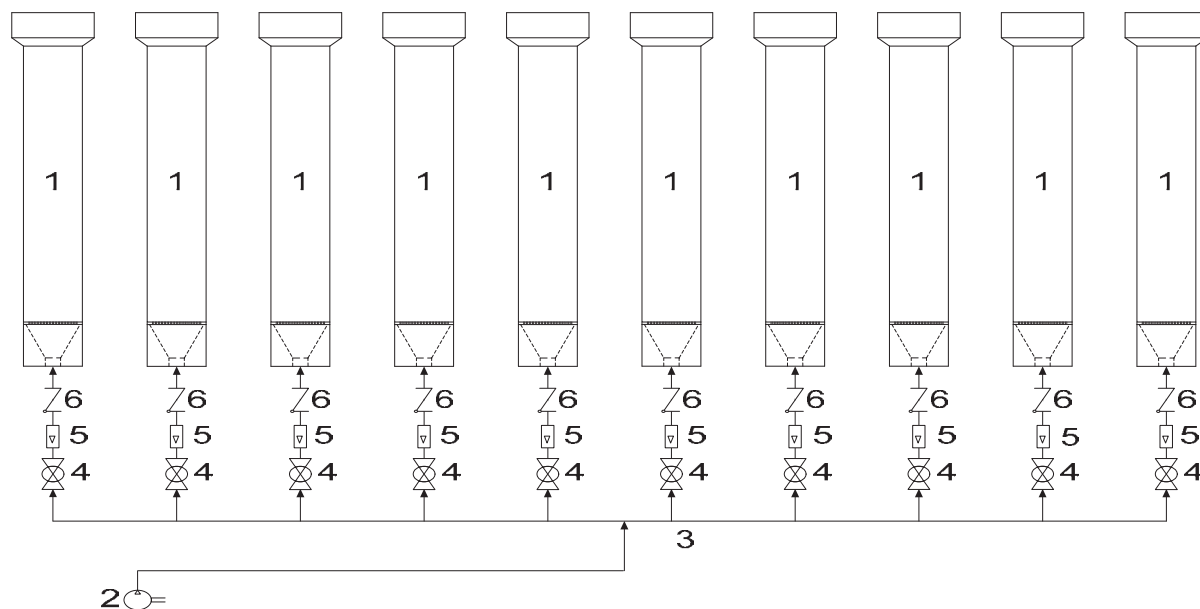


Fig. 5.1: Experimental set up. (1) Reactor, (2) Air compressor, (3) common header, (4) Ball valve, (5) Rotameter, (6) Non-return valve

It has been reported that 10 is the optimum aspect ratio for air fluidization (Ochieng et al., 2002). In order to carry out experiments with variable aspect ratio, the maximum aspect ratio of the reactor column was set at 15 resulting in a column height of 480 mm. A thickness of 1.5 mm for the glass of the reactor body was chosen in order to give enough strength without being too thick to interfere with transmission of UV rays. A gas disengaging section with a diameter of 67 mm and a height of 50 mm was provided on top of the reactor body to prevent the movement of liquid and solids out of the reactor. Therefore, the glass section of the reactor has a total length of 569 mm with a maximum capacity of 629 ml and a working solution volume of 450 ml. Four sampling ports were provided on the reactor body to be used for hydrodynamic experiments.

The air compressor (Jun-air) that was used could deliver 50 litres per minute (LPM) of uncompressed air into the reactors. Variable air flowmeters (rotameters) were mounted on the reactor frame and were capable of metering air flow within the range of 0.167-1.33 LPM. Excess air was vented to minimize pressure in the gas lines. The system was operated in batch mode for the liquid and solid, with air being used to induce fluidization of the bed and also as a source of oxygen which was used as an electron acceptor. The experimental rig was mounted on a rooftop where there were no obstructions to the rays of the sun.

5.2.1.2 Solar radiation sensor

A silicon pyranometer solar radiation sensor (Kipp & Zonen) was used for quantifying the global solar radiation intensity at the Vaal University of Technology (VUT). The radiation sensor is one of the components in the VUT weather station which was installed by the South African Weather Services (SAWS). The radiation data was recorded, stored and retrieved by the VUT weather station data logger. The

recorded global solar radiation data was averaged every 5 minutes. Hourly, daily and monthly radiation data was obtained by summing the 5 minute averaged data.

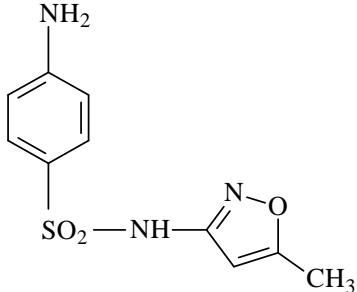
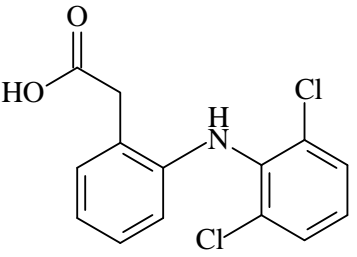
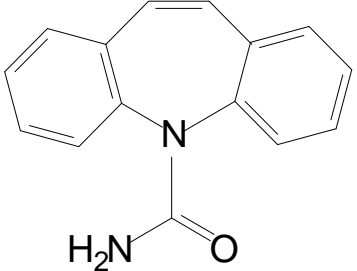
5.2.1.3 Material preparation and sampling equipment

Other equipment that were used for the experiments included test sieves (38 μm , 75 μm and bottom plate) for sieving the catalysts. A magnetic stirrer (Wisestir) was used to homogenize the composite catalyst mixtures. An oven (Labotech) was used to dry the composite photocatalyst samples. Several 0.45 μm GHP syringe filters with glass fibre prefilter (Pall Acrodisc) were used for filtering samples before analysis.

5.2.2 Materials

Aeroxide P25 titanium (IV) oxide (P25-TiO₂) was purchased from Acros Organics. Ludox HS-30 colloidal silica and the pharmaceuticals sulfamethoxazole (SMX), diclofenac sodium salt (DCF) and carbamazepine (CBZ) were obtained from Sigma-Aldrich (South Africa). The structure and some properties of SMX, DCF and CBZ are shown in Table 5.1. Hydrochloric acid (32%), sulphuric acid (98%), sodium hydroxide and commercial powdered activated charcoal (PAC) were purchased from Labchem (South Africa). All experiments were carried out with deionized water (Resistivity 18.2 M Ω cm) from a Millipore Direct Q reverse osmosis unit.

Table 5.1: Properties of diclofenac, sulfamethoxazole and carbamazepine. (^aBrogat et al., 2013; ^bYu et al., 2008)

Compound	Structure	Log K _{ow}	pK _a	Natural pH in deionized water
Sulfamethoxazole C ₁₀ H ₁₁ N ₃ O ₃ S		0.9 ^a	1.8 ^a 5.6 ^a	4.6
Diclofenac C ₁₄ H ₁₀ Cl ₂ NO ₂		0.7 ^a	4.2 ^a	5.0
Carbamazepine C ₁₅ H ₁₂ N ₂ O		2.45 ^b	2.3 ^b 13.9 ^b	6.0

5.2.3 Experimental methods

5.2.3.1 Preparation of PAC-TiO₂-silica xerogel composite catalyst

Known quantities of PAC, TiO₂ and colloidal silica were mixed in a capped bottle and stirred magnetically until the mixture was homogeneous. Then 15 ml of the slurry mixture in the bottle was spread on 30 × 30 cm glass plates to make thin layers of the slurry. The glass plates were then put in an oven at 90°C for quick gelling of the colloidal silica sol. It was necessary to form the gel quickly in order to prevent settling of the PAC in the silica sol which would result in non-uniform distribution of the PAC in the composite. The resulting dry flakes of PAC and TiO₂ bound by silica xerogel on the glass plates were then crushed and sieved to a size range of 38-75 μm. This composite catalyst powder was then shaken in 100 ml of 0.05 M HCl solution for every 40 g of colloidal silica used to make the composite. The acid was used to remove the excess alkalinity due to the NaOH used to stabilize the colloidal silica. The acid wash was followed by several washes with deionized water to remove the excess acid and loose particles of PAC, TiO₂ and silica xerogel. Between each wash, the pH of the water was monitored and washing stopped when the pH value remained constant at around 6.5. Finally, the composite catalysts were dried in an oven at 50°C to obtain the PAC-TiO₂-silica xerogel (CTS) composite catalyst. Pure silica xerogel and a composite of TiO₂ and silica xerogel (TS composite) were also prepared using a procedure similar to that of the CTS composite. However, for the pure silica xerogel, only colloidal silica was used as a precursor while for the TS composite, both TiO₂ and colloidal silica were used as precursors.

5.2.3.2 Adsorption and photodegradation experiments

The adsorption and photocatalysis experiments were carried out between 9.30 am and 2.30 pm on sunny days in the fluidized bed photocatalytic reactor. Dark adsorption experiments were carried out first by inclining the reactors at an appropriate angle from the horizontal and then covering the reactors with a black polythene plastic to keep off sunlight. Then the required mass of the CTS composite catalyst/pure silica xerogel/TS composite was added into 450 ml of the target substrate in the covered photocatalytic reactor to start adsorption. Air sparging was then started and air flow regulated and maintained at the required level using the rotameters. After reaching the adsorption equilibrium, the black polythene plastic covering the reactors was removed to let sunlight irradiate the reactors in order to start photocatalysis. During adsorption and photocatalysis, 3 ml of the substrate was sampled periodically for analysis using a UV-vis spectrophotometer. All adsorption and photocatalysis experiments were carried out in duplicate in order to statistically confirm the experimental results. The azimuth angle of the reactors was adjusted every hour so that the reactors always faced the sun in order to increase the solar intensity on the reactors. For the pH experiments, the pH of the substrate solutions was adjusted with 0.1 N H₂SO₄ or 0.1 N NaOH.

5.2.3.3 CTS composite adherence stability experiments

The CTS composite adherence stability was determined by analysing the turbidity of the reaction solution collected under the distributor. After the photodegradation experiments, the non-return valves were opened and the reaction solution collected from under the distributor. The solution was then analysed for turbidity. The turbidity gave an indication of the detachment of PAC, TiO₂ and silica from the CTS composite.

5.2.3.4 PAC regeneration experiments

The regeneration of the spent PAC by photodegradation was determined by measuring the adsorption of the PAC after photodegradation. At the end of photodegradation, the solution from the reactors was drained leaving the CTS composite in the reactors. Then the CTS composite in the reactors was contacted with a fresh substrate solution to carry out a second adsorption. The mass adsorbed by the spent PAC during the second adsorption of the substrates (m_{AT}) included the mass adsorbed due to photocatalytic regeneration (m_{AP}) and also due to adsorption by unsaturated sites that were not occupied during the first adsorption (m_{AU}). Even though the solution reached adsorption equilibrium during the first adsorption, there were still

unsaturated active sites in the spent PAC. Therefore, the spent PAC would still adsorb the substrates when in contact with a fresh substrate solution. The mass adsorbed by these originally unsaturated sites (m_{AU}) was determined by carrying out a second adsorption without running a photodegradation experiment after the first adsorption. The mass of the substrate adsorbed due to photocatalytic regeneration was calculated as:

$$m_{AP} = m_{AT} - m_{AU} \quad (5.1)$$

The regeneration efficiency (%) was calculated as:

$$RE = 100 \times \frac{Q_{EAP}}{Q_{EA}} \quad (5.2)$$

where Q_{EAP} is the equilibrium adsorption capacity of the spent PAC due to photocatalytic regeneration and Q_{EA} is the equilibrium adsorption capacity of the fresh PAC.

5.2.3.5 Hydrodynamics experiments

Hydrodynamic experiments were carried out to determine the effect of the reactor inclination angle and superficial fluidization velocity on the solid concentration distribution and global gas holdup. The solid concentration distribution was determined by the method used by Matsumura et al. (2007) which involved sampling slurry solution from several points along the reactor height and analysing the solid concentration. In this method, 5 g/L of the CTS composite was added to 400 ml of water in the reactors. The reactors were then inclined to the appropriate angle and air sparging started and maintained at the required flow rate. The air sparging was continued for 10 minutes in order to stabilize the hydrodynamic behaviour of the reactor. Thereafter, 10 ml samples containing water and CTS composite particles were taken from the 4 sampling ports on the side of the reactor. The eye of the sampling needle was situated in the middle of the reactor. This ensured that the sampled solids were those that were fluidized and not those which may have settled on the reactor walls. The solid concentration in the samples was then analysed gravimetrically by filtering the liquid through a filter paper to retain the solids followed by drying the solid laden filter paper. The difference in weight of the filter paper before sample filtration and after drying was used to compute the solid concentration in the sample. The solid concentration at the different sampling ports in the reactor was used to determine the solid concentration distribution.

Global gas holdup measurement was carried out for all the reactors to characterize the fluidization behaviour of the individual reactors. The gas holdup measurement was carried out using the quick stop method (Abraham et al., 1992). In this method, the reactor was inclined at the appropriate angle and then a certain volume of water corresponding to the required aspect ratio was poured into the reactor. A mark was then made on the reactor wall corresponding to the gas-free level of the liquid. Then air sparging was started and maintained at the appropriate flow rate for 10 minutes for the reactor hydrodynamics to stabilize. After the flow had stabilized, another mark was made on the reactor wall to indicate the top level of the sparged liquid. The difference in the two marks gave an indication of the volume of the gas in the liquid and was used to determine the gas holdup.

5.2.4 Chemical analyses

The concentration of the target pharmaceuticals was determined using a UV-vis spectrophotometer (PG instruments T60) at λ_{max} of 256, 276, and 285 nm for sulfamethoxazole, diclofenac and carbamazepine, respectively. The samples were prepared for UV-vis analysis by removing solids through filtration using 0.45 μm GHP syringe filters. Solution turbidity was measured using a Hach DR2000 photometer using the FAU turbidity function. The pH measurements were performed using an Orion Star A111 pH meter (Thermo Scientific). The SEM analysis was carried out at magnifications of 500, 2000, 5000 and 200000 using a Carl Zeiss Auriga system at an accelerating voltage of 5.00 kV. X-Ray Fluorescence (XRF) analysis was carried

out by a Rigaku Primini machine. The XRF machine could only detect elements with element numbers above 8 and as such only TiO₂ and silica xerogel could be detected but not carbon. X-Ray Diffraction (XRD) measurements were carried out on a Shimadzu XRD-7000 X-Ray Diffractometer using CuK α radiation in the range $2\theta = 10-80^\circ$.

The anatase to rutile ratio in the TiO₂ was calculated as (Zhou et al., 2007).

$$\chi = \left(1 + \frac{0.8I_A}{I_R}\right)^{-1} \quad (5.3)$$

where χ is the weight fraction of rutile phase, I_A is the intensity of anatase (101) phase and I_R is the intensity of the rutile (110) phase.

5.2.5 Experimental design

A one factor at a time (OFAT) experimental design was used for the experiments. Table 5.2 shows the various experiments and the experimental parameters that were varied. There were two sets of parameter variation; the first set were those that were related to the material preparation while the other set were the operating parameters for photodegradation and hydrodynamics.

Table 5.2: The parameters investigated during the experiments using OFAT experimental design

Experiment	Parameters varied
Adsorption and photodegradation experiments	<ul style="list-style-type: none"> • Amount of silica xerogel in the CTS composite • PAC/TiO₂ ratio in the CTS composite • Mass of the CTS catalyst • Reactor inclination angle • Superficial air velocity • Initial concentration of the substrate solution • Initial pH of the substrate solution
Catalyst adherence experiments	<ul style="list-style-type: none"> • Amount of silica xerogel in the CTS composite
Regeneration experiments	<ul style="list-style-type: none"> • PAC/TiO₂ ratio in the CTS composite
Hydrodynamics experiments	<ul style="list-style-type: none"> • Reactor inclination angle • Superficial air velocity • Reactor aspect ratio

5.2.6 Data analyses

Microsoft Excel was used for all mathematical analyses. For the adsorption studies, the equilibrium adsorption capacity (q_e) (mg/g) was calculated as:

$$q_e = \frac{(C_0 - C_e)V}{m} \quad (5.4)$$

where C_0 is the initial substrate concentration (mg/L), C_e is the equilibrium substrate concentration (mg/L), V is the volume of the substrate solution (l) and m is the mass of the adsorbent (g).

The Langmuir adsorption isotherm was fitted by:

$$\frac{C_e}{q_e} = \frac{1}{K \cdot q_m} + \frac{C_e}{q_m} \quad (5.5)$$

where C_e is the equilibrium substrate concentration (mg/L), q_e is the equilibrium adsorption capacity (mg/g) and q_m is the maximum Langmuir adsorption capacity (mg/g)

The Freundlich adsorption isotherm was fitted by:

$$\log q_e = \log K_F + \frac{1}{n} \log C_e \quad (5.6)$$

where q_e is the equilibrium adsorption capacity (mg/g), C_e is the equilibrium substrate concentration (mg/L), K_F is the Freundlich capacity factor (mg/g(1/mg)^{1/n}) and $1/n$ is the Freundlich intensity parameter.

5.3 Results and discussion

5.3.1 Solar radiation at VUT

Solar photodegradation depends solely on sunlight for the energy source to activate the TiO₂ catalyst. For practical utility, it is important to know the quantity of solar energy available at the point-of-use and how the intensity of the solar radiation varies with seasons, weather and time of day. In order to obtain this information, the 5-minute radiation data collected at VUT weather station was summed up to obtain hourly, daily and monthly solar radiation data. The hourly, daily and monthly solar irradiation data gave a very good indication of how solar radiation intensity varies with time of day, weather and seasons, respectively. The solar photodegradation experiments in this work were carried out at the Vaal University of Technology (VUT) in Southern Gauteng region of South Africa.

5.3.1.1 Monthly solar irradiation data

Solar radiation data was collected from the month of May to November 2012. The irradiation data (Fig. 5.2) shows an increase in irradiation from the months of June to November at VUT. This is due to the fact that VUT is located in the southern hemisphere (26.7000° S, 27.8167° E) in the South Temperate Zone where winter starts late May as the sun moves towards the northern hemisphere of the earth. By June 21, during the winter solstice in the southern hemisphere, the sun is furthest from the equator resulting in the lowest monthly solar irradiation being recorded in the month of June. The movement of the sun to the northern hemisphere results in less radiation intensity and shorter days on the southern hemisphere. The combination of low solar radiation intensity and short days results in very low daily solar radiation during the winter months.

As the sun travels back to the southern hemisphere, the solar radiation increases gradually from June to December. By October, summer begins as the sun comes closer to VUT resulting in high radiation and longer days. The combination of high radiation intensity and longer days results in high daily radiation at VUT. Since solar photodegradation depends on the intensity of solar radiation, higher degradation is expected in the summer months than during winter. Therefore, photodegradation experiments were carried out during summer when the solar intensity was highest.

The preliminary data obtained at the VUT are significantly higher than those reported by Dekker et al. (2012) for the University of KwaZulu-Natal (UKZN) and University of Stellenbosch (US). In May, for example, the irradiation was 825 MJ/m² for VUT, and the figures are 387 MJ/m² and 291 MJ/m² for UKZN and US, respectively (Dekker et al., 2012). This shows a logical decreasing trend in the amount of radiation with an increase in the distance from the equator, US being the furthest from the equator compared to the other two locations.

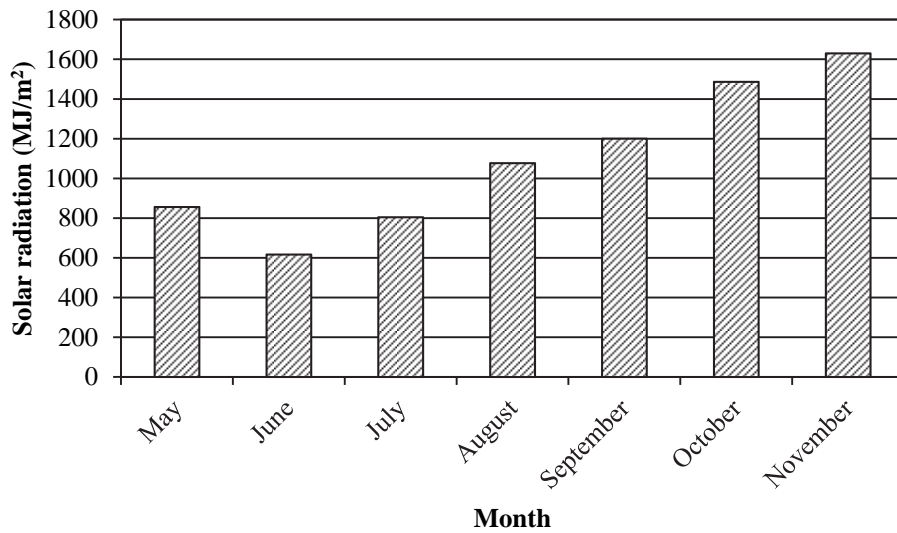


Fig. 5.2: Monthly solar radiation for May to November 2012 at VUT

5.3.1.2 Daily solar radiation data

The month of October 2012 was used as an example to show how the daily radiation varies from day to day during a single month. The daily radiation data (Fig. 5.3), shows great variations in radiation intensity between different days ranging from of 22 MJ/m² on 24th October to 66 MJ/m² on 31st October. The length of days in October was more or less similar; therefore, the days with low radiation intensity must have been due to the cloudiness of the sky. The solar radiation sensor that was used to collect the radiation data measured the global solar radiation which includes both direct and diffuse solar radiation. The direct solar radiation refers to the light that comes directly from the sun while diffuse radiation is light reflected from the clouds, lands, buildings and other objects. During cloudy days, the diffuse radiation remains more or less constant while the direct radiation reduces due to the fact that clouds block the direct sunlight. This reduction in direct solar radiation results in a reduction in the measured global solar radiation. In order to ensure the repeatability in the results of photodegradation, experiments were only carried out during sunny days.

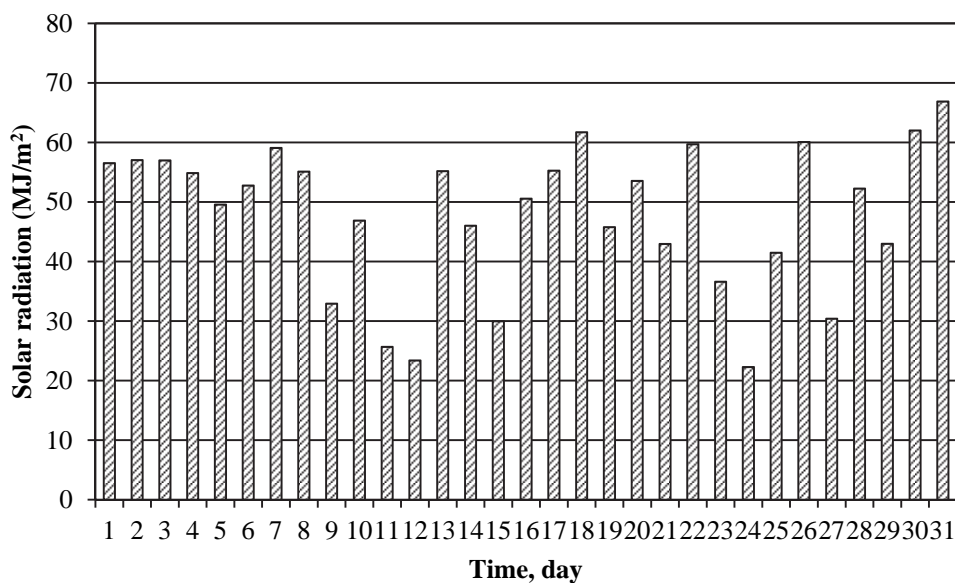


Fig. 5.3: Daily solar radiation for October 2012 at VUT

5.3.1.3 Hourly solar radiation data

Solar irradiation data for the cloudy day of 24/10/2012 (Fig. 5.4a) and the sunny day of 31/10/2012 (Fig. 5.4b) were used to determine the changes in radiation within a single day. The data show a general increase in radiation from sunrise to midday followed by a general reduction in irradiation as the day progresses to sunset with no solar radiation at night. The sun is furthest from the radiation sensor during sunrise and sunset resulting in low solar radiation. At noon, the sun comes closest to the radiation sensor resulting in an increased global radiation. These hourly radiation patterns were observed during both winter and summer. The rate of photodegradation is expected to decrease in the mornings and evenings as the rate of radiation decreases. During mid-morning, noon and early afternoon, the rate of photodegradation is expected to be highest due to high radiation. Therefore, photodegradation experiments were carried out between 9.30 am and 2.30 pm in order to ensure little change in the intensity of sunlight during the duration of the photodegradation.

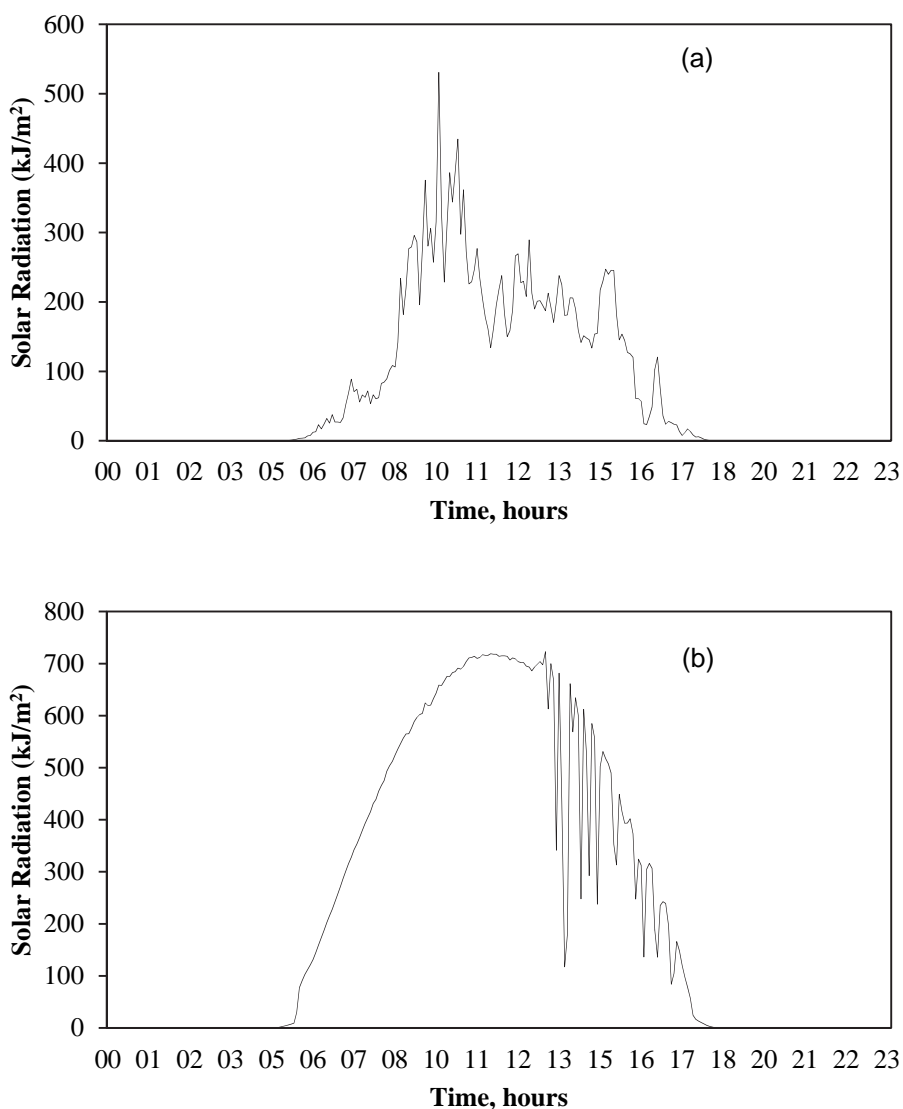


Fig. 5.4: Solar radiation data for (a) 24th October 2012 and (b) 31st October 2012 at VUT

5.3.2 Catalyst characterization

Catalyst characterization studies were carried out to analyse various features of the synthesized CTS composite, pure silica xerogel and the TS composite as well as their precursors: PAC and TiO_2 . The instruments used for catalyst characterization included SEM, XRD and XRF.

5.3.2.1 SEM analysis

SEM micrographs were taken in order to analyse the surface morphology and determine the sizes of the PAC, TiO_2 , pure silica xerogel, the TS composite and the CTS composite. The SEM micrographs of pure silica xerogel particles (Fig. 5.5a) and CTS (Fig. 5.5b) at a magnification of x500 indicate clearly that the size range of the pure silica xerogel and CTS composite particles was between 20 and 70 μm . The sizes of pure silica xerogel and CTS composite particles were consistent with the size range of the sieves used when preparing the pure silica xerogel and CTS composite (38-75 μm). There were very few particles of pure silica xerogel and CTS composite below 38 μm while the largest quantity of the particle size was between 38 and 75 μm . The shapes of both the pure silica xerogel and CTS composite particles in the SEM micrographs were irregular due to crushing when preparing the catalyst.

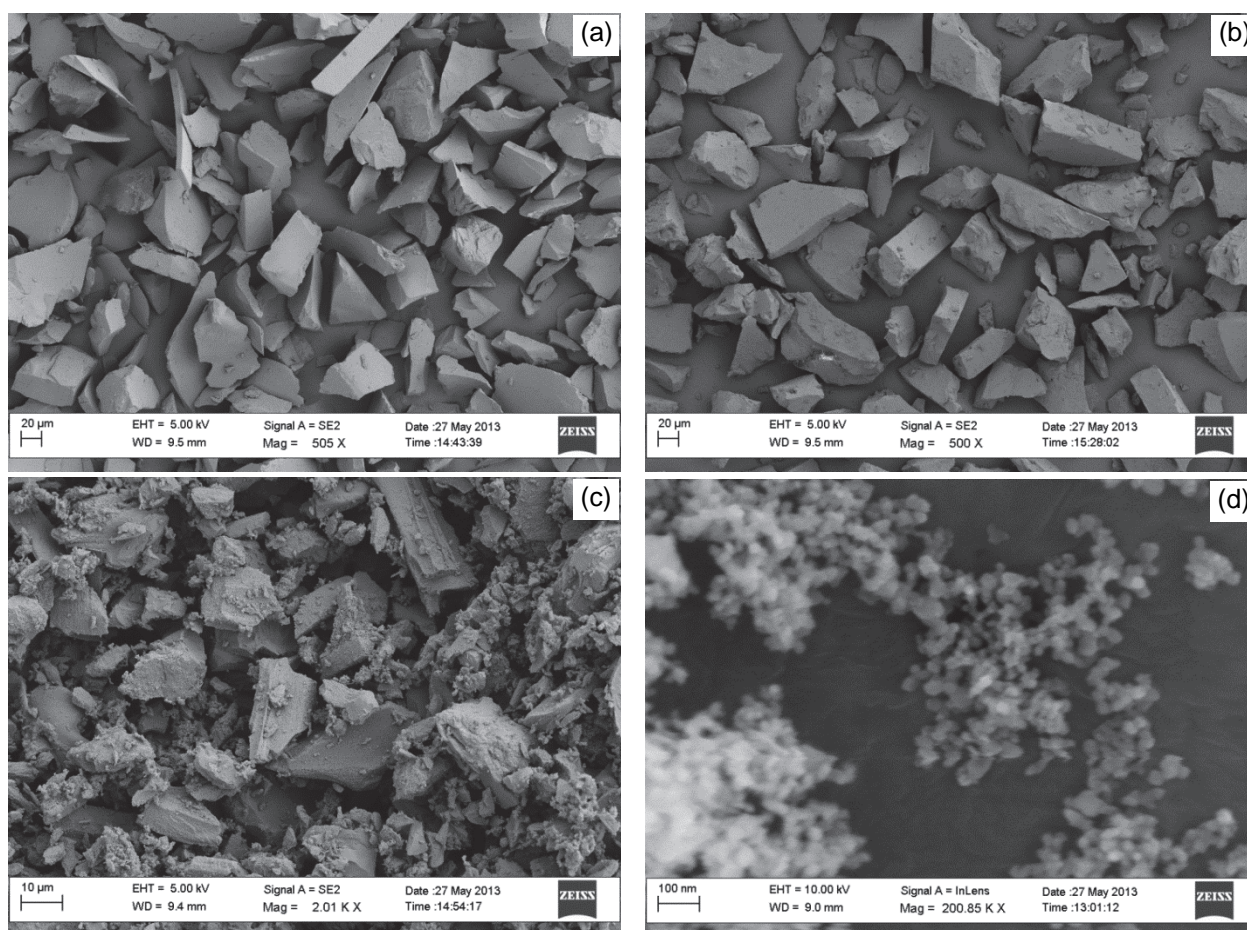


Fig. 5.5: SEM images of (a) pure silica xerogel, (b) CTS composite, (c) PAC and (d) TiO_2 ; CTS composition: 60% silica xerogel, 10% PAC/ TiO_2 ratio

At low magnifications, the SEM micrograph of the CTS composite particles appears similar to that of pure silica xerogel particles due to the fact that gelled silica was the matrix of both the CTS composite and the pure silica xerogel. Therefore, during the crushing step when the CTS composite and pure silica xerogel were being prepared, it is the gelled silica matrix that was crushed. Since the gelled matrix became irregular during crushing, both the SEM micrographs of pure silica xerogel particles and CTS composite particles looked similar.

The micrograph of the PAC particles (Fig. 5.5c) at a magnification of x2000, shows a wide size range with most particles having sizes of almost 5 μm and a few particles having large sizes of 20 μm . During the preparation of the CTS composite, a mixture of the small-sized PAC and the large sized PAC entered the CTS composite matrix. Although SEM is not effective in determining the sizes of nanoparticles such as the P25 TiO_2 , an approximation in size could be made at high magnifications of x200,000 (Fig. 5.5d). The TiO_2 nanoparticles were observed to be approximately 25 nm and the particles seemed to be spherical with a uniform size. Similar particle sizes (15-25 nm) of P-25 TiO_2 have been reported by Porter et al. (1999).

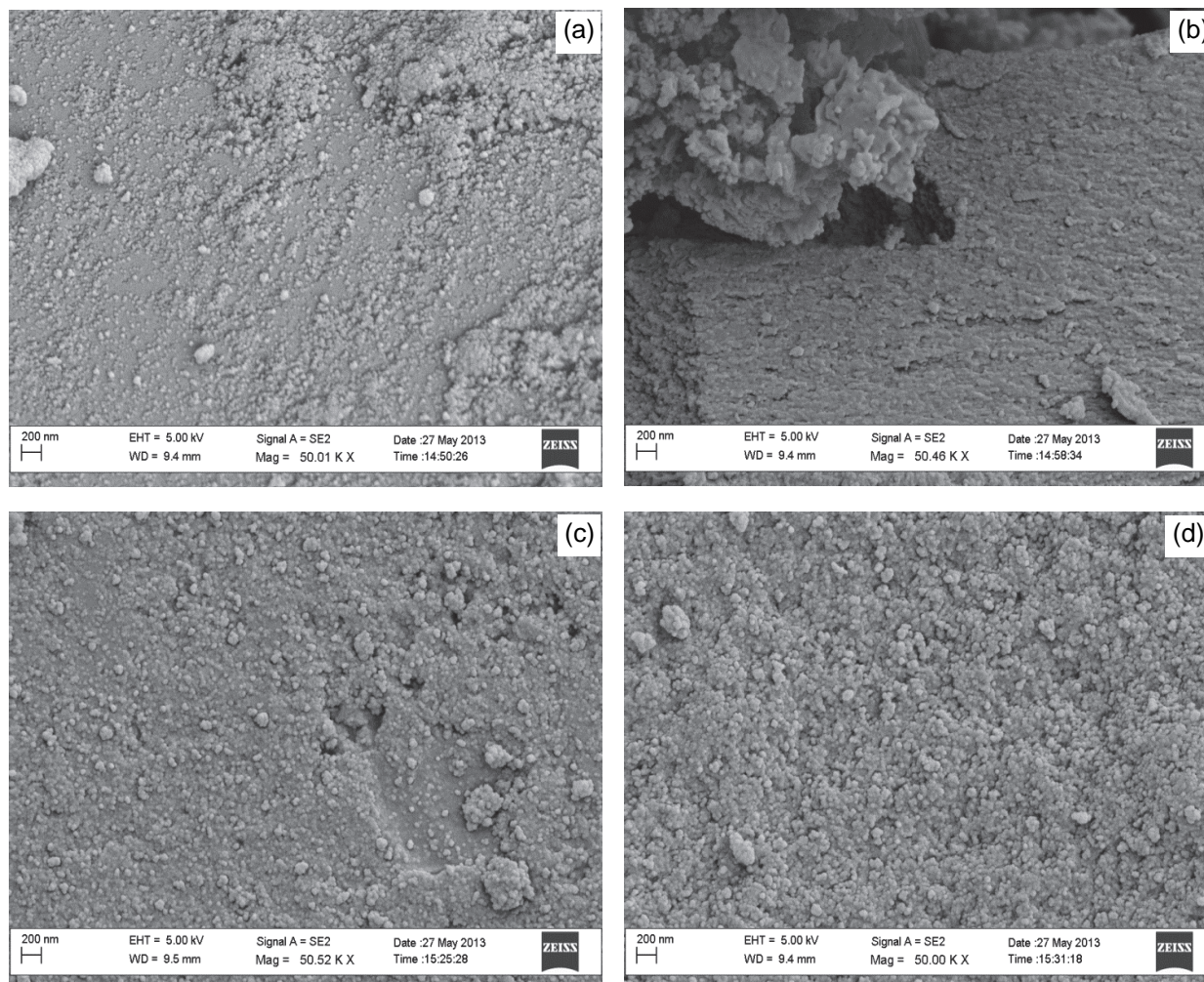


Fig. 5.6: High magnification SEM images of (a) silica xerogel, (b) small sized PAC and large sized PAC, (c) TS composite and (d) CTS composite; CTS composition: 60% silica xerogel, 10% PAC/ TiO_2 ratio

The high magnification (x50,000) SEM images of pure silica xerogel (Fig. 5.6a), PAC (Fig. 5.6b), TS composite (Fig. 5.6c) and the CTS composite (Fig. 5.6d) show the surface morphology of the various catalyst compositions. The SEM images of pure silica xerogel (Fig. 5.6a) and that of the TS composite (Fig. 5.6c) show very little porosity. However, when PAC was added to the silica xerogel and TiO_2 matrix to form the CTS composite, the porosity increased markedly as shown in Fig. 5.6d. PAC increased the porosity of the CTS composite due to the high porosity of PAC formed during the activation of its precursors (Suhass et al., 2007). Figure 5.6b shows the SEM image of two sizes of PAC, the large sized PAC occupying most of the figure with the small-size PAC by the top-left corner. The small-sized PAC has a very high porosity as compared to the large sized PAC. A mixture of the small-sized PAC and the large-sized PAC formed part of the CTS composite increasing the porosity of the composite. The high porosity of the CTS composite is expected to result in a higher rate of adsorption of pollutants on the CTS composite than on either the pure

silica xerogel or the TS composite. Therefore, a high rate of degradation of the pharmaceutical pollutants is expected with the CTS composite.

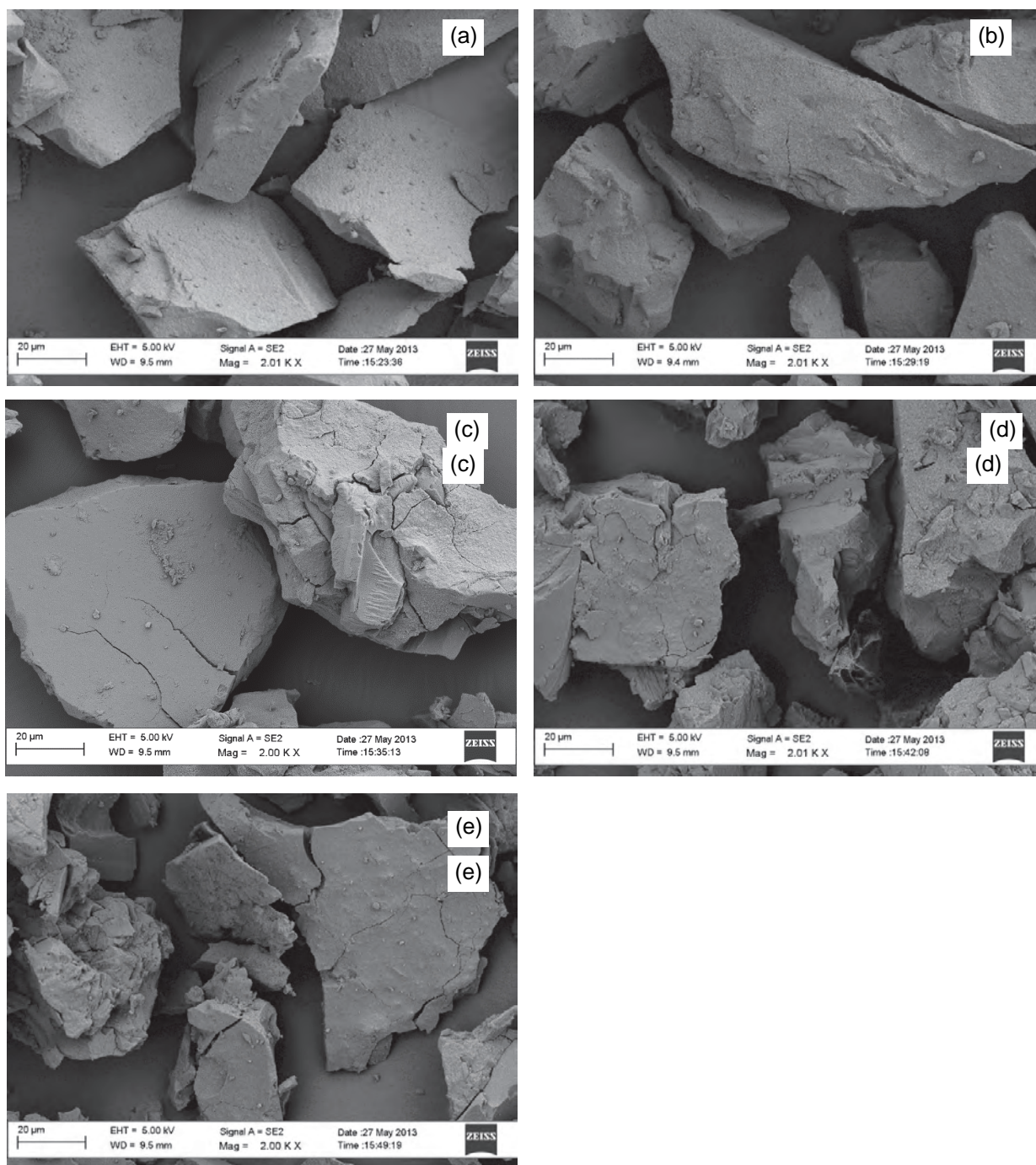


Fig. 5.7: SEM images of various CTS composites with varying PAC/TiO₂ ratios: (a) 100%, (b) 80% (c) 60% (d) 40% (e) 20%; CTS composition: 60% silica xerogel loading

SEM images of various CTS composites with different PAC/TiO₂ ratios were taken in order to analyse the effect of the PAC/TiO₂ ratio on the morphology of the CTS composite. The SEM images (Fig. 5.7) show an increase in cracks in the CTS composite with increase in the PAC/TiO₂ ratio. Increasing the PAC in the CTS composite led to an increase in the number of the large sized PAC (Fig. 5.6b) entering the CTS composite matrix. Therefore cracks tended to form in the CTS composite at the edges of the large sized PAC. This is due to the fact that the large sized PAC of up to 20 µm occupied a large volume of the 38 µm CTS

composite. The cracks exposed the surface of the PAC that would have been covered by the silica xerogel.

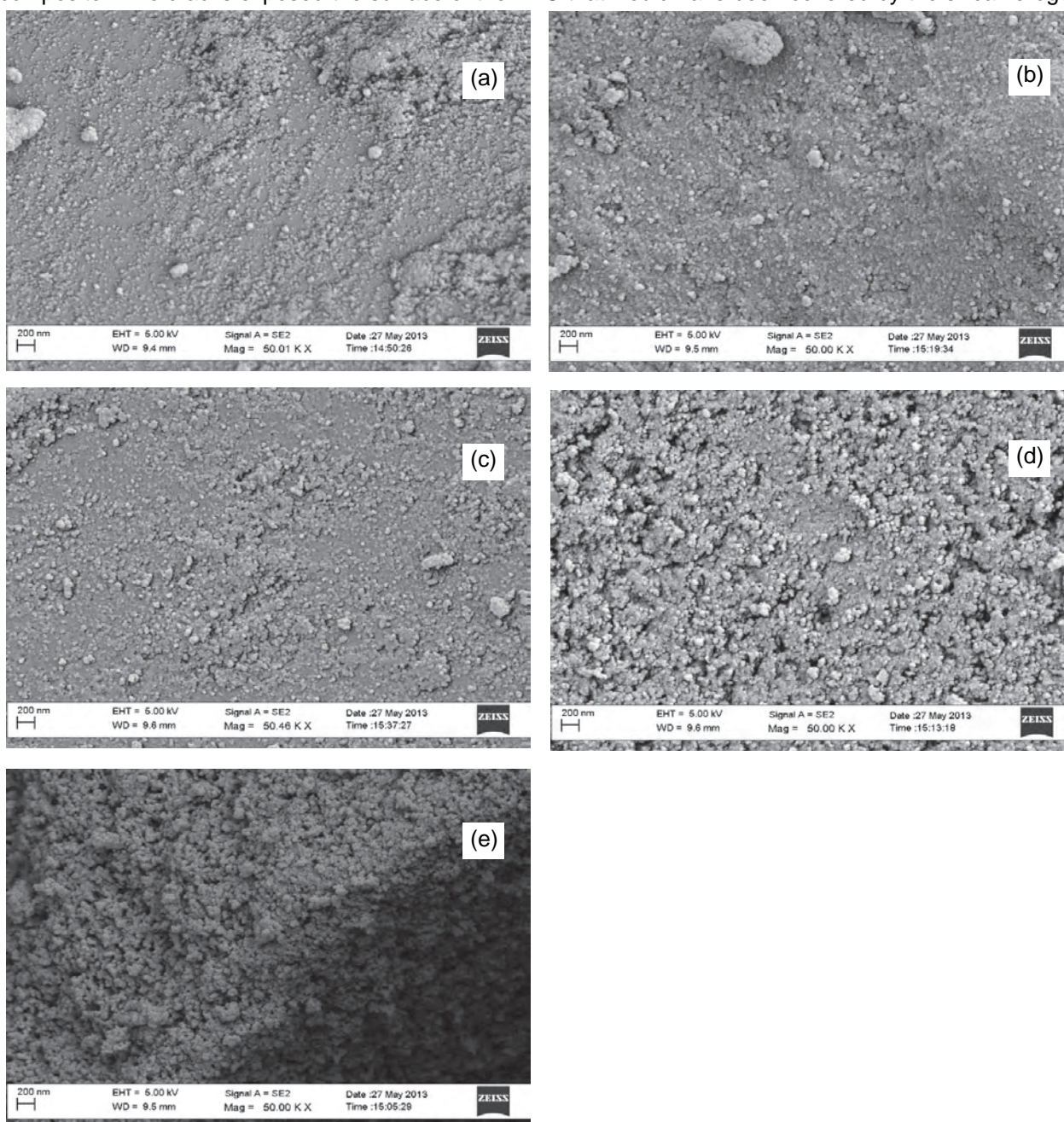


Fig. 5.8: SEM images of various CTS composites with varying silica xerogel loading: (a) 100%, (b) 80% (c) 60% (d) 40% (e) 20%; CTS composition: 20% PAC/TiO₂ ratio

The presence of these cracks increased the surface area available for adsorption of the substrates. Therefore an increase in adsorption of the substrates with an increase in the PAC/TiO₂ ratio was expected.

The SEM analysis was also carried out in order to determine the effect of silica xerogel loading on the morphology of the CTS composite. To analyse the effect of silica xerogel loading, SEM images of various CTS composites at a fixed PAC/TiO₂ ratio of 20% were taken. The images (Fig. 5.8) show an increase in the porosity of the CTS composite with decreasing silica xerogel loading. This porosity is mostly pronounced in the CTS composites with 20% silica xerogel loading and 40% silica xerogel loading. In order to bind the PAC and TiO₂ together, the silica xerogel traps together the PAC and TiO₂ in its matrix. This process may lead to some PAC and TiO₂ particles having their surfaces covered by the silica xerogel. Decreasing the amount of silica xerogel in the CTS composite therefore exposes more of the porous PAC surfaces. An increase in the exposure of the porous PAC surfaces led to an increase in the porosity of the CTS composite

with decreasing silica xerogel loading. This increase in the porosity of the CTS composite is expected to result in an increase in the adsorption of the substrates with increasing PAC/TiO₂ ratios.

5.3.2.2 XRD analysis

XRD analysis was used to obtain the crystallographic composition of the PAC, TiO₂, pure silica xerogel and CTS composite. The XRD spectra (Fig. 5.9) show that both the CTS composite and the P-25 TiO₂ had anatase and rutile phases. The anatase and rutile phases originate from the P-25 TiO₂ and can remain visible in any mixtures of P-25 TiO₂ with other materials. The I_A/I_R as well as the percentage of rutile and anatase phases in P-25 TiO₂ and CTS composite as calculated by Eqn. (5.3) are shown in Table 5.3.

Table 5.3: Percentage of rutile and anatase in the P-25 TiO₂ and CTS composite

Sample	I_A/I_R	Rutile (%)	Anatase (%)
P-25 TiO ₂	6.05	17.1	82.9
CTS composite	4.53	21.6	78.4

The percentage of rutile phase in the P-25 TiO₂ was found to be 17.1%. This is very similar to the value 20% rutile reported by Guillard et al. (1999). There is a marked similarity between the rutile and anatase peaks in both the XRD spectra of P-25 TiO₂ and the CTS composite. The percentage of rutile and anatase phases in the P-25 TiO₂ and the CTS composite were also very close. These similarities between the anatase and rutile phases of P-25 TiO₂ and the CTS composite show that incorporating PAC and silica xerogel in a matrix with P-25 TiO₂ did not significantly change the rutile/anatase phase ratio of P-25 TiO₂ in the CTS composite. This suggests that neither silica xerogel nor PAC reacted with either the rutile or anatase phase of the TiO₂ and that the mixture of PAC, silica xerogel and TiO₂ was merely physical. This is important since one of the reasons Aeroxide P-25 TiO₂ grade has been found to be highly active is due to its well-balanced rutile/anatase phase ratio (Hurum et al., 2003). Maintaining the rutile/anatase phase ratio of the TiO₂ in the CTS composite was therefore very crucial in order to maintain the high reactivity of the P-25 TiO₂.

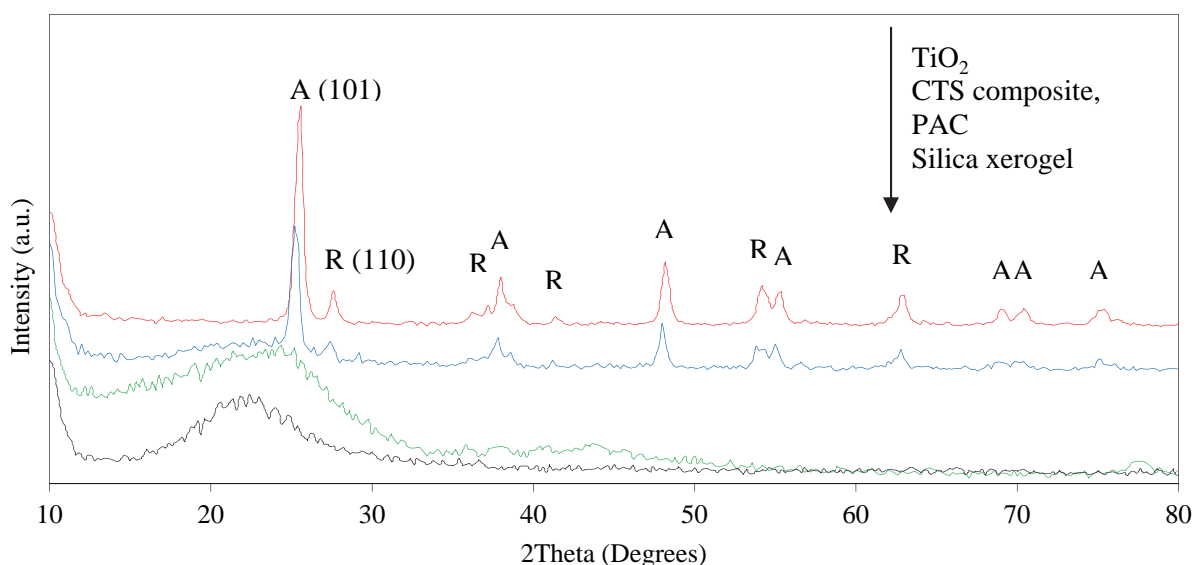


Fig. 5.9: XRD spectra of CTS, TiO₂, PAC, and pure silica xerogel; A-Anatase, R-Rutile; CTS composition: 60% silica xerogel, 10% PAC/TiO₂ ratio

The pure silica xerogel remained in amorphous state as shown by the absence of peaks due to the fact that the low temperature (90°C) used during the preparation was far below the 300°C temperature at which amorphous silica starts crystallizing into cristobalite (Bettermann and Liebau, 1975). Similarly, the as-

received activated carbon which did not show any peaks in the XRD spectrum was amorphous. Other studies have also found from XRD analysis that AC is amorphous (Zieliński et al., 2005).

5.3.2.3 X-Ray Fluorescence Spectroscopy (XRF) analysis

XRF analysis was carried out to determine the molecular composition of CTS composites of different silica xerogel loading. Carbon could not be quantified by the XRF spectroscope used in this work but silica xerogel and TiO₂ could be quantified therefore all results were expressed in carbon-free basis. The results of the XRF analysis for the various samples together with the theoretical compositions are shown in Table 5.4. The theoretical amount of silica xerogel which refers to the quantity of silica xerogel measured during the preparation of the CTS composite was more than the true quantity of silica xerogel in the CTS composite as measured by XRF. This shows that a more significant portion of colloidal silica or silica xerogel was lost during preparation than TiO₂. A significant portion of the colloidal silica contains NaOH used to stabilize the silica sol to prevent gelling while in storage. The acid wash during the synthesis of the CTS composite resulted in the removal of the NaOH in the CTS composite. Since the NaOH was part of the theoretical silica xerogel during measurement, its removal in the process of preparation resulted in the observed difference between the theoretical and true loading of silica xerogel onto the CTS composite. However, the difference is small (less than 10%) showing that the preparation process did not significantly affect the desired composition of the CTS composite. The XRF results thus validate the effectiveness of the method used to synthesize the CTS composite.

Table 5.4: Carbon free basis XRF results vs theoretical compositions for various silica loadings

CTS composition (silica xerogel, %)	Silica xerogel (Theoretical)	Silica xerogel (XRF)	Difference	TiO ₂ (Theoretical)	TiO ₂ (XRF)	Difference
20	23.8	20.2	-3.6	76.2	79.8	3.6
40	45.4	36.2	-9.2	54.5	63.8	9.3
60	65.2	56.2	-9.0	34.8	43.8	9.0
80	83.3	73.5	-9.8	16.6	26.5	9.9
100	100.0	100.0	0.0	0.0	0.0	0.0

5.3.3 Catalyst composition and performance

The CTS catalyst consisted of three components: PAC, TiO₂ and silica xerogel. When analysing the relative amounts of silica in the CTS composite, the amount of silica xerogel was used and not the colloidal silica. The relative amounts of each of the components in the CTS composite had an effect on the percentage adsorption and degradation of the substrates, the regeneration efficiency of the PAC, as well as the attachment stability of TiO₂ and PAC on the silica xerogel. Therefore, it was crucial to investigate the effects of the proportion of silica xerogel in the CTS composite and the PAC/TiO₂ ratio of the composite on the rate of adsorption and photodegradation of the substrates. The optimum composite catalyst characteristics were decided based on the percent adsorption and photodegradation of the substrates, the regeneration efficiency of PAC and the adherence stability of TiO₂ and PAC on the silica xerogel.

5.3.3.1 Effect of silica xerogel in the CTS composite on adsorption and photodegradation

Silica xerogel is an important constituent of the CTS composite as it binds together the TiO₂ catalyst and the PAC adsorbent. The proportion of silica xerogel in the CTS composite influences the catalyst adherence stability and also affects the fraction of TiO₂ and PAC in the composite. The quantity of TiO₂ and PAC in turn affects the photoactivity and adsorption capacity of the CTS composite. Several experiments were carried out to determine the effect of the proportion of silica xerogel in the CTS composite on the rate of adsorption and photodegradation of SMX, DCF and CBZ. The results (Fig. 5.10a-c) show an increase in the adsorption

and photodegradation of the substrates with a decrease in the percentage of silica xerogel in CTS composite.

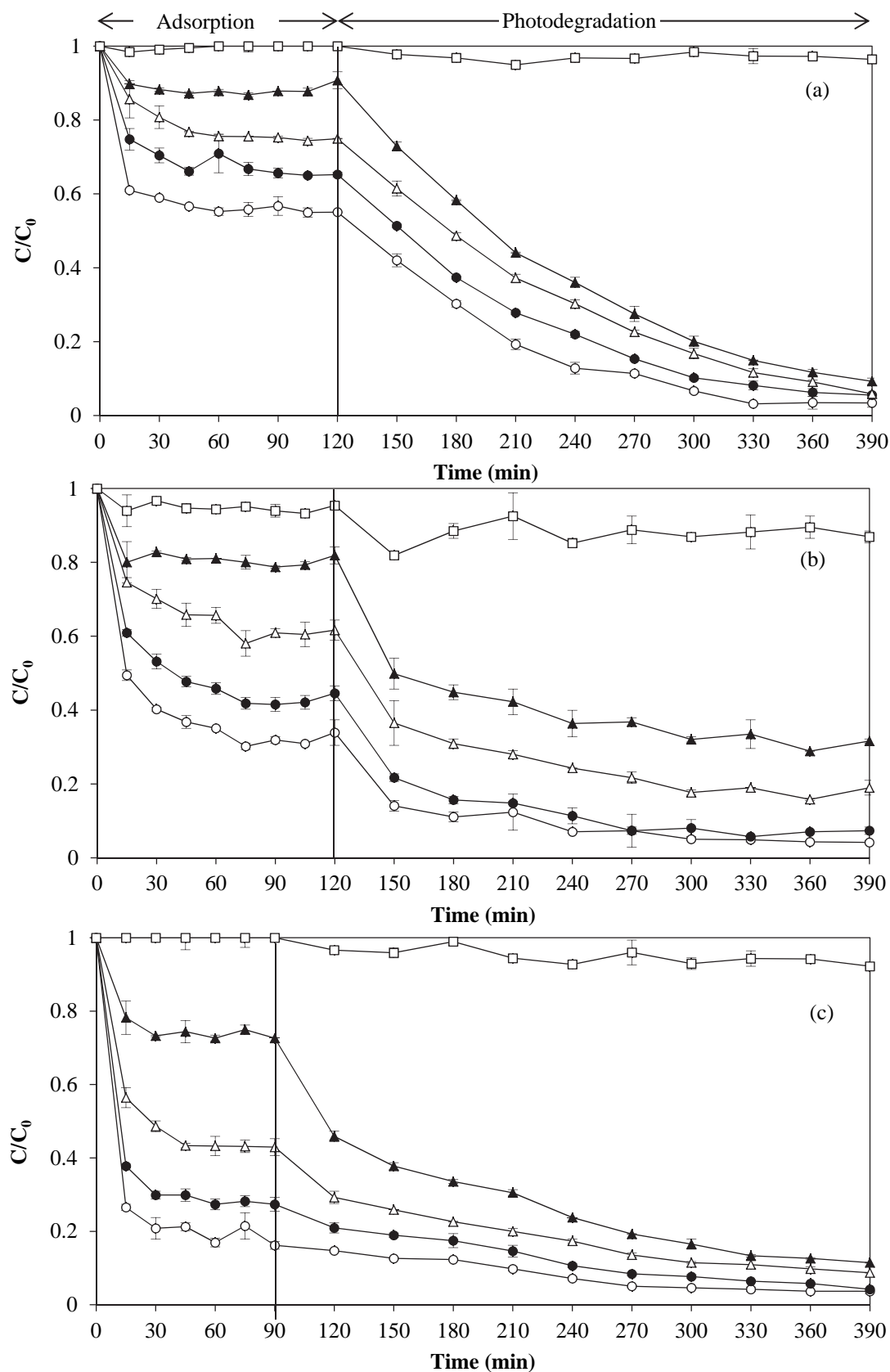


Fig. 5.10: Effect of proportion (%) of silica xerogel in the CTS composite on the rate of adsorption and photodegradation of (a) SMX, (b) DCF and (c) CBZ; $C_0 = 10$ mg/L, mass of CTS = 0.5 g, AC/TiO₂ ratio = 20%, superficial air velocity = 0.014 m/s

This observation could be explained in terms of the effect of silica on the other constituents of the CTS composite: TiO₂ and PAC. The major function of silica is the binding of TiO₂ onto PAC. However, an increase in the silica xerogel loading in the CTS composite could reduce the porosity of the CTS composite and this could lead to a decrease in adsorption and consequently in photodegradation. Also, the increase in the detachment of TiO₂ and PAC from the composite during the experiment (evidenced by an increase in solution turbidity) led to an increase in adsorption and photodegradation. This is due to the fact that the TiO₂ and PAC had a higher surface area for adsorption and photodegradation when detached than when attached onto the silica xerogel.

There was very little adsorption and photodegradation when pure silica xerogel (100%) was used in the control experiment. Pure silica xerogel exhibited very little adsorption capacity due to its low porosity (Fig. 5.6a) which resulted in the silica xerogel having few active sites for adsorption of substrate molecules. The low photodegradation efficiency of silica xerogel was due to the fact that silica xerogel is an insulator and not an active photocatalyst (Fox and Dulay, 1993). Decreasing the proportion of silica xerogel in the CTS composite resulted in an increase in the amount of TiO₂ and PAC in the composite. An increase in the amount of PAC in the CTS composite resulted in an increase in PAC active sites for adsorption of the substrates leading to the observed increase in adsorption. Similarly, an increase in the amount of TiO₂ led to an increase in the number of active sites for photocatalytic degradation of the substrates resulting in an increase in photodegradation of the substrates. Similar results were reported by Zainudin et al. (2010) when phenol was degraded using a composite catalyst made of nano-TiO₂ and ZSM-5 attached onto large 0.5 mm silica gel beads using colloidal silica. They found that increasing the proportion of colloidal silica in the composite catalyst decreased the rate of degradation of phenol but they did not offer an explanation for their result.

Some of the results from Fig. 5.10a-c are summarised in Table 5.5 which shows the percentage adsorption, adsorption equilibrium time and percentage photodegradation of the substrates using the CTS composite with 60% silica xerogel. The results show that the percentage adsorption increased as: CBZ>DCF>SMX while the percentage photodegradation increased in the opposite direction as: SMX>DCF>CBZ. The equilibrium adsorption time for SMX and CBZ was 60 minutes while that of DCF was 90 minutes. The differences in adsorption and photodegradation are related to the hydrophobicity and ionic states of the SMX, DCF and CBZ solutions and how they interact with PAC and TiO₂ surfaces.

Activated carbon can adsorb substrates through electrostatic interactions and also through non-electrostatic interactions such as hydrophobic interactions. Electrostatic interactions refer to the attraction that occurs between activated carbon and a substrate molecule with a charge opposite to the surface charge of activated carbon. Hydrophobic interactions occur when hydrophobic substrates are rejected by water and are thus attracted to the hydrophobic activated carbon (Moreno-Castilla, 2004).

Table 5.5: Adsorption, adsorption equilibrium time and photodegradation of SMX, DCF and CBZ of CTS composite catalyst with 60% silica xerogel

Chemical	Adsorption (%)	Equilibrium time (min)	Photodegradation (%)
SMX	25	60	69
DCF	38	90	43
CBZ	57	60	34

The activated carbon used in the synthesis of the CTS composite had a zero point charge of 6.3 (Fig. A 7). In solutions of SMX, DCF and CBZ, the PAC surface was positively charged. SMX has two pK_as: 1.8 and 5.6 (Brogat et al., 2013). Below pH 1.8, SMX is positively charged while above pH 5.6, it is negatively charged. Between pH 1.8 and 5.6, SMX is uncharged. Therefore the SMX molecules were uncharged at pH 4.6, the natural pH of SMX solution. There was relatively little attraction between the positively charged activated carbon surface and the uncharged SMX molecules resulting in low percent adsorption. There was also little adsorption of SMX through hydrophobic interaction with activated carbon due to the low

hydrophobicity of SMX evidenced by its low $\text{Log } K_{ow}$ of 0.9. DCF has a $\text{p}K_a$ of 4.2 (Brogat et al., 2013) and natural pH of 5.0, therefore in the DCF natural solution, the DCF molecules were negatively charged. The positively charged PAC surface attracted and adsorbed the DCF molecules resulting in a high adsorption. However, there was very little adsorption of DCF onto PAC through hydrophobic interactions due to its low $\text{Log } K_{ow}$ of 0.7. CBZ has 2 $\text{p}K_a$ s: 2.3 and 13.9 (Yu et al., 2008) and was therefore uncharged in its solution of pH 6. There was very little adsorption of the uncharged CBZ molecules onto the negatively charged PAC by the mechanism of electrostatic attractions. However, CBZ is very hydrophobic as shown by its high $\text{Log } K_{ow}$ value of 2.5. Therefore, a lot of the hydrophobic CBZ molecules were adsorbed on the PAC. Higher $\text{Log } K_{ow}$ values indicate that a substrate is relatively more hydrophobic (Moreno-Castilla, 2004).

Both SMX and DCF had low hydrophobicity as indicated by their low $\text{Log } K_{ows}$ of 0.9 and 0.7, respectively. However, CBZ had a high hydrophobicity as indicated by its high $\text{Log } K_{ow}$ of 2.5. Therefore, the adsorption mechanism of CBZ was primarily hydrophobic interactions while the adsorption mechanism of SMX and DCF was primarily electrostatic attractions. Although the adsorption of SMX was primarily through electrostatic attraction, more SMX was adsorbed through hydrophobic interactions than DCF. The adsorption of DCF was higher than that of SMX due to the fact that SMX was uncharged while DCF was positively charged. The adsorption of CBZ through hydrophobic interactions was higher than the adsorption of DCF through electrostatic attraction. This is probably due to a higher density of chemical species on the PAC surface responsible for hydrophobicity than those species responsible for electrostatic attractions. This would also explain the fact that adsorption via hydrophobic interactions was faster than that via electrostatic interactions. The difference in the rate of adsorption is indicated by the short equilibrium adsorption time (60 min) achieved by CBZ and the long adsorption equilibrium time (90 min) achieved by DCF.

The varying extent of photodegradation of SMX, DCF and CBZ in solution was determined by the adsorption of the substrates by the PAC. With an increase in the adsorption of the substrates, more of the hydroxyl radicals photodegraded the substrates adsorbed on the PAC and concentrated near the TiO_2 . Therefore, there were fewer hydroxyl radicals to photodegrade the substrates in solution. This explains the decrease in the photodegradation of the substrates in solution with an increase in the adsorption of the substrates at the beginning of the experiment.

Silica xerogel was used in the CTS composite to bind PAC and TiO_2 together. To determine the adherence stability of CTS composite with different silica xerogel loadings, the turbidity of the reaction solution was analysed after photodegradation. The turbidity gave an indication of the amount of fines that detached from the CTS catalyst during the experiment. The results (Fig. 5.11a-c) show a decrease in turbidity with increasing proportion of silica xerogel in the composite catalyst up to an optimum of 60% silica xerogel in the CTS composite catalyst. However, the turbidity of DCF solution (Fig. 5.11b) showed a slight increase when the proportion of silica xerogel in the composite was increased from 60% to 100%. This increase in the turbidity of DCF was due to the change in colour of the DCF solution from clear to brown during photolysis caused by brown coloured intermediates. Similar brown colouring of DCF solution during photolysis was observed by Pérez-Estrada et al. (2005) and was attributed to the formation of carbazole structures. The composite catalyst of 80% and 100% silica xerogel could not degrade these brown intermediates within the reaction time. Therefore, the brown colour persisted and increased the measured turbidity values of DCF solutions catalysed by composites of 80% and 100% silica xerogel. Turbidity is due to the presence of particles in solution that reflect light. The carbazole structures have low solubility and therefore they form precipitates which result in higher readings during turbidity measurements.

If there had been no precipitates in DCF solutions, the measured turbidity of DCF solution would have decreased with increasing proportion of silica xerogel in the CTS composite as was the case with SMX and CBZ solutions. These results are expected since decreasing the proportion of silica xerogel in the composite resulted in a decrease in the binding power of silica xerogel which lead to the loss of TiO_2 and PAC fines. The loss of TiO_2 and PAC fines from the CTS catalyst is undesirable in continuous operation as this would result in the reduction in the activity of the catalyst during the succeeding cycles of reuse. The fines would

also end up in treated wastewater leading to a secondary pollution problem from nanoparticles in the effluent of the wastewater treatment system. Since the prevention of detachment of the components of the CTS catalyst was a priority, the CTS catalyst with a silica xerogel loading of 60% was chosen as the optimum. This is due to the fact that the CTS with 60% silica xerogel loading had a good balance between high adsorption and photodegradation efficiency and excellent adherence stability.

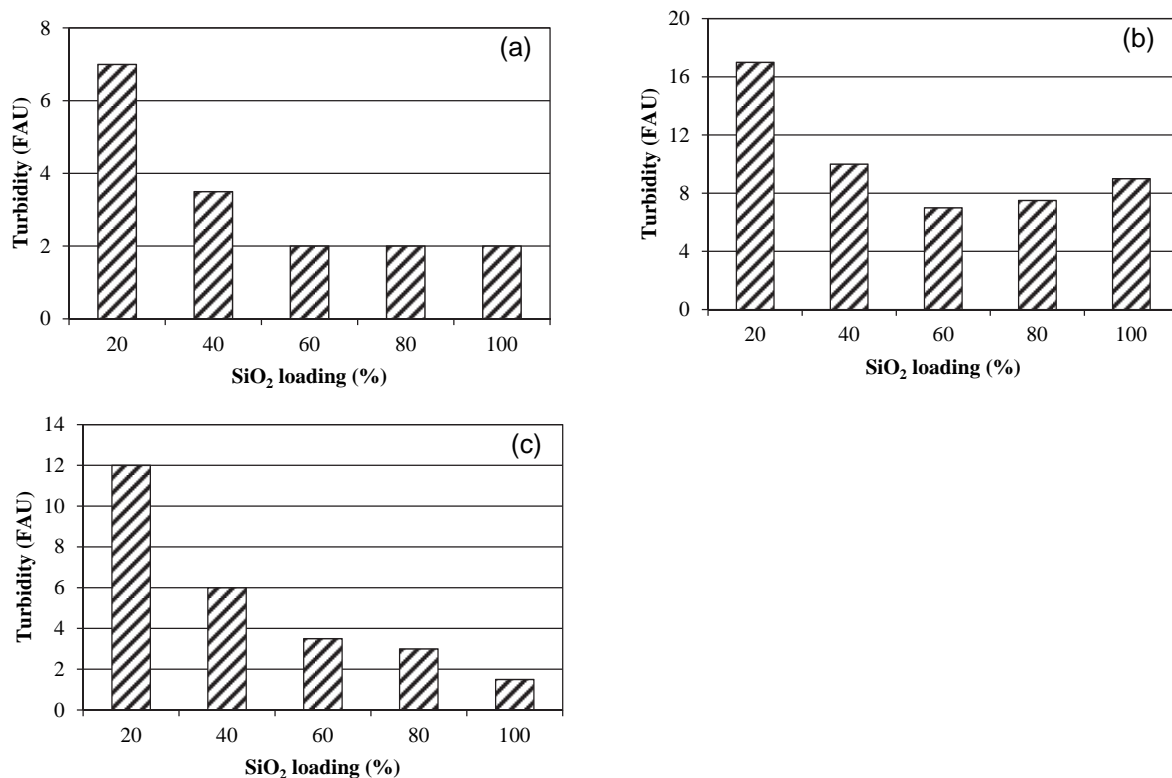


Fig. 5.11: Effect of proportion of silica xerogel (10%) in the composite on the turbidity of (a) SMX, (b) DCF and (c) CBZ; $C_0 = 10$ mg/L, mass of CTS = 0.5 g, AC/TiO₂ ratio = 20%, superficial air

5.3.3.2 Effect of PAC/TiO₂ ratio in the composite catalyst on adsorption and photodegradation

After obtaining the optimum silica xerogel loading in the CTS composite, the amount of the PAC and TiO₂ in the composite was determined by varying the PAC/TiO₂ ratio in the composite. Obtaining the optimum PAC/TiO₂ ratio in the CTS composite was crucial since the ratio determined the effectiveness of the regeneration of the PAC by TiO₂. Experiments were carried out to determine the effect of PAC/TiO₂ ratio in the composite catalyst on the adsorption and photodegradation of SMX, DCF and CBZ. The results (Fig. 5.12a-c) show an increase in adsorption but a decrease in photodegradation of the substrates with increasing PAC/TiO₂ ratio in the composite catalyst. The TS composite (0% PAC/TiO₂ ratio) which was made of only silica xerogel and TiO₂ showed very poor adsorption due to its low porosity (Fig. 5.6c) and therefore few active sites for adsorption. Adding the PAC to the TS composite to form the CTS composite increased the adsorption of the substrates due to the presence of PAC in the composite. This is due to the fact that the PAC had very high porosity (Fig. 5.6d) which provided sufficient active sites for the adsorption of the substrates.

An increase in the fraction of PAC in the CTS composite resulted in an increase in sites for adsorption at the expense of sites for photodegradation. Therefore increasing the PAC/TiO₂ ratio increased the extent of adsorption but reduced the extent of photodegradation. However, during photodegradation, the removal of the substrates reduced with increasing PAC/TiO₂ ratio, which is due to the reduction in the amount of TiO₂ in the CTS composite. The removal of the substrates by the CTS composites with low PAC/TiO₂ ratios increased markedly during photodegradation. However, the composites with high PAC/TiO₂ ratios had lowered the

residual concentration of the substrates in solution so much during adsorption that the composites with low PAC/TiO₂ ratio only achieved a similar residual concentration after 300 minutes of treatment.

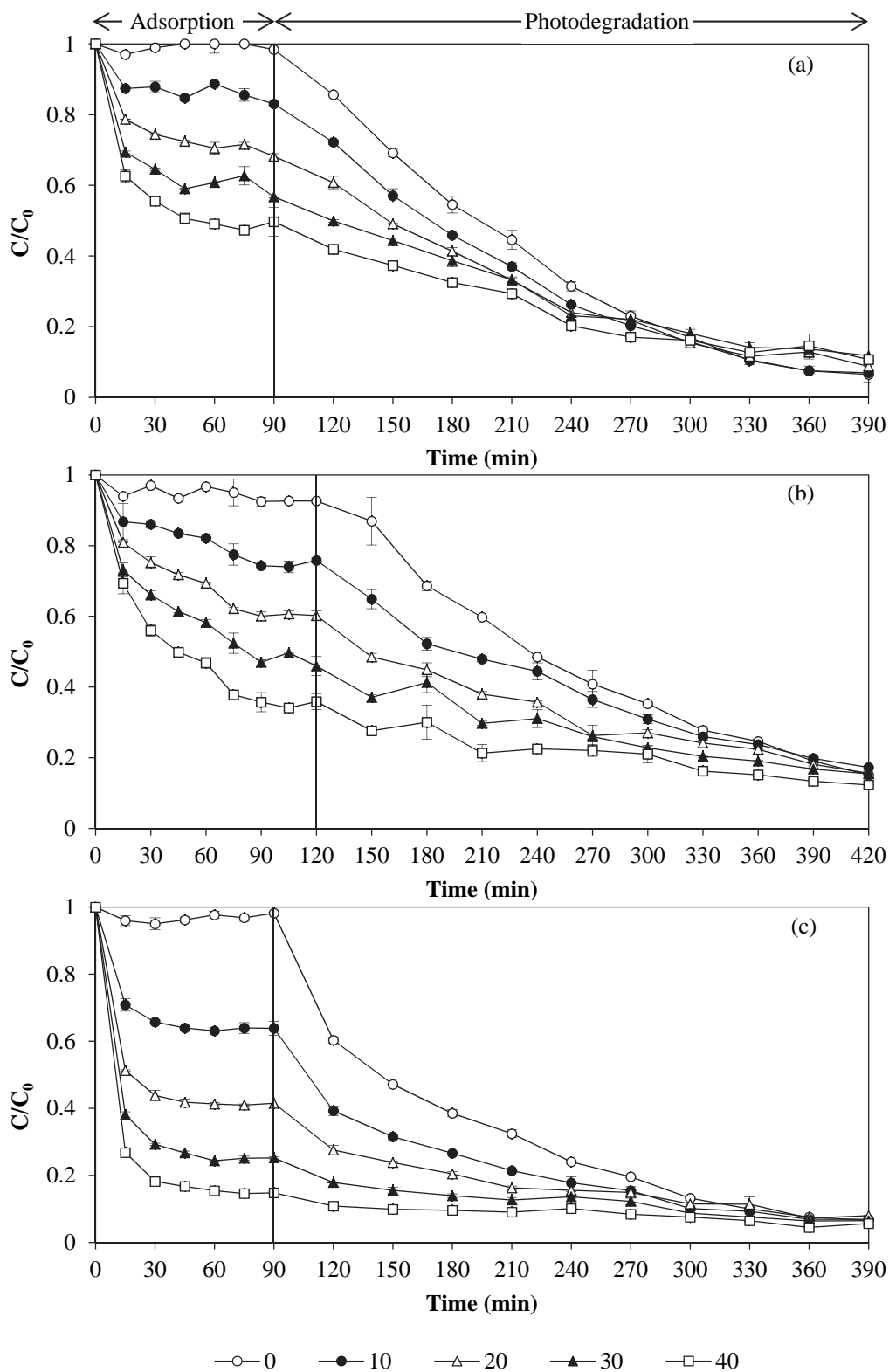


Fig. 5.12: Effect of PAC/TiO₂ ratio (%) on the rate of adsorption and photodegradation of (a) SMX, (b) DCF and (c) CBZ; $C_0 = 10$ mg/L, mass of CTS = 0.5 g, silica xerogel loading = 60%, superficial air velocity = 0.014 m/s

Table 5.6 summarises various performance parameters of different CTS composites with varying PAC/TiO₂ ratios for the removal of the substrates from wastewater. The adsorption capacity of the substrates on the fresh PAC adsorbent (Q_{EA}) decreased with an increase in the mass of the PAC adsorbent. For a fixed initial concentration of the substrate and a fixed volume of the substrate solution, the concentration gradient between the bulk substrate solution and the surface of the PAC decreased with an increase in the mass of the PAC adsorbent. This was due to the splitting effect of the concentration gradient between the bulk solution and the surface of the PAC. Since the adsorption capacity is proportional to the concentration gradient, the adsorption capacity decreased with a decrease in the concentration gradient when the mass of the PAC was increased (Kumar and Porkodi, 2007).

The TiO₂ in the CTS composite was responsible for the photodegradation of the substrates after exposure of the CTS composite to sunlight. This is due to the fact that P-25 TiO₂ has a band gap energy of 3.10 eV and therefore could be activated by light of wavelength below 400 nm (Nagaveni et al., 2004). Solar UV in the range of 310-400 nm (UV class A) could therefore activate the TiO₂ in solution to form hydroxyl radicals which then attacked and degraded the substrates in the solution. During photodegradation, the TiO₂ photodegraded both the substrates in solution and the substrates that had been adsorbed onto the PAC. The photodegradation of the substrates that was adsorbed onto the PAC regenerated the PAC and the efficacy of this regeneration was expressed as the regeneration efficiency (RE).

The regeneration efficiency of PAC using CTS composites of different PAC/TiO₂ ratios (Table 5.6) show a decrease in the regeneration efficiency of PAC with an increase in the PAC/TiO₂ ratio. This is due to the fact that decreasing the amount of TiO₂ in the CTS composite led to a decrease in active sites for photodegradation of the adsorbed substrate and regeneration of the PAC. Yap and Lim (2012) found similar results when they degraded bisphenol-A, sulfamethazine and clofibric acid using nitrogen doped TiO₂ attached onto AC. Their results were due to the fact that decreasing the amount of TiO₂ in the composite led to a reduction in the number of active sites for the regeneration of the AC.

The removal of the substrates from the solution was not the only factor taken into consideration when selecting the optimum PAC/TiO₂ ratio. The other factor was the regeneration efficiency of the CTS composite. Increasing the PAC/TiO₂ ratio increased the removal of the substrates from solution but decreased the regeneration efficiency which would reduce the reusability of the CTS composite. In order to achieve a high removal of substrates in solution without compromising its reusability, the CTS composite with 10% PAC/TiO₂ ratio was selected as the optimum.

Table 5.6: Performance characteristics of CTS composites with different PAC/TiO₂ ratios

PAC/TiO ₂ ratio (%)	DCF			CBZ		
	Q_{EA} (mg/g)	Q_{EAP} (mg/g)	RE (%)	Q_{EA} (mg/g)	Q_{EAP} (mg/g)	RE (%)
10	120.9	26.8	22.1	141.4	73.3	51.8
20	99.5	2.7	2.7	144.6	49.5	34.2
30	90.1	0.0	0.0	121.8	23.2	19.0
40	80.1	0.0	0.0	105.1	2.3	2.2

where Q_{EA} is the equilibrium adsorption capacity of the fresh PAC (mg/g), Q_{EAP} is the equilibrium adsorption capacity of the spent PAC due to photocatalytic regeneration (mg/g) and RE is the regeneration efficiency.

5.3.3.3 Effect of the CTS loading

The effect of the CTS mass on the adsorption and photodegradation of the substrates was determined by varying the mass of the CTS composite catalyst. The results (Fig. 5.13a-c) show an increase in the adsorption and photodegradation of the substrates with increase in mass of the CTS composite. Increasing the mass of the CTS composite resulted in an increase in the amount of PAC and TiO₂ in solution.

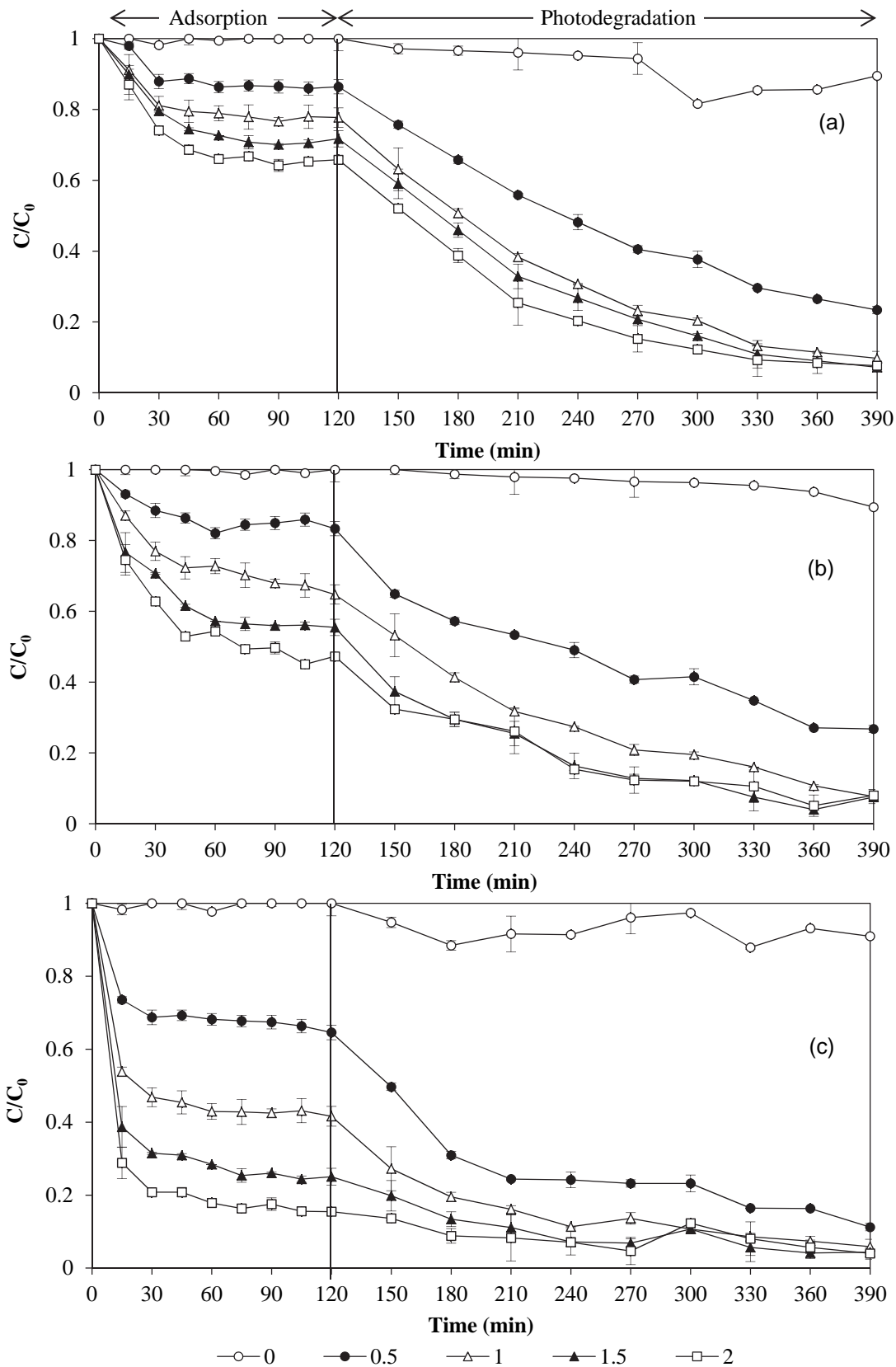


Fig. 5.13: Effect of mass of the CTS composite (g/L) on the adsorption and photodegradation of (a) SMX, (b) DCF and (c) CBZ; $C_0 = 10$ mg/L, silica xerogel loading = 60%, PAC/TiO₂ ratio = 10%, superficial air velocity = 0.014 m/s, reactor inclination angle = 75°

More PAC in solution resulted in an increase in active sites for adsorption of the substrates resulting in an increase in the adsorption of the substrates.

Similarly, an increase in the amount of TiO_2 in solution resulted in an increase in the number of active sites for photodegradation thus resulting in an increase in the photodegradation of the substrates. However, increasing the composite mass beyond 1.5 g/L did not show any significant increase in the photodegradation of the substrates. This is due to the fact that increasing the CTS catalyst mass beyond 1.5 g/L resulted in some of the CTS catalyst shielding others and preventing them from receiving sunlight (Malato et al., 2009). The shielded TiO_2 were not activated and therefore did not photodegrade the substrates thus resulting in no further increase in photodegradation.

When shielding occurs in a given solution, the shielded catalysts become inactive. It would be cost effective not to have any inactive catalyst particles at any time during photodegradation. The optimum mass of the CTS composite would be that which would ensure the highest number of catalyst particles in solution without some catalyst particles shielding others. Therefore a composite mass of 1.5 g/L was selected as the optimum CTS composite mass due to the fact that this mass resulted in the highest degradation without some of the CTS catalysts shielding others.

5.3.4 Hydrodynamics

The hydrodynamic parameters such as the solid concentration distribution and gas holdup of the fluidized bed photocatalytic reactor, greatly influence the substrate photodegradation. The solid concentration distribution determines the rate of substrate-catalyst mass transfer which influences the rate of adsorption and photodegradation of the substrate. Similarly, the gas holdup affects the rate of gas-liquid mass transfer which determines the amount of dissolved oxygen, an electron scavenger necessary for photocatalysis. Hydrodynamic studies were therefore carried out to determine the solid concentration distribution and the gas holdup at different superficial air velocities and reactor inclination angles. These hydrodynamic studies gave the optimum superficial air velocity and reactor inclination angle at which the adsorption and photodegradation were to be carried out. Gas holdup was also used as a hydrodynamic standard to ascertain that the different reactors had similar hydrodynamic behaviour. It was necessary for hydrodynamics to be similar for the different reactors during other experiments so as to eliminate hydrodynamic influence on the adsorption and photodegradation data.

5.3.4.1 Gas holdup

The effect of aspect ratio, reactor inclination angle and superficial air velocity (u_g) on the global gas holdup was determined using 2 g/L of the CTS composite. The results (Fig. 5.14) show an increase in the gas holdup (ϵ_g) with an increase in u_g . The gas holdup increased from 0.03 to 0.26 when u_g was increased from 0.007 to 0.028 m/s. This was due to the fact that increasing u_g increased the number of bubbles in the solution which resulted in an increase in the fraction of the reactor volume occupied by air. Figure 5.14 also shows a pronounced decrease in u_g with decreasing aspect ratio when the superficial air velocity was increased above 0.014 m/s. For example, at a u_g of 0.028 m/s, the gas holdup decreased from 0.26 to 0.17 when the aspect ratio was increased from 2 to 8. There was little decrease in ϵ_g when the aspect ratio was increased beyond 8. The decrease in ϵ_g with an increase in the aspect ratio can be attributed to the fact that increasing the aspect ratio increases the path length of bubbles in the reactor column. As these bubbles have a longer distance to travel in solution, the probability of the bubbles coalescing increases (Ochieng et al., 2002). Therefore, most of the bubbles coalesce and increase in size. The bigger bubbles rise faster in solution taking a shorter time in the liquid. The decrease in the residence time of the bubbles in the solution results in a decrease in the gas holdup.

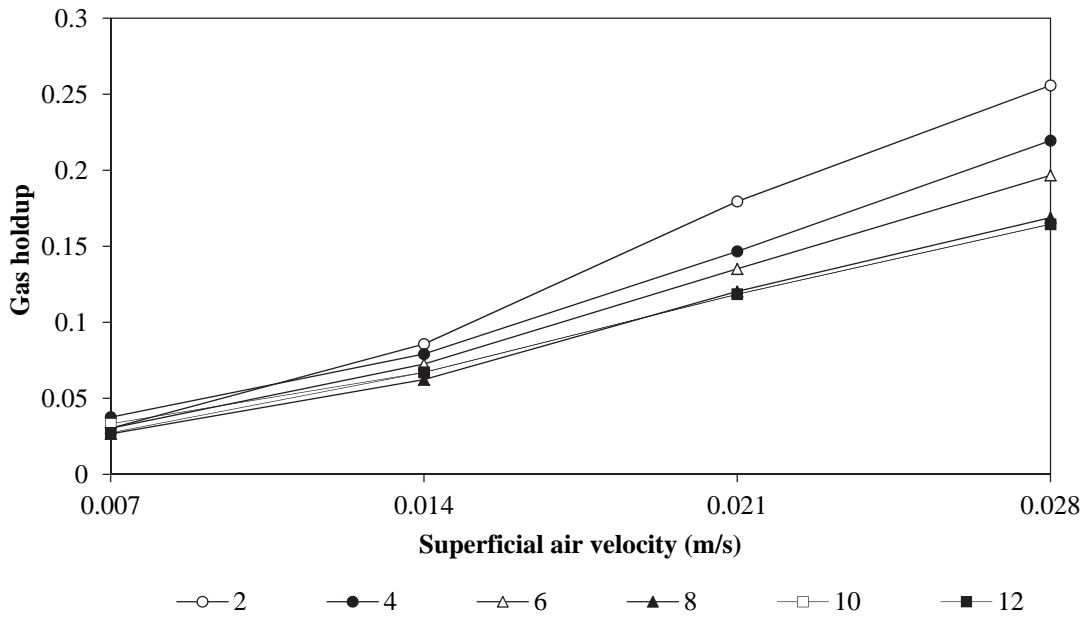


Fig. 5.14: The effect of aspect ratio and superficial air velocity on gas holdup, inclination angle = 90°, solid loading = 1 g/L

The effect of the reactor inclination angle on the ϵ_g was also investigated, and the results (Fig. 5.15) show a marked decrease in the ϵ_g with a decrease in the reactor inclination angle at high u_g . For example, the ϵ_g reduced from 0.2 to 0.12 when the inclination angle was reduced from 90° to 60°, where 90° represents the vertical position. This reduction is due to the fact that as the reactor was inclined, the air bubbles had a shorter distance to travel in the liquid before leaving the reactor. Also, when the reactor was inclined, the bubbles rose to the upper inclined wall of the reactor and crawled on the surface of the reactor until they reach the gas disengaging section. The high number of bubbles on the upper inclined wall of the reactor increased bubble coalescence. The shorter bubble travel distance coupled with an increased bubble size due to coalescence resulted in a shorter bubble residence time in the reactor thus reducing the ϵ_g . Similar results were reported by Ugwu et al. (2002), who reported a decrease in ϵ_g from 0.022 to 0.016 when they reduced the inclination angle from 45° to 8° in their inclined airlift reactor.

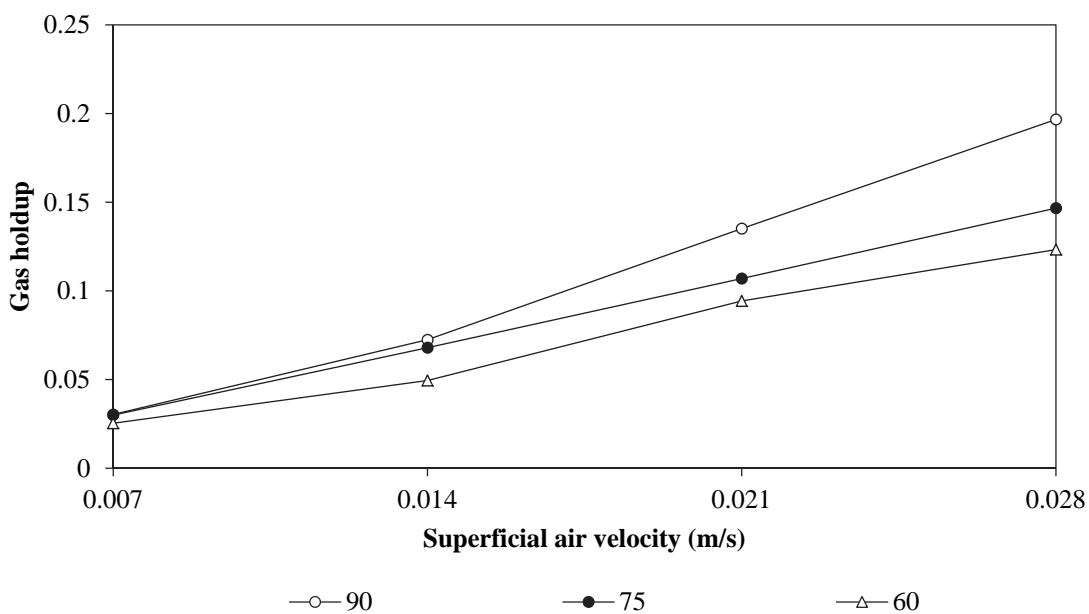


Fig. 5.15: The effect of inclination angle (°) on gas holdup, aspect ratio = 6, solid loading = 2 g/L

5.3.4.2 Solid concentration distribution

The solid concentration distribution gives an indication of the dispersion of the solid catalyst particles in the reactor. It is affected by the superficial air velocity and the reactor inclination angle. Experiments were carried out using different superficial air velocities and reactor inclination angles to investigate the effect of these parameters on the solid concentration distribution. The results (Fig. 5.16a-d) show a general decrease in solid concentration with an increase in distance from the distributor at different superficial air velocities. This decrease in solid concentration with increasing distance from the distributor was sharper when the reactor was vertical (inclination angle of 90°). At this position, the solid concentration dropped by 99% from 14.3 g/L to 0.16 g/L between 5.7 cm and 48.6 cm from the distributor, respectively. Also, at 90° inclination angle, the rate of decrease in solid concentration with increasing distance from the distributor did not change significantly with an increase in superficial air velocity after 20 cm from the distributor. When the reactor inclination angle was reduced below 90°, there was a significant improvement in solid concentration distribution. For example, at 75° inclination angle and air superficial velocity of 0.014 m/s, the solid concentration decreased by only 38% from 5.4 g/L to 3.3 g/L between 5.7 cm and 48.6 cm from the distributor, respectively. At angles below 90°, it was found that the solid concentration distribution was significantly affected by the superficial air velocity.

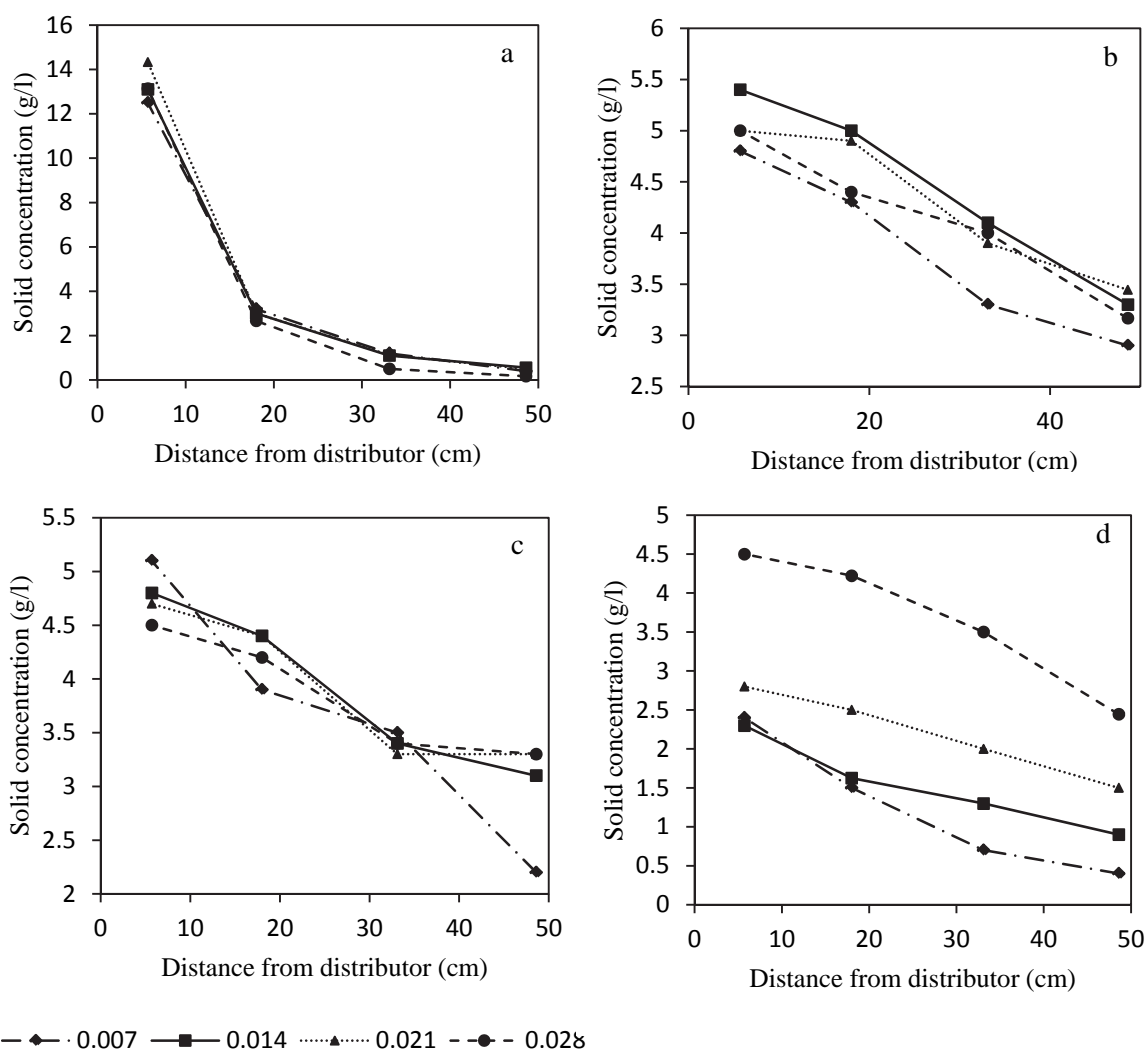


Fig. 5.16: Variation of solid concentration with distance from the distributor at different superficial air velocities (m/s) and inclination angles: (a) 90°; (b) 75° (c) 60° (d) 45°; solid loading = 5 g/L, liquid volume = 400 ml

Figure 5.17 summarizes Fig. 5.16a-d and shows the mean and standard deviation of the solid concentration in the samples. The mean of the solid concentration in the samples gave an indication of how much solid settled on the distributor or the reactor walls and thus could not be sampled. Therefore the mean of the solid concentration gave a rough approximation of the radial solid distribution. The standard deviation on the other hand, showed how well the solid particles were distributed along the length of the reactor. The standard deviation therefore gave a good indication of the axial solid distribution. The best hydrodynamic conditions at which there was an optimum solid distribution with no settling of the solids would be at a mean solid concentration of 5 g/L and a standard deviation of 0.

Both Fig. 5.16a-d, and Fig. 5.17 show a sudden increase in solid concentration distribution with a decrease in reactor inclination angle from 90° to 75°. A good solid concentration distribution was maintained when the inclination angle was further reduced to 60°. However, when the angle was reduced further to 45°, the solid concentration distribution worsened. When the reactor was inclined, air bubbles moved along the upper surface of the reactor creating a low density region. The liquid in this low density region moved up the reactor carrying solid particles along to the top of the reactor. The space left by the upward moving liquid was filled by the liquid occupying the lower denser region of the reactor. This downward moving liquid carried the solid particles back to the bottom of the reactor which were in turn picked and moved up by the upward moving liquid. In this way, air induced a bulk circulation of the liquid in an inclined reactor which carried the solids along, thus fluidizing them. A similar behaviour has been observed for airlift reactors (Christi and Moo-Young, 1993; Vunjak-Novakovic et al., 2005). The inclined reactor essentially behaved as an airlift reactor with the inclined upper section of the reactor being analogous to the airlift riser while the inclined lower section acted like an airlift downcomer. In the reactor used in this work, there was no physical separation between the riser and the downcomer as found in airlift reactors. However, the region occupied by air bubbles was small enough for there to be sufficient hydrodynamic separation between the high and low density regions in the reactor.

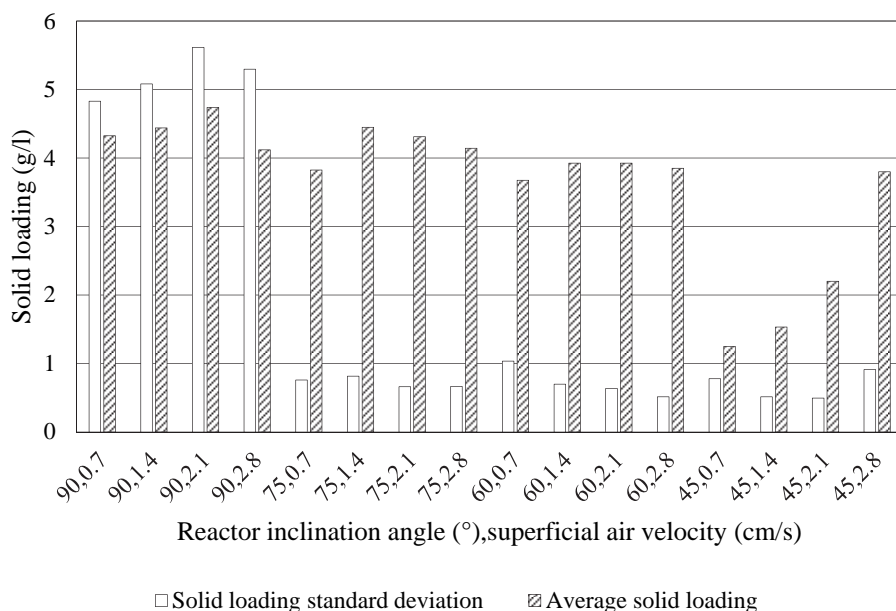


Fig. 5.17: Mean catalyst loading and standard deviation of samples at different distances from the distributor at different inclination angles and superficial air velocities (cm/s), solid loading = 5 g/L, liquid volume = 400 ml

The lower part of the inclined reactor was not as turbulent as the upper part, and therefore particles tended to settle on the lower wall even as they were dragged towards the distributor. Particles also tended to settle on the distributor since at least half of the distributor was not sparged when the fluidized bed reactors were inclined. This is due to the fact that in the inclined reactors, bubbles on the distributor tended to rise upwards

towards the upper reactor wall leaving the lower section of the distributor unsparged. The tendency of the solids to settle on the reactor walls and distributor was especially pronounced at an inclination angle of 45°. This settling of the solids on the walls and distributor increased with decreasing superficial air velocity due to the reduction in turbulence at low superficial air velocities. However, very little settling was observed at 90° inclination angle due to the fact that the reactor being vertical, there could be no solid settling on the reactor walls. Instead, all the solid particles tended to settle on the distributor where air passing through the entire surface of the distributor lifted the solids thus preventing the solids from settling on the distributor.

5.3.4.3 *Optimum hydrodynamic conditions*

The optimum hydrodynamic conditions were chosen with respect to the gas holdup and the solid concentration distribution. The vertical position (90°) resulted in a good gas holdup but poor solid concentration distribution. At the extreme end, the 45° inclination angle had high solid settling, good distribution of the unsettled solids but poor gas holdup. Both 90° and 45° inclination angles were not suitable for the hydrodynamics of the reactors. The 75° and 60° inclination angles had comparable hydrodynamic characteristics: low solid settling, good solid concentration distribution and average gas holdup with 75° being slightly better. Therefore, 75° inclination angle and 0.021 m/s superficial air velocity were chosen as the optimum hydrodynamic conditions for further adsorption and photodegradation experiments.

5.3.5 *Effect of hydrodynamics on adsorption and photodegradation*

High solid-liquid and liquid-gas mass transfer rates are essential to achieve a high rate of adsorption and photodegradation. For photodegradation, the substrates have to come into contact with the photocatalyst and also oxygen in air has to dissolve into the liquid for efficient photodegradation to take place. Therefore, both the liquid-solid and gas-liquid mass transfer rates influence photodegradation. For the adsorption, only the liquid-solid mass transfer rate determines the rate of adsorption. These liquid-solid and gas-liquid mass transfer rates depend on the solid concentration distribution and the gas holdup, respectively. Hydrodynamic studies have shown that the reactor inclination angle and superficial gas velocity affect the solid concentration distribution and the gas holdup. It is imperative therefore to determine whether factors such as the reactor inclination angle and superficial velocity also affect the rate of adsorption and photodegradation.

5.3.5.1 *Effect of reactor inclination angle on adsorption and photodegradation*

The effect of reactor inclination angle on the adsorption and photocatalytic degradation of SMX, DCF and CBZ was investigated using 1.5 g/L of CTS composite. The angle was varied from 60° to 90° while maintaining the u_g at 0.014 m/s. The results (Fig. 5.18a-c) show that the extent of adsorption of the various substrates was virtually similar at the different reactor inclination angles while the photodegradation was relatively low at inclination angles of 60° and 90° but increased at inclination angle of 75°. It has been previously observed that there was very poor solid concentration distribution at 90°. At the bottom of the reactor where there were more of the catalyst particles, the catalyst particles near the reactor walls shaded the ones in the middle of the reactor keeping them from being activated by the sunlight. At the top of the reactor, there were few catalyst particles, and consequently sunlight was not fully utilized to activate the catalyst. Therefore, both at the bottom and at the top of the reactor there was inefficiency in the utilization of sunlight for photodegradation, resulting in low photodegradation.

At 75°, there was better photodegradation of substrates as compared to that at 60° and 90°. It is important to note that it was at this angle of 75° that there was good solid concentration distribution and little settling of the solids. This meant that sunlight did not have to travel very far into the reactor to activate the catalyst nor were there huge areas in the reactor where catalyst could not be reached by the light. This efficient utilization of sunlight resulted in an increase in the photodegradation of the substrates. Gas holdup was lower at an inclination angle of 75° than at 90° and yet the overall rate of photodegradation was higher at an inclination angle of 75°. These results suggest that solid concentration distribution was more important for

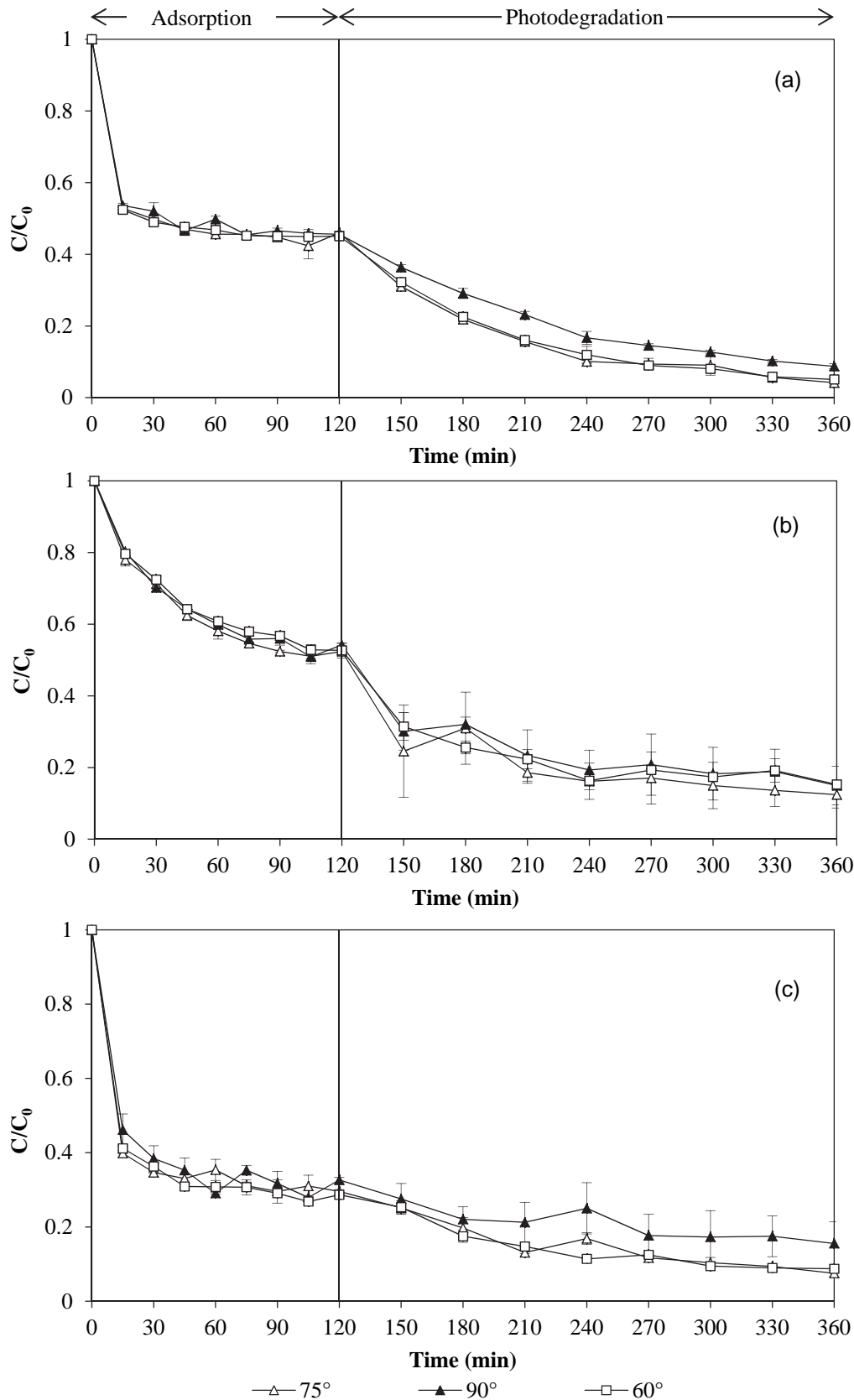


Fig. 5.18: Effect of reactor inclination angle on the rate of adsorption and photodegradation at 1.5 g/L CTS loading, 0.014m/s superficial air velocity for: (a) DCF; (b)

photodegradation than gas-holdup. This is an indication that the gas-liquid mass transfer was not a limiting factor but solids distribution was. Matsumura et al. (2007) observed an increase in the degradation of o-cresol by introducing a draft tube in their vertical three phase reactor. It has been concluded previously that when the reactor in this work was at 90°, it was analogous to a vertical three phase reactor without a draft

tube. However, when the reactor was inclined it behaved like a draft tube three phase reactor used by Matsumura et al. (2007). In their study, Matsumura et al. (2007) attributed the increase in photodegradation of *o*-cresol in the draft tube three phase reactor to the induced liquid circulation created by the draft tube. Therefore, the findings in this work are similar to those obtained by Matsumura et al. (2007).

At an inclination angle of 60°, there was a considerable settling of the catalyst on the lower inclined reactor walls. Sunlight which had to pass through the substrate to reach the catalyst was absorbed or reflected by the substrate so that only a little solar radiation could activate the catalyst on the reactor walls. This inefficiency in the utilization of sunlight resulted in the low rate of photodegradation at an inclination angle of 60°. Reactors inclined at both 90° and 60° suffered inefficiencies in utilizing sunlight for catalyst activation. Consequently, an inclination angle of 75° was chosen as the optimum reactor inclination angle. This conclusion agrees well with what was obtained during hydrodynamic experiments.

The percentage equilibrium adsorption of SMX, DCF and CBZ were 47, 55 and 71, respectively. Therefore, there was an increase in the adsorption of the substrates in the order SMX>DCF>CBZ. This was due to the fact that CBZ was adsorbed onto the PAC mainly due to hydrophobic interactions while DCF was adsorbed mainly due to electrostatic attractions. SMX, however, had weak hydrophobic interactions and electrostatic attractions. Therefore, SMX exhibited the lowest adsorption onto the PAC followed by DCF whose electrostatic attraction was weaker than the hydrophobic interactions responsible for the adsorption of CBZ.

5.3.5.2 *Effect of superficial air velocity on adsorption and photodegradation*

The effect of superficial air velocity on the adsorption and photocatalytic degradation of SMX, DCF and CBZ was investigated using 1.5 g/L of CTS composite. The superficial air velocity was varied from 0 to 0.028 m/s while maintaining the angle at 75°. The results (Fig. 5.19a-c) show that the adsorption and photodegradation increased with increasing superficial air velocity up to an optimum of 0.007 m/s, beyond which no further increase was observed. When the reactors were not sparged with air (0 m/s), some adsorption occurred during the mixing of CTS composite and the substrate at the start of the experiment. After the mixing, some adsorption continued to take place as the CTS composite started settling in the reactor. By the time photocatalysis started, almost all the CTS composite particles had settled onto the distributor. Only those CTS particles on the very top of the distributor were exposed to sunlight and could therefore degrade the substrates. Photocatalysis using these few CTS composite particles coupled with direct photolysis of the substrate resulted in the little degradation of the substrate at a superficial air velocity of 0 m/s.

When the superficial air velocity was increased to 0.003 m/s, some fluidization of the catalyst was observed. There was also considerable settling of the CTS catalyst on the lower wall and on the distributor of the reactor. Due to the settling of the CTS composite, only a portion of the optimum amount of catalyst was fluidized and was therefore available for adsorption and photodegradation. At a superficial air velocity of 0.007 m/s, settling of the CTS on the reactor walls and distributor reduced and almost all the CTS composite particles remained suspended in solution. The fluidized CTS composite particles had enough surface area exposed to the substrate and sunlight for adsorption and photodegradation. Increasing the superficial air velocity above 0.007 m/s, resulted in further reduction in the settling of the catalyst on the reactor walls and the distributor, but did not increase the adsorption and photodegradation. Matsumura et al. (2007) found similar results by fluidizing larger (500 µm) but lighter (570 kg/m³) particles in a larger (96 mm ID) reactor. They found a trend similar to that in this work in which the rate of photodegradation of *o*-cresol increased with increasing superficial gas velocity up to a 'critical gas velocity' beyond which no further increase in degradation was observed. They found an optimum superficial air velocity of 0.006 m/s which is comparable to the optimum superficial velocity observed in this work (0.007 m/s).

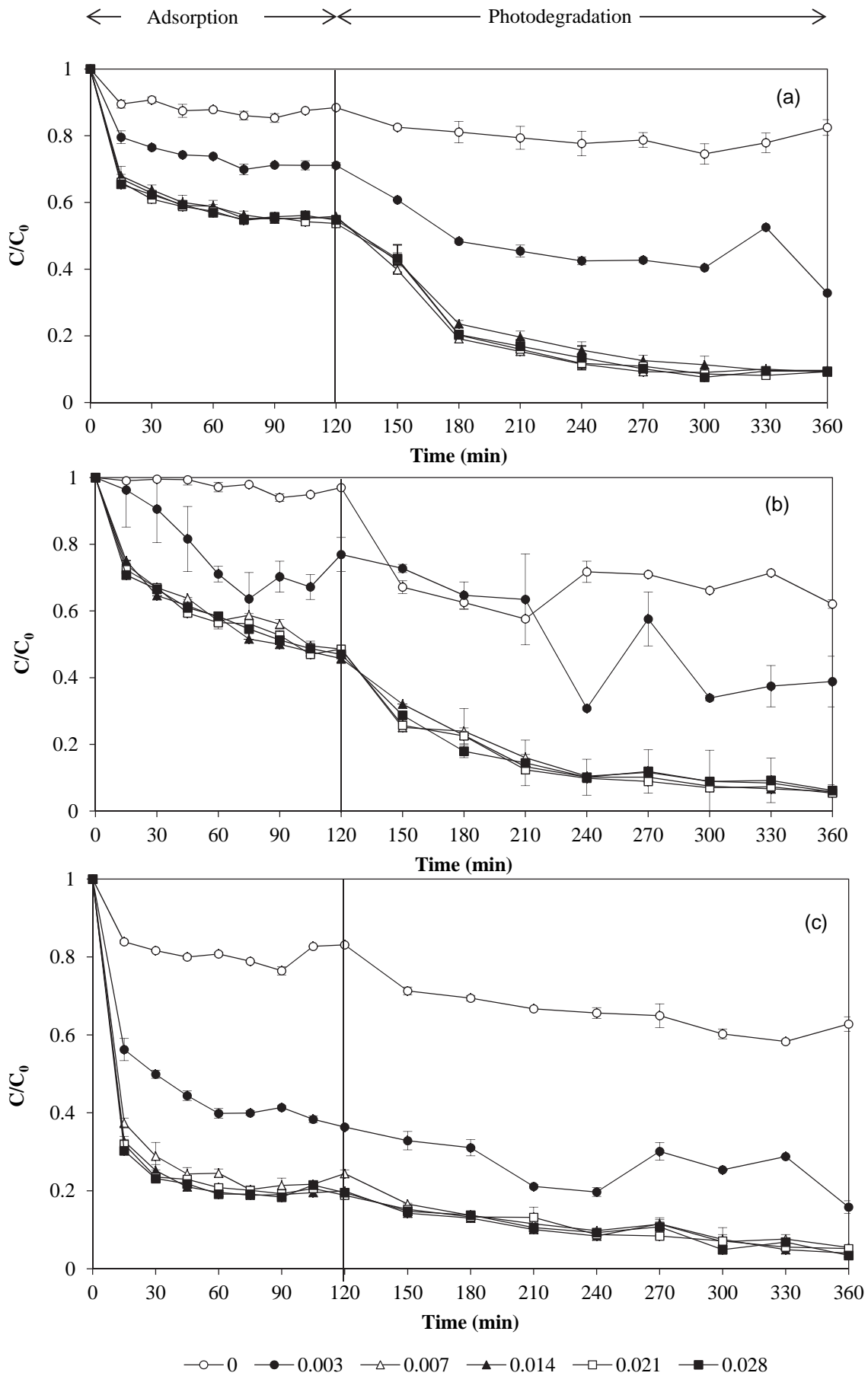


Fig. 5.19: Effect of superficial air velocity (m/s) on the rate of adsorption and photocatalysis at 1.5 g/L CTS loading reactor and inclination angle = 75° for: (a) SMX; (b) DCF; (c) CBZ.

Fluidization is costly due to the electric energy required to run the compressor. From an economics point of view, the lowest superficial air velocity resulting in the maximum adsorption and photodegradation was chosen as the optimum superficial air velocity. Therefore, 0.007 m/s was chosen as the optimum superficial velocity. It is worth noting that the optimum superficial air velocity found during adsorption and photocatalysis experiments (0.007 m/s) is lower than the optimum superficial velocity found during hydrodynamic experiments (0.014 m/s). These findings suggest that a sub-optimum superficial air velocity is sufficient for adsorption and photocatalysis. Obtaining an optimum rate of adsorption and degradation with sub-optimal superficial air velocity is desirable from an economical point of view to reduce the cost of operation of the wastewater treatment system.

The equilibrium percentage adsorption of SMX, DCF and CBZ in this experiment were 45, 53 and 80, respectively. The difference in the adsorption was due to the fact that the hydrophobic interactions responsible for the adsorption of CBZ were stronger compared to the electrostatic interactions responsible for the adsorption of the DCF. The SMX with the weak electrostatic attractions and hydrophobic interactions had the lowest adsorption. The photodegradation of the substrates in the solution decreased in the order SMX>DCF>CBZ. This was due to the fact that the rate of photodegradation depends on the initial concentration of the substrate (Malato et al., 2009). At the end of the adsorption experiment and the start of the photodegradation experiment, CBZ had the lowest residual concentration in solution followed by DCF with SMX having the highest concentration.

5.3.6 Solution characteristics

Wastewater has inherent characteristics due to the identity and concentration of the chemicals that make up the wastewater. The characteristics of the wastewater such as the concentration of the substrates and the solution pH affect the adsorption and photodegradation of substrates. Therefore, it is crucial to determine the effect of the solution characteristics on the adsorption and photodegradation of the substrates. Experiments were carried out to determine the effect of the solution characteristics on the adsorption and photodegradation of SMX, DCF and CBZ. The results of these experiments would give an indication of how effective the adsorption and photodegradation system would be when used to remove real wastewater.

5.3.6.1 Effect of initial substrate concentration on adsorption and photodegradation

The effect of the initial substrate concentration on the adsorption and photodegradation of the substrates was determined using 1.5 g/L of the CTS composite catalyst. The results (Fig. 5.20a-c) show a decrease in the time of removal of the substrates with a decrease in the initial substrate concentration. There was a fixed number of active sites on the CTS composite for adsorption and photodegradation of the substrate molecules. Only a certain number of the substrate molecules could be adsorbed by the CTS active sites. Increasing the number of substrate molecules in the solution beyond the number of available adsorbent active sites meant that some substrate molecules would remain in the solution. Therefore, an increase in the initial concentration of the substrates left more substrate molecules to be photodegraded. Only a fixed number of active sites were available for photodegradation of the substrates at any one time. Therefore, it would take longer to photodegrade the solution with more substrate molecules.

The typical concentration of pharmaceutical pollutants in wastewater has been reported to be in the order of ng/L to low µg/L (Houtman, 2010). The experiments in this work were carried out at higher concentrations of mg/L. However, the results of this work could still be applicable to the pharmaceutical contaminants at lower concentrations. This is due to the fact that the increase in the removal of substrates with decreasing initial concentration from 15 to 2 mg/L shows that the substrate removal would keep increasing at substrate concentrations below 2 mg/L. However, the optimum mass of the CTS composite used will have to be reduced when removing lower concentrations of substrates.

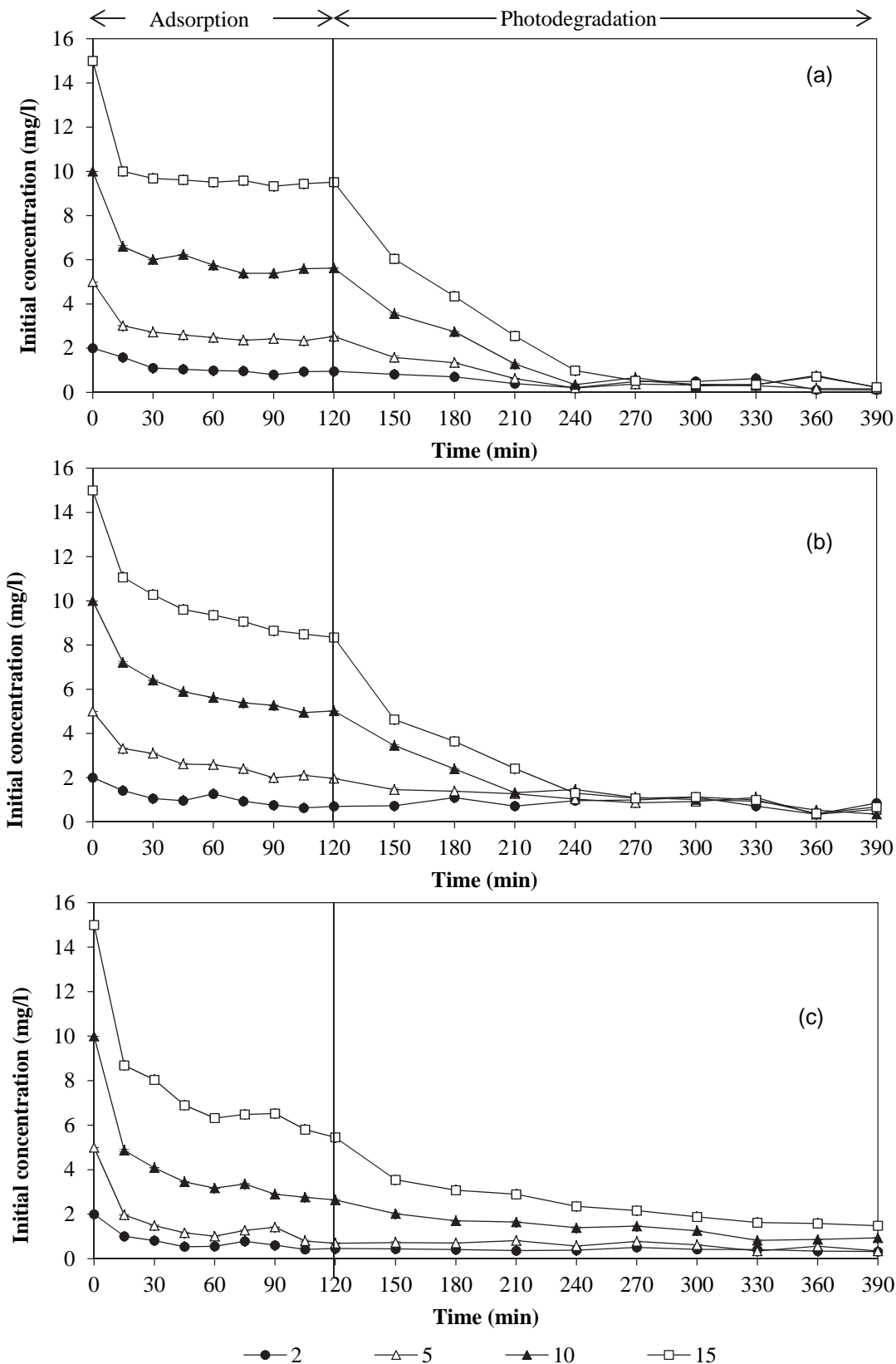


Fig. 5.20: Effect of substrate initial concentration (mg/L) on the adsorption and photodegradation of (a) SMX, (b) DCF and (c) CBZ; silica xerogel loading = 60%, PAC/TiO₂ ratio = 10%, CTS loading = 1.5 g/L, superficial air velocity = 0.014 m/s, reactor inclination angle = 75°

5.3.6.2 Effect of initial pH on adsorption and photodegradation

The effect of the initial pH of the substrate solution on the adsorption and photodegradation of the substrates was determined by varying the pH of the substrate solution from 4 to 10. The results (Fig. 5.21) show an

increase in the adsorption and photodegradation of SMX with a decrease in solution pH. With a ZPC of 6.3, the PAC was positively charged in SMX solutions of pH 4 and 4.6 and negatively charged in solutions of pH 7 and 10. The SMX molecules with two pK_a s: 1.8 and 5.6 were uncharged at SMX solution pH 4 and 4.6 and negatively charged at solution of pH 7 and pH 10. At pH 4 and 4.6, there was relatively little attraction between the positively charged activated carbon surface and the uncharged SMX molecules resulting in low

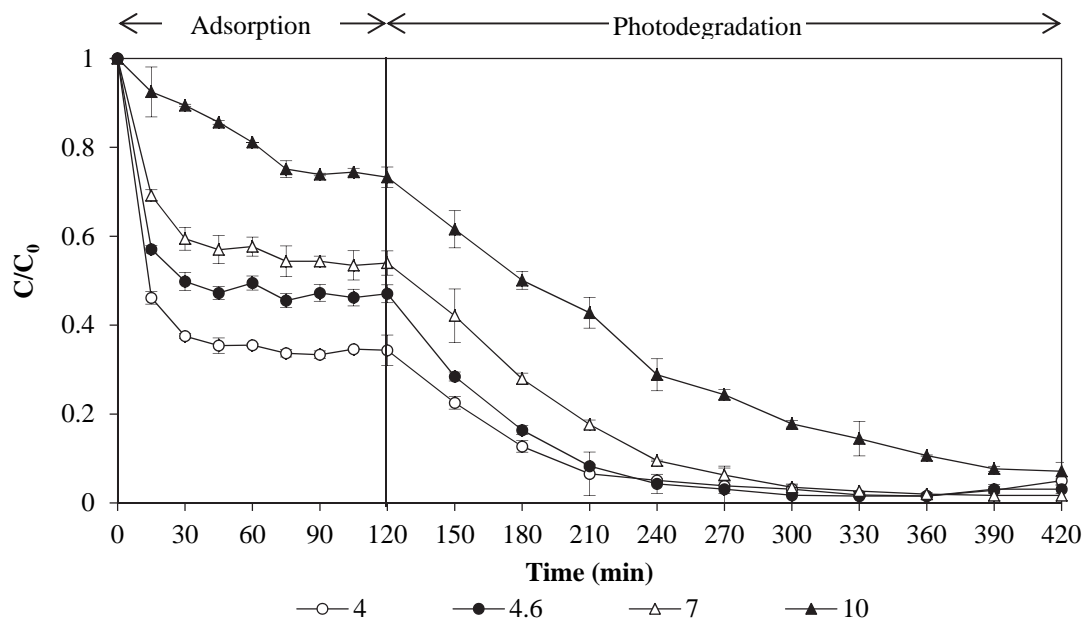


Fig. 5.21: Effect of initial pH of solution on the adsorption and photodegradation of SMX; $C_0 = 10$ mg/L, silica xerogel loading = 60%, PAC/TiO₂ ratio = 10%, CTS loading = 1.5 g/L, superficial air velocity = 0.014 m/s, reactor inclination angle = 75°

percent adsorption. However there was some adsorption due to hydrophobic interactions of the SMX molecules and the PAC surface. Increasing the solution pH to 7 and 10 resulted in a decrease in adsorption of SMX on the PAC surface due the repulsion between the positively charged SMX molecules and the positively charged surface of the PAC. This repulsion reduced the adsorption due to hydrophobic interactions since the SMX molecules were repelled from the surface of the PAC.

5.3.6.3 Equilibrium isotherms

The data in Fig. 5.20a-c were fitted to the Langmuir and Freundlich isotherms and the results in Table 5.7 show a good fit for the Langmuir isotherm for SMX and DCF. Unlike the other two, a good fit for both Langmuir and Freundlich was obtained with DCF. With SMX, a good fit was obtained for Langmuir but not Freundlich isotherm. The CBZ showed a poor fit for both Langmuir and Freundlich isotherms. Therefore, both SMX and DCF were adsorbed on the PAC on a monolayer fashion. The maximum Langmuir adsorption capacity of SMX and DCF were equal but lower than that of CBZ. This roughly follows the equilibrium adsorption of the substrates which had been observed to increase in the order: SMX>DCF>CBZ except that the adsorption of DCF was higher than that of SMX.

Table 5.7: Langmuir and Freundlich isotherms of the adsorption of SMX onto the CTS composite

	Langmuir isotherm			Freundlich isotherm		
	q_m	K	R^2	n	K_F	R^2
SMX	172.4	0.122	0.991	0.518	2.196	0.837
DCF	172.4	0.204	0.990	1.539	29.208	0.988
CBZ	243.9	0.360	0.862	1.557	60.576	0.838

5.4 Conclusion

In this study, adsorption and photodegradation of pharmaceuticals using a composite catalyst of TiO₂, activated carbon and silica xerogel (CTS composite) was carried out in a three phase fluidised bed reactor system using sunlight as the source of energy. The analysis of solar radiation data revealed that photodegradation should be carried out between 9.30 am and 2.30 pm on sunny days during the summer months. Characterisation of the CTS composite showed an increase in the porosity of the composite with the introduction of the activated carbon. It was also found that the addition of the PAC and the silica xerogel to the TiO₂ did not significantly affect the composition of the TiO₂. The optimum CTS composition was determined to be 60% silica xerogel loading and 10% PAC/TiO₂ ratio while the best mass of the CTS composite was 1.5 g/L. The best catalyst composition resulted in over 95% removal of the substrates.

The hydrodynamic experiments showed that the optimum hydrodynamic conditions in the reactor were obtained at an air superficial velocity of 0.014 m/s and an inclination angle of 75°. However, the adsorption and photodegradation experiments revealed that the optimum hydrodynamic conditions were at an air superficial velocity of 0.007 m/s and reactor inclination angle of 75°. There was an increase in the adsorption of the pharmaceuticals on the PAC in the order carbamazepine>diclofenac>sulfamethoxazole. It was observed that decreasing the initial concentration of the substrates resulted in an increase in the removal of the substrates by adsorption and photodegradation. The adsorption and photodegradation of the sulfamethoxazole increased with a decrease in pH. The adsorption of sulfamethoxazole and diclofenac followed Langmuir isotherm while the carbamazepine did not show good fit for both Langmuir and Freundlich isotherms.

The effect of metal ions was not investigated in the previous two sections. However, for practical utilization of photocatalysis, it is crucial to investigate the effect of coexisting metal ions on photocatalysis. Industrial and municipal wastewaters seldom exist without the presence of metal ions. Metal ions in wastewater is important since the ions affect the rate of photodegradation.

References

- Abraham, M., Khare, A.S., Sawant, S.B., Joshi, J.B. (1992). Critical gas velocity for suspension of solid particles in three-phase bubble columns. *Industrial & Engineering Chemistry Research*, 31(4), 1136-1147.
- Bettermann, P., Liebau, F. (1975). The transformation of amorphous silica to crystalline silica under hydrothermal conditions. *Contributions to Mineralogy and Petrology*, 53(1), 25-36.
- Braham, R.J., Harris, A.T. (2009). Review of major design and scale-up considerations for solar photocatalytic reactors. *Industrial & Engineering Chemistry Research*, 48(19), 8890-8905.
- Brogat, M., Cadiere, A., Sellier, A., Thomas, O., Baures, E., Roig, B. (2013). MSPE/UV for field detection of micropollutants in water. *Microchemical Journal*, 108(0), 215-223.
- Christi, Y., Moo-Young, M. (1993). Improve the Performance of Airlift Reactors. *Chemical Engineering Progress*, 39.

- Dekker, J., Nthontho, M., Chowdhury, S., Chowdhury, S. (2012). Investigating the effects of solar modelling using different solar irradiation data sets and sources within South Africa. *Solar Energy*, 86(9), 2354-2365.
- Fox, M.A., Dulay, M.T. (1993). Heterogeneous photocatalysis. *Chemical reviews*, 93(1), 341-357.
- Guillard, C., Disdier, J., Herrmann, J., Lehaut, C., Chopin, T., Malato, S., Blanco, J. (1999). Comparison of various titania samples of industrial origin in the solar photocatalytic detoxification of water containing 4-chlorophenol. *Catalysis Today*, 54(2-3), 217-228.
- Houtman, C.J. (2010). Emerging contaminants in surface waters and their relevance for the production of drinking water in Europe. *Journal of Integrative Environmental Sciences*, 7(4), 271-295.
- Hurum, D.C., Agrios, A.G., Gray, K.A., Rajh, T., Thurnauer, M.C. (2003). Explaining the Enhanced Photocatalytic Activity of Degussa P25 Mixed-Phase TiO₂ Using EPR. *The Journal of Physical Chemistry B*, 107(19), 4545-4549.
- Kimura, T., Yoshikawa, N., Matsumura, N., Kawase, Y. (2004). Photocatalytic degradation of nonionic surfactants with immobilized TiO₂ in an airlift reactor. *Journal of Environmental Science and Health, Part A*, 39(11-12), 2867-2881.
- Kumar, K.V., Porkodi, K. (2007). Mass transfer, kinetics and equilibrium studies for the biosorption of methylene blue using *Paspalum notatum*. *Journal of hazardous materials*, 146(1), 214-226.
- Malato Rodríguez, S., Blanco Gálvez, J., Maldonado Rubio, M.I., Fernández Ibáñez, P., Alarcón Padilla, D., Collares Pereira, M., Farinha Mendes, J., Correia de Oliveira, J. (2004). Engineering of solar photocatalytic collectors. *Solar Energy*, 77(5), 513-524.
- Malato, S., Fernández-Ibáñez, P., Maldonado, M., Blanco, J., Gernjak, W. (2009). Decontamination and disinfection of water by solar photocatalysis: Recent overview and trends. *Catalysis Today*, 147(1), 1-59.
- Matsumura, T., Noshiroya, D., Tokumura, M., Znad, H.T., Kawase, Y. (2007). Simplified model for the hydrodynamics and reaction kinetics in a gas-liquid-solid three-phase fluidized-bed photocatalytic reactor: degradation of o-cresol with immobilized TiO₂. *Industrial & Engineering Chemistry Research*, 46(8), 2637-2647.
- Moreno-Castilla, C. (2004). Adsorption of organic molecules from aqueous solutions on carbon materials. *Carbon*, 42(1), 83-94.
- Nagaveni, K., Hegde, M.S., Ravishankar, N., Subbanna, G.N., Madras, G. (2004). Synthesis and Structure of Nanocrystalline TiO₂ with Lower Band Gap Showing High Photocatalytic Activity. *Langmuir*, 20(7), 2900-2907.
- Ochieng, A., Ogada, T., Sisenda, W., Wambua, P. (2002). Brewery wastewater treatment in a fluidised bed bioreactor. *Journal of hazardous materials*, 90(3), 311-321.
- Pérez-Estrada, L., Maldonado, M., Gernjak, W., Agüera, A., Fernández-Alba, A., Ballesteros, M., Malato, S. (2005). Decomposition of diclofenac by solar driven photocatalysis at pilot plant scale. *Catalysis Today*, 101(3), 219-226.
- Porter, J., Li, Y., Chan, C. (1999). The effect of calcination on the microstructural characteristics and photoreactivity of Degussa P-25 TiO₂. *Journal of Materials Science*, 34(7), 1523-1531.
- Shan, A.Y., Ghazi, T.I.M., Rashid, S.A. (2010). Immobilisation of titanium dioxide onto supporting materials in heterogeneous photocatalysis: a review. *Applied Catalysis A: General*, 389(1), 1-8.
- Suhas, Carrott, P.J.M., Ribeiro Carrott, M.M.L. (2007). Lignin – from natural adsorbent to activated carbon: A review. *Bioresource technology*, 98(12), 2301-2312.
- Ugwu, C., Ogbonna, J., Tanaka, H. (2002). Improvement of mass transfer characteristics and productivities of inclined tubular photobioreactors by installation of internal static mixers. *Applied Microbiology and Biotechnology*, 58(5), 600-607.
- Vunjak-Novakovic, G., Kim, Y., Wu, X., Berzin, I., Merchuk, J.C. (2005). Air-lift bioreactors for algal growth on flue gas: mathematical modeling and pilot-plant studies. *Industrial & Engineering Chemistry Research*, 44(16), 6154-6163.
- Yap, P., Lim, T. (2012). Solar regeneration of powdered activated carbon impregnated with visible-light responsive photocatalyst: Factors affecting performances and predictive model. *Water research*, 46(9), 3054-3064.

- Yu, Z., Peldszus, S., Huck, P.M. (2008). Adsorption characteristics of selected pharmaceuticals and an endocrine disrupting compound – Naproxen, carbamazepine and nonylphenol – on activated carbon. *Water research*, 42(12), 2873-2882.
- Zainudin, N.F., Abdullah, A.Z., Mohamed, A.R. (2010). Characteristics of supported nano-TiO₂/ZSM-5/silica gel (SNTZS): Photocatalytic degradation of phenol. *Journal of hazardous materials*, 174(1-3), 299-306.
- Zhou, J., Takeuchi, M., Ray, A.K., Anpo, M., Zhao, X.S. (2007). Enhancement of photocatalytic activity of P25 TiO₂ by vanadium-ion implantation under visible light irradiation. *Journal of colloid and interface science*, 311(2), 497-501.
- Zieliński, M., Wojcieszak, R., Monteverdi, S., Mercy, M., Bettahar, M. (2005). Hydrogen storage on nickel catalysts supported on amorphous activated carbon. *Catalysis Communications*, 6(12), 777-783.

CHAPTER 6

6 PHOTOCATALYTIC DEGRADATION OF DYES IN THE PRESENCE OF IONS

6.1 Introduction

The accelerated growth in civilization and industrial activities has revealed the great problem of water pollution by inorganic and organic compounds such as heavy metals, dyes and pesticides. (Bhatnagar and Sillanpää, 2009). These chemicals enter the aquatic medium in numerous different ways, either dumped directly, such as industrial effluents or from wastewater treatment plant. The most problematic recalcitrant organics co-contaminated with metal ions are dyes from the textile industrial effluents. These organic compounds usually have synthetic origins and complex aromatic molecular structures which make them more stable and difficult to biodegrade (Robinson et al., 2001). Due to their high toxicity and the associated environmental hazards, occurrence of dyes and metal ions in water and wastewater can cause serious damage to human beings even at very low concentrations. Metals are also not biodegradable and can accumulate in living tissues, which means they become concentrated throughout the food chain. Although at low doses they are essential micronutrients for plants and animals, in high doses they can negatively affect the health of most living organisms. Heavy metals ions such as chromium, copper, lead and zinc (Bhatnagar and Sillanpää, 2009) often co-exist with these organic compounds in wastewater generated from different sources. Metallic ions usually are not degradable and have an unlimited lifetime. Also, while their concentrations are increased by several industrial processes, they produce a disturbing ecological imbalance in the environment. This condition occurs more frequently with chromium ion. The application of chromium has increased due to the extensive use of chromate and dichromate in textile, photoengraving processes, and leather tanning (Park et al., 2005).

Treatment of wastewater containing organic and metal pollutants is a complex worldwide environmental problem, as the two components must be treated independently. In addition these chemicals revealed a significant difference in molecular weight, chemical composition and toxicity (Aksu, 2005). With this growing demand for good quality water, one of a few attractive alternatives to resolve these environmental issues is the possible reuse of wastewater. Countless practical strategies and solutions have been implemented to produce more viable water resources. Currently water treatment methods such as adsorption or coagulation simply concentrate the pollutants present by transferring them to other phases, thus not reducing them into an active compound. These have led to the rapid R&D in the field of "Advanced Oxidation Processes (AOPs)" as innovative and low cost wastewater treatment methods (Chong et al., 2010). Heterogeneous photocatalysis employing TiO_2 semiconductor catalyst has revealed its efficiency in degrading a wide range of recalcitrant organics into readily biodegradable compounds and ultimately mineralizing them to harmless carbon dioxide and water. Up to now, the post-separation of the semiconductor TiO_2 catalyst after water treatment remains the major problem in industrial process. To solve this problem, in this work TiO_2 catalyst powder is loaded onto silica in such a way as to provide high surface area and accessibility of the catalyst.

6.2 Methodology

Chemicals used were of analytical reagent grade, used as received and purchased from the same company, Sigma Aldrich Chemical Co. Methyl orange, an azo dye (MO, 99%,) and potassium dichromate (99.8% $\text{K}_2\text{Cr}_2\text{O}_7$) as the source of Cr(VI), were selected as model compounds co-existing in various industrial and municipal wastes. Titanium dioxide containing mainly anatase, with 30% rutile was used as photocatalyst with Ludox Hs-30 colloidal silica as the supporting material. Commercial TiO_2 with an average particle size of 12 nm was used for reference.

6.2.1 Synthesis of TiO_2 /silica composite photocatalysts

Titanium dioxide supported-silica samples were prepared by adding Ludox Hs-30 colloidal silica solution to plain TiO_2 with proper mixing to ensure a homogeneous TiO_2 coating onto silica. After mixing, the mixture was dried at 110°C and screened to 75-150 μm particle. The coated particles were then dispersed in Mill Q-plus water, till the pH of the suspension was close to 6.5. By this procedure, a sample of 15 wt% of TiO_2 onto 75-150 μm silica particle size was prepared.

6.2.2 Characterization of composite photocatalysts

Prior to photodegradation experiments, material characterization was done using Scanning Electron Microscopy and Energy Dispersive Spectroscopy (SEM- EDS), Raman spectroscopy (RS) and zeta potential (ZP) analysis techniques. These techniques helped to interpret the photocatalysis process under different operating conditions. In order to ensure the crystalline structure of prepared TiO₂/silica composite, the morphology of the prepared composite photocatalyst was examined by SEM analysis equipped with EDS. The isoelectric point of the TiO₂/silica composite was measured by Zetasizer.

6.2.3 Photocatalysis experiments

A 100 ml semi-batch reactor (Fig. 6.1) was used for the photocatalytic experiments of methyl orange and reduction of metal ions. In all experiments, 80 ml of an aqueous solution containing either the dye alone, metal alone or their mixture was used throughout and experiments were performed at room temperature (25 ± 3°C). Milli Q-plus water (resistance = 18.2 M.Ω) was used for all experimental work. The UV lamp (low-pressure mercury lamp, wave length, 254 nm (Pen-Ray), with an intensity of 5.5 mW/m²), protected by a quartz sleeve was used. All experiments were conducted in duplicate. For all experiments, the solution was left to equilibrate

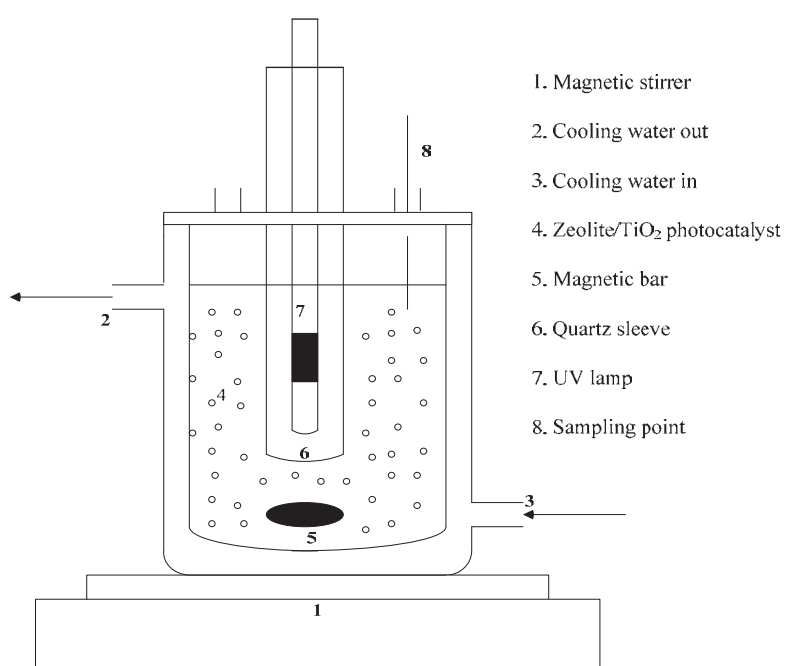


Fig. 6.1: Experimental setup

for 0.5 h in the dark before the lamp was switched on. This was sufficient to reach an equilibrated adsorption as deduced from the steady-state concentrations. Samples were taken at desired time intervals and immediately filtered through a polypropylene syringe filter (0,45 μm).

6.3 Results and discussion

6.3.1 SEM- EDS analysis

The morphology of the silica alone and the prepared TiO₂/silica composite photocatalyst is shown in Fig. 6.2. From Fig. 6.2a, the morphology may be described as the close packed cubic arrangement. This morphology remained the same even after supporting TiO₂ (Fig. 6.2c) on silica with 75-150 μm size particle. Taking into account the EDS spectra (Fig. 6.2b) this arrangement could be that of oxygen ions, with the silicon ions dispersed on tetrahedral interstices, since Si⁴⁺ is very much smaller than O²⁻ (Papirer, 2000).

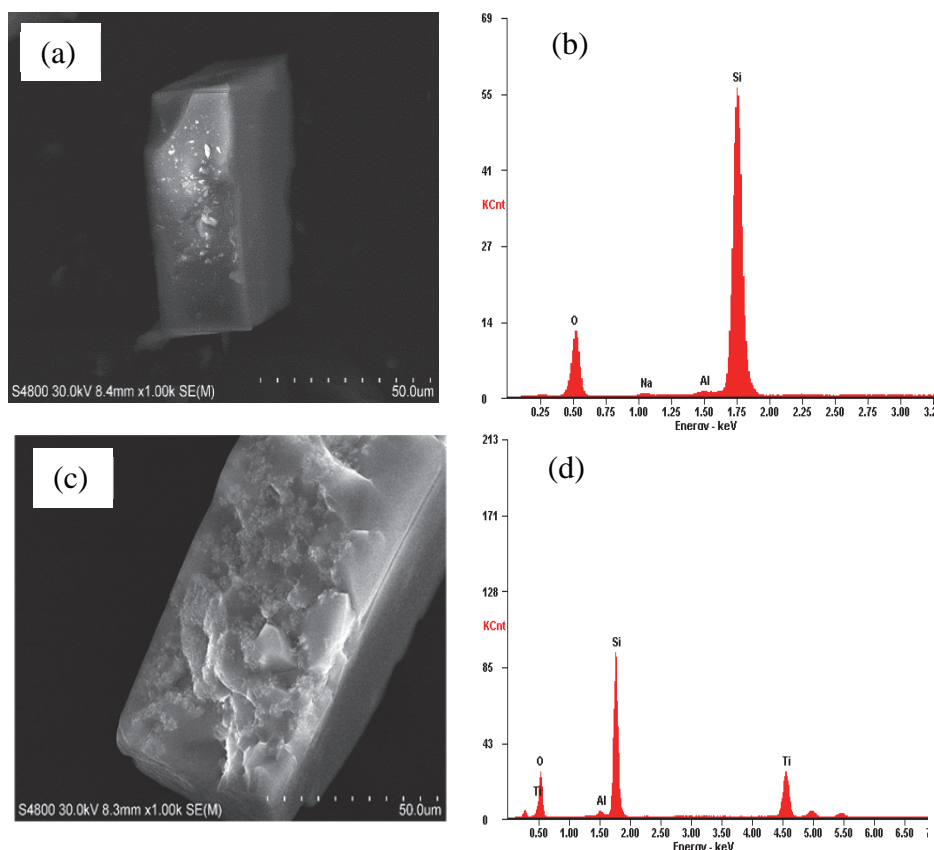


Fig. 6.2: SEM images and EDS spectra: (a and b) silica alone (c and d) 15% TiO₂/silica

6.3.2 Raman spectra analysis

The Raman spectra of 15% TiO₂/silica composite photocatalyst before and after the photocatalytic treatment of methyl orange are displayed in Fig. 6.3. A very strong sharp band at 196.1 cm⁻¹, a medium band at about 641.2 cm⁻¹ and three small bands at 198, 397.6, 517.4 cm⁻¹ are observed in Fig. 6.3a. These well-defined bands observed indicate that anatase crystallites prevail in the structure of the prepared photocatalyst composite. The peaks correspond well with those observed for a single-crystal anatase (640, 515, 400, 197, 144 cm⁻¹) (Beattie and Gilson, 1968). Further analysis of the Raman spectra unveil the existence of the other two Raman signals, close to 146 and 437.4 cm⁻¹ that can be associated with the occurrence of rutile phase in TiO₂ structure. The TiO₂ was still present in silica supporting material even after the 180 min photocatalysis treatment. The characterization by Raman spectroscopy is in agreement with the findings obtained from the SEM-EDS images (Fig. 6.2).

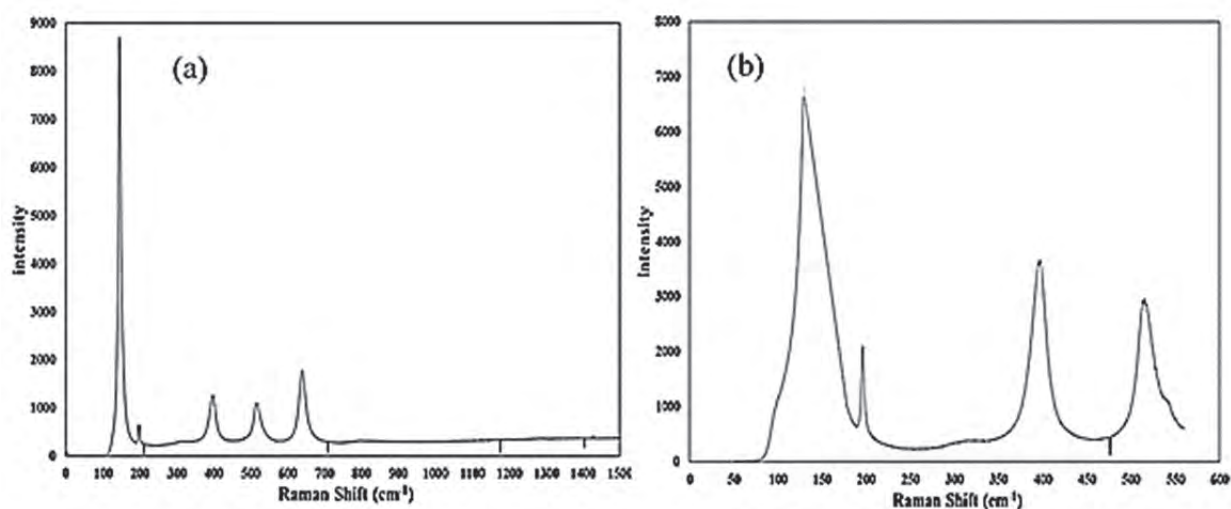


Fig. 6.3: Raman spectra of TiO₂/silica (a) before and (b) after the photocatalysis treatment

6.3.3 Isoelectric point measurements (IEP)

The point of zero charge (PZC) of TiO₂/silica with the diameter between 38-75 μm was determined by zeta potential measurements (Fig. 6.4). The differences in acid-base properties of TiO₂-SiO₂ oxide composites have an impact on the obtained zeta potential values (Nowacka *et al.*, 2013). Upon evaluating the course of the electro kinetic curve for the TiO₂/silica composite, it can be seen that its zeta potential is decreasing with an increase in the pH values, which confirms that the zeta potential value strongly depends on the pH value. The IEP for the TiO₂/silica particles is found at a pH value of around 2 and reaches zeta potential values from 10 to -34 mV in the studied pH range. In addition, the stability of TiO₂-silica composite photocatalyst is high in the pH values from 4 to 6, as indicated by high zeta potentials. The IEP for TiO₂ was reported to be around 6 (Londeree, 2002). The differences in the electrokinetic properties of the studied composite photocatalyst and that of TiO₂ are a result of the proposed synthesis method and the percent composition of a given oxide. Lower IEP value of the prepared synthetic composite photocatalyst is most likely caused by a higher percent composition of silica, which is characterized by an isoelectric point at a pH value of 2. These results were consistent with the findings revealed by Papirer (2000) where the silica's point of zero charge ranged between 2 and 3. In addition, the surface charges were changed from positive to negative as a function of pH due to the unprotonation of the surface groups. At a pH less than the IEP, the TiO₂/silica surface was positively charged due to the formation of Si-OH₂⁺. At a pH above the IEP, the surface of the TiO₂/silica had a negative charge due to the deprotonation of the silanol group resulting in Si-O⁻. As the pH approached 6, the Si-O⁻ become dominant (the pKa for SiOH = Si-O⁻ + H⁺ is around 6 and 7) (Cox, 1993). Londeree (2002) reported that these Si-O⁻ sites react with cations in solution and an increase in pH would significantly improve the adsorption of organic and inorganic compounds on composite surface. For nonionic compounds in solution, adsorption could take place at the silanol groups by either Van der Waals forces or hydrogen bonding. It was further reported (Londeree, 2002) that for anionic compounds, adsorption could occur at a pH above the PZC of silica, but instead it would be occurring at the TiO₂ surface which is positively charged at pH < 6.0.

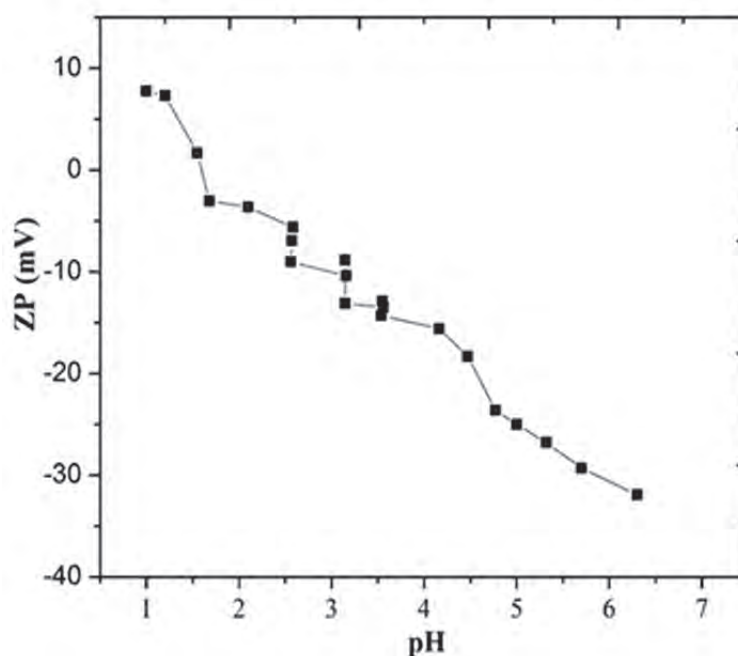


Fig. 6.4: Zeta potential of TiO₂/silica as a function of pH

6.3.4 Photocatalytic degradation of methyl orange dye by TiO₂/silica photocatalyst

Control experiment was conducted at two different conditions, dark adsorption over composite photocatalysts and photolysis under UV light only (Fig. 6.5). No significant dye degradation was observed during the adsorption test even for prolonged time. This elucidates the attainment of adsorption equilibrium and hence, for all experiments, the solution was left to equilibrate for 0.5 h in the dark. In direct photolysis, 42% colour removal was achieved in 3.5 h irradiation time by the assistance of light. To recognize the role of

support material during the photocatalytic degradation of methyl orange, the 15 wt% TiO₂/silica composite was compared with unsupported TiO₂ amount equivalent to the one available on both photocatalyst for the degradation efficiency. It can be clearly seen from Fig. 6.5 that the 90% degradation of methyl orange was observed over supported system (TiO₂/silica), whereas the degradation over TiO₂ alone did not reach

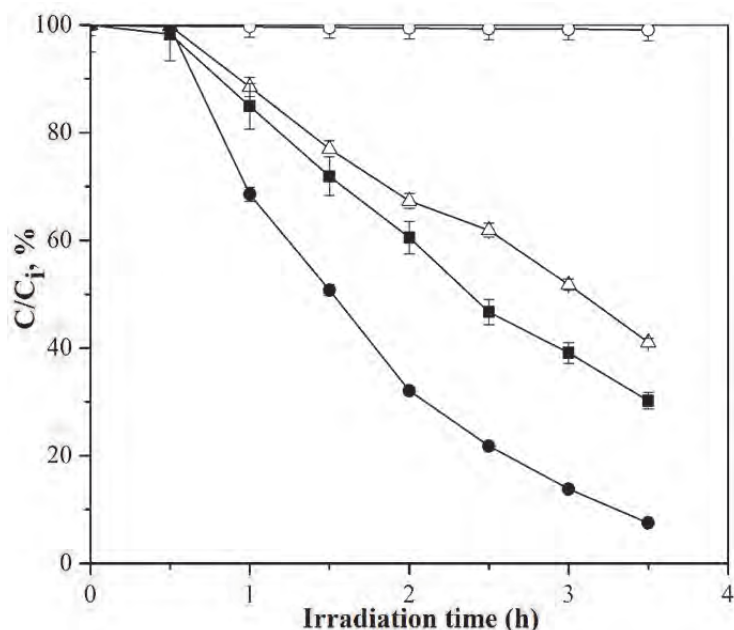


Fig. 6.5: Adsorption of methyl orange over TiO₂/silica (○); photocatalytic degradation of methyl orange over UV (Δ); UV-TiO₂ (■); UV-TiO₂/silica (●)

complete degradation even at 3.5 h. This can be explained in terms of the interaction between TiO₂ and supporting materials (silica), as well as the different structure from bulk TiO₂. Apart from that, this high degradation percentage could be due to the presence of a higher amount of hydroxyl radicals within the solution (Auguliaro et al., 1990).

6.3.5 Effect of photocatalyst composite loading

The composite photocatalyst loading is an important parameter in photocatalysis studies due to the fact that it determines the capacity of the composite photocatalyst for a given initial concentration of dye solution. The effect of composite photocatalyst concentration on the dye degradation is shown in Fig. 6.6. The effect of TiO₂/silica composite photocatalyst concentration was determined from 1.25-12.75 gL⁻¹. It is observed in Fig. 6.6 that initially the degradation of methyl orange reduced significantly with an increase in composite photocatalyst concentration. This was more pronounced at 1.25 gL⁻¹ TiO₂/silica composite photocatalyst concentration which can be due to the partial deactivation of activated molecules by collision with ground state molecules. Furthermore, the significant reduction in degradation percentage of the dye above 1.25 gL⁻¹ TiO₂/silica photocatalyst concentration can be explained in terms of the availability of active sites on TiO₂/silica surface and the light penetration of photoactivating light into the suspension. The availability of active sites increases with the suspension of photocatalyst loading (Neppolian *et al.*, 2002). When the amount of photocatalyst increases above an optimum level, the light photon absorption coefficient usually declines. The optimum concentration of 1.25 gL⁻¹ TiO₂/silica composite photocatalyst was found and used in further experiments. Many studies have reported the effect of photocatalyst concentration on the process efficiency (Gaya and Abdullah, 2008; Herrmann, 1999). These results are mostly independent and a direct comparison cannot be made, as the photoreactor, radiation fluxes, intensity and wavelengths used were different.

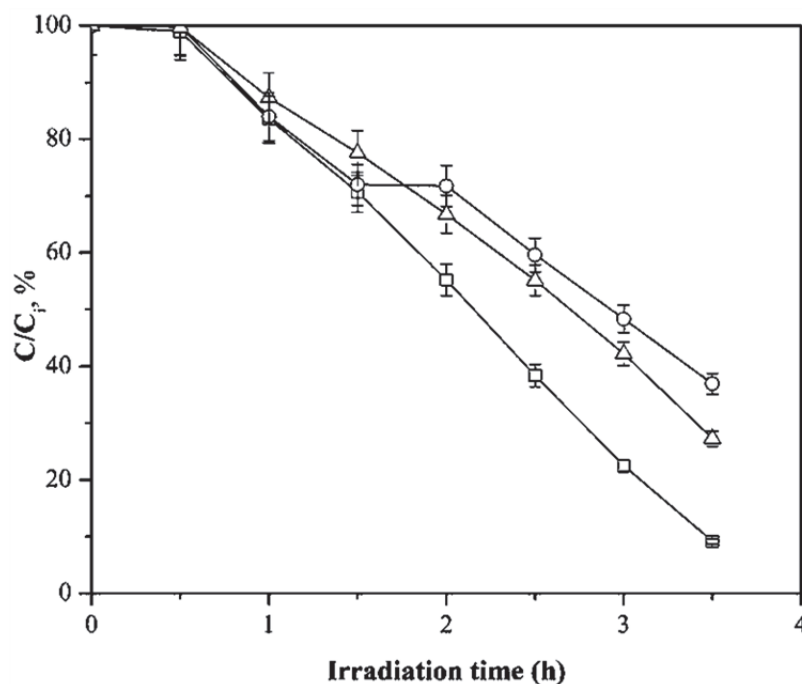


Fig. 6.6: Effect of TiO₂/silica composite photocatalyst concentration on dye degradation: 1.25 gL⁻¹ (□); 6.25 gL⁻¹ (○); 12.25 gL⁻¹ (Δ). Condition: C₀= 25 mgL⁻¹; pH= 6.5

6.3.6 Effect of dye initial concentration

Efficient application of the photocatalytic oxidation system requires the investigation of the dependence of photocatalytic degradation rate on the substrate concentration. The characteristic of organic dye concentrations in wastewater from the textile industry is usually in the range of 10-50 mgL⁻¹ (Kansal et al., 2007). Therefore, methyl orange solution concentration was varied in the range 5-50 mgL⁻¹ during the photocatalytic degradation at solution pH 6.3. The degradation was found to increase up to an initial concentration of 35 mgL⁻¹ and then decreased (Fig. 6.7). The inadequate number of surface sites on TiO₂/silica composite photocatalyst particles may affect the photodegradation efficiency. As the concentration of methyl orange pollutant increases, more molecules of the compound get adsorbed on the surface of the photocatalyst. As a result, the reactive species ([•]OH and [•]O²⁻) needed for the degradation of dye also increase. However, the formation of [•]OH and [•]O²⁻ on the composite photocatalyst surface remains constant for a 5.5 mW/m² light intensity and 1.25 gL⁻¹ photocatalyst concentration for 210 minutes duration of

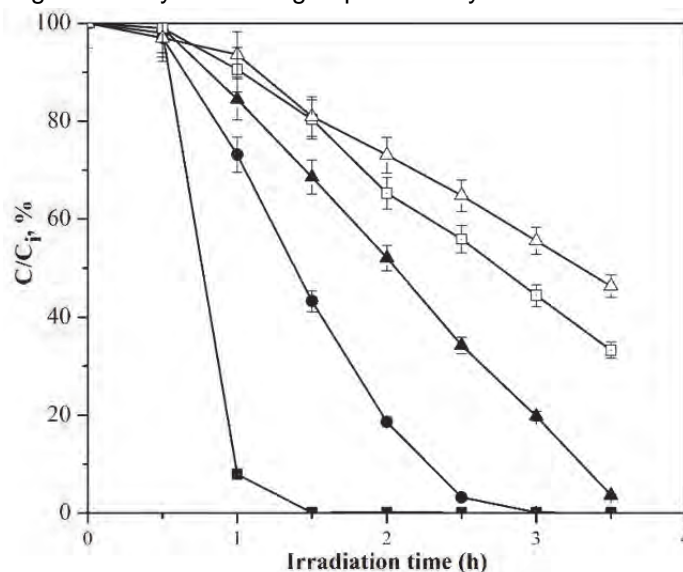


Fig. 6.7: Effect of initial concentration on TiO₂/silica photocatalyst 5 mgL⁻¹ (■); 15 mgL⁻¹ (●); 25 mgL⁻¹ (▲); 35 mgL⁻¹ (□); 50 mgL⁻¹ (Δ)

irradiation. Hence, the available OH radicals are inadequate to attack the methyl orange molecules at higher concentrations due to constant reaction conditions. Consequently the degradation rate of the methyl orange decreases as the concentration increases (Bahnmann et al., 2007). In addition, an increase in substrate concentration can lead to the generation of intermediates which may adsorb on the surface of the photocatalyst. Slow diffusion of the generated intermediates from the catalyst surface can result in the deactivation of active sites of the photocatalyst, and consequently result in a reduction in the degradation rate. In contrast, at low concentration the number of catalytic sites will not be a limiting factor and the rate of degradation is proportional to the substrate concentration in accordance with apparent first-order kinetics (Hermann, 1999; Ollis et al., 1991).

6.3.7 Effect of solution pH

The solution pH does not only affect the surface charge of a photocatalyst, but also the degree of ionization or speciation (pKa) of an organic pollutant during the reaction. Electrostatic interaction between semiconductor surface, substrate and charged radicals formed during photocatalytic oxidation is profoundly dependent on the pH of the solution (Saien and Khezrianjoo, 2008). Therefore, the pH of the solution plays a key role in the photocatalytic oxidation of pollutants. To study the effects of H⁺ concentrations on dye degradation, comparative experiments were performed at three pH values: 3, 7 and 9 and results are shown on Fig. 6.8. At pH 3, the surface of silica/TiO₂ is positively charged and thus attracting the largest amount of negatively charged anions of methyl orange, hence there is a substantial degradation. Zeta potential measurements (Fig. 6.4) indicate that the surface charge of the TiO₂/silica composite photocatalyst decreased as the pH increased, signifying repulsive forces between photocatalyst surface and dye in alkaline media. Furthermore, the limiting behaviour in alkaline medium is due to the negative charge of a composite photocatalyst and therefore methyl orange transformation products can be repelled away from the silica/TiO₂ surface which opposes the adsorption of substrate molecules on the surface of the composite photocatalyst. As a result, methyl orange degradation declines in alkaline medium.

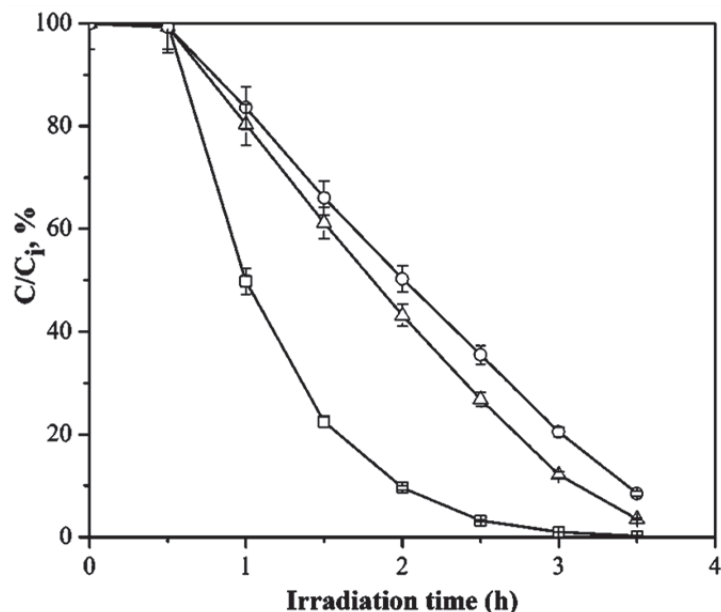


Fig. 6.8: Effect of solution pH on TiO₂/silica photocatalyst pH 3 (□); pH 7 (Δ); pH 9 (○).

6.3.8 Photodegradation isotherms and kinetics of methyl orange

The isotherm modelling basically reflects the interaction between substrate and photocatalyst until the state of equilibrium is reached. In order to optimize the effectiveness of the TiO₂/silica on the photodegradation of methyl orange, linear form of Langmuir (Fig. 6.9a) and Freundlich models (Fig. 6.9b) were applied for the TiO₂/silica composite photocatalyst. For brevity, the linear form of the Langmuir and Freundlich isotherm model are described by equation (1) (Langmuir, 1918) and equation (2), (Freundlich, 1906). The correlation coefficients (R²) along with other parameters for two different models were calculated and listed in Table 6.1. Clear deviations were observed in the Langmuir and Freundlich isotherm models. A straight line (Fig. 6.9a)

with a correlation coefficient (R^2) of 0.995 signifying that the degradation of methyl orange onto the composite photocatalyst fits the Langmuir isotherm reasonably well. The Freundlich constants, K_f and n , calculated from this investigation, are 2.3×10^{-3} and 0.399, respectively. The R^2 obtained from the Freundlich isotherm model implies poor fitting for the Freundlich isotherm model. Comparison of the correlation coefficients of both models suggests that the Langmuir model is suitable. The fact that the Langmuir isotherm fits the experimental data well can be due to homogeneous distribution of active sites on the $\text{TiO}_2/\text{silica}$ surface.

$$q_e = \frac{q_m K_L C_e}{1 + K_L C_e} \quad (6.1)$$

7

where, q_m (mgL^{-1}) and K_L (Lmg^{-1}) are the Langmuir constants related to adsorption capacity and rate of adsorption, respectively, q_e is dye concentration at equilibrium onto adsorbent (mgL^{-1}), C_e is dye concentration at equilibrium in solution (mgL^{-1}).

$$q_e = K_f C_e^{1/n_f} \quad (6.2)$$

where K_f is the Freundlich constant related to adsorption capacity, n_f is measure of the surface heterogeneity, ranging between 0 and 1. For linearization of the data, the Freundlich equation is written in logarithmic form:

$$\log q_e = \log k_f + \left(\frac{1}{n}\right) \log C_e \quad (6.3)$$

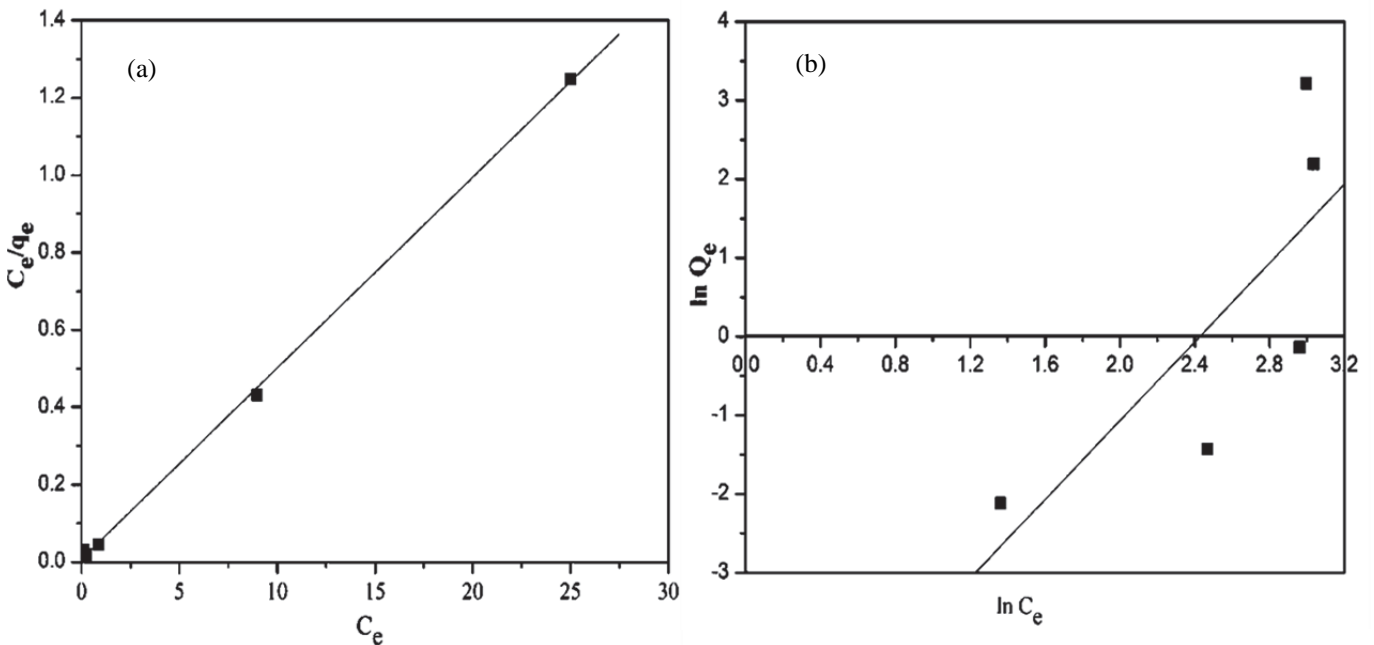


Fig. 6.9: Linear transform of (a) Langmuir and (b) Freundlich isotherm

Fig. 6.10 shows the plot obtained by applying the nonlinear form of Langmuir and Freundlich model (Eqs. 1 and 2) and its output is given in Table 6.1. The Langmuir model showed a moderate fit with R^2 of 0.949 $\text{TiO}_2/\text{silica}$. At moderate values R^2 of $\text{TiO}_2/\text{silica}$ composite photocatalyst was supported by low values of the RMSE and χ^2 . In the case of nonlinear Freundlich model, the 'n' values were higher than 1, suggesting that the adsorption is possibly favourable. Thus, the adsorption of methyl orange on $\text{TiO}_2/\text{silica}$ composite

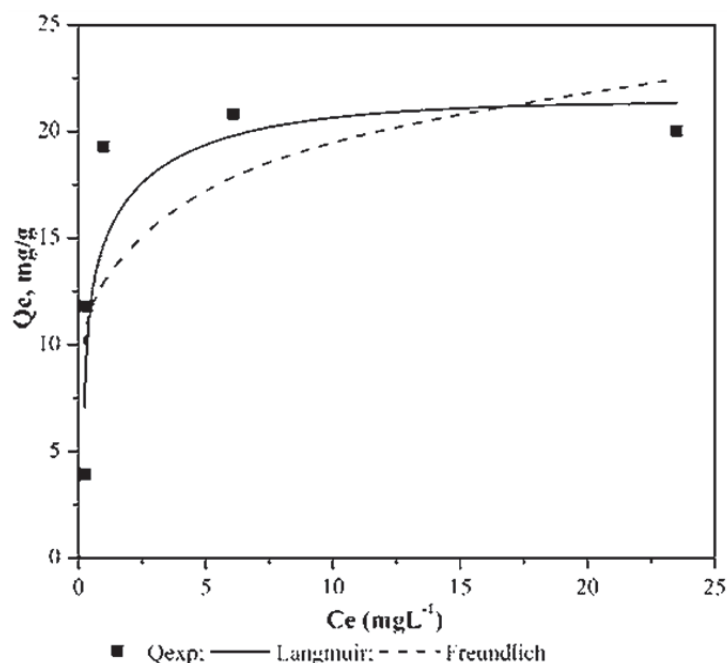


Fig. 6.10: Photodegradation isotherms of methyl orange on TiO₂/silica

photocatalyst represents a favourable uptake. Furthermore, a moderate Freundlich fit with R^2 value of 0.929 and low values of RMSE and χ^2 for TiO₂/silica composite photocatalyst was also obtained. This demonstrate that the nonlinear Freundlich model could be able to fit the experimental data as supported by the value of 'n' as 7.7186 which lies between 1 and 10. However, the Freundlich model was found not to be representative enough to describe the data, as reflected by the low correlation coefficients as compared to the Langmuir model. Hence, the linear regression of Langmuir model suggesting homogeneous distribution of active sites on composite photocatalyst surface was found to be the best fit. In addition, for TiO₂/silica composite photocatalyst, the linear regression of Langmuir model gave a better value of the maximum adsorption capacity of 20.24 mg/g for methyl orange without significantly affecting the quality of the fit, as the experimental values were close to the estimated values obtained by the model.

Table 6.1: Isotherms constants and correlation coefficients for the degradation of Methyl orange onto TiO₂/silica composite photocatalyst

Linear regression										
Composite photocatalyst	Langmuir isotherms			Freundlich isotherms						
	qm (mg/g)	K (L/mg)	R ²	n	K _f (L/mg)	R ²				
TiO ₂ /silica	20.24	6.5	0.999	0.399	2.3*10 ⁻³	0.5987				
Nonlinear regression										
Composite photocatalyst	Langmuir isotherm					Freundlich isotherm				
	Qm	K	R ²	χ^2	RMSE	n	K _f	R ²	χ^2	RMSE
TiO ₂ /silica	2.559	4.072	0.949	0.054	0.194	7.7186	1.680	0.929	0.044	-4.413

Photocatalysis is a time dependent process and it is very imperative to determine the rate of photocatalysis for designing and evaluating the photocatalyst in removing the pollutants from waste water. The data for the photodegradation of methyl orange on the composite photocatalyst was applied to pseudo-first and second-order kinetic model, and the results are presented in Table 6.2. The plot of pseudo-first-order and pseudo-second-order kinetic model, are shown in Fig. 6.11 and Fig. 6.12, respectively. The correlation coefficient for the second-order kinetic model (0.999) is greater than that of the first-order kinetic model (0.936). Therefore

the dye photocatalytic system by TiO₂/silica is a second-order reaction. The pseudo-first-order and second-order model equation are given in equation (4) and (5) (Repo et al., 2012).

$$\ln(q_e - q_t) = \ln q_e - k_1 t \quad (6.4)$$

where q_t and q_e are the adsorption capacity (mmol/g) at time t and at equilibrium respectively, while k_1 represents the pseudo first order rate constant (min⁻¹). The pseudo first order model was generalized to two-site-occupancy adsorption to form a pseudo-second-order equation:

$$\frac{t}{q_t} = \frac{1}{k_2 q_e^2} + \frac{t}{q_e} \quad (6.5)$$

where k_2 is the pseudo second order rate constant (g/mmol min). It has been distinguished that this model is able to estimate experimental q_e values quite well and is not very sensitive for the influence of the random errors (Repo et al., 2012).

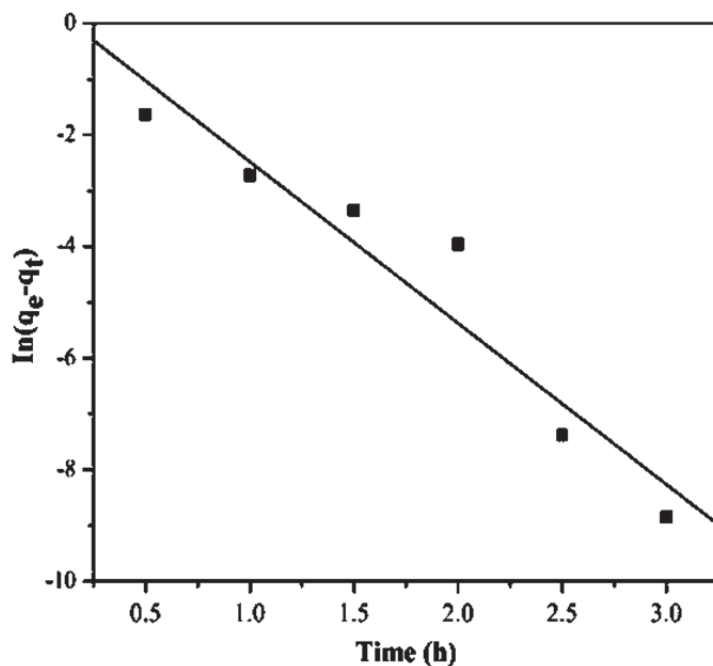


Fig. 6.11: Pseudo-first-order plot for the photocatalytic degradation of methyl orange dye onto TiO₂/silica

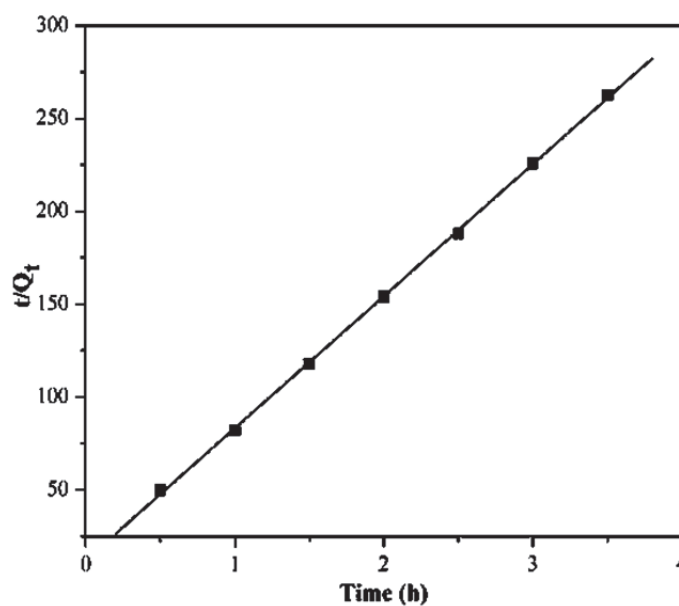


Fig. 6.12: Pseudo-second-order plot for the photocatalytic degradation of methyl orange dye onto TiO₂/silica

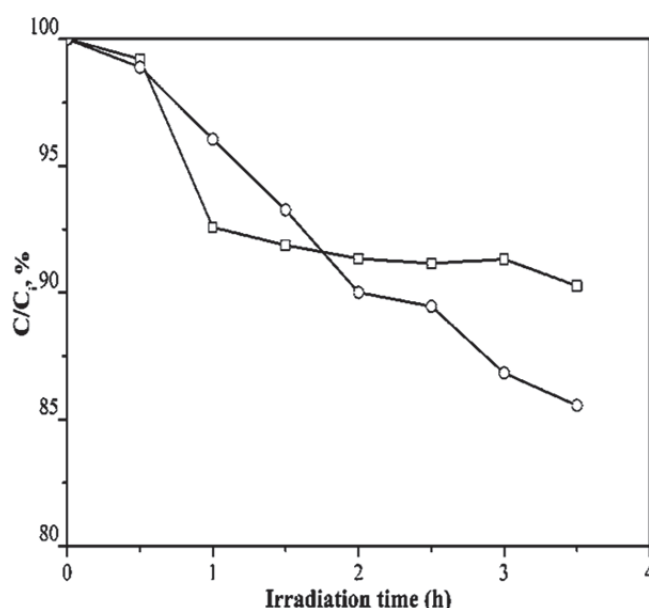
Table 6.2: Kinetic parameters for degradation of methyl orange

Pseudo-first-order model	k (min ⁻¹)	q _e (mg/g)	R ²
	0.122	0.95	0.936
Pseudo-second-order model	k (min ⁻¹)	q _e (mg/g)	R ²
	0.118	0.844	0.999

Since Cr(VI) and dye co-exist in wastewater from the leather tanning and textile industry, further experiments were conducted to remove the dye from synthetic Cr(VI) wastewater. To understand the effect of Cr(VI) in the presence of methyl orange dye, the photoreduction experiment of Cr(VI) alone was investigated at pH 6.3 and pH 3.

6.3.9 Photocatalytic reduction with a single substrate: Cr(VI)

Photocatalytic reduction of Cr(VI) has been investigated by several researchers using CdS and WO semiconductor catalyst (Chen and Ray, 2001). The general results showed that Cr(VI) can be easily reduced photocatalytically under UV irradiation, however, this is not in agreement with the results found in the present study. In this study, photocatalytic reduction of Cr(VI) was conducted with solution containing 5 mgL⁻¹ Cr(VI) and 1.25 gL⁻¹ composite photocatalyst, for 3.5 h at pH 3 and 6.5. As shown in Fig. 6.13, the photocatalytic reduction of Cr(VI) is much slower even in acidic medium. The slow photocatalytic reduction of Cr(VI) in the absence of methyl orange is due to the fact that the net photocatalytic reaction in a completely inorganic aqueous solution is the three electron-reduction of Cr(VI) to Cr(III) with oxidation of water to oxygen, in which the reduction kinetics of Cr(VI) is a slow four-electron process (Schrank et al., 2002) and hence, the photocatalytic reduction of the metal alone is relatively slow. Furthermore, the speciation in different solution pH plays an important role in the photocatalytic reduction of Cr(VI). A decrease in pH did not contribute

**Fig. 6.13: Photoreduction of Cr(VI) on TiO₂/silica at pH 3 (○); pH 6.5 (□)**

significantly to the reduction of Cr(VI) as illustrated in Fig. 6.13. This can be explained by the surface charge properties of the composite photocatalysts. At pH 3 the predominant species of chromium are the negatively charged HCrO₄⁻ and Cr₂O₇²⁻ ions, whilst at pH values around 6.3, Cr(VI) exists mainly as HCrO₄⁻ and CrO₄²⁻ (Papadam et al., 2007). The change in the amount of OH⁻ on the photocatalyst surface can also contribute to the pH influence. Since, the point of zero charge (PZC) of TiO₂/silica composite photocatalysts is at pH 2 (Fig. 6.4), the photocatalyst surface is negatively charged at pH greater than their PZC, whereas they are positively charged in more acidic conditions (pH < PZC), which favors the reduction of Cr(VI) anions. As the pH of the solutions increased, the negatively charged sites of the composite photocatalyst increased, thus,

the reduction of Cr(VI) anions was prevented due to electrostatic repulsion and consequently their reduction on the prepared composite photocatalyst surface.

6.3.10 Photocatalytic degradation of the dye and reduction of Cr(VI), ternary system

The effect of Cr(VI) on the photocatalytic degradation of methyl orange, an azo dye, was studied at various experimental conditions in further experiments. Fig. 6.14 shows the degradation-time profiles as well as the final Cr(VI) reduction at different composite photocatalyst concentration which was conducted at pH 6.5 and 3. The initial methyl orange concentration was kept constant at 25 mgL^{-1} . It can be seen (Fig. 6.14 a and b) that photocatalytic degradation efficiency decreased with the increasing loading at pH 6.5 and pH 3 compared to the preliminary experiment of dye alone. It is remarkable to note from Fig. 6.6 and Fig. 6.8 that for the binary dye/TiO₂-silica system, dye removal continuously proceeded faster than that of the respective ternary dye/Cr(VI)/ TiO₂-silica system (Fig. 6.14) irrespective of the photocatalyst loading and solution pH. This was more evident for the experiments performed at pH 6.5 and 1.25 gL^{-1} photocatalyst concentration. The photocatalytic reduction of Cr(VI) was expected to be more efficient in the Cr(VI)-dye system than in the single system due to the promoter effect by photocatalytic degradation of the dye.

It is important to note that high metal reduction on TiO₂/silica composite photocatalyst was achieved (12.5 gL^{-1}) in spite of the pH solution (Fig. 6.15a and b). This clearly indicates that during the ternary system, an extent of Cr(VI) reduction and methyl orange degradation was achieved at the same optimum composite photocatalyst concentration. In such organic and metal ion compound coexisting systems, the dye receives holes from the electrons band directly or indirectly and is oxidized (Fu et al., 1998). It was manifested that the photoreduction of Cr(VI) was much faster in the mixed system than the single one. This fact could be attributed to the oxidation of dye consuming photo-excited holes quickly, which weakens electron-hole recombination promoting the photocatalytic reduction of Cr(VI) on the photocatalyst surface. The diminished photocatalytic efficiency in the mixed system can be attributed to the competition between dye and dichromate anions for the composite photocatalyst active sites and, therefore, they have more reduced probabilities to adsorb onto the photocatalyst surface and undergo photocatalytic reactions than in the individual binary systems.

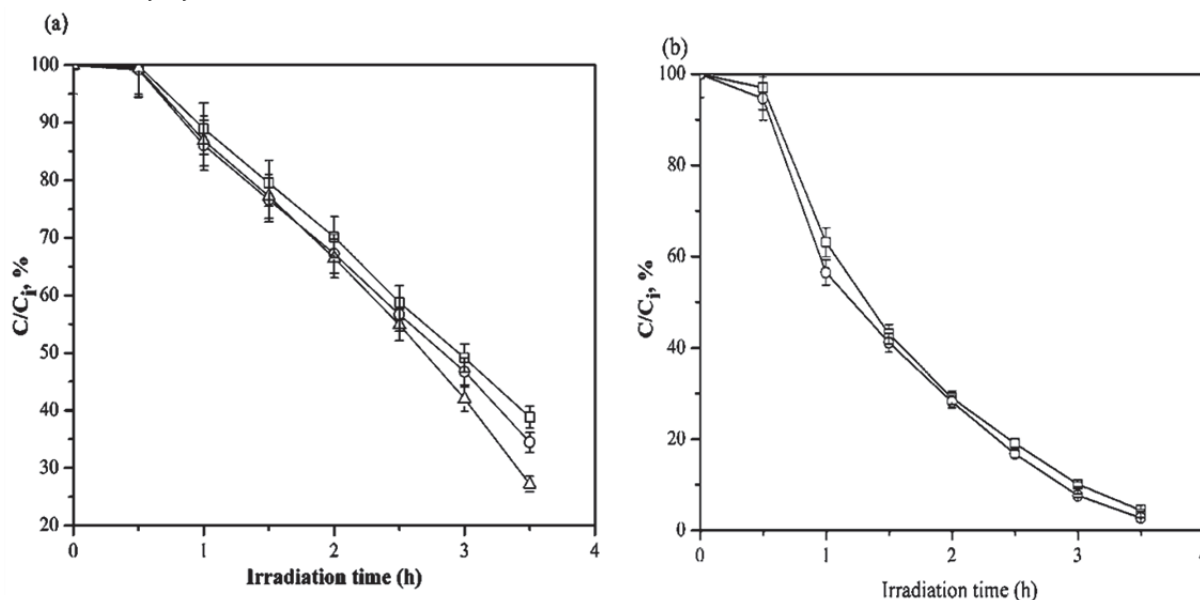


Fig. 6.14: Effect of TiO₂/silica photocatalyst concentration on dye degradation in the presence of Cr(VI) at (a) pH 6.5: 1.25 gL^{-1} (□); 6.25 gL^{-1} (Δ) 12.5 gL^{-1} (○) and (b) pH 3: 6.25 gL^{-1} (◐) 12.5 gL^{-1} (□)

Moreover, the composite photocatalyst to some extent, becomes deactivated due to the formation of stable precipitates that hindered the active sites of the photocatalyst. For example, Chen and Cao (2005) reported that Cr³⁺ is likely to precipitate as Cr(OH)₃ at pH values beyond 4-5, therefore covering the composite photocatalyst surface. This agrees with the results obtained when Cr(VI) alone (Fig. 6.13) was photocatalytically reduced due to the slow reduction of Cr(VI) to Cr(III). Hence, the decline in photocatalytic

activity was more distinguishable at near-neutral rather than acidic conditions. Furthermore, dye degradation intermediate products and chromic species can form complexes that also contribute to composite photocatalyst deactivation. Colon et al. (2001) investigated the simultaneous photocatalytic treatment of salicylic acid and Cr(VI) over various TiO₂ suspensions at pH 2 and reported that the conversion of both pollutants in the ternary system was extensively lower than that in the corresponding binary systems. This was due to the occurrence of photocatalyst deactivation as a result of trivalent chromium deposition on the active sites.

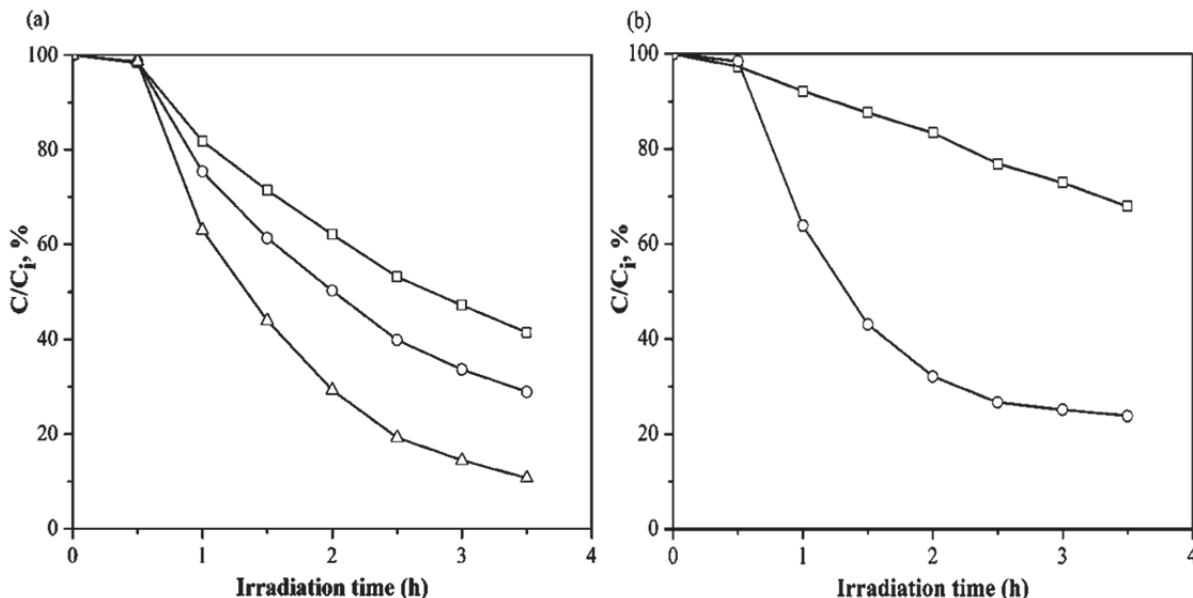


Fig. 6.15: Effect of TiO₂/silica concentration on Cr(VI) reduction in the presence of dye; (a) pH 6.5: 1.25 gL⁻¹ (□); 6.25 gL⁻¹ (○); 12.5 gL⁻¹ (Δ) and (b) pH 3: 6.25 gL⁻¹ (□); 12.5 gL⁻¹ (○).

In the final set of experiments, the effect of Cr(VI) concentration on the photocatalytic efficiency of methyl orange was evaluated at optimum conditions. Fig. 6.16 shows that high photocatalytic degradation efficiency of methyl orange on TiO₂/silica composite photocatalyst was achieved with an increase of Cr(VI) concentration initially, however, decrease was observed when Cr(VI) concentration was beyond 2 mgL⁻¹. The degradation efficiency was 94.8% at 2 mgL⁻¹ and decreased to 76.1% and 65.6% at 5 and 10 mgL⁻¹ metal concentration, respectively (Fig. 6.16). The increase in degradation efficiency at low metal initial concentration can be due to the fast reaction in the hole photogenerated in the presence of Cr(VI) whose photoreduction is also favoured in the presence of organic compounds as reported. This aspect is important due to the high affinity of the dye to the composite photocatalyst surface as well as the production of more electrons in the conduction band. However, as the metal concentration increased, the dye degradation

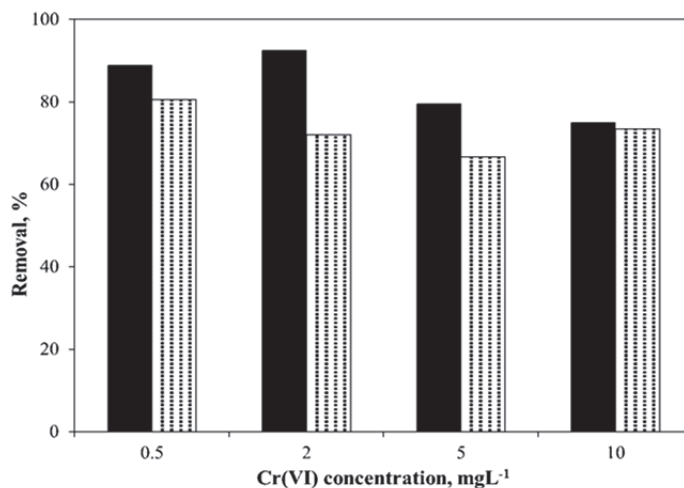


Fig. 6.16: Effect of Cr(VI) initial concentration on dye degradation (black bars) over TiO₂/silica and final Cr(VI) reduction (hatched bars). Condition: C₀= 25 mgL⁻¹; pH= 3

decreased and this may be attributed to more metal ions adsorbed onto TiO₂/zeolite and TiO₂/silica composite photocatalyst surface which then block the adsorption of methyl orange molecules

6.4 Conclusion

In the first part of the work, TiO₂ was supported on silica material for the photodegradation of methyl orange in the absence and presence of ions. The characterization of TiO₂ supported silica revealed the good dispersion of TiO₂ on the surface of silica. The optimum operating conditions found during photocatalytic experiments include 1.25 gL⁻¹ photocatalyst composite concentration, 25 mgL⁻¹ dye concentration and pH 3. The dye degradation at 3.5 h of irradiation was 96.4% and 72.8% for the binary and ternary systems, respectively, with the compatible values at pH 3 being 99.8% and 76.17% for the binary and ternary systems, respectively. The Langmuir model was found to be best fitting for methyl orange photodegradation on TiO₂/silica composite photocatalyst. Significant deviations between experimental and predicted data were observed with Freundlich model, implying that all the binding sites were similar on the composite photocatalyst in accordance with Langmuir's theory. The degradation of dye/TiO₂-silica system proceeds faster than that of the respective ternary dye/Cr(VI)/ TiO₂-silica system at neutral pH. It is evident that the photo reduction of Cr(VI) was much faster in the mixed system than in the single one. This could be attributed to the oxidation of dye consuming photo-excited holes rapidly and proficiently, attenuating electron-hole recombination and improving the Cr(VI) reduction on photocatalyst surface. A higher composite photocatalyst loading is required in order for the faster reduction of Cr(VI) to Cr(III) to take place during the mixed system.

References

- Aksu, Z. (2005). Application of biosorption for the removal of organic pollutants: a review. *Process Biochemistry*, 40:997-1026.
- Auguliaro, V., Davi, E., Palmisano, L., Schiavello, M., Sclafani, A. (1990). Influence of hydrogen peroxide on the kinetics of phenol photodegradation in aqueous titanium dioxide dispersion. *Applied Catalysis*, 65(1), 101-116.
- Beattie, I.R. and Gilson, T.R. (1968). *Proc. Roy. Soc. London. A*, 307:407.
- Bhatnagar, A., Sillanpää, M. (2009). Applications of chitin-and chitosan-derivatives for the detoxification of water and wastewater – a short review. *Advances in Colloid and Interface Science*, 152(1), 26-38.
- Chen, D., Ray, A. K. (1999). Photocatalytic kinetics of phenol and its derivatives over UV irradiated TiO₂. *Applied Catalysis B: Environmental*, 23(2), 143-157.
- Colon, G., Hidalgo, M.C., Navio, J.A. (2001). Photocatalytic deactivation of commercial TiO₂ samples during simultaneous photoreduction of Cr (VI) and photooxidation of salicylic acid. *Journal of Photochemistry and Photobiology A*, 138(1):79-85
- Cox, G. (1993). The influence of silica structure on reversed-phase retention. *Journal of Chromatography*, 656:353-367
- Freundlich, H. M. F. (1906). Over the adsorption in solution. *J. Phys. Chem*, 57(385471), 1100-1107.
- Fu, H., Lu, G., Li, S. (1998). Adsorption and photo-induced reduction of Cr (VI) ion in Cr (VI)-4CP (4-chlorophenol) aqueous system in the presence of TiO₂ as photocatalyst. *Journal of Photochemistry and Photobiology A: Chemistry*, 114(1), 81-88.
- Gaya, U.I. and Abdullah, A.H. (2008). Heterogeneous photocatalytic degradation of organic contaminants over titanium dioxide: a review of fundamentals, progress and problems. *Journal of Photochemical. Photobiology, C: Photochemical: review*, 9:1-12.
- Kansal, S. K., Singh, M., Sud, D. (2007). Studies on photodegradation of two commercial dyes in aqueous phase using different photocatalysts. *Journal of hazardous materials*, 141(3), 581-590.
- Langmuir, I., (1918). The Constitution and Fundamental Properties of Solids and Liquids. *Journal of the American Chemical Society*. 40 (9), 1361-1403.
- Londeree, D.J. (2002). Silica-titania composites for water treatment, MSc. Dissertation. University of Florida

- Neppolian, B., Choi, H. C., Sakthivel, S., Arabindoo, B., Murugesan, V. (2002). Solar light induced and TiO₂ assisted degradation of textile dye reactive blue 4. *Chemosphere*, 46(8), 1173-1181.
- Neppolian, B., H.C. Choi, S. Sakthivel, B. Arabindoo and V. Murugesan. (2002). Solar light induced and TiO₂ assisted degradation of textile dye reactive blue 4. *Chemosphere*, 46, 1173-1181.
- Nowacka, M., Ambrohewicz, D., Jesionowski, T. (2013). TiO₂-SiO₂/Ph-POSS Functional Hybrids: Preparation and Characterisation. *Journal of Nanomaterials*, 1-10.
- Ollis, D. F., Pelizzetti, E., Serpone, N. (1991). Photocatalyzed destruction of water contaminants. *Environmental Science & Technology*, 25(9), 1522-1529.
- Papadam, T., Xekoukoulotakis, N. P., Poullos, I., Mantzavinos, D. (2007). Photocatalytic transformation of acid orange 20 and Cr (VI) in aqueous TiO₂ suspensions. *Journal of Photochemistry and Photobiology A: Chemistry*, 186(2), 308-315.
- Papirer, E. (2000). *Adsorption on silica surfaces*. CRC Press.
- Park, D., Yun, Y. S., Park, J. M. (2005). Use of dead fungal biomass for the detoxification of hexavalent chromium: screening and kinetics. *Process Biochemistry*, 40(7), 2559-2565.
- Persello, J., (2000). Surface and interface structure of silicas, in: *Adsorption on Silica Surfaces*, Papirer, E. (Ed), John Wiley and Sons Ltd., New York, 297-342,.
- Saien, J., Khezrianjoo, S. (2008). Degradation of the fungicide carbendazim in aqueous solutions with UV/TiO₂ process: Optimization, kinetics and toxicity studies. *Journal of hazardous materials*, 157(2), 269-276.
- Sharma, M. V. P., Lalitha, K., Durgakumari, V., Subrahmanyam, M. (2008). Solar photocatalytic mineralization of isoproturon over TiO₂/HY composite systems. *Solar Energy Materials and Solar Cells*, 92(3), 332-342.

CHAPTER 7

7 INTEGRATED BIODEGRADATION AND PHOTODEGRADATION

7.1 Introduction

Molasses-based distilleries and textile industries are among the most polluting industries that generate large volumes of high strength wastewater. On the one hand, distillery effluent is characterized by an extremely high organic load as well as strong odour and recalcitrant dark brown colour (Satyawali and Balakrishnan, 2008). The recalcitrant dark brown pigment in the distillery wastewater is called melanoidin. On the other hand, textile industry effluent is characterized by huge amounts of a wide variety of recalcitrant dyes (Chen et al., 2008). Anaerobic digestion (AD) has been considered to be a very suitable technique for the treatment of distillery and textile effluent due to its energy generation potential (Somasari et al., 2008). However, the recalcitrant and toxic nature of the organic pollutants generated from dye stuff have posed a great challenge in the adoption of AD in the treatment of the textile effluent (Oller et al., 2011). This leads to low digestion which results in low energy generation. The low digestion efficiency always calls for long hydraulic retention times in order to achieve significant elimination of the biorecalcitrant components, and at times there could be digester failure. Chu and Tsui, (Chu and Tsui, 2002) reported that most dyes cannot be totally eliminated by biological wastewater treatment methods due to their biorecalcitrant nature.

In contrast, distillery effluent contains a high amount of biodegradable organic contaminants which can be converted into biogas in the AD process. However, the major challenge facing the AD treatment of distillery wastewater is the fact that this process is incapable of removing the colour associated with the distillery wastewater (Satyawali and Balakrishnan, 2008; Pant and Adholeya, 2007). The colour is caused by melanoidins which are biorecalcitrant due to their antioxidant property which makes them toxic to many micro-organism species involved in the AD process (Satyawali and Balakrishnan, 2008; Pant and Adholeya, 2007). The AD process therefore has been pointed out to be inefficient when used as an individual technique in the treatment of distillery effluent (Satyawali and Balakrishnan, 2008; Simate et al., 2011; Oller et al., 2011).

Recently, there has been a considerable interest in the utilization of advanced oxidation processes (AOPs) for complete removal of the recalcitrant components of distillery and textile effluent (Forgacs et al., 2004). The chemistry of AOP is based on the production of hydroxyl radicals as oxidizing agents which mineralize organic contaminants. The AOPs which have been used with good pollutant removal efficiencies include: $\text{H}_2\text{O}_2/\text{UV}$, UV/TiO_2 (UV photocatalysis) (Huang et al., 2008) and UV photolysis (Wong and Chu, 2003). However, the cost associated with the AOPs is often prohibitive for wastewater treatment (Al-Momani et al., 2002).

Previous studies have attempted integration of AOPs and biological treatment processes as an economical means for treating bio-recalcitrant organic contaminants in wastewater (Oller et al., 2011; Al-Momani et al., 2002; Parra et al., 2002). These studies, however, focused mainly on aerobic digestion rather than the anaerobic digestion. Therefore integration of AOP and anaerobic digestion needs more studies to evaluate its performance not only in organic load reduction but also in energy generation. In one instance, the AOP can be used as a pre-treatment technique in order to increase the biodegradability of the wastewater. Conversely, in an instance where the AOP cannot improve the biodegradability of the biorecalcitrant compounds, it can be used as a post-treatment method to totally remove the biorecalcitrant compounds that would otherwise require longer digestion time in the AD unit. In either of the two scenarios, the two technologies must be integrated to provide a technically and economically feasible option. In the design of the integrated process, whether the AOP or the biological process comes first in the treatment line, the overall purpose of reducing cost will be nearly the same as minimizing AOP treatment and maximizing the biological stage (Oller et al., 2011). This is due to the fact that AOP is a more costly technology than the biological process (Oller et al., 2011). If UV photocatalysis is employed as the AOP of choice, then irradiation time is of high consideration because it directly affects the operation cost.

One likely advantage of using AOP pre-treatment in the treatment of textile dyes and distillery effluent is that it can improve biodegradability of the recalcitrant compounds (Al-Momani et al., 2002; Parra et al., 2002). Similarly, the advantage of employing a biological method as pre-treatment is in the fact that textile wastewater is characterized by very intense colour, which can lead to light attenuation during UV treatment unless high dilution is employed; the biological pre-treatment can therefore be employed to reduce the colour before final UV treatment. This is likely to result in shorter irradiation time thereby lowering the operational cost considerably. Furthermore, in the integrated system, the energy required by the UV photodegradation process can be supplied by the anaerobic process, thereby making the integrated system to be self-sufficient. This section aims at studying the feasibility of using an integrated UV photocatalytic degradation (AOP) and anaerobic digestion (AD) in the treatment of methylene blue dye which is a model textile dye, molasses wastewater and real distillery wastewater. Zeolite, which is an adsorbent, is used as support medium for the TiO_2 photocatalyst and biomass support in the photoreactor and bioreactor, respectively. The efficiency of using the UV photocatalyst process as either a pre-treatment or post-treatment method to the AD process is evaluated in a fixed bed up-flow bioreactor and photocatalytic reactor. The results in this section have been published elsewhere (Apollo et al., 2013; 2014).

7.2 Methodology

7.2.1 Materials

Distillery effluent was obtained from Talbot & Talbot (Pty), Pietermaritzburg, South Africa. Raw molasses was purchased from a local commercial outlet at Vanderbijlpark, South Africa and was diluted to make synthetic molasses wastewater. The South African natural zeolite was purchased from Pratley mining company in South Africa and crushed to particle size of 2 mm diameter. Titanium dioxide powder (Technical grade, 99% purity) and Methylene blue dye was purchased from Sigma Aldrich.

7.2.2 Inoculum and wastewater preparation

Inoculum used was obtained from a digester treating distillery effluent and a secondary digester of municipal wastewater treatment plant (Sebokeng water plant, South Africa). The distillery wastewater, synthetic molasses wastewater (MWW) and methylene blue (MB) dye were diluted as appropriate, mixed with inoculum in the ratio of 7:3, this was the best ratio obtained from batch preliminary studies. The mixture was then supplemented with various nutrients: KHPO_4 (20 mg/L), $\text{MgSO}_4 \cdot 7\text{H}_2\text{O}$ (5 mg/L), NiSO_4 (10 mg/L), NH_4NO_3 (20 mg/L), FeSO_4 (5 mg/L) and $\text{Ca}(\text{HCO}_3)_2$ (20 mg/L) (Somasiri et al., 2008; Sreekrishnan et al., 2004; Andalib et al., 2012). The inoculum, wastewater samples and inoculated wastewater samples were characterized.

7.2.3 Experimental set-up

Laboratory scale anaerobic up-flow fixed bed reactor and annular photoreactor (Fig. 7.1) were used in this study. The outer wall of the photoreactor was made of Perspex while the inner wall, which was the UV shield (protector), was made of borosilicate glass in such a way as to create an annular space of volume 0.52 L between the inner wall of the Perspex tube and the outer wall of the borosilicate tube. The inside diameter of the inner borosilicate tube was 36 mm and it was 2 mm thick while the inside diameter of the Perspex tube was 56 mm and it was 3 mm thick. Each reactor had a working volume of 0.45 L. At the bottom of both the reactors (the inlet section) there was a distribution compartment fitted with a distribution plate which had 34 evenly distributed holes each of 1 mm in diameter. This compartment was to ensure an even distribution of the influent during reactor feeding and recycling so as to minimize channelling across the bed. For a better comparison of the overall performance of the integrated system, according to this study, the photoreactor and bioreactor used were of similar dimensions.

The photocatalytic reactor was packed with the TiO_2 /zeolite (TZ) composite catalyst, 15 W UV-C was used as source of irradiation. The TZ composite catalyst used was prepared by solid-solid dispersion method

(Durgakumari et al., 2008) with a TiO₂ composition of 15%. The bioreactor was packed with zeolite of 2 mm particle size. Peristaltic pumps were used to feed and circulate wastewater in the reactors.

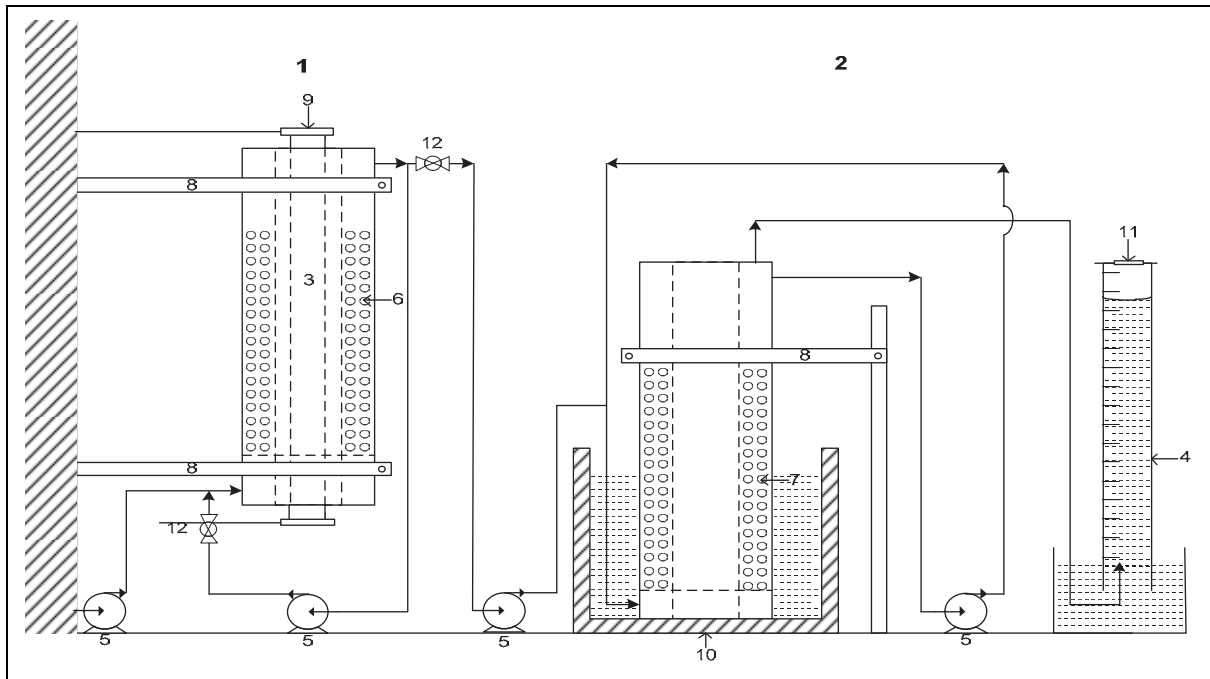


Fig. 7.1: The integrated photocatalytic degradation and anaerobic digestion set up: (1) photodegradation unit (2) biodegradation unit, (3) 15 W UV lamp, (4) measuring cylinder for gas collection, (5) peristaltic pump, (6) TiO₂/zeolite catalyst, (7) zeolite, (8) clamp, (9) UV tube holder, (10) water bath, (11) butyl rubber septum, (12) valve.

7.2.4 Photodegradation and biodegradation experiments

Photodegradation and biodegradation experiments were carried out separately in the respective reactors; this was then followed by an integration of the two processes. The experiments were carried out in batch. In the integrated system, the two processes were arranged in series so that, in the first case, the photodegradation process was followed by the AD process while in the second case the AD process was followed by the photodegradation process. Photodegradation was carried out at pH 4 for molasses and distillery and pH 9 for MB since these were the optimum pH conditions for the photodegradation as was observed in preliminary experiments conducted in 100 ml conical flasks irradiated with 15 W UV-C lamp. In the case where photodegradation (AOP) preceded the AD, the pH of the photodegraded effluent was adjusted to about 7 before feeding to the bioreactor. Also, in the case where the AD process preceded AOP, the pH of the AD treated effluent was adjusted to 4 for molasses and distillery and 9 for MB dye before feeding to the photoreactor. The effluent was recirculated at 40 cm³/min and 10 cm³/min in the photoreactor and bioreactor, respectively. The biogas produced during the AD process was collected using Mariotte water displacement method. In this case, the measuring cylinder which was used to collect the gas had a butyl rubber septum at the top for gas sampling. Adsorption experiments on TZ catalyst and zeolite were conducted as control. Degraded wastewater was left to settle then filtered before measuring its absorbance at 475 nm to evaluate degradation efficiency. Percentage colour removal (\emptyset) was calculated as;

$$\emptyset = \frac{(A_0 - A_t)}{A_0} \times 100 \quad (7.1)$$

where A_0 is the initial absorbance and A_t is the absorbance at time t .

7.2.5 Experimental analysis

To evaluate the performance of the system, various performance indicators were analysed. The COD and BOD were analysed in accordance with the standard laboratory procedure (Clesceri et al., 2005). In the COD analysis, closed reflux method using dichromate solution as oxidant was employed and Nanocolor colorimeter was used for analysis. The analysis for COD was done in triplicate and average value used. Phosphates and nitrates were analysed using spectrophotometer (HACH DR 2000) while colour was measured using UV-vis spectrophotometer model DR 2800 (HACH). The amount of biogas produced was read directly from the inverted measuring cylinder used for gas collection. The methane composition of the gas was determined using gas chromatograph (GC) model SRI 8610C, fitted with thermal conductivity detector (TCD). Scanning electron microscopy (SEM), model FEI NOVANO SEM 230, fitted with energy dispersive X-ray spectrophotometry (EDX), was used to study the surface morphology of the TiO₂-zeolite catalyst and the elemental composition of zeolite.

7.2.6 Statistical Analysis

To compare the performances of AD and integrated AOP-AD or AD-AOP system, t-test for two-independent samples was carried out. Sampling was done in triplicate and the mean colour and COD removal efficiencies for these treatment processes were compared against each other.

7.3 Results and discussion

The integrated anaerobic digestion and photocatalysis of both distillery and textile wastewaters was investigated in an annulus reactor. Both the materials and wastewater were characterized using standard methods. The results showed that photodegradation improves biodegradability of the wastewater used and methane yield. However, the optimal reactor sequence was dependent on the type of waste.

7.3.1 Distillery wastewater

7.3.1.1 Zeolite, catalyst and wastewater characterization

The EDX analysis of the South African clinoptilolite (natural zeolite) showed the following elemental composition: O (57.41%), Na (1.52%), Mg (0.63%), Al (6.5%), Si (30.63%), K (1.99%), Ca (0.73%) and Fe (0.57%). The SEM analysis for the TZ catalyst is shown in Fig. 7.1, where it can be seen that the TiO₂ attached well on zeolite (Fig. 7.2a). Even after photodegradation, TiO₂ was still attached on zeolite surface (Fig. 7.2b).

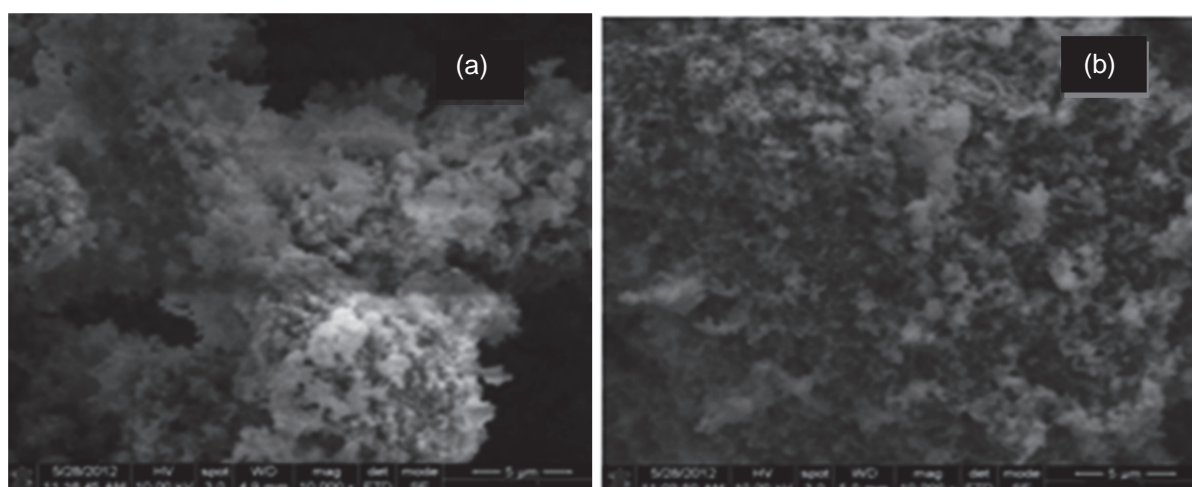


Fig. 7.2: SEM analysis for TiO₂-zeolite catalyst (a) before photodegradation and (c) after photodegradation

The characteristics of real distillery wastewater, synthetic commercial molasses wastewater, inoculum and inoculated wastewater samples are shown in Table 7.1.

Table 7.1: Wastewater characteristics

Characteristics	Inoculum	Distillery	MWW	Inoculated distillery	Inoculated MWW
Total COD (mg/L)	2942± 127	5761± 105	4980± 117	5050 ± 59	4738 ± 56
Soluble COD (mg/L)	900 ± 35	4125± 87	3820± 64		
BOD (mg/L)	526	1160	1118	1701	1652
Total nitrogen (mg/L)	59	142	392	206	455
Total phosphates (mg/L)	36	34	7	72	40
Total suspended solids (mg/L)	112	87	62	205	181
pH	6.8-7.2	4.2-4.5	4.6-4.8	6.8-7.1*	6.8-7.1*

* Adjusted values

7.3.1.2 Photodegradation in the annulus photocatalytic reactor

Results for photodegradation of the distillery effluent and MWW at their natural pH (4) are shown in Fig. 7.3. After irradiation time of 3 hours, MWW and distillery attained colour removal of 69% and 54%, respectively. However, a low corresponding reduction in COD of 20% and 15% was recorded for MWW and distillery wastewater, respectively. The observed reduction in colour during photodegradation can be explained by the reaction mechanism involving photogenerated hydroxyl radicals and the organic contaminants. The chromophores of melanoidin which is a constituent of the MWW and distillery wastewater are contributed by conjugated C=C and C=O (Kwak et al., 2004). The photogenerated hydroxyl radicals are known to react with organic compounds by addition to the double bond or by abstraction of hydrogen atoms from aliphatic organic molecules (Buxton et al., 1988). Therefore, it follows that the double bonds of the melanoidin present in the MWW and distillery wastewater were broken by the photogenerated hydroxyl radicals leading to colour reduction.

The low COD removal observed during photodegradation of MWW and distillery wastewater has also been observed in previous studies (Pala and Erden, 2005; Peña et al., 2003). The possible explanation is that the change in the structure of melanoidin during photodegradation, which resulted in colour reduction did not lead to total mineralization of the melanoidin thus resulting in the low COD reduction (Dwyer et al., 2008). It could also be observed that MWW experienced a better colour removal (69%) than that of the distillery wastewater (54%) yet they both contain melanoidin as the major colour-imparting compound. This difference can be attributed to the fact that the real distillery wastewater is more complex as it contained some other additives used during the fermentation process unlike raw molasses. In addition, the processes involved during fermentation and distillation could have altered, to some extent, the physical and chemical properties of the melanoidin in the real distillery wastewater unlike melanoidin in the raw molasses wastewater. Moreover, distillery effluent contains some traces of ethanol since the distillation process is not always 100% efficient (Wilkie et al., 2000), and it has been reported that ethanol retards hydroxyl radical production during the photodegradation process (Daneshvar et al., 2004). It was further observed that there was a negligible decrease in BOD during photodegradation of both the wastewater samples.

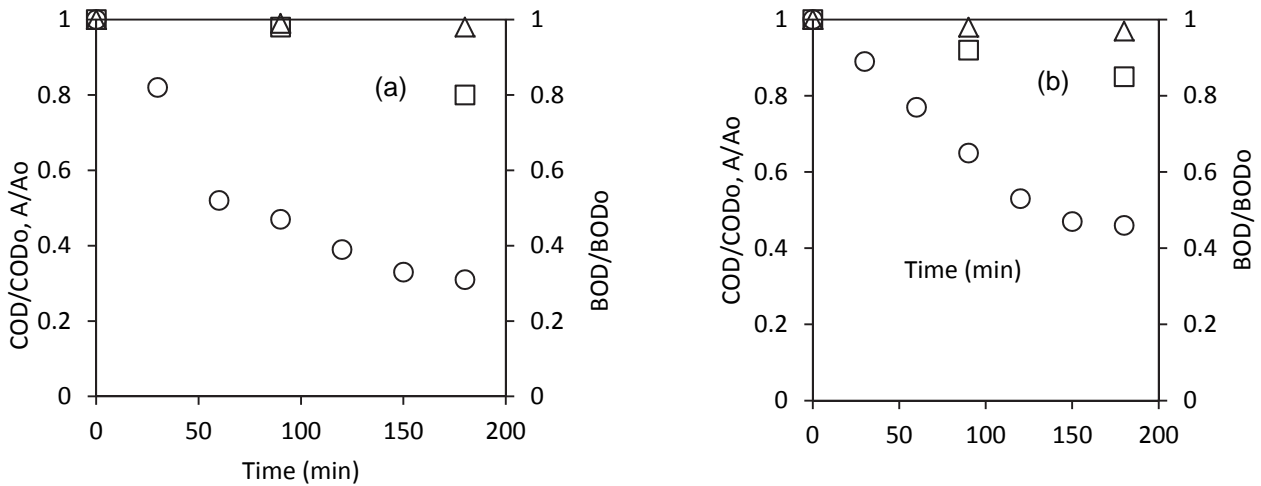


Fig. 7.3: Photodegradation of; MWW (a) and distillery wastewater (b) in the annular photocatalytic reactor; colour (○), COD (□) and BOD (△)

7.3.1.3 Anaerobic degradation of UV pre-treated and non-UV pretreated wastewater

The effect of the UV pre-treatment on the anaerobic digestion of the wastewater samples was studied whereby the effluent from the photoreactor was fed into the bioreactor unit. In Fig. 7.4a it can be seen that the non-UV pretreated MWW had higher COD removal (80%) compared to the UV-pretreated stream (47%). BOD reduction also showed a similar trend with the non-UV pretreated MWW attaining a reduction of 99% while the UV pretreated stream had 88% reduction. In Fig. 7.4b, the non-UV pretreated distillery had COD and BOD removals of 75% and 97%, respectively, while the UV pretreated stream had COD and BOD reduction of 70% and 94%, respectively. The relatively low COD removal observed in the UV-pretreated samples, may suggest that the UV process might have generated some less biodegradable intermediates. It has been reported that sometimes AOP pre-treatment of biorecalcitrant components of wastewater may lead to formation of stable intermediates which are less biodegradable than the original molecules (Oller et al., 2011).

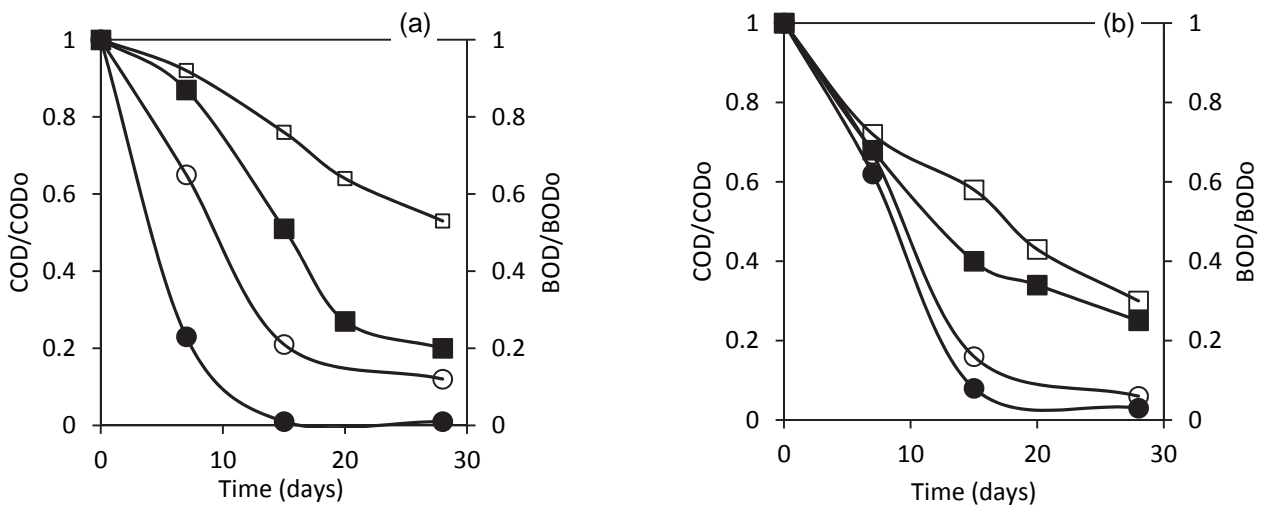


Fig. 7.4: Anaerobic degradation of; MWW (a) and distillery (b) wastewater streams. UV pretreated wastewater streams (open symbols), COD (□) and BOD (○) and non UV treated streams (closed symbols), COD (■) and BOD (●)

Generally, the performance of the anaerobic process in BOD removal from molasses-based distillery industries is reported to be higher than 80% while COD removal can vary from about 40% to above 95% depending on process parameters and reactor configuration used (Satyawali and Balakrishnan, 2008).

7.3.1.4 Removal by adsorption in the photoreactor and bioreactor

Contribution of adsorption to the contaminant removal or concentrating the pollutants on the TZ composite catalyst surface in the photoreactor was studied. In this study, the wastewater stream was circulated in the reactor without irradiating with the UV light. Also, contaminant removal by adsorption on the zeolite surface in the bioreactor was studied (no inoculum was added) and results are presented in Table 7.2.

Table 7.2: Colour and COD reduction by adsorption in the photoreactor and bioreactor

Wastewater stream	Photoreactor		Bioreactor	
	Colour reduction, %	COD reduction %	Colour reduction %	COD reduction %
Distillery	17.4	<10	19	<10
MWW	19.2	<10	26	<10

It is important to note that the adsorption on zeolite coated with TiO₂ (in the photoreactor) was slightly lower than that of the unmodified zeolite (in the bioreactor), this may be attributed to the blockage of some adsorptive pores of zeolite by TiO₂ in the former case. In both cases, adsorption onto zeolite and onto TiO₂ coated on zeolite, did not result in any appreciable BOD removal for both the wastewater samples.

7.3.1.5 Cumulative biogas production and methane yield

Daily biogas production during the anaerobic degradation of non-UV pretreated and UV pretreated wastewater samples were recorded and the cumulative amounts are shown in Fig. 7.5.

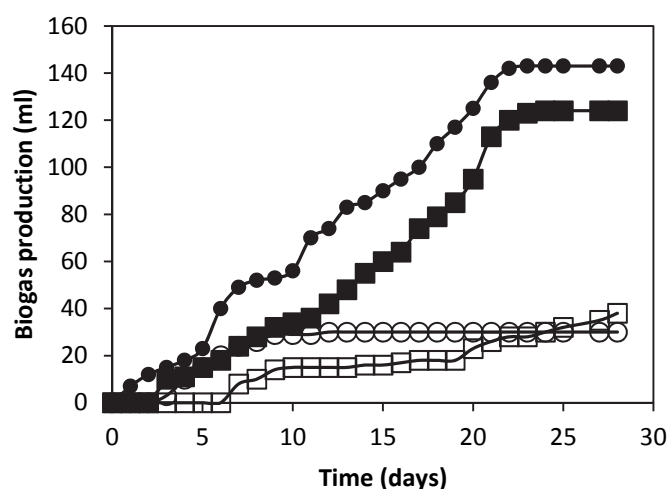


Fig. 7.5: Cumulative biogas production during the anaerobic process; non-UV pretreated MWW (■), UV pretreated MWW (□), non-UV pretreated distillery (●) and UV pre-treated distillery (○)

Both the non-UV pretreated MWW and real distillery wastewater had better gas production than their UV pretreated counterparts suggesting the presence of more toxic photodegradation by-products. This is also reflected in the fact that the non-UV pretreated samples had shorter lag periods as compared to the UV pre-

treated samples. However, the biogas production was relatively low due to high COD loading considering the small reactor volume used. Biogas analysis showed that the non-UV pretreated MWW had methane yield of 75.9% after 25 days of digestion while the UV pretreated stream had 71.2% for the same period. On the other hand, both the distillery samples had almost equal methane yield of 73.9% and 73% for the non-UV pretreated and UV pretreated, respectively.

7.3.1.6 Volatile fatty acids (VFAs) and pH

It is reported that accumulation of VFAs in the digester may lead to process failure as this results in low pH in the digester which inhibits microbial growth. For digestion to proceed optimally, the concentration of the VFAs in the digester should be less than 250 mg/L (Somasiri et al., 2008)[27]. It is therefore important to monitor the concentration of VFA and pH during the anaerobic degradation process. In Fig. 7.6, there was a high initial VFAs concentration for MWW and this might have led to the low gas production during the onset of degradation of MWW as shown in Fig. 7.5.

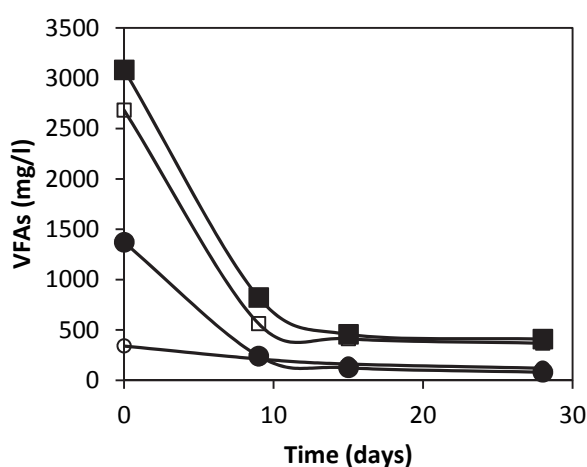


Fig. 7.6: VFA removal during the anaerobic process, non- UV pre-treated MWW (■), UV pre-treated MWW (□), non- UV pre-treated distillery (●) and UV pre-treated distillery (○)

Also, UV pretreated wastewater had lower VFAs concentration compared to the non-pretreated wastewater. This may be due to the fact that the UV pretreatment led to degradation of the VFAs in these wastewater samples. This may also be evidenced by the reduction in COD during UV pretreatment observed in Fig. 7.3. Even though low VFA concentration is likely to lead to higher biogas production, this was not observed in the pre-treated wastewater samples. This may be due to the generation of more toxic photodegradation intermediates (Oller et al., 2011)

In Fig. 7.6, it can further be seen that after about 10 days of degradation the concentration of VFA stabilized in the digesters. This is most likely due to the fact that the amount of VFAs produced from the acidogenesis process was being consumed in the methanogenesis process resulting in process stability. Somasiri et al. (2008) reported that under a constant VFA concentration, H₂ and acetic acid formed due to acidogenic and acetogenic bacterial activities were utilized immediately and converted into methane by methanogens. Similar trend of VFA reduction has been reported (Vavilin and Lokshina, 1996; Wang et al., 1999) in mesophilic anaerobic degradation of VFAs.

The pH of the various wastewater samples were monitored during the entire digestion period and results presented in Table 7.3. It can be seen that during the digestion period the pH values were within the expected range of 6.0-8.0 in anaerobic digester (Acharya et al., 2008). However, there was a slight increase in pH values with the degradation time from day 0 to day 28. This observation might have been due to the

corresponding reduction in VFAs concentration with time as shown in Fig. 7.6, which led to a slight reduction in the acidity of the media.

Table 7.3: pH variation during the anaerobic degradation process

pH of wastewater				
Day	MWW		Distillery	
	UV pretreated	non-UV pretreated	UV pretreated	non-UV pretreated
0	7.15	7.08	7.2	7.18
15	7.31	7.46	7.42	7.58
20	7.73	7.87	7.64	7.32
28	7.93	8.02	7.77	7.98

7.3.1.7 Nitrates and phosphates

A reduction in nitrate concentration during the anaerobic digestion process was observed in all wastewater samples treated under various conditions as shown in Fig. 7.7. From the figure, it can also be observed that the initial nitrogen concentration of the UV pretreated wastewater samples were generally lower than those of the non-UV pretreated wastewater samples for the MWW while the trend for the distillery wastewater was not very distinct. During photodegradation pre-treatment, ammonia nitrogen could have been removed in the photoreactor by an ion exchange process, since zeolite is reported to be a very good ammonia exchanger (Montalvo et al., 2012; Milán, 2001). This leads to the lower nitrogen concentration in the UV pretreated MWW stream. Also, some dissolved organic nitrogen (DON) and ammonia nitrogen could have been removed by the photodegradation process (Dwyer et al., 2008).

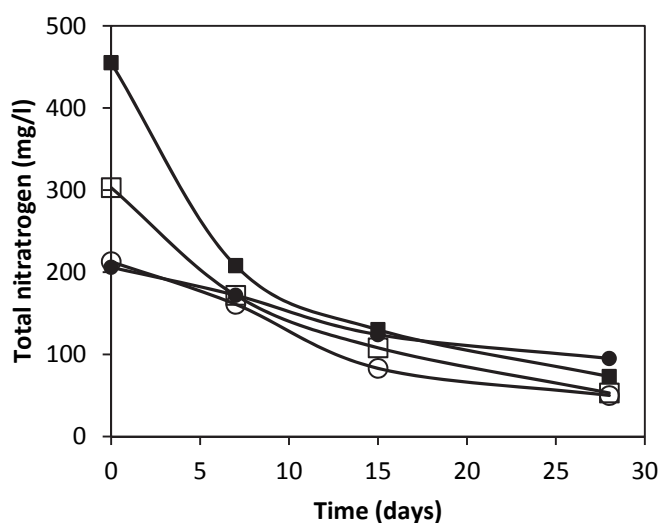


Fig. 7.7: Nitrates removal during the anaerobic process, non- UV pretreated MWW (■), UV pretreated MWW (□), non- UV pretreated distillery (●), UV pretreated distillery (○)

The general reduction in nitrate concentration during the anaerobic digestion is due to the denitrification process in the anaerobic conditions. Del Pozo and Diez (2003) reported that during the anaerobic degradation process, both the denitrification of oxidized nitrogen and methanogenic degradation occur simultaneously in the bioreactor. Similar reduction in nitrates was also reported by Acharya et al. (2008) during anaerobic treatment of distillery spent wash in an up-flow anaerobic fixed film bioreactor. A general nitrate removal was observed during the AD process in this study. However, the final values attained were still higher than the permissible total nitrogen limit in effluent which is 5 mg/L (Dwyer et al., 2008). In Fig. 7.8,

a general reduction in phosphate concentration during AD was observed. The lower initial phosphate concentration in the UV pretreated wastewater compared to the non-UV wastewater samples may be due to phosphate adsorption onto the TZ catalyst in the photoreactor. This difference, however, is too small for any meaningful quantification. The general reduction in phosphates concentration observed during the anaerobic degradation process is due to the fact that it is consumed by microbes since it is essential in the metabolic process (Hesselmann, 2000).

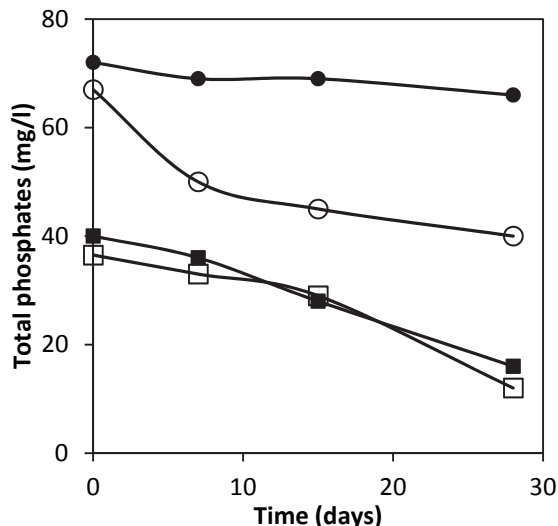


Fig. 7.8: Phosphates removal during the anaerobic process, non- UV pretreated MWW (■), UV pretreated MWW (□), non- UV pretreated distillery (●), UV pretreated distillery (○)

7.3.1.8 Overall performance of the integrated biological and photochemical process

(a) Colour removal

The AD and photodegradation processes were integrated in two ways; in the first case, AD was performed before photodegradation (AOP) while in the second case the AOP was conducted before AD. In Fig. 7.9 and Fig. 7.10, the results for the biological process is shown first, followed by the result obtained when the effluent of the bioreactor was fed into the photoreactor. The cumulative performance of this arrangement (i.e. AD followed by AOP) is then presented as the performance of integrated biological-photochemical process. This was then compared to the performance of the arrangement in which photodegradation is used as the first treatment step and the effluent is fed into the bioreactor (integrated AOP-AD process).

In Fig. 7.9, it can be seen that AD treatment alone was a very poor technique for colour removal for MWW. In fact, it can be seen that the colour of MWW even increased by about 13% during the anaerobic treatment process. A similar observation has been reported, and it is attributed to repolymerization of colour imparting compounds during the anaerobic process (Pant and Adholeya, 2007). However, the AD achieved colour removal of 51% for distillery wastewater. Molasses wastewater and distillery wastewater have a lot in common as it is reported that about 88% of the molasses constituent used in the distillery industry ends up as waste in the spent wash. However, the disparity observed in the colour removal during AD treatment of these wastewater samples may be due to the fact that the distillery wastewater and the MWW were from different sources; the MWW was synthetically prepared from raw molasses while distillery effluent was a real industrial wastewater from the distillery industry.

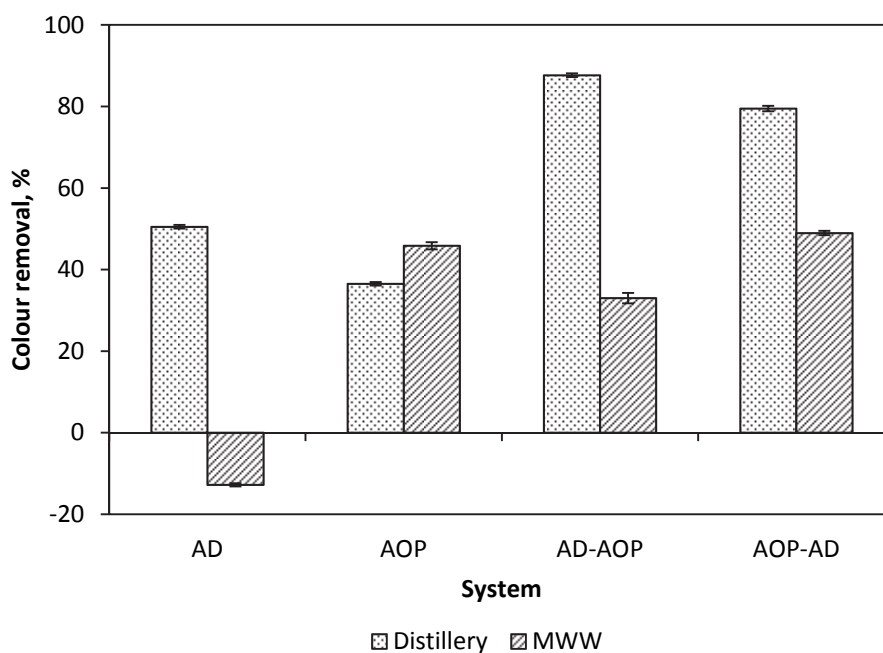


Fig. 7.9: Overall colour removal for the integrated system

The AD process was then followed by AOP. In this case it was observed that the photodegradation step further removed 37% of the original colour for the distillery wastewater while for MWW, 46% colour was further removed. It therefore follows that the integrated process in which AD treatment was followed by AOP achieved an overall colour removal of 33% and 88% for MWW and distillery wastewater, respectively, as shown in Fig. 7.9. The low overall colour removal observed in MWW is due to the increment in colour which was observed during the AD treatment. This therefore means that the colour intensity increased thus hindering light penetration in the subsequent photodegradation process. Also, real distillery wastewater had good colour removal in both the AD and photodegradation processes, hence high overall performance. However, it can be pointed out that the colour removal of 51% for the real distillery wastewater in AD treatment is not good enough for AD to be applied as a stand-alone technique for the treatment of such wastewater stream. In other studies, Dwyer et al. (2008) obtained 35% and 16% degradation of dissolved organic nitrogen and dissolved organic carbon, respectively, during biodegradation of synthetic melanoidin, while Gonzalez et al. (2000) reported 6-7% melanoidin removal in an anaerobic-aerobic treatment of distillery wastewater.

It can further be seen (Fig. 7.9) that the integration of the two processes whereby photodegradation was followed by anaerobic digestion achieved colour removal of 79% and 49% for distillery and MWW, respectively. Distillery wastewater still showed reasonable colour reduction in this arrangement, though less than in the AD-AOP case. However, MWW still had poor colour reduction. It is also significant to note that this arrangement is not efficient in the treatment of distillery wastewater as it is characterized by very low biogas production as shown in Fig. 7.4.

The t-test analysis showed that there was a significant difference in the performance of the integrated AD-AOP and AOP-AD systems in colour removal, for the distillery effluent; $t(4) = 2.78$, $P = 1.3 \times 10^{-4}$ and for MWW; $t(3) = 3.2$, $P = 9 \times 10^{-4}$. Also, a comparison of the mean efficiency of colour removal of the AD process with that of either of the two integrated systems for both the wastewater samples also gave $P < 0.05$ indicating that there was a significance difference in their mean efficiencies.

(b) COD reduction

The observed colour reductions in Fig. 7.9 can be related to the corresponding overall COD reduction shown in Fig. 7.10. It can be observed that anaerobic digestion alone achieved COD removal of 80.4% for MWW while photodegradation removed a further 5.3% of the initial COD, therefore, the overall COD removal for

integrated biological-photochemical process was 85.7%. On the other hand, the integrated photodegradation biological process attained an overall COD removal efficiency of just 47 % for the MWW.

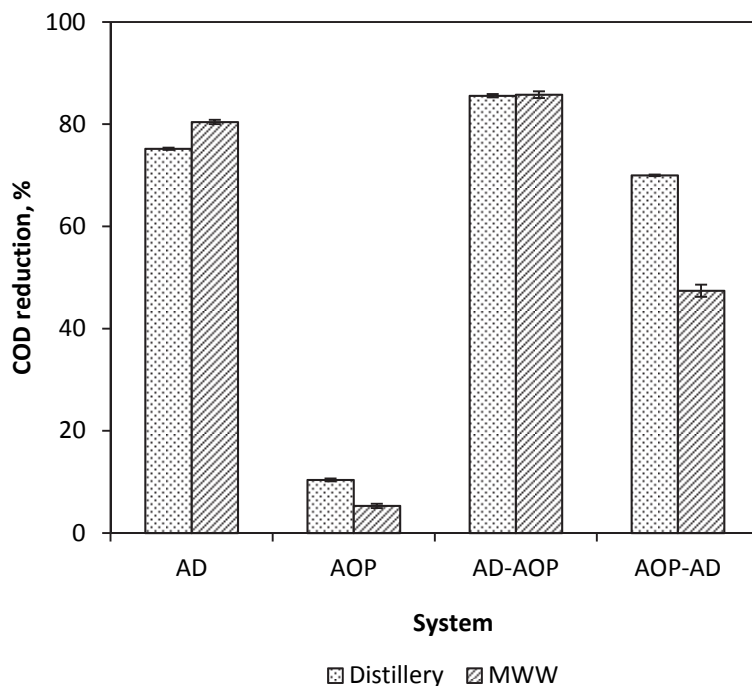


Fig. 7.10: Overall COD reduction for the integrated system

Figure 7.10 further shows that the AD process alone achieved a COD removal of 75% for the distillery wastewater while photodegradation removed an additional 10.4% of the initial COD. Therefore the integrated AD-AOP process achieved an overall COD removal of 85.4% while the integrated AOP-AD process achieved 70% COD removal for the distillery wastewater, which was almost equivalent to that of AD alone. The lower COD removal achieved in the AOP-AD process as compared to the AD-AOP process may be due to the generation of some toxic intermediates during the photo-pretreatment (Oller et al., 2011). It could not be well established how long some residual hydroxyl radicals or organic peroxide intermediates generated during photo-pretreatment lasted in the solution. These could have inhibited microbial activity during anaerobic treatment of distillery wastewater.

The t-test analysis showed that there was a significant difference in the performance of the integrated AD-AOP and AOP-AD systems in COD removal, for the distillery effluent; $t(3) = 3.18$, $P = 9.3 \times 10^{-6}$ and for MWW; $t(3) = 3.2$, $P = 4.3 \times 10^{-5}$. Also, a comparison of the mean efficiency of COD removal of the AD process with that of either of the two integrated systems for both the wastewater samples also gave $P < 0.05$ indicating that there was a significant difference in their mean efficiencies.

7.3.2 Textile wastewater

7.3.2.1 Wastewater characteristics

The characteristics of methylene blue dye solution, inoculum and inoculated wastewater are shown in Table 7.4. The MB dye was found to have low biodegradability as indicated by the low BOD/COD ratio, it was also slightly acidic with high COD. Similar characteristics have been reported in literature (Oller et al., 2011)

Table 7.4: Wastewater characteristics

Characteristics	Inoculum	MB dye	Inoculated MB
Total COD (mg/L)	2820±54	5217±112	4503± 75
BOD (mg/L)	1450	1512	1485
BOD/COD	0.5	0.28	0.33
Total nitrogen (mg/L)	242 ± 9	-	385 ± 14
Total phosphates (mg/L)	43 ± 4	-	32 ± 3
Total suspended solids (mg/L)	186 ± 8	-	18 ± 2
pH	7.0-7.2	5.4-5.6	7.0-7.2 ^a

^aAdjusted values

The low biodegradability of MB is attributed to the bio-recalcitrant nature of dyes, which are generally complex aromatic compounds. The COD and BOD of the inoculated sample was less than that of the non-inoculated dye, which has a lower pH. The inoculation acted as a diluent and lowered both the COD and BOD values. However, it increased the concentration of the inorganic compounds.

7.3.2.2 Photodegradation in the annulus photocatalytic reactor

During photodegradation, 71% colour removal was achieved after irradiation time of 90 minutes as shown in Fig. 7.11. It was also observed that the colour removal was accompanied by a reduction in COD of 54%. The observed reduction in colour and COD during photodegradation can be explained by the reaction mechanism involving the photogenerated hydroxyl molecules and the double bonds of the MB dye during the photodegradation process (Rauf et al., 2010; Houas et al., 2001). This reaction led to cleaving of the aromatic rings of the MB resulting in production of simpler organic intermediates such as simpler aromatic compounds and aliphatic organic acids (Stylidi, 2003; Tanaka et al., 2000). Further oxidation of these acids results in eventual evolution of CO₂ (Konstantinou and Albanis, 2004). It was also observed that the BOD increased by 48% during photodegradation. This is an indication that photodegradation converted the MB dye into a more digestible substrate for the microorganisms (Al-Momani et al., 2002).

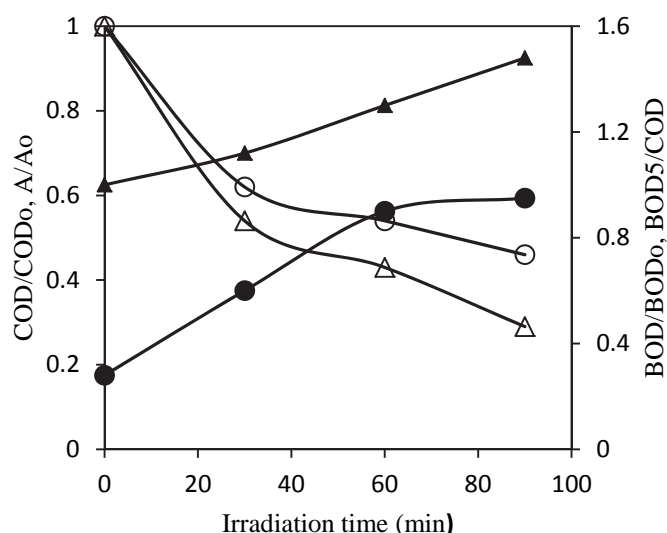


Fig. 7.11: Photodegradation in the annular photocatalytic reactor; COD/COD₀ (○), A/A₀ (△), BOD/BOD₀ (△) and BOD₅/COD (●)

7.3.2.3 Biodegradability enhancement during photodegradation

Biodegradability index (BOD₅/COD ratio) has been used as a measure of the biodegradability of various wastewater streams (Al-Momani et al., 2002; Parra et al., 2002). Normally, a BOD₅/COD ratio higher than

0.4 is an indication that the wastewater is readily biodegradable, while a ratio below 0.4 is an indication of the presence of low biodegradable contaminants in wastewater streams (Parra et al., 2002). In Fig. 7.11, the biodegradability index of MB before photodegradation was 0.28, which indicates that it was not readily biodegradable. It was observed that photodegradation increased the biodegradability of MB dye from 0.28 to around 0.95 after 90 minutes of irradiation. However, 60 minutes was taken as the best irradiation time due to the fact that there was only a 0.05 increase in biodegradability between irradiation time of 60 minutes and 90 minutes. Therefore, irradiation time of 60 minutes was chosen as the optimum since increase in biodegradability levelled off at this point. The UV pre-treated effluent could then be fed into the bioreactor where the remaining COD could be further reduced in a more economical way than if the photodegradation process alone was employed for total COD removal. This is attributed to the fact that photodegradation is a more expensive technique than biological treatment due to its high energy demand (Oller et al., 2011).

Methylene blue has aromatic rings in its structure and therefore its degradation is expected to produce aromatic amines, which are more toxic, as intermediate products. However, due to the observed increase in biodegradability after UV treatment, it can be inferred that this process did not produce such compounds. Similar observations were reported by Al-Momani et al. (2002) in a case of UV photodegradation of dyes which have aromatic rings in their structures such as nylanthrene, intercon and direct dyes. An increase in biodegradability of real textile wastewater using UV photodegradation has also been reported (Al-Momani et al., 2002). These previous studies, however, were only carried out in aerobic systems and therefore information on how UV pretreatment of textile wastewater impacts on energy generation from such wastewater is inadequate in the literature.

7.3.2.4 Degradation of pre-treated wastewater

Anaerobic digestion of the UV pretreated and non-UV pretreated wastewater samples was carried out in the bioreactor. Fig. 7.12 shows that there was a higher COD and BOD reduction in the UV pretreated samples as compared to the non-UV pretreated samples.

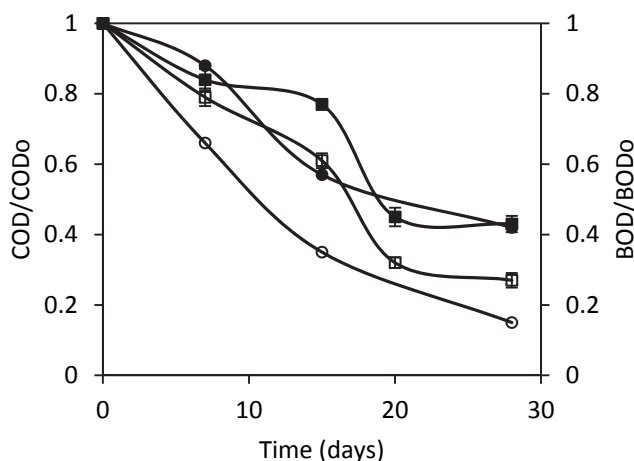


Fig. 7.12: Anaerobic degradation of UV pre-treated wastewater sample; COD (□), BOD (○) and non-UV pre-treated sample; COD (■) and BOD (●)

The COD reductions were 73% and 57% for the UV pretreated and non-UV pretreated samples, respectively, while the corresponding BOD reductions were 85% and 58%, respectively. The UV pretreatment enhanced degradation due to its ability to improve the biodegradability of the MB as shown in Fig. 7.11. Table 7.5 shows colour reduction efficiencies during degradation of UV pre-treated and AD pre-treated samples. It was observed that UV pretreatment did not result in any appreciable increase in colour reduction during AD treatment. Also, the colour reduction of non-AD pre-treated sample was higher than that of AD pre-treated sample in the succeeding photodegradation treatment unit. This could have been due

to the fact that effluent from AD pre-treatment unit had particulate matter, from sludge, which could have not been totally removed by filtration. This led to light attenuation during ensued photodegradation treatment. Moreover, the particulate matter could have led to reduced mass transfer resulting in low reaction rate.

Table 7.5: Comparison between UV pre-treatment and AD pre-treatment in colour reduction

Time(days)	Colour removal %, Anaerobic digestion		Colour removal%, UV photodegradation		
	non pretreated	UV pretreated	Time (min)	non- AD pretreated	AD pretreated
0	0	0	0	0	0
7	9	10	30	46	23
15	23	23	60	57	31
20	30	31	90	71	38
28	32	35			

7.3.2.5 Adsorption in the photoreactor and bioreactor

Contribution of adsorption to the contaminant removal or concentrating the pollutants on the catalyst or zeolite surface in the photoreactor and bioreactor was studied. The data in Table 7.6 give an insight into the role played by adsorption in concentrating the MB molecules on the surface of both the zeolite (in bioreactor) and catalyst (in photoreactor). This enhances the reaction by ensuring that the organic pollutants are in close contact with microbes attached on the zeolite surface in the bioreactor (Montalvo et al., 2012). Also, concentrating the pollutants on the catalyst surface in the photoreactor enhances photodegradation by ensuring that the reactant and the catalyst are always in contact (Huang et al., 2008). Moreover, previous studies have generally established that the application of zeolite improves the anaerobic degradation process due to its ability to immobilize microbes on its surface and its good buffering capacity (Montalvo et al., 2012; Tada et al., 2005).

Table 7.6: Adsorption on TiO₂/zeolite and zeolite surface in the reactors

Photoreactor		Bioreactor	
Colour reduction, %	COD reduction %	Colour reduction %	COD reduction %
30	21	35	27

7.3.2.6 Biogas production

Daily biogas production during the anaerobic degradation of the non-UV pretreated and UV pretreated samples was recorded. The methane content of the biogas produced was analysed after every four days. Figure 7.13 shows the cumulative biogas production and methane composition. UV pre-treatment improved biogas production and methane composition. This is due to the fact that UV pre-treatment improved anaerobic biodegradability of MB and therefore more of the organic compounds generated by the UV pre-treatment could be easily converted to biogas. The methane composition of the biogas produced increased with time due to the fact that during the initial stages of anaerobic digestion (acidogenesis) CO₂ and H₂ are the major gases produced, these gases are then converted into methane in the ensued methanogenesis process (Aiyuk et al., 2006). Moreover, during the start of the anaerobic process the micro-organisms need time to acclimatise and therefore they have low activity.

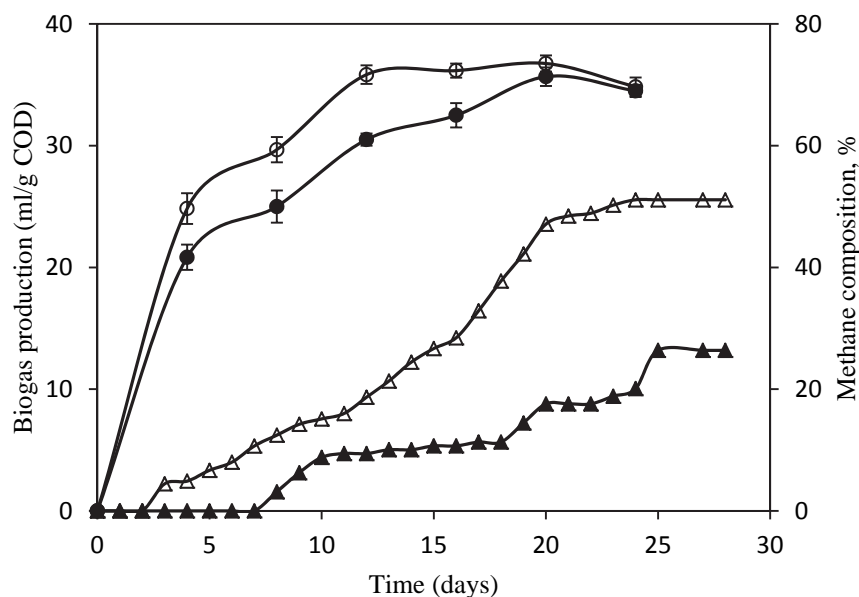


Fig. 7.13: Biogas production (triangles) and methane composition (circles) during the anaerobic process; non- UV pretreated MB (closed symbols) and UV pretreated MB (open symbols)

7.3.2.7 Volatile fatty acids (VFAs) and pH

In Fig. 7.14a initially the UV pretreated MB had higher VFAs than the non-UV pretreated sample. This may be an indication that in the photodegradation of the MB dye, VFAs were among the products or intermediates produced. This is in agreement with the improved biodegradability observed during photodegradation (Fig. 7.11) as VFAs are more readily biodegradable than the original MB dye molecules. It has been reported (Stylidi, 2003; Tanaka et al., 2000; Konstantinou and Albanis, 2004) that VFAs are major intermediates in the photodegradation of some textile dyes. It was also observed that after 15 days of digestion the VFAs concentration of both the wastewater samples had reduced significantly to reach a stable concentration. This is most likely due to the fact that the amount of VFAs produced from the acidogenesis process was being consumed in the methanogenesis process resulting in the stability in VFAs concentration (Somasiri et al., 2008). The degradation of VFAs obeyed first order kinetics (Wang et al., 1999; Vavilin and Lokshina, 1996) with rate constants of $1.06 \times 10^{-1} \text{ day}^{-1}$ and $1.03 \times 10^{-1} \text{ day}^{-1}$ for the non-UV pretreated and UV pretreated samples, respectively (Fig. 7.14b)

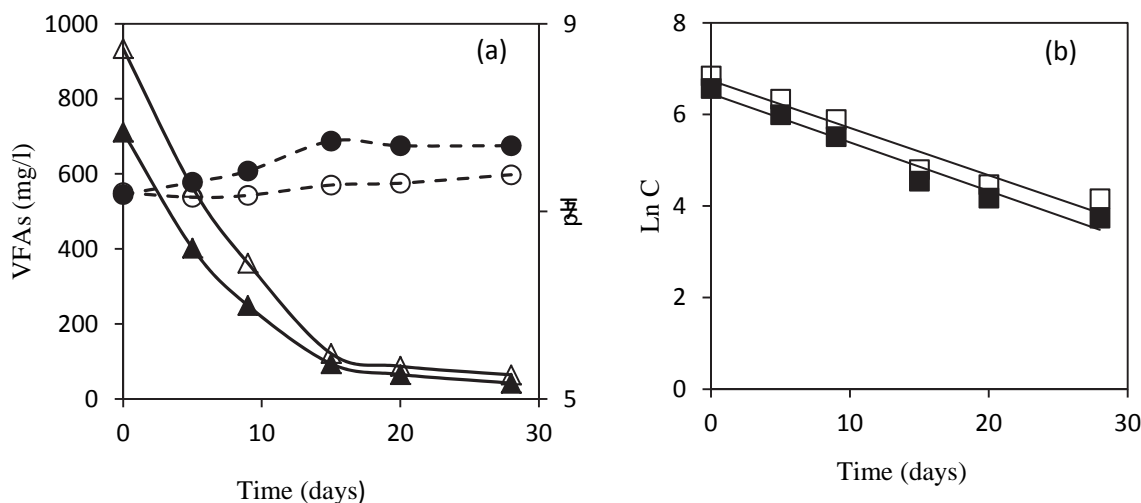


Fig. 7.14: (a) VFA removal during AD process; non-UV pretreated MB (\blacktriangle) and (\square) UV pretreated MB (Δ) and pH; non-UV pre-treated MB (\bullet) and UV pre-treated MB (\circ). (b) Degradation kinetics of the VFAs; non-UV pre-treated MB (\blacksquare) and UV pre-treated MB (\square)

The pH of the wastewater samples was monitored during the entire digestion period. It was observed that during the digestion period the pH values were within the expected pH range in the anaerobic digester. However, there was a slight increase in pH values with the degradation time from day 0 to day 28. This observation might have been due to the corresponding reduction in VFAs concentration with time as shown in Fig. 7.14a, which led to a slight reduction in the acidity of the media. Apart from the good buffering effect provided by KH_2PO_4 and NaHPO_4 which were added at the start of the digestion, zeolite which was used as biomass support also had a good buffering capacity and could have also contributed to the observed pH stability (Tada et al., 2005).

7.3.2.8 Nitrates and phosphates

In Fig. 7.15 it was observed that the initial nitrate and phosphate concentrations of the UV pretreated stream were lower than those of the non-UV pretreated stream. This could have been due to the removal of nitrates and phosphates by adsorption on the TiO_2 /zeolite composite catalyst surface. Moreover, dissolved organic nitrogen (DON) and ammonia nitrogen could have been removed by the photodegradation process (Dwyer et al., 2008). The general reduction in nitrate concentration during the anaerobic digestion is due to denitrification under anaerobic conditions. Del Pozo and Diez (2003) reported that during anaerobic degradation, both the denitrification of oxidized nitrogen and methanogenic degradation occur simultaneously in the bioreactor. The general reduction in phosphates concentration observed during the anaerobic degradation process is due to the fact that it is consumed by microbes since it is essential in the metabolic process (Hesselmann, 2000).

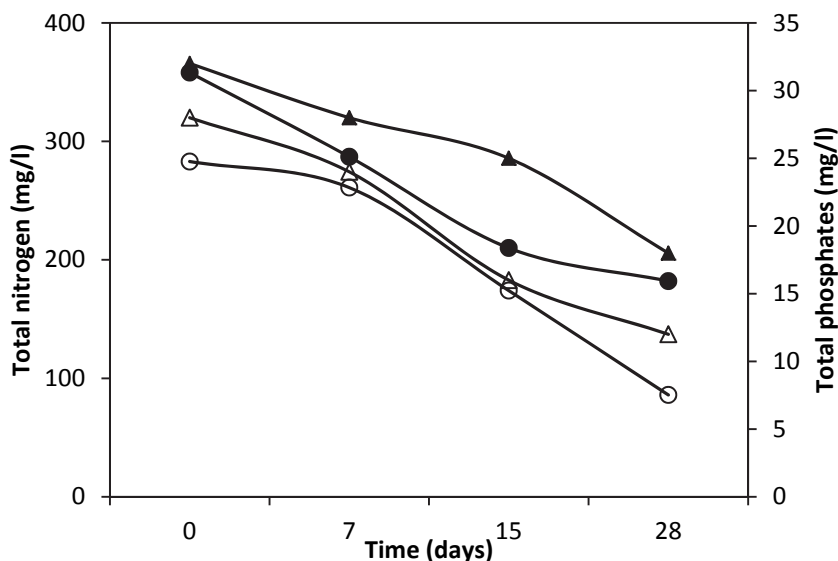


Fig. 7.15: Nitrate (circles) and phosphate (triangles) removal during the anaerobic process, non- UV pretreated sample (closed symbols), UV pre-treated sample (open symbols)

7.3.2.9 Efficiency of the integrated biological and photochemical process

The photodegradation (AOP) and AD processes were integrated in two ways; in the first case, AD was performed before the AOP (AD-AOP) while in the second case the AOP was conducted before the AD (AOP-AD). In Fig. 7.16, the results for colour and COD reduction are shown. In the first place, results for the AD system as a single treatment process is shown, the effluent from the AD system was then fed into the AOP system and the additional pollutant removal was recorded. The sum of removal by AD and AOP is then presented as the overall removal by the AD-AOP system. Removal by the AD-AOP system is then

compared with that of the AOP-AD system. In both cases AD was conducted for a period of 28 days while AOP was carried out for 60 minutes since this was the optimum irradiation time.

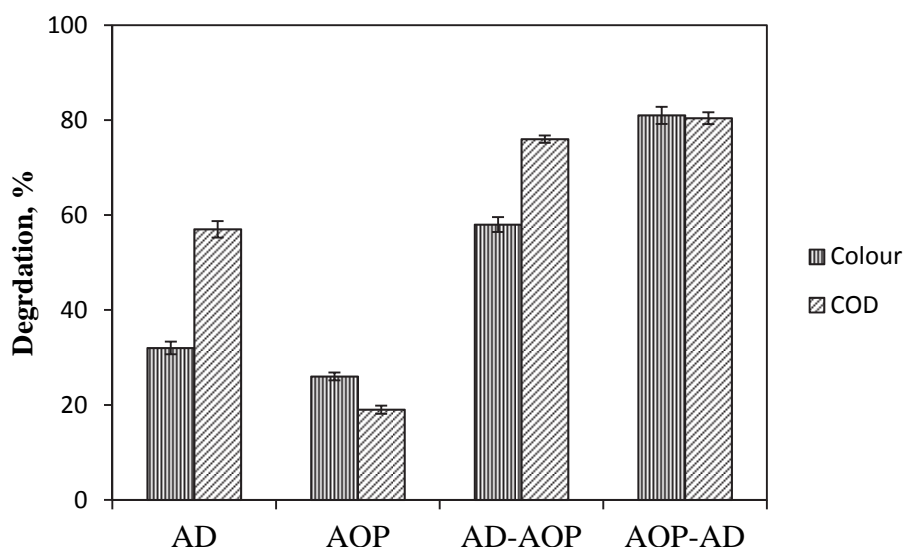


Fig. 7.16: Overall COD reduction for the integrated system

Figure 7.16 shows that AD treatment alone achieved colour removal of 32% and COD reduction of 57%. This low degradation can be attributed to the fact that the MB had low biodegradability (Fig. 7.11). When the effluent from the bioreactor was then fed into the photoreactor, additional colour and COD reductions of 26% and 19%, respectively, were obtained. Therefore, in the case where AD was followed by the AOP (AD-AOP) colour removal of 58% and COD reduction of 76% were achieved. For the integrated process in which the AOP was followed by the AD process (AOP-AD) an improved colour removal of 81% and a COD removal of 73% were achieved. It can therefore be deduced that photodegradation pre-treatment of MB converted the MB molecules into a form that could easily be degraded by the consortia of microbes in the bioreactor. Also, the good COD reduction efficiency of the AD-AOP (76%) can be attributed to the fact that the initial AD step reduced the colour of the sample and this reduced light attenuation in the subsequent AOP unit.

The t-test analysis showed that there was a significant difference in the mean performance of the integrated AD-AOP and AOP-AD systems in COD and colour reduction, for COD; $t(4) = 2.7$, $P = 0.029$ and for colour; $t(3) = 3.18$, $P = 4.43 \times 10^{-4}$. Also, a comparison of the mean efficiency of the AD as a stand-alone process with that of either of the two integrated systems also gave $P < 0.05$ indicating that there was a significant difference in their mean efficiencies.

7.3.2.10 Energy consumption

If UV photodegradation (AOP) was employed as the only treatment method to reduce colour and COD to above 75% as was achieved by the integrated AOP-AD system, then higher energy would be required to drive the process. It required irradiation time of 120 minutes to achieve colour and COD reduction of about 75% using a 15 W UV lamp and this consumed 108 kJ of energy. However, in the AOP-AD integrated system an overall COD and colour removal of above 80% were achieved with shorter irradiation time of 60 minutes and this consumed 54 kJ. Therefore, the AOP-AD integration consumed 50% less energy to achieve the same pollutant removal than if AOP was applied as a stand-alone process. Moreover, considering that the energy content of methane is about 38 MJ/m^3 , the energy produced by the AD process was about 3.06 kJ and this can further reduce the energy consumption of the integrated AOP-AD system. However, it is important to note that energy consumed by the pumps and other units was not considered in these calculations.

7.4 Conclusion

Anaerobic up-flow fixed bed reactor and annular photocatalytic reactor were used to study the efficiency of integrated anaerobic digestion (AD) and ultraviolet (UV) photodegradation of real distillery effluent, raw molasses wastewater (MWW) and methylene blue textile dye. It was found that UV photodegradation as a stand-alone technique achieved colour removal of 54% and 69% for the distillery and MWW, respectively, with a COD reduction of < 20% and a negligible BOD reduction. On the other hand, AD as a single treatment technique was found to be effective in COD and BOD reduction with efficiencies of above 75% and 85%, respectively, for both wastewater streams. However, the AD achieved low colour removal efficiency, with an increase in colour intensity of 13% recorded when treating MWW, while a colour removal of 51% was achieved for the distillery effluent. The application of UV photodegradation as a pre-treatment method to the AD process reduced the COD removal and biogas production efficiency. However, an integration in which UV photodegradation was employed as a post-treatment to the AD process achieved high COD removal of above 85% for MWW and distillery wastewater samples, and colour removal of 88% for the distillery effluent. Thus, photodegradation can be employed as a post-treatment technique to an AD system treating distillery effluent for complete removal of the biorecalcitrant and colour imparting compounds.

For the textile dye, it was found that anaerobic degradation performed better in COD reduction than in colour reduction, achieving 57% and 32% reduction, respectively. In contrast, photodegradation performed better than the AD in colour reduction achieving 70% efficiency but achieved a lower COD reduction of 54%. The efficiency of the two processes applied separately in the degradation of MB dye was generally low. However, the integrated AOP-AD system achieved better degradation with colour and COD reductions of 81% and 80%, respectively. Moreover, it was found that UV photodegradation pretreatment improved the biodegradability of the MB dye by 3- folds after irradiation time of 60 minutes. Thus integration of the two processes in such a way that UV photodegradation precedes the AD process, led to higher biogas production than that of the stand-alone AD process.

All the results reported up to this stage are from batch processes. Batch operation of reactors is important for validation of technology and optimisation of basic operating parameters. However, batch reactors are not efficient and cost effective and are therefore seldom used where continuous reactors can be employed. The use of batch systems for photocatalysis has been extensively studied. However, there is very little data on the use of continuous reactors for photocatalysis.

References

- Acharya, B. K., Mohana, S., Madamwar, D. (2008). Anaerobic treatment of distillery spent wash – A study on upflow anaerobic fixed film bioreactor. *Bioresource technology*, 99(11), 4621-4626.
- Aiyuk, S., Forrez, I., Lieven, D. K., Van Haandel, A., Verstraete, W. (2006). Anaerobic and complementary treatment of domestic sewage in regions with hot climates – A review. *Bioresource Technology*, 97(17), 2225-2241.
- Al-Momani, F., Touraud, E., Degorce-Dumas, J. R., Roussy, J., Thomas, O. (2002). Biodegradability enhancement of textile dyes and textile wastewater by VUV photolysis. *Journal of photochemistry and Photobiology A: Chemistry*, 153(1), 191-197.
- Andalib, M., Hafez, H., Elbeshbishy, E., Nakhla, G., Zhu, J. (2012). Treatment of thin stillage in a high-rate anaerobic fluidized bed bioreactor (AFBR). *Bioresource technology*, 121, 411-418.
- Apollo, S., Onyango, M. S., Ochieng, A. (2013). An integrated anaerobic digestion and UV photocatalytic treatment of distillery wastewater. *Journal of hazardous materials*, 261, 435-442.
- Bush, S., Dickson, A., Harman, J., Anderson, J. (1999). *Australian Energy: market developments and projections to 2014-15* ABARE Research Report (No. 99.4).
- Buxton, G. V., Greenstock, C. L., Helman, W. P., Ross, A. B. (1988). Critical review of rate constants for reactions of hydrated electrons, hydrogen atoms and hydroxyl radicals ($\cdot\text{OH}$ / $\cdot\text{O}^-$ in aqueous solution. *Journal of physical and chemical reference data*, 17(2), 513-886.

- Chamarro, E., Marco, A., Esplugas, S. (2001). Use of Fenton reagent to improve organic chemical biodegradability. *Water research*, 35(4), 1047-1051.
- Chandra, R., Pandey, P.K, (2000) Decolorization of anaerobically treated distillery effluent by activated charcoal adsorption method. *Indian Journal of environmental protection* 21 134-137.
- Chen, Y., Cheng, J. J., Creamer, K. S. (2008). Inhibition of anaerobic digestion process: a review. *Bioresource technology*, 99(10), 4044-4064.
- Chu, W., Tsui, S. M. (2002). Modeling of photodecoloration of azo dye in a cocktail photolysis system. *Water research*, 36(13), 3350-3358.
- Clesceri, L. S., Greenberg, A. E., Eaton, A. D. (1998). Standard methods for the examination of water and wastewater. *American Public Health Association, Washington, DC*.
- Daneshvar, N., Salari, D., Khataee, A. R. (2004). Photocatalytic degradation of azo dye acid red 14 in water on ZnO as an alternative catalyst to TiO₂. *Journal of Photochemistry and Photobiology A: Chemistry*, 162(2), 317-322.
- Del Pozo, R., Diez, V. (2003). Organic matter removal in combined anaerobic-aerobic fixed-film bioreactors. *Water Research*, 37(15), 3561-3568.
- Durgakumari, V., Subrahmanyam, M., Subba Rao, K. V., Ratnamala, A., Noorjahan, M., Tanaka, K. (2002). An easy and efficient use of TiO₂ supported HZSM-5 and TiO₂+ HZSM-5 zeolite combineate in the photodegradation of aqueous phenol and p-chlorophenol. *Applied Catalysis A: General*, 234(1), 155-165.
- Dwyer, J., Kavanagh, L., Lant, P. (2008). The degradation of dissolved organic nitrogen associated with melanoidin using a UV/H₂O₂ AOP. *Chemosphere*, 71(9), 1745-1753.
- Forgacs, E., Cserhati, T., Oros, G. (2004). Removal of synthetic dyes from wastewaters: a review. *Environment international*, 30(7), 953-971.
- Francisca Kalavathi, D., Uma, L., Subramanian, G. (2001). Degradation and metabolization of the pigment – melanoidin in distillery effluent by the marine cyanobacterium *Oscillatoria boryana* BDU 92181. *Enzyme and microbial technology*, 29(4), 246-251.
- González, T., Terrón, M. C., Yagüe, S., Zapico, E., Galletti, G. C., González, A. E. (2000). Pyrolysis/gas chromatography/mass spectrometry monitoring of fungal-biotreated distillery wastewater using *Trametes* sp. I-62 (CECT 20197). *Rapid communications in mass spectrometry*, 14(15), 1417-1424.
- Gupta, V. K., Jain, R., Varshney, S. (2007). Removal of Reactofix golden yellow 3 RFN from aqueous solution using wheat husk – an agricultural waste. *Journal of Hazardous Materials*, 142(1), 443-448.
- Hao, O. J., Kim, H., Chiang, P. C. (2000). Decolorization of wastewater. *Critical reviews in environmental science and technology*, 30(4), 449-505.
- Hesselmann, R. P. X., Von Rummell, R., Resnick, S. M., Hany, R., Zehnder, A. J. B. (2000). Anaerobic metabolism of bacteria performing enhanced biological phosphate removal. *Water Research*, 34(14), 3487-3494.
- Houas, A., Lachheb, H., Ksibi, M., Elaloui, E., Guillard, C., Herrmann, J. M. (2001). Photocatalytic degradation pathway of methylene blue in water. *Applied Catalysis B: Environmental*, 31(2), 145-157.
- Huang, M., Xu, C., Wu, Z., Huang, Y., Lin, J., Wu, J. (2008). Photocatalytic discolorization of methyl orange solution by Pt modified TiO₂ loaded on natural zeolite. *Dyes and Pigments*, 77(2), 327-334.
- Jain, N., Minocha, A. K., Verma, C. L. (2002). Degradation of predigested distillery effluent by isolated bacterial strains. *Indian journal of experimental biology*, 40(1), 101-105.
- Konstantinou, I. K., Albanis, T. A. (2004). TiO₂ assisted photocatalytic degradation of azo dyes in aqueous solution: kinetic and mechanistic investigations: A review. *Applied Catalysis B: Environmental*, 49(1), 1-14.
- Kwak, E. J., Lee, Y. S., Murata, M., Homma, S. (2004). Effect of reaction pH on the photodegradation of model melanoidins. *LWT-Food Science and Technology*, 37(2), 255-262.
- Lata, K., Kansal, A., Balakrishnan, M., Rajeshwari, K. V., Kishore, V. V. N. (2002). Assessment of biomethanation potential of selected industrial organic effluents in India. *Resources, Conservation and Recycling*, 35(3), 147-161.
- Maas, R., Chaudhari, S. (2005). Adsorption and biological decolourization of azo dye Reactive Red 2 in semicontinuous anaerobic reactors. *Process Biochemistry*, 40(2), 699-705.

- Metcalf, L., Eddy, H. P., Tchobanoglous, G. (1972). *Wastewater engineering: treatment, disposal, and reuse*. McGraw-Hill.
- Milán, Z., Sánchez, E., Weiland, P., Borja, R., Martín, A., Ilangovan, K. (2001). Influence of different natural zeolite concentrations on the anaerobic digestion of piggery waste. *Bioresource technology*, 80(1), 37-43.
- Montalvo, S., Guerrero, L., Borja, R., Sánchez, E., Milán, Z., Cortés, I., Angeles de la Rubia, M. (2012). Application of natural zeolites in anaerobic digestion processes: A review. *Applied Clay Science*, 58, 125-133.
- Naik, N., Jagadeesh, K. S., Noolvi, M. N. (2010). Enhanced degradation of melanoidin and caramel in biomethanated distillery spentwash by microorganisms isolated from mangroves. *Iranica Journal of Energy and Environment*, 1, 347-351.
- Navgire, M., Yelwande, A., Tayde, D., Arbad, B., Lande, M. (2012). Photodegradation of Molasses by a MoO₃-TiO₂ Nanocrystalline Composite Material. *Chinese Journal of Catalysis*, 33(2), 261-266.
- Oller, I., Malato, S., Sánchez-Pérez, J. A. (2011). Combination of advanced oxidation processes and biological treatments for wastewater decontamination – a review. *Science of the total environment*, 409(20), 4141-4166.
- Pala, A., Erden, G. (2005). Decolorization of a baker's yeast industry effluent by Fenton oxidation. *Journal of hazardous materials*, 127(1), 141-148.
- Pant, D., Adholeya, A. (2007). Biological approaches for treatment of distillery wastewater: a review. *Bioresource technology*, 98(12), 2321-2334.
- Parra, S., Malato, S., Pulgarin, C. (2002). New integrated photocatalytic-biological flow system using supported TiO₂ and fixed bacteria for the mineralization of isoproturon. *Applied Catalysis B: Environmental*, 36(2), 131-144.
- Pena, M., Coca, M., Gonzalez, G., Rioja, R., Garcia, M. T. (2003). Chemical oxidation of wastewater from molasses fermentation with ozone. *Chemosphere*, 51(9), 893-900.
- Prasad, R. K. (2009). Color removal from distillery spent wash through coagulation using *Moringa oleifera* seeds: Use of optimum response surface methodology. *Journal of hazardous materials*, 165(1), 804-811.
- Rajor, A., Singh, R., Mathur, R. P. (2002). Colour removal of distillery waste by saccharomyces. *Indian Journal of Environmental Protection*, 22(11), 1241-1252.
- Rauf, M. A., Meetani, M. A., Khaleel, A., Ahmed, A. (2010). Photocatalytic degradation of methylene blue using a mixed catalyst and product analysis by LC/MS. *Chemical Engineering Journal*, 157(2), 373-378.
- Satyawali, Y., Balakrishnan, M. (2008). Wastewater treatment in molasses-based alcohol distilleries for COD and color removal: a review. *Journal of environmental management*, 86(3), 481-497.
- Shan, A. Y., Ghazi, T. I. M., Rashid, S. A. (2010). Immobilisation of titanium dioxide onto supporting materials in heterogeneous photocatalysis: a review. *Applied Catalysis A: General*, 389(1), 1-8.
- Simate, G. S., Cluett, J., Iyuke, S. E., Musapatika, E. T., Ndlovu, S., Walubita, L. F., Alvarez, A. E. (2011). The treatment of brewery wastewater for reuse: State of the art. *Desalination*, 273(2), 235-247.
- Somasiri, W., Li, X. F., Ruan, W. Q., Jian, C. (2008). Evaluation of the efficacy of upflow anaerobic sludge blanket reactor in removal of colour and reduction of COD in real textile wastewater. *Bioresource technology*, 99(9), 3692-3699.
- Song, Z., Williams, C. J., Edyvean, R. G. J. (2001). Coagulation and anaerobic digestion of tannery wastewater. *Process Safety and Environmental Protection*, 79(1), 23-28.
- Stylidi, M., Kondarides, D. I., Verykios, X. E. (2003). Pathways of solar light-induced photocatalytic degradation of azo dyes in aqueous TiO₂ suspensions. *Applied Catalysis B: Environmental*, 40(4), 271-286.
- Tada, C., Yang, Y., Hanaoka, T., Sonoda, A., Ooi, K., Sawayama, S. (2005). Effect of natural zeolite on methane production for anaerobic digestion of ammonium rich organic sludge. *Bioresource technology*, 96(4), 459-464.
- Tanaka, K., Padermpole, K., Hisanaga, T. (2000). Photocatalytic degradation of commercial azo dyes. *Water research*, 34(1), 327-333.

- Vavilin, V. A., Lokshina, L. Y. (1996). Modeling of volatile fatty acids degradation kinetics and evaluation of microorganism activity. *Bioresource Technology*, 57(1), 69-80.
- Wang, Q., Kuninobu, M., Ogawa, H. I., Kato, Y. (1999). Degradation of volatile fatty acids in highly efficient anaerobic digestion. *Biomass and Bioenergy*, 16(6), 407-416.
- Wilkie, A. C., Riedesel, K. J., Owens, J. M. (2000). Stillage characterization and anaerobic treatment of ethanol stillage from conventional and cellulosic feedstocks. *Biomass and Bioenergy*, 19(2), 63-102.
- Wong, C. C., Chu, W. (2003). The direct photolysis and photocatalytic degradation of alachlor at different TiO₂ and UV sources. *Chemosphere*, 50(8), 981-987.
- Sreerishnan, T. R., Kohli, S., Rana, V. (2004). Enhancement of biogas production from solid substrates using different techniques – a review. *Bioresource technology*, 95(1), 1-10.
- Zhang, F. Feng, C. Cui, J. Hao, G. Li, W., (2009). Photocatalytic degradation of ammonia nitrogen with suspended TiO₂. 3rd International Conference on Bioinformatics and Biomedical Engineering 11-13 June Beijing China.

CHAPTER 8

8 CONTINUOUS PHOTODEGRADATION OF DISTILLERY EFFLUENT

8.1 Introduction

Studies on continuous application of photodegradation in the decolourization of distillery wastewater is limited in literature. A study of photodegradation in a continuous mode is important as it can give information which is vital in scaling up the process to industrial application. Distillery industries are major environmental pollutants due to their large discharge of wastewater which contains significant amounts of recalcitrant compounds (Acharya et al., 2008). Melanoidins, which are polymers responsible for the dark brown colour of distillery effluent, are the major recalcitrant component of distillery effluent (Kalavathi et al., 2001). Anaerobic digestion (AD) has been widely considered as an attractive treatment technique for distillery effluent due to its reputation as a low cost and environmentally friendly technique. Even though AD is able to remove a significant amount of chemical oxygen demand (COD) of the distillery effluent, it is incapable of removing the colour associated with the biorecalcitrant melanoidins (Satyawili and Balakrishnan, 2008). Therefore it is necessary to employ a post-treatment method to decolourise the AD pre-treated effluent (Rizzo et al., 2011). Photodegradation is one of the processes which can be employed to efficiently decolorize distillery wastewater (Pena et al., 2003). The aim of this work was to apply a continuous UV/TiO₂ photodegradation in the decolouration of distillery effluent. A fluidized bed reactor was used due to its ability to achieve efficient mixing.

8.2 Methodology

8.2.1 Materials

Distillery effluent was outsourced from Talbot and Talbot wastewater solutions Pty and stored in a fridge at 4°C before use. Titanium dioxide catalyst, Degussa P 25, was purchased from Sigma Aldrich (the catalyst was used as it is, without modification, it will be modified for future work as this is work in progress). The sources of radiation were 15 W UV-A and UV-C lamps, and compressed air was used as source of oxygen and to fluidize the catalyst.

8.2.2 Experimental set up

The experimental set up (Fig. 8.1) consisted of a 0.5 L photoreactor with an effective volume of 0.4 L. The outer wall was made of Perspex while the inner UV shield wall was made of either quartz or borosilicate glass and a UV lamp was suspended at the centre of the reactor. The wastewater was pumped into and out of the reactor by a digital peristaltic pump. Compressed air was continuously pumped into the reactor to supply oxygen and to fluidise the catalyst, excess air was vented out through an air outlet at the top of the reactor. Air rotameter was used to monitor the air flow rate.

8.2.3 Experimental procedure

Distillery wastewater of varied concentrations was prepared and mixed with an appropriate amount of catalyst in a beaker. The reservoir containing wastewater and catalyst was continuously stirred on a magnetic stirrer plate to ensure uniform catalyst distribution. The mixture was fed into the reactor and air from the compressor was passed upward through a column of distillery wastewater containing suspended TiO₂ catalyst via a flow distributor compartment at the bottom of the reactor. Liquid and gas flow rates ranged from 2 to 25 mL/min and 10 to 80 L/h. The performance of the system was monitored in terms of decolouration. The colour analysis was carried out using UV-Vis spectrophotometer (T80+ UV/VIS Spectrophotometer, PG instruments Ltd). The samples were filtered using a 0.45 µm filter syringe.

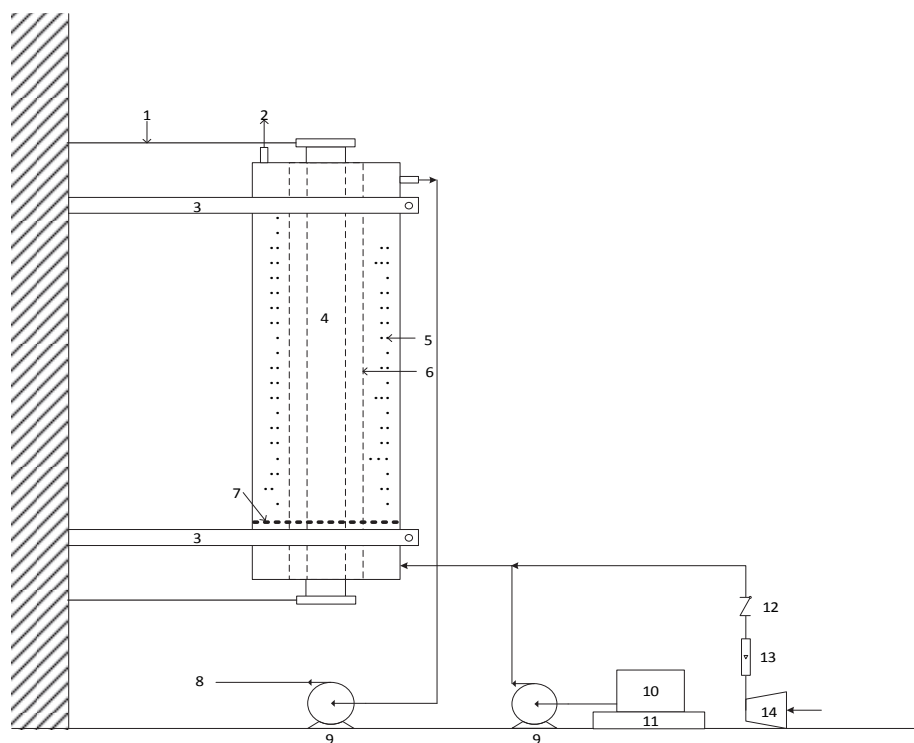


Fig. 8.1: Reactor set up; (1) UV lamp holder (2) air outlet (3) Clamp (4) UV lamp (5) suspended catalyst (6) UV lamp shield (7) distributor holes (8) effluent (9) peristaltic pump (10) wastewater reservoir (11) magnetic stirrer (12) non-return valve (13) air rotameter (14) compressor

8.3 Results and Discussion

The UV photodegradation was carried out in a continuous operation. The wastewater was continuously fed into the reactor and the catalyst concentration was maintained constant in each run. The effect of wastewater concentration, air flow rate, wastewater flow rate, catalyst concentration, UV irradiation type and reactor construction material were studied. In the continuous degradation studies, before UV irradiation was introduced adsorption was carried out for 60 minutes until equilibrium was attained. UV radiation was therefore conducted after the 60th minute.

8.3.1 Effect of UV type and reactor construction material

The effect of material used in the construction of the UV shield of the reactor and the effect of UV type was investigated. Quartz and borosilicate as construction material and UV-A and UV-C as radiation source were studied. The wastewater was passed in the reactors until adsorption equilibrium was reached. This was then followed by photodegradation studies. The reactor made of quartz achieved colour removal of about 99% after 100 minutes while the borosilicate reactor achieved colour reduction of about 75% within the same period of time (Fig. 8.2a). Applying UV-A and UV-C in a quartz glass reactor showed that UV-C achieved higher degradation within a shorter time as compared to that of UV-A, as shown in Fig. 8.2b. Due to these observations, the subsequent studies were conducted using UV-C as source of radiation in a reactor made of quartz glass.

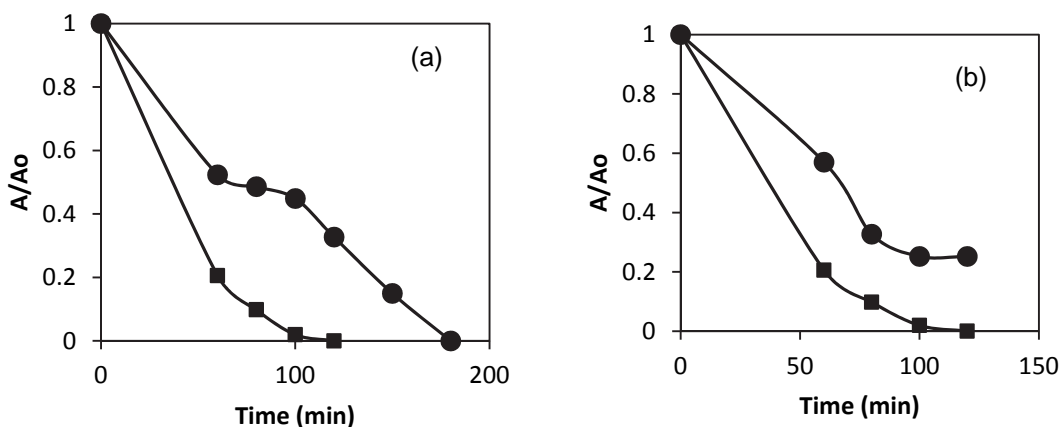


Fig. 8.2: Effect of (a) construction material, (●) borosilicate, (■) quartz and (b) UV type, (●) UV-A, (■) UV-C on photodegradation

8.3.2 Effect of concentration

Degradation of different concentrations of the distillery effluent was studied at a fixed air flow rate of 40 L/h, effluent flow rate of 2 mL/min and catalyst loading of 2 g/L. The concentrations which were studied were 5 mL/l, 10 mL/l and 15 mL/l of distillery wastewater with corresponding chemical oxygen demand (COD) of about 500 mg/L, 1000 mg/L and 1500 mg/L, respectively. In Fig. 8.3, it was observed that colour removal proceeded faster at low concentrations than at high concentrations. This is due to the fact that at high concentrations the effluent was darker than at low concentrations, therefore there was higher light attenuation at high concentrations than at low concentrations. Moreover, at high concentrations there was low mass transfer caused by interparticle collision.

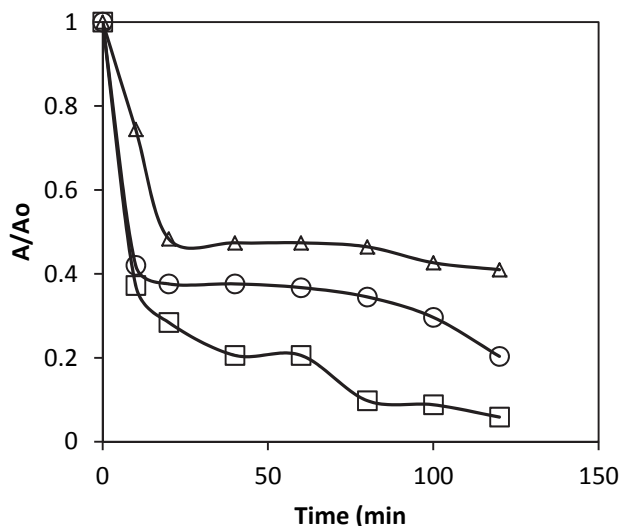


Fig. 8.3: Effect of the initial wastewater concentration on the colour removal efficiency, (Δ) 15 mL/l, (○) 10 mL/l (□) 5 mL/l

8.3.3 Air flow rate and effluent flow rate

Figure 8.4 shows the effect of the air flow rate on decolourisation rate at a fixed liquid flow rate of 2 mL/min. The optimum air flow rate was 40 L/h, the observed low degradation at low air flow rate can be attributed to poor mixing at low air flow rates. Pareek et al. (2001) reported a similar trend when conducting degradation

of bayer liquor using similar reactor. The study showed that at low flow rates there was poor mixing which hindered the reaction.

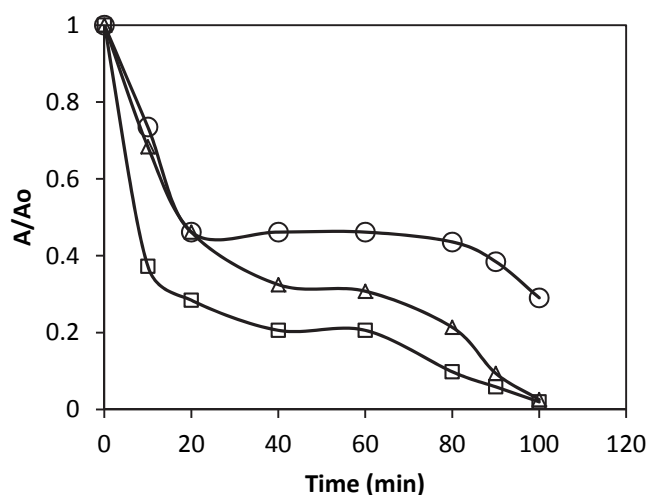


Fig. 8.4: Effect of air flow rate in the degradation of distillery effluent at effluent flow rate of 2 mL/min, catalyst loading of 2 g/L and initial effluent concentration of 5 mL/L (500 mg/L COD), (○) 10 L/h (□) 40 L/h (Δ) 80 L/h

Wei and Wan (1991) attributed a similar observation to the dominance of mass transfer resistance at low gas flow rates in a similar reactor containing a stationary liquid column. Figure 8.5 shows that higher decolouration was achieved at low effluent flow rate. This can be attributed to the fact that at low effluent flow rate there is high residence time and this leads to an increased contact time between the pollutants, UV irradiation and the catalyst.

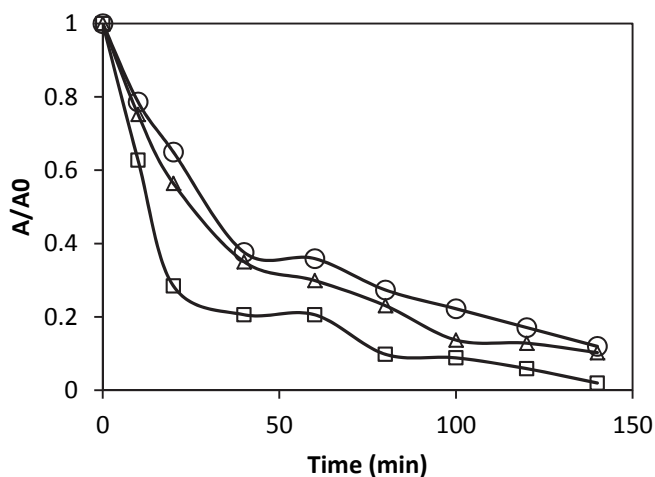


Fig. 8.5: Effect of liquid flow rate in the degradation of distillery effluent at air flow rate of 40 l/h, catalyst loading of 2 g/L, and effluent concentration of 5 mL/L (500 mg/L COD), (○) 25 mL/min (Δ) 12 mL/min (□) 2 mL/min

8.3.4 Catalyst loading

The experiments were conducted with catalyst loading ranging from 0.5 g/L to 5 g/L while keeping other parameters constant (air flow rate 40 L/h, liquid flow rate 2 mL/min and concentration 5 mL/L). In Fig. 8.6, the reaction rate increased with an increase in catalyst loading from 0.5 g/L attaining maximum at 2 g/L, then there was a decrease in reaction rate when the catalyst was increased to 5 g/L. This may be attributed to the shielding effect caused by the catalyst at high loading, leading to a reduction in reaction rate. Moreover,

at very high catalyst loading mass transfer is reduced due to the increased viscosity of the solution (Zhu et al., 2011; Nawi et al., 2012).

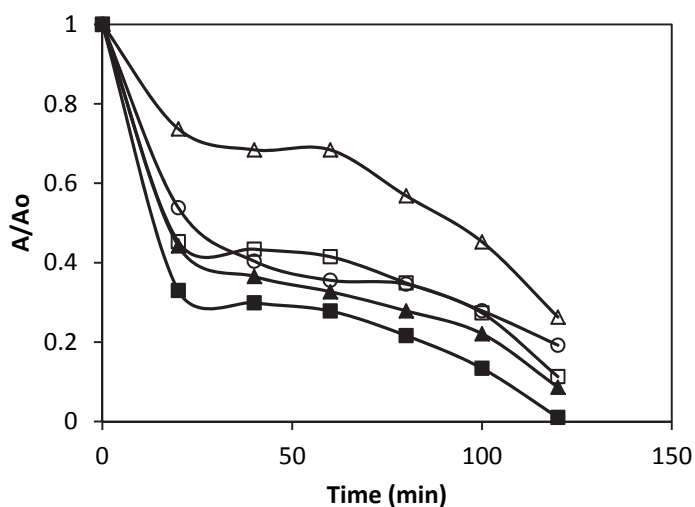


Fig. 8.6: Effect of catalyst loading on degradation of distillery effluent at air flow rate of 40 L/h, liquid flow rate of 2 mL/min and concentration of 5 mL/L, (Δ) 0.5 g/L, (□) 1 g/L, (■) 2 g/L, (▲) 3 g/L, (○) 5 g/L

8.4 Conclusion

UV decolouration of distillery effluent was carried out in a continuous system. It was found that the efficiency of the degradation process depended on air flow rate, effluent flow rate, effluent concentration, catalyst loading, reactor construction material, UV radiation source and irradiation time. The optimum catalyst loading was found to be 2 g/L while optimum air flow rate was found to be 40 l/h resulting in a maximum photodegradation of 99%. It was also found that degradation was faster at low effluent flow rate than at high effluent flow rate.

References

- Acharya, B. K., Mohana, S., Madamwar, D. (2008). Anaerobic treatment of distillery spent wash – A study on upflow anaerobic fixed film bioreactor. *Bioresource technology*, 99(11), 4621-4626.
- Francisca Kalavathi, D., Uma, L., Subramanian, G. (2001). Degradation and metabolization of the pigment – melanoidin in distillery effluent by the marine cyanobacterium *Oscillatoria boryana* BDU 92181. *Enzyme and microbial technology*, 29(4), 246-251.
- Nawi, M. A., Sabar, S. (2012). Photocatalytic decolourisation of Reactive Red 4 dye by an immobilised TiO₂/chitosan layer by layer system. *Journal of colloid and interface science*, 372(1), 80-87.
- Pareek, V. K., Brungs, M. P., Adesina, A. A. (2001). Continuous process for photodegradation of industrial bayer liquor. *Industrial & engineering chemistry research*, 40(23), 5120-5125.
- Rizzo, L. (2011). Bioassays as a tool for evaluating advanced oxidation processes in water and wastewater treatment. *Water research*, 45(15), 4311-4340.
- Satyawali, Y., Balakrishnan, M. (2008). Wastewater treatment in molasses-based alcohol distilleries for COD and color removal: a review. *Journal of environmental management*, 86(3), 481-497.
- Wei, T. Y., Wan, C. C. (1991). Heterogeneous photocatalytic oxidation of phenol with titanium dioxide powders. *Industrial & engineering chemistry research*, 30(6), 1293-1300.
- Zhu, H., Jiang, R., Fu, Y., Guan, Y., Yao, J., Xiao, L., Zeng, G. (2012). Effective photocatalytic decolorization of methyl orange utilizing TiO₂/ZnO/chitosan nanocomposite films under simulated solar irradiation. *Desalination*, 286, 41-48.
- Pena, M., Coca, M., Gonzalez, G., Rioja, R., Garcia, M. T. (2003). Chemical oxidation of wastewater from molasses fermentation with ozone. *Chemosphere*, 51(9), 893-900.

CHAPTER 9

9 CONCLUSIONS AND RECOMMENDATIONS

This work was carried out in five work packages. In the first case, anaerobic digestion of molasses and methylene blue was carried out. In the second study, UV photodegradation of molasses and methylene blue wastewater was carried out in the shaker using a composite catalyst of TiO_2 and zeolite. In the third study, solar photocatalytic degradation and adsorption of pharmaceuticals in a fluidised bed reactor was investigated. The fourth study looked into the photodegradation of a combined methyl orange and Cr(VI) solution. In the fifth study, the efficiency of an integrated anaerobic digestion and UV photodegradation in the treatment of methylene blue dye, distillery effluent and molasses wastewater was investigated. Lastly, photodegradation of distillery effluent was carried out in a continuous reactor.

9.1 Conclusions

9.1.1 *Anaerobic digestion of molasses wastewater and methylene blue dye*

The biodegradation of MWW was observed to increase with an increase in concentration. On the other hand, the degradation of MB, a model textile wastewater, was inhibited at high concentrations (concentrations above 2000 mg/L). In both wastewater types, it was found that the use of zeolite as biomass support material led to an improvement in biogas yield and COD removal. Biodegradation was found to be suitable for colour removal only for the MB but not MWW.

9.1.2 *UV photodegradation of molasses wastewater and methylene blue dye*

It was also found that a UV/ TiO_2 system alone could not effectively treat molasses wastewater as low degradation was achieved. However, a H_2O_2 /UV/ TiO_2 /zeolite hybrid system was found to be a viable technology for the decolourization of the molasses wastewater, even though this technology does not perform well in COD removal.

9.1.3 *Adsorption and solar photodegradation of pharmaceutical wastewater*

The analysis of solar radiation data revealed that photodegradation should be carried out between 9.30 am and 2.30 pm on sunny days during the summer months. Characterisation of the CTS composite showed that the constituents of the CTS composite increased porosity without affecting the reactivity of the TiO_2 . The optimum CTS composition was determined to be 60% silica xerogel loading and 10% PAC/ TiO_2 ratio while the best mass of the CTS composite was 1.5 g/L. The hydrodynamic experiments showed that the optimum hydrodynamic conditions in the reactor were obtained at an air superficial velocity of 0.007 m/s and an inclination angle of 75° . It was observed that decreasing the initial concentration of the substrates resulted in an increase in the removal of the substrates by adsorption and photodegradation. The adsorption and photodegradation of the sulfamethoxazole increased with decrease in pH. The adsorption of sulfamethoxazole and diclofenac followed the Langmuir isotherm while the carbamazepine did not show good fit for both Langmuir and Freundlich isotherms.

9.1.4 *Photodegradation of methyl orange in the presence of ions*

The characterization of TiO_2 supported silica revealed the good dispersion of TiO_2 on the surface of silica. The equilibrium studies showed that the Langmuir model was most accurate and the methyl orange dye photocatalytic system by TiO_2 /silica composite photocatalyst is a second order reaction. The degradation of dye/ TiO_2 -silica system proceeds faster than that of the respective ternary dye/ Cr(VI) / TiO_2 -silica system at neutral pH. It is evident that the photo reduction of Cr(VI) was much faster in the mixed system than in the single one.

9.1.5 *Integrated anaerobic biodegradation and photodegradation of molasses wastewater and methylene blue*

In the integrated UV photodegradation and anaerobic degradation studies, it was observed that UV pre-treatment improved biodegradability of MB dye but not that of distillery wastewater and MWW. It was also observed that UV treatment is good for colour removal for all the wastewater streams under study but its performance on COD removal depends on the wastewater being treated. Finally, it was observed that an integrated system in which AOP is followed by AD performs better in the treatment of MB dye while an arrangement in which AD is followed by AOP is more efficient for treatment of MWW and real distillery wastewater. The optimum sequence of reactor arrangement is waste specific.

9.1.6 *Continuous photodegradation of distillery effluent*

The optimum catalyst loading was found to be 2 g/l while optimum air flow rate was found to be 40 l/h. It was also found that degradation was faster at low effluent flow rate than at high effluent flow rate.

9.2 Recommendations

Even though photodegradation performs well in mineralization of toxic and recalcitrant organic compounds which cannot be easily biodegraded, it is faced with some challenges such as high energy requirement. It is recommended that UV light be replaced with sunlight in order to reduce the energy footprint of photocatalysis. Further, the optimisation of solar biodegradation can be achieved using a solar simulator. Another problem is encountered in the treatment of wastewater with high colour intensity which hinders the penetration of light rays thus lowering the performance of the process. Dilution of such high intensity wastewater could improve their photodegradation.

Sunlight intensity fluctuates with time of day while artificial UV light sources output reduces with time of use. In order to ensure accurate experimental results, the intensity of UV needs to be determined. The use of a UV radiometer during experiments is therefore recommended. Analysis of the substrates and degradation products was carried out using a UV-vis spectrophotometer. Although this method is fast, less costly and fairly accurate for homogeneous samples, the method becomes inaccurate in heterogeneous samples such as a photodegraded solution. A High Performance Liquid Chromatography (HPLC) instrument would be best for such analyses. Also, the chromatograms of a HPLC-MS would better identify the photodegradation products than UV-vis spectra.

During hydrodynamic experiments, solid concentration distribution was determined by sampling slurry at different points along the reactor height and analysing the solid concentration from the slurry gravimetrically. This method has been used in the past but it is not very accurate. In future experiments, it is suggested to use the method of Optical Attenuation Technology (AOT) to determine the solid concentration distribution.

APPENDICES

A1 Reactor Design and Pictures

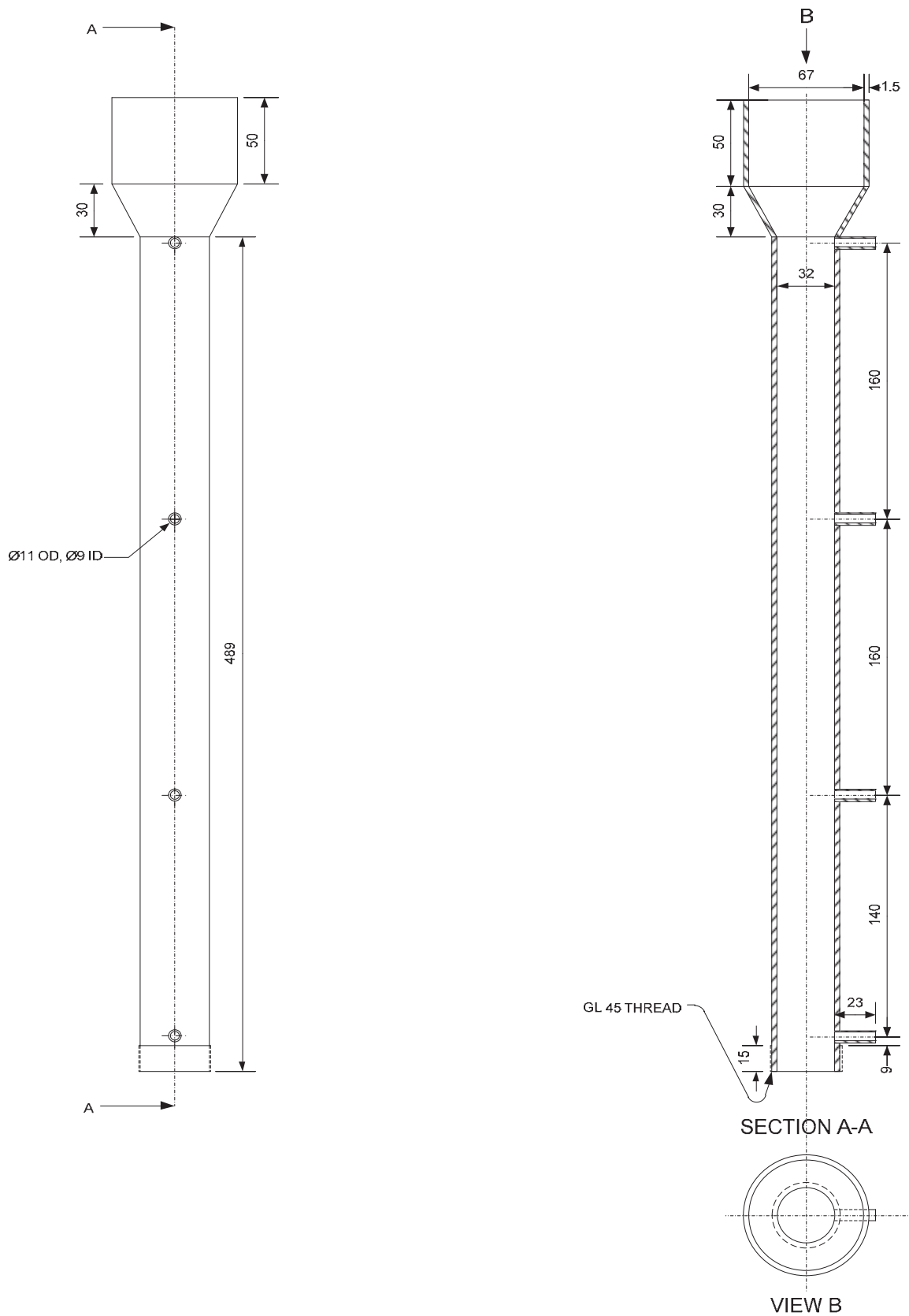


Fig. A1: Fluidized bed photocatalytic reactor (all dimensions in mm)



Fig. A2: Picture of fluidized bed photocatalytic reactor array



Fig. A 4: Photodegradation reactor setup



Fig. A 5: Anaerobic degradation reactor setup

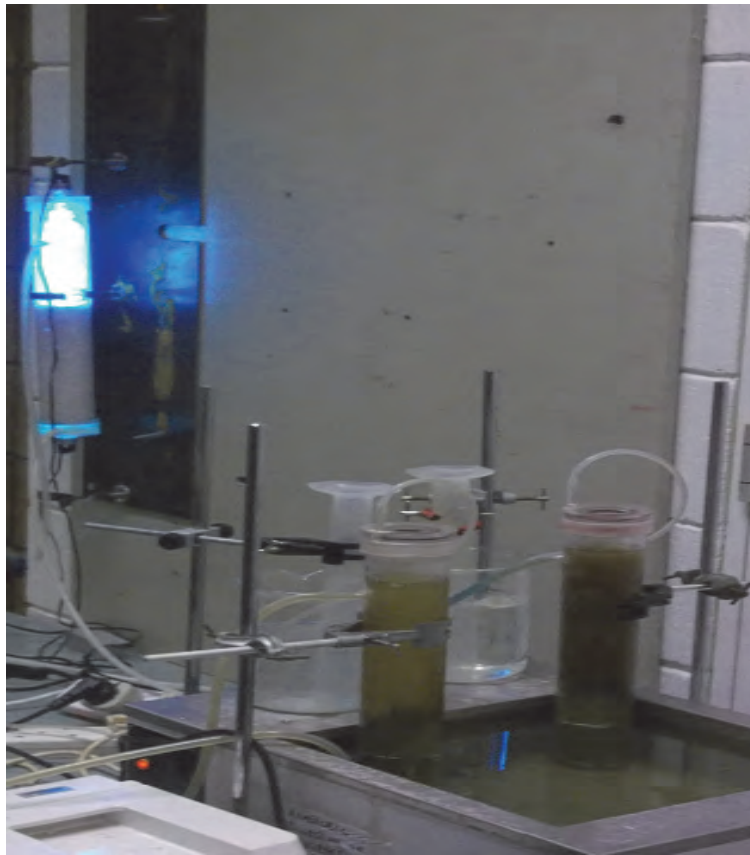


Fig. A 6: Integrated photodegradation and anaerobic degradation

A2 Supplementary data

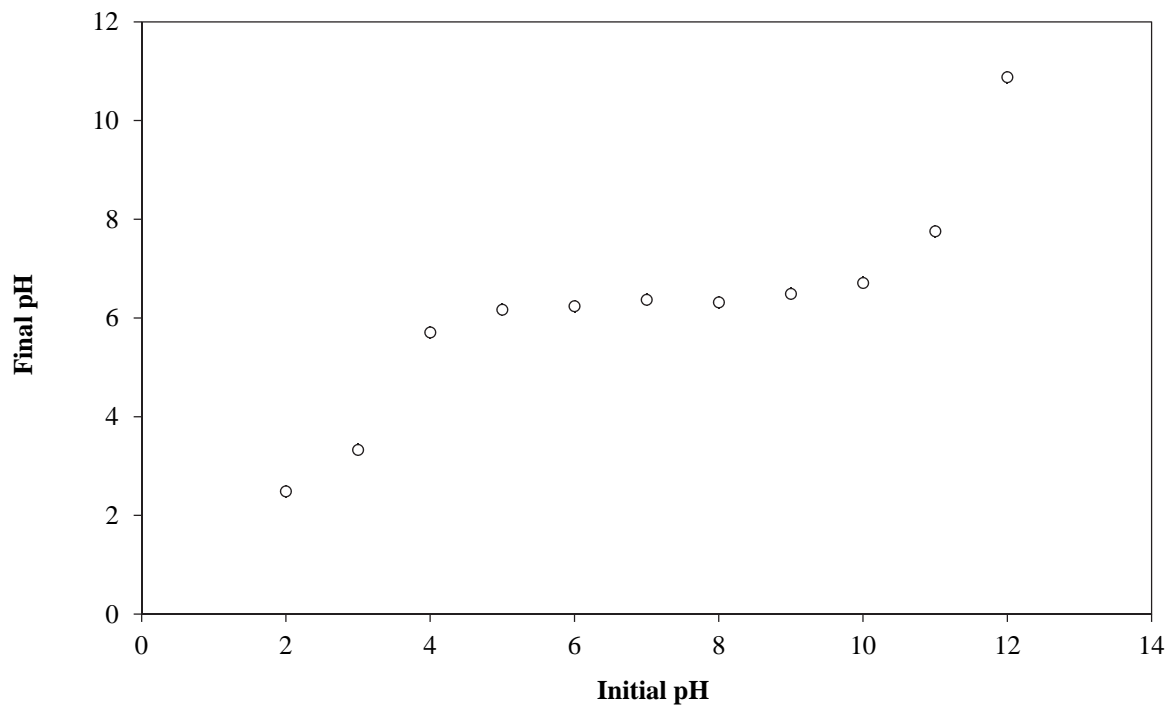


Fig. A 7: Zero point charge of powdered activated carbon

A3 Workshop/conferences

Date	Venue	Theme	Attendance	Institutions represented
28/3/2013	VUT Science Park	Renewable Energy and Water Postgraduates Conference	50	4
19/11/2013	Emerald and Gauteng	Resort Casino, centre: Renewable energy & water	85	5

A4 Other outputs

1. Review of biological wastewater treatment in Southern Gauteng; Project K8/935/3 Part I; 1st August, 2010
2. Wastewater characterization and treatment methods; Project K8/935/3 Part II, 15th October 2010.
3. Biogas production and photocatalytic degradation Project; K8/935/3 Part III, 30th November, 2011.
4. The use of zeolite based support material and photocatalysis to improve biogas production, Project K8/935/3 Part IV, 30th March, 2011.
5. Review of integrated photo-catalytic and anaerobic treatment of industrial wastewater for biogas production; Project no K5/2105 Part I, 6th August, 2011
6. Experimental setup and material preparation for integrated photo-catalytic and anaerobic treatment; Project no K5/2105 Part II, 6th November, 2011.
7. Preliminary operational results on photo degradation; Project no K5/2105 Part III, 3rd March, 2012.
8. Evaluation of operating parameters for biogas production; Project no K5/2105 Part IV, 18th July 2012.
9. Optimization of the operating parameters for photocatalytic and biodegradation process Project no K5/2105 Part V, 14th November, 2012.
10. Interim report on Photodegradation in fluidized bed and annular reactors; Project no K5/2105 Part VI, 1st, April, 2013.
11. Photodegradation in fluidized bed and annular reactors; Project no K5/2105; Part VII, 1st, June 2013.
12. Operation of integrated photodegradation and biodegradation on batch and continuous mode Project no K5/2105 Part VIII, 20th November, 2013.
13. Final report (the present one) Operation of integrated photodegradation and biodegradation on batch and continuous mode Project no K5/2105 Part VIII, 6th May, 2014.